Departament d'Enginyeria
del Terreny, Cartogràfica i Geofísica
UNIVERSITAT POLITÈCNICA DE CATALUNYA

Expansion mechanisms in sulphated rocks and soils

PhD Thesis

Department of Geotechnical Engineering and Geosciences
Universitat Politècnica de Catalunya

Anna Ramon Tarragona

Supervisor: Prof. Eduardo Alonso Pérez de Ágreda

Barcelona, October 2014

Abstract

Geological formations containing sulphates are commonly associated with the development of severe expansions when they are involved in tunnel excavation. The intensity of the observed expansive behaviour in these materials is greater than in other expansive soils and rocks free of sulphates. Swelling in sulphated formations can also occur in the rock mass although no tunnel is excavated, and also within fills made of compacted material from excavations in sulphated rocks. The functionality and stability of engineering works are affected in the majority of the cases.

The prediction of strains and swelling pressures in sulphated formations is a difficult task. On that direction, the Thesis analyses and describes the mechanisms and conditions leading to expansions in sulphated rocks through the detailed investigation of three exceptional cases of damage induced by expansions involving sulphated formations in Spain.

Lilla tunnel, the first case-history analysed, was excavated in Tertiary anhydritic claystone. Expansions developed led to severe tunnel floor heaving and to very high pressures against tunnel lining. The second case, a bridge founded on piles within an anhydritic claystone, Pont de Candí bridge, experienced an unexpected and sustained heave of the central pillars as a consequence of the development of swelling strains below the deep pile foundations. The third case, the compacted access embankments to another bridge, Pallaressos embankments, experienced a very significant volumetric expansion. As a result, the bridge was axially compressed and damaged.

Mechanisms leading to swelling in tunnels in sulphated rocks have been described in the literature; however, an alternative interpretation is proposed. In the first two cases the development of swelling phenomena is explained by the precipitation of gypsum crystals in rock discontinuities. The presence of anhydrite plays a central role in the phenomenon because its dissolution leads to supersaturation conditions of groundwater in calcium sulphate with respect to gypsum, which will result into gypsum precipitation. The process of precipitation of gypsum in discontinuities is thought to act as local jacks inducing swelling strains. The maximum pressure exerted by crystal growth has been estimated under a thermodynamical point of view.

Expansions in the third case analysed are a result of massive growth of ettringite and thaumasite minerals in embankments reinforced by Portland cement due to sulphate attack to cementitious materials. Mineralogical analysis and the simulation of the chemical reactions involved in sulphate attack have shown that expansions in this type of embankments would proceed for a long time because of the availability of the necessary components for ettringite and thaumasite formation. A finite element model of embankment swelling developed has shown that great loads can be generated due to swelling against rigid structures restraining the expansion in some direction.

A coupled Hydro Mechanical and Chemical model formulated in a porous media has been developed to simulate volumetric expansions explained by gypsum precipitation. The model is consistent with field and laboratory observations and describes the kinetics of precipitation and dissolution of gypsum and anhydrite, the solute transport and the development of strains induced by crystallization. The model has been applied to interpret and simulate the heave experienced by Pont de Candí viaduct. Modelling capabilities were checked against the long term history of viaduct heave and also, against the foundation response when the vertical load from a surface embankment was added to counteract swelling.

Resumen

Las formaciones geológicas que contienen sulfatos están asociadas tradicionalmente al desarrollo de expansiones severas cuando son atravesadas por túneles. La intensidad del comportamiento expansivo observado en estos materiales es mayor que en otras rocas y suelos expansivos libres de sulfatos. El hinchamiento asociado a formaciones sulfatadas también puede ocurrir en el macizo rocoso aunque no se excave un túnel, y también en rellenos construidos con material compactado procedente de excavaciones en rocas sulfatadas. En la mayoría de casos la funcionalidad y estabilidad de las obras de ingeniería se ven afectadas.

La predicción de deformaciones y presiones de hinchamiento en formaciones sulfatadas es una tarea difícil. En este sentido, la Tesis analiza y describe los mecanismos y las condiciones que conducen a expansiones en rocas sulfatadas, a través de la investigación detallada de tres casos excepcionales de daño debido a expansiones que involucran formaciones sulfatadas en España.

El túnel de Lilla, el primer caso analizado, se excavó en arcillita anhidrítica. El desarrollo de expansiones condujo a un levantamiento severo de la solera y a presiones contra el revestimiento muy altas. El segundo caso, un puente cimentado en pilotes en una arcillita anhidrítica, el viaducto de Pont de Candí, experimentó un levantamiento inesperado de los pilares centrales debido al desarrollo de hinchamientos por debajo de las cimentaciones profundas. En el tercer caso, los terraplenes de acceso a otro puente, los terraplenes de Pallaressos, experimentaron una expansión volumétrica muy significativa y el puente resultó comprimido axialmente y dañado.

Los mecanismos que conducen al hinchamiento en túneles en rocas sulfatadas se han descrito en la literatura; sin embargo, se propone una interpretación alternativa. La precipitación de cristales de yeso en discontinuidades de la roca explica el desarrollo de fenómenos de expansión en los dos primeros casos. La presencia de anhidrita juega un papel central en el fenómeno expansivo porque su disolución conduce a condiciones de sobresaturación del agua del macizo en sulfato cálcico respecto el yeso, que resulta en la precipitación de yeso. Se cree que el proceso de precipitación de yeso en discontinuidades actúa como gatos locales

generando deformaciones. La presión máxima ejercida por crecimiento de cristales se ha estimado desde un punto de vista termodinámico.

Las expansiones en el tercer caso son el resultado del crecimiento masivo de los minerales de etringita y thaumasita en terraplenes estabilizados con cemento Portland debido al ataque sulfático a los materiales cementantes. Ensayos mineralógicos y la simulación de las reacciones químicas involucradas en el ataque sulfático han mostrado que las expansiones en este tipo de terraplenes continuarían durante un periodo de tiempo largo, debido a la disponibilidad de los componentes necesarios para la formación de etringita y thaumasita. Un modelo de elementos finitos del hinchamiento del terraplén ha mostrado que estas expansiones pueden generar presiones muy altas contra estructuras rígidas.

Se ha desarrollado un modelo acoplado Hidro-Mecánico y Químico formulado en medio poroso para simular expansiones volumétricas explicadas por la precipitación de yeso. El modelo es consistente con observaciones de campo y laboratorio y describe la cinética de la precipitación y disolución, el transporte de soluto y el desarrollo de deformaciones inducidas por cristalización. El modelo se ha aplicado para interpretar y simular el levantamiento experimentado por el viaducto. La capacidad de modelación se ha verificado frente a las medidas de levantamiento del viaducto en el tiempo y también, frente a la respuesta de las cimentaciones a la construcción de un terraplén en superficie para contrarrestar el hinchamiento.

Acknowledgements

My research adventure began some years ago when I engaged on my final degree thesis with Professors Eduardo Alonso and Enrique Romero. It was a great experience, and this, together with my inquisitiveness and will to continue learning, the little push from Professor Xavier Oliver, the proposal from Professor Eduardo Alonso, and maybe also, as some would say, my unawareness, made me decide to enrol in a PhD program after I finished my degree. And I can say it has been worthwhile, beyond my expectations. But I have not been alone.

First of all I would like to sincerely thank my supervisor, Professor Eduardo Alonso, for ensuring I received a complete training. I am grateful for the invaluable discussions we had, in which he always listened to me, with the goal of transmitting all his knowledge with clarity, making sure everything was understood. I also would like to express my gratitude for the opportunity he gave me of participating in real engineering, academic and scientific projects with a high level of rigour and demand. His interest and wish to understand the scientific background of unexpected behaviours in geotechnics, the way he analyses the problems under a wide point of view and his interest for innovation have been an excellent encouragement and example.

I would like to especially thank Professor Sebastià Olivella for his kind and patient help when modelling with CODE_BRIGH and for solving the difficulties that appeared throughout the process. Thank you for spending so much valuable time with me.

I am grateful for the interest and implication of the Department professors: M. Saaltink, J. M. Salvany, J. Gili, J. Vaunat, I. Carol, A. Lloret, A. Gens, J. Suriol, M. Arroyo, E. Romero, A. Ledesma, J. Corominas, X. Sánchez and E. Custodio. And also for the contributions of I. Berdugo, D. Tarragó and L. Oldecop to the Thesis.

I appreciate the conceptual discussions on the nature of swelling and crystal growth maintained with E. Tauler, M. Labrador, A. Canals and S. Seguí, professors from the Dept. of Crystallography of the UB; Dr. C. Ayora from the J. Almera Institute; Professors E. Vázquez and M. Barra from the Dept. of Building Engineering of the UPC; and Dr. J. M. García-Ruiz and Dr. A. van Driessche from the Laboratory of Crystallographic Studies of Granada/CSIC.

I have felt very welcomed at the Department of Geotechnical Engineering & Geosciences from the start. I would like to thank Mar, Víctor, Eva, Óscar, M. Carmen R., Geni and Marta, from the department, and M. Carmen L., from the CIMNE, for their help in dealing with the

administrative matters; Albert and Joan for the IT support and Raúl for his help with the graphs. I am also grateful to Tomás, José and Victor for their friendship, help and time spent in the progress of the experimental part.

I am thankful for the funding I received from the “Departament d’Innovació, Universitats i Empresa” of the “Generalitat de Catalunya”; the “Ministerio de Ciencia e Innovación”; the “Col·legi d’Enginyers de Camins, Canals i Ports”; the “Ministerio de Fomento” of Spain, and also from the CIMNE.

The Spanish National Agency for Railway Infrastructure (ADIF) provided the main technical and financial support during an important part of the field research developed. I would like to specially thank ADIF engineers R. Rodríguez, J. García-Germán, S. Martínez Priego, A. Alba and I. Macías. I greatly appreciate the support to the field research provided on site by engineers A. Alba, M. Alfonso, and A. López Polín (INECO-TIFSA); J. Torres, J. M. Gutiérrez Manjón and M. V. Gil (FCC); C. Sanz (IIC); Dr. J.M. Suso (AITEMIN); and also to CEDEX, Cepasa, Eptysa and Laboratorio Collado Villalba, for the laboratory tests.

The friendship and support from my Department colleagues have also contributed to the successful completion of this Thesis. I bear very much in mind the conversations and encouragement from the time I started the Doctorate from Nubia, Sergio, and Núria, who has been with me from day one. This trip has been easier thanks to the discussions and good times I have shared with Tere, Dani, Alessandra, Mauricio, Nadia, Rodrigo, Enrique, Octavio, Vladimir, Yeudy, Zhifeng, Karim, Benoit, Héctor, Ernesto, Ricardo, Analice, Samuel, Diego, Marité, Kantha, Clara, Lurdes M., Jubert, Rafaela, Francesca, Joaquín, Laura, Abel, Daniel, Mariana, Carme C., Josbel, Amadeu, Joanna, Claudia, Alfonso, Clàudia, Natàlia, Guillem, Víctor, Ignasi, Cristian, Agustín, Lluís, Jordi, Ramón, Olga; and Alba and Ivan with whom I started a nice friendship in the Alps.

I want to extend my gratitude to all the people, quite a few, that have helped me during all these years and whose names are impossible for me to list all here. I would like to thank Marta S., Maria del Mar, Gemma, Rubén, Anna, Cris, Marta T., Carmen, Andrea, Matías, Catalina, Míriam, Carlos, Astrid, Giorgio, Aïda, David L. and David B. for staying close to me in this adventure. I would also like to express my gratitude to Manuel’s family for their support.

Finally, I would like to specially thank my parents, grandparents, Ester and Manuel for their support, understanding, encouragement and patience during all these years, to them and to the much-missed Tote I dedicate this Thesis.

Agradecimientos

Mi aventura con la investigación empezó hace unos años con la tesina de final de carrera con los Profesores Eduardo Alonso y Enrique Romero. Fue una muy buena experiencia, y esto hizo que junto a mi inquietud y ganas de seguir aprendiendo, el empujoncito del Profesor Xavier Oliver, la propuesta del Profesor Eduardo Alonso, y alguien diría que quizá también mi inconsciencia, después de terminar la carrera decidiera empezar el Doctorado. Y puedo decir que ha valido la pena, con creces. Pero no lo he conseguido sola.

Para empezar quiero agradecer muy sinceramente a mi tutor el Profesor Eduardo Alonso. Quiero darle las gracias por haberse preocupado por mi formación completa. Le agradezco las discusiones enriquecedoras que hemos mantenido, él siempre escuchando y con mucho interés por transmitir todos sus conocimientos con claridad, asegurándose de que todo quedara entendido. También le agradezco la oportunidad de haber participado en proyectos de ingeniería reales, académicos y científicos con un nivel de rigor y exigencia altos. Su interés y voluntad de querer comprender el trasfondo científico de comportamientos inesperados en geotecnia, el análisis con una perspectiva amplia de los problemas y el interés por innovar ha constituido un excelente estímulo y ejemplo del que aprender durante este tiempo.

Agradezco especialmente al Profesor Sebastià Olivella su amable y paciente ayuda en las modelaciones con CODE_BRIGHT y en la resolución de las dificultades que han surgido. Gracias por dedicarme tu tiempo.

Estoy agradecida por el interés e implicación de los profesores del Departamento: M. Saaltink, J. M. Salvany, J. Gili, J. Vaunat, I. Carol, A. Lloret, A. Gens, J. Suriol, M. Arroyo, E. Romero, A. Ledesma, J. Corominas, X. Sánchez y E. Custodio. Y por las contribuciones de I. Berdugo, D. Tarragó y L. Oldecop.

Valoro las discusiones provechosas sobre la naturaleza de los hinchamientos y el crecimiento cristalino que he mantenido con E. Tauler, M. Labrador, A. Canals y S. Seguí profesores del Dept. de Cristalografía de la UB; Dr. C. Ayora del Institut J. Almera; los Profesores E. Vázquez y M. Barra del Dept. de Ingeniería de la Construcción de la UPC; y Dr. J. M. García-Ruiz y Dr. A. van Driessche del Laboratorio de Estudios Cristalográficos de Granada/CSIC.

Me he sentido muy acogida en el Departamento de Ingeniería del Terreno desde el principio. Gracias Mar, Víctor, Eva, Óscar, M. Carmen, Geni, Marta, del departamento, y M. Carmen L.,

del CIMNE, por haberme facilitado la burocracia y temas administrativos. Gracias Albert y Joan por el soporte informático y Raúl por la ayuda con las figuras. A Tomás, José y Víctor estoy agradecida por la amistad, la dedicación y la ayuda en avanzar en la parte experimental.

Agradezco la financiación recibida del "Departament d'Innovació, Universitats i Empresa" de la Generalitat de Catalunya; del Ministerios de Ciencia e Innovación; del "Col·legi d'Enginyers de Camins, Canals i Ports"; del Ministerio de Fomento, y también del CIMNE.

La agencia ADIF proporcionó el principal apoyo técnico y económico de una parte importante de la investigación de campo de la Tesis. Doy las gracias especialmente a los ingenieros de ADIF R. Rodríguez, J. García-Germán, S. Martínez Priego, A. Alba y I. Macías. También agradezco la ayuda a pie de obra para realizar la investigación de campo a los ingenieros M. Alfonso, A. Alba y A. López Polín de INECO-TIFSA; J. Torres, J. M. Gutiérrez Manjón y M. V. Gil de FCC; a C. Sanz de IIC; a AITEMIN (Dr. J. M. Suso); y a las instituciones CEDEX, Cepasa, Eptysa y Laboratorio Collado Villalba por los ensayos realizados.

La amistad y apoyo de los compañeros Estudiantes y Doctores del Departamento también ha colaborado a que esta Tesis haya llegado a buen fin. Tengo muy presentes las conversaciones y ánimos de cuando empecé el Doctorado de Nubia, Sergio y Núria, que aparte de recibirme ya cuando empecé la tesina, me ha ido acompañando durante todo este tiempo. Han hecho más fácil el camino los buenos momentos y las discusiones compartidas con Tere, Dani, Alessandra, Mauricio, Nadia, Rodrigo, Enrique, Octavio, Vladimir, Yeudy, Zhifeng, Karim, Benoit, Héctor, Ernesto, Ricardo, Analice, Samuel, Diego, Marité, Kantha, Clara, Lurdes M., Jubert, Rafaela, Francesca, Joaquín, Laura, Abel, Daniel, Mariana, Carme C., Josbel, Amadeu, Joanna, Claudia, Alfonso, Clàudia, Natàlia, Guillem, Víctor, Ignasi, Cristian, Agustín, Lluís, Jordi, Ramón, Olga; y Alba y Ivan con quienes inicié una buena amistad en la alta montaña.

Quiero extender mi agradecimiento a todas aquellas personas, que son muchas, que a lo largo de todos estos años me han ayudado y que no me es posible nombrarlas a todas aquí. Gracias Marta S, Maria del Mar, Gemma, Rubén, Anna, Cris, Marta T., Carmen, Andrea, Matías, Catalina, Míriam, Carlos, Astrid, Giorgio, Aïda, David L. y David B. por acompañarme de cerca en la aventura y estar presentes siempre que ha hecho falta. Agradezco también muy afectuosamente el apoyo recibido por la familia de Manuel.

Finalmente quiero agradecer a mis padres, abuelos, a Ester y a Manuel su apoyo, comprensión, ánimos y paciencia durante estos años, a ellos y a la añorada Tote dedico esta Tesis.

Agraïments

La meva aventura amb la investigació va començar ja fa uns anys amb la tesina de final de carrera amb els Professors Eduardo Alonso i Enrique Romero. Va ser una molt bona experiència, i això va fer que juntament amb la meva inquietud i ganes de seguir aprenent, l'empenteta del Professor Xavier Oliver, la proposta del Professor Eduardo Alonso, i algú diria que potser també la meva inconsciència, després d'acabar la carrera decidís començar el Doctorat. I puc dir que ha valgut la pena, amb escreix. Però no ho he aconseguit sola.

Per començar vull agrair molt sincerament al meu tutor el Professor Eduardo Alonso. Vull donar-li les gràcies per haver-se preocupat per la meva formació completa. Li agraeixo les discussions enriquidores que hem mantingut, ell sempre escoltant i amb molt interès per transmetre tots els seus coneixements amb claredat, assegurant-se que tot quedés entès. També li agraeixo l'oportunitat d'haver participat en projectes d'enginyeria reals, acadèmics i científics amb un nivell de rigor i exigència alt. El seu interès i voluntat de voler comprendre el rerefons científic de comportaments inesperats en geotècnia, l'anàlisi amb una perspectiva àmplia dels problemes i l'interès per innovar ha constituït un excel·lent estímul i exemple d'on aprendre durant aquest temps.

Agraeixo especialment al Professor Sebastià Olivella la seva amable i pacient ajuda en les modelacions amb el CODE_BRIGHT i en la resolució dels entrebancs que han sorgit. Gràcies per estirar el teu temps per mi.

Estic agraïda per l'interès i implicació dels professors del Departament: M. Saaltink, J. M. Salvany, J. Gili, J. Vaunat, I. Carol, A. Lloret, A. Gens, J. Suriol, M. Arroyo, E. Romero, A. Ledesma, J. Corominas, X. Sánchez i E. Custodio. I per les contribucions de l'I. Berdugo, D. Tarragó i L. Oldecop.

Aprecio les discussions profitoses sobre la naturalesa dels inflaments i el creixement cristal·lí que he mantingut amb E. Tauler, M. Labrador, A. Canals i S. Seguí professors del Dept. de Cristal·lografia de la UB; Dr. C. Ayora de l'Institut Jaume Almera; els Professors E. Vázquez i M. Barra del Dept. d'Enginyeria de la Construcció de la UPC; i Dr. J. M. García-Ruiz i Dr. A. van Driessche del Laboratori d' Estudis Cristal·logràfics de Granada/CSIC.

M'he sentit molt acollida al Departament d'Enginyeria del Terreny des del principi. Gràcies Mar, Víctor, Eva, Óscar, M. Carmen R., Geni i Marta, del departament, i M. Carmen L., del

CIMNE, per haver-me facilitat la burocràcia i temes administratius. Gràcies Albert i Joan pel suport informàtic i Raúl per l'ajuda amb les figures. Al Tomás, José i Víctor estic agraïda per l'amistat, la dedicació i l'ajuda en avançar en la part experimental.

Agraeixo el finançament rebut del Departament d'Innovació, Universitats i Empresa de la Generalitat de Catalunya; del Ministerio de Ciencia e Innovación; del Col·legi d'Enginyers de Camins, Canals i Ports; del Ministerio de Fomento, i també del CIMNE.

L'agencia ADIF va proporcionar el principal suport tècnic i econòmic d'una part important de la investigació de camp de la Tesi. Dono les gràcies especialment als enginyers d'ADIF R. Rodríguez, J. García-Germán, S. Martínez Priego, A. Alba i I. Macías. També agraeixo l'ajuda a peu d'obra per dur a terme el treball d'investigació de camp als enginyers M. Alfonso, A. Alba i A. López Polín d'INECO-TIFSA; J. Torres, J. M. Gutiérrez Manjón i M. V. Gil de FCC; a C. Sanz de IIC; a l'empresa AITEMIN (Dr. J.M. Suso); i a les institucions CEDEX, Cepasa, Eptysa i Laboratorio Collado Villalba pels assajos realitzats.

L'amistat i suport dels companys Estudiants i Doctors del Departament també han col·laborat a que aquesta Tesi hagi arribat a bon fi. Tinc molt present les converses i ànims de quan vaig començar el Doctorat de la Nubia, el Sergio, i la Núria, que a part de rebre'm ja quan vaig començar la tesina, m'ha anat acompanyant tot aquest temps. Han fet més fàcil el camí els bons moments i les discussions compartides amb Tere, Dani, Alessandra, Mauricio, Nadia, Rodrigo, Enrique, Octavio, Vladimir, Yeudy, Zhifeng, Karim, Benoit, Héctor, Ernesto, Ricardo, Analice, Samuel, Diego, Marité, Kantha, Clara, Lurdes M., Jubert, Rafaela, Francesca, Joaquín, Laura, Abel, Daniel, Mariana, Carme C., Josbel, Amadeu, Joanna, Claudia, Alfonso, Clàudia, Natàlia, Guillem, Víctor, Ignasi, Cristian, Agustín, Lluís, Jordi, Ramón, Olga; i Alba i Ivan amb qui vaig iniciar una bona amistat a l'alta muntanya.

Vull estendre el meu agraïment a totes aquelles persones, que són moltes, que al llarg de tots aquests anys m'han ajudat i que no m'és possible nombrar-les a totes aquí. Gràcies Marta S., Maria del Mar, Gemma, Rubén, Anna, Cris, Marta T., Carmen, Andrea, Matías, Catalina, Míriam, Carlos, Astrid, Giorgio, Aïda, David L. i David B. per acompanyar-me d'aprop en l'aventura i estar presents sempre que ha fet falta. Agraeixo també molt afectuosament el suport que he rebut de la família del Manuel.

Finalment vull agrair als meus pares, padrins, a l'Ester i al Manuel el seu recolzament, ànims, comprensió i paciència durant aquests anys, a ells i a l'enyorada Tote dedico aquesta Tesi.

Table of contents

CHAPTER 7 MODELLING GYPSUM CRYSTAL GROWTH AND SWELLING BEHAVIOUR. APPLICATION TO PONT DE CANDÍ BRIDGE

CHAPTER 8 ANALYSIS OF MASSIVE SULPHATE ATTACK TO CEMENT TREATED RAILWAY EMBANKMENTS AND TRACK BASES

Notation

a : activity

a_0 : activity of a reference state

b : parameter defining γ_i

b : vector of body forces

c_u : undrained strength

D : diffusion coefficient

E_c : elastic modulus of concrete

E_s : elastic modulus of steel

e : void ratio

f_{ck} : characteristic compressive cylinder strength of concrete at 28 days

f^w : sink or source of water

G_s : specific gravity

$\mathbf{j}_l^w$: total mass flux of water

K : intrinsic permeability

K_0 : at rest pressure coefficient

L : length

m_{anh} : precipitated mass of anhydrite

m_{gyp} : precipitated mass of gypsum

MV_a : molar volume of anhydrite

MV_g : molar volumes of gypsum

PI: plasticity index

p : pressure applied on the crystals

$p_{c,a}$: pressure experience by the crystal at zone a

$p_{c,b}$: pressure experience by the crystal at zone b

p_d : pressure exerted by a crystal against pore walls, reaction pressure against crystal growth

p_l : liquid pressure

p_s : swelling pressure

$\mathbf{q}_l$: flow rate of water, advective flow

q_u : unconfined compression strength

$R,\ r,\ r_1,\ r_2$: radius

R_g : ideal gas constant

S_r : degree of saturation

T : temperature

T : absolute temperature (in equations)

t : time

$\boldsymbol{u}$: solid displacements

w : water content

w_L : liquid limit

w_p : plastic limit

α : load angle

γ_{cl} : interfacial energy at the crystal-solution interface

γ_h : bulking coefficient in the horizontal direction

γ_i : bulking coefficients

$\gamma_{\max}$: bulking coefficient for zero pressure stress

γ_s / γ_w : solid specific unit weight

γ_z : bulking coefficient in the vertical direction

δ : displacement

ε_i : strain in the direction i

η : coefficient of kinetic laws (equations (10a) and (10b))

μ_c : chemical potential of the crystal

θ : coefficient of kinetic laws (equations (10a) and (10b))

κ : kinetic constant

κ_{anh} : kinetic constant parameter for anhydrite

κ_{gyp} : kinetic constant parameter for gypsum

ν : Poisson's ratio

ν_c : molar volume of the crystal

ν_i : stoichiometric coefficients of a chemical reaction

ξ : sign of the equation (7.10)

ρ_{anh} : anhydrite density

ρ_d : dry density

ρ_{gyp} : gypsum density

ρ_l : density of water

ρ_s : density of solid species

ρ_t : total density

$\boldsymbol{\sigma}$: stress tensor

σ_c : specific surface

$\sigma'_{crystal}$: pressure applied on the crystals

σ'_h : horizontal swelling stresses

σ'_i : effective confining stress in the direction *i*

σ_v : applied vertical stress

σ'_z : effective vertical stress

σ'_z : effective vertical confining stress

ϕ : porosity

ϕ_{anh} : current volumetric fraction of anhydrite

ϕ_{gyp} : current volumetric fraction of gypsum

ϕ_{ini}^{anh} : initial volumetric fraction of anhydrite

ϕ_{ini}^{gyp} : initial volumetric fraction of gypsum

ω_l^m : current mass fraction of mineral in liquid phase

$\omega_{l_{sat}}^m$: current equilibrium mass fraction of dissolved sulphate in water

$\omega^m_{0l_{sat}}$: equilibrium mass fraction of dissolved sulphate in water for an unloaded crystal

$\omega^m_{l_{sat,anh}}$: current equilibrium mass fraction of dissolved sulphate in water with respect to anhydrite

$\omega^m_{0l_{sat,anh}}$: equilibrium mass fraction of dissolved sulphate in water with respect to anhydrite without pressure applied on crystals

$\omega^m_{l_{sat,gyp}}$: current equilibrium mass fraction of dissolved sulphate in water with respect to gypsum

$\omega^m_{0l_{sat,gyp}}$: equilibrium mass fraction of dissolved sulphate in water with respect to gypsum without pressure applied on crystals

CHAPTER 1

Introduction

1.1 Interest of the Thesis

Severe expansive phenomena often occur in excavations performed in sulphated claystone just after the end of the excavation. These phenomena cause great displacements at non confined surfaces; or important swelling pressures against structural elements. Two interesting characteristics of these problematic phenomena are the sudden occurrence and their uncertain evolution in time, without an apparent stabilisation of swelling pressures and deformations. Therefore, the expansion occurring in this type of rocks is a phenomenon capable of severely affect the stability and functionality of excavations.

A rock mass can swell due to two reasons:

– Because it contains intrinsically expansive minerals, like montmorillonite or chlorite, and, besides, if one of the following additional circumstance takes place:

  - The interstitial water in the rock is under suction, which means, in stress terms that its pressure is negative. The suction decreases in the presence of free water (that can have different origins), and that facilitates the hydration of the expansive minerals.

- The rock was cemented under stress. Or, as Bjerrum (1967) would say, the rock acquires a "frozen" energy by deformation ("*strain energy locked in*"). The stress changes induced by the excavation break the bonds of the matrix rock and release its expansive potential, which in general also requires the presence of water to allow the hydration of clay minerals.

– Because it contains soluble salts capable of being dissolved in water and precipitate as crystals in joints or voids in the rock. The sulphated rocks are, in general, affected by this mechanism; therefore expansion is related to the precipitation of gypsum crystals, or ettringite and thaumasite crystals. Apparently the most dangerous and extreme cases of swelling occur in sulphated clayey formations, and the Thesis dedicates the attention to them.

Heave and structural damage in natural formations containing sulphate species have often been associated with tunnelling when gypsum ($CaSO_4 \cdot 2H_2O$) and anhydrite (CaSO4) are present in the rock. Triassic claystone formations containing sulphates in Central Europe (Baden-Wütemberg, in Germany; Jura Mountains, in Switzerland) have been crossed by tunnels for decades. A significant proportion has experienced severe heave problems as a result of expansions within the material below tunnel floor, which have been described by several authors (Kovári et al., 1988; Wittke 1990, 2006; Anagnostou 1993, 2007; Madsen et al., 1995; Wittke-Gattermann & Wittke 2004; Anagnostou et al., 2010).

In Spain there are three well-known tunnels affected by extreme sulphate-related heave. They belong to the high-speed railway from Madrid to Barcelona: Camp Magré, Lilla and Puig Cabrer. They were excavated through Tertiary claystone formations containing gypsum and anhydrite. Lilla tunnel is the one that experienced the most damaging expansive behaviour. At the end of summer of 2002, an increasing heave of the floor of the tunnel was detected during the construction of Lilla tunnel, just a few months after the end of the excavation, and this led rapidly to the failure of the concrete flat slab (Figure 1.1). The heave rates in Lilla were very high in some points (600mm/year!). A total of 1500 m out of the total tunnel length (2000 m) was severely affected by a rapid development of heave. The distribution of the intensity of swelling was not homogeneous along the total length of the tunnel. Some stretches experienced extreme expansions while in others heave was barely measured. The exceptional ground expansions in Lilla led to a total reconstruction of the tunnel in a highly reinforced

circular structure made up with a high characteristic strength concrete, with a cost that tripled the initial prevision of the project. Later, high swelling pressures against the lining of Lilla tunnel, which exceed 6 MPa at some points, have been measured.

(a) (b) (c)

Figure 1.1. Heave and failure of the tunnel flat-slab at chainage 411+880: (a) March 2003; (b) May 2003; (c) September 2003

A case of development of swelling in a deep sulphated formation not related with tunnelling has been detected recently in Spain. This is the case of the significant heave of Pont de Candí bridge for the high-speed railway link Madrid-Barcelona, located next to Lilla tunnel, in the province of Tarragona. The heave mainly concerned the two central pillars, which reach a height of 56 m over foundations. The central pillars of the bridge were founded on a hard anhydritic Tertiary claystone of Tertiary age by means of large diameter (1.65 m) 20 m long bored piles. As it will be described in detail later, the measured sustained heave rates ranging from 5 to 10 mm/month were found to be a result of the development of expansions in depth, within a sulphated formation located below the tips of the piles.

Some similarities with the heave affecting Pont de Candí bridge can be found in the problems reported in relation to two European towns. Lately, an area of the French town of Lochwiller in Alsace and the historic town of Staufen in Germany are experiencing damaging heave apparently related with the development of swelling within an anhydritic formation.

The origin of the swelling phenomena in sulphated formations inducing severe heave in tunnels in Central Europe above mentioned, has often been described as a transformation of anhydrite ($CaSO_4$) into gypsum ($CaSO_4 \cdot 2H_2O$). At a molecular level the two added water molecules imply a theoretical increase of 62% in volume, which is then made responsible for the observed heave (Sahores, 1962; Einfalt & Götz, 1976; Einstein, 1979, 1996; Wittke &

Pierau, 1979; Serrano et al., 1981; Zanbak & Arthur, 1986; Wittke, 1990 and 2006; Madsen & Nüesch, 1991; Kolymbas, 2005).

However, this explanation has been challenged by some authors arguing that the orthorhombic crystals of anhydrite cannot be distorted to become the monoclinic crystals of gypsum (Holliday, 1970; Ortí, 1977). Other authors (Pina et. al., 2000; Krause, 1976; Pimentel, 2003) reject also the direct transformation of anhydrite to gypsum as the basic expansion mechanism. On the other hand, the analysis of field and laboratory observations indicates that the development of expansions is related with the precipitation of gypsum crystals. In fact, evaporation processes at the excavation boundaries of Lilla tunnel were the explanation initially given to the development of swelling in the expanding active layer below the tunnel floor, and hence the mechanism leading to swelling behaviour in tunnels. Evaporation of sulphated water produces supersaturated conditions in calcium sulphate. However, this interpretation doesn't fit the swelling deformations found at depth below the piles of Pont de Candí bridge. No evaporation process is possible to occur at those depths. In this Thesis a different interpretation is suggested for the swelling phenomenon.

Expansions involving calcium sulphated materials can also be found when sulphate attack to cement or lime treated sulphated clay material occurs. This process has been found to be capable of inducing high swelling pressures against rigid structures and important heave when the attack affects massively to layers of certain thickness. In those cases, precipitation of ettringite and thaumasite are involved. An example is the phenomenal swelling of two railway embankments located in Spain, Pallaressos embankments. The scale of the reaction of sulphate attack in these embankments is considered to be quite unique.

In a natural way, a civil engineering work involves the performance of cuts and fills. Commonly the material used to build the embankments and fills comes from previously excavated nearby cuts. Then, embankments consisting on compacted marls containing gypsum will be probably built along civil engineering works involving sulphated rocks. Therefore, the danger of development of sulphate attack to those embankments and fills, if they are treated with lime or cement, has to be taken into account during their design and construction. In addition, transition wedges close to a more rigid structure placed next to an embankment is a common practice. Frequently, cement is used in the design of the transition

wedges, this situation may result in sulphate attacks. These are the reasons explaining the interest of studying this phenomenon.

Calcium sulphated rock formations are common in extensive regions of Spain in Tertiary formations in sedimentary basins and in Triassic formations. They are found in outcrops covering the 7.2% of the surface of Spain. That is a large area. However, sulphated formations are present at depth in a significantly larger extension. Therefore, sulphated formations can be apparently quite often involved in underground excavations and foundations, and therefore a certain evidence of a high potential risk of development of sulphate-related swelling in possible future excavations exists in Spain. However, experience indicates that not all tunnels and bridge foundations in anhydritic or gypsiferous rocks develop expansive phenomena. This is also the case of embankments or compacted layers performed with the material excavated from cuts in anhydritic gypsiferous formations. The reasons for differences in behaviour are not clear. Identifying the conditions leading to a critical swelling problem is not an easy task. The main characteristics of the expanding phenomenon are well known from the reported cases of tunnels affected by expansions. However, the knowledge of the consequences and phenomenology of the expansive behaviour of sulphated rocks and soils doesn't correspond with the insufficient knowledge about the basic mechanisms that generate and control it.

In view of the high presence of sulphated formations in Spain, having the capability for predicting the swelling development and estimating the intensity of the expansions is fundamental for the proper design of tunnels, excavations and embankments or fills in sulphated materials, capable of coping with the requirements of functionality and safety of the structure but also capable of resisting the swelling exerted against structures. In addition, knowing the maximum pressure that could be exerted by expansions related to precipitation of crystals is also necessary because it would be used during the design or repair of the tunnel cross-section shape and lining characteristics.

The design criteria adopted in Lilla tunnel for the final solution (to resist high swelling pressures up to 4.5 MPa for the most critical distribution of applied pressure against the external surface of the tube) have been adopted as a reference in the recent design of other tunnels simply because they will cross rock formations containing gypsum and anhydrite. A reference is made here to Oliola tunnel in the Segarra-Garrigues canal; Albertia and

Montezkue tunnels in Álava, in the high-speed railway Madrid-Valladolid-Norte and Sorbes tunnel in the railway Alicante to Almería.

Questions often raised when an underground work has to be built in sulphated geological formations are typically:

- Will swelling phenomena occur?
- Will the expanding phenomena be intense?
- Which is the convenient excavation and building methodology to avoid or mitigate the development of swelling?
- Which values of maximum swelling pressure against the lining have to be considered in the design of the resisting cross sections in tunnels?

All these questions must be answered in order to build safety infrastructures and to avoid expensive overdesigned structures. However, it is not possible to answer those questions if the fundamental mechanisms that lead to expansions are not well known. The economic impact of these questions is very high.

The knowledge on the mechanisms involved during the development of swelling and the conditions in the rock mass leading to the triggering of the phenomenon will probably allow defining practical criteria valuable for the identification of the swelling potential from field investigation, for the design of tunnels and foundations and for the definition of construction procedures to minimize or avoid the development of expansions.

A better knowledge of the fundamental mechanisms of crystal growth is also required to develop computational methods useful for predicting the occurrence of sulphate-related swelling phenomena, quantifying its intensity and selecting design and construction processes to avoid or resist swelling deformations and pressures.

1.2 Objectives of the Thesis

The analysis of the existing knowledge on the phenomenology of expansions in anhydritic gypsiferous claystone prior to the Thesis allowed extracting that:

- The phenomenon of expansion is well described in tunnels built through these materials due to the reported cases in the literature form Central Europe, and also thanks to the

wide instrumentation installed in Lilla tunnel and the characterization performed on the materials crossed by the excavation in Lilla.

– There is a certain indication that precipitation of crystals explains the swelling in sulphated rocks.

However, a number of gaps related to the phenomenology of expansions in sulphated claystones, which still haven't being clarified, exist, as mentioned before, and demonstrate that it is worthwhile to investigate further this subject.

1.2.1 Gaps found in the available knowledge

a) Gaps in practice

Although the swelling phenomenon in Lilla tunnel could be described well thanks to field observations, the phenomenon couldn't be predicted. No methodology existed for predicting the occurrence of swelling, with the extreme severity observed in Lilla, from the results of a usual field reconnaissance programme (and from the associated laboratory tests).

A relationship between the measured extreme expansive phenomena at floor level and the large swelling pressures against the lining in Lilla, and the information collected during the field investigation prior to the excavation could not be established.

b) Gaps at theoretical level

Predicting and quantifying tools for swelling didn't exist; therefore the development of a general swelling model was needed.

The modelling of swelling phenomena requires the formulation of each of the mechanisms involved in the development of expansions and the conditions leading to precipitation of crystals.

1.2.2 Detailed objectives of the Thesis

The previous comments guided the definition of the objectives of the Thesis. The main objective of the Thesis is to develop methodologies for the prediction of the occurrence of swelling in the excavations when sulphated rock masses are involved. These methodologies

should be able to be applied by designers and contractors dealing with excavations in these materials.

The Thesis will pursue the following specific objectives to achieve the main goal:

- Identify precisely the mechanisms that take place during the development of swelling phenomena related to sulphate formations.
- Identify the conditions triggering the development of expansions.
- Estimate the maximum pressure that could be exerted by expansions induced by precipitation of crystals.
- Develop practical criteria for the prediction of both the development of swelling behaviour and the estimation of the intensity of expansions from a field geotechnical reconnaissance.
- Develop a general theoretical model for simulating precipitation of crystals and the resulting swelling deformations and pressures consistent with field and experimental observations.
- Develop a general computational tool which could be used at design as well as at construction and operation stages of a given infrastructure involving sulphated rocks.
- Validate the model developed against the real case of heave of Pont de Candí Bridge.
- Understand the phenomenon of massive sulphate attack to large embankments and its effect on structures such as bridges.

1.3 Methodology applied in the Thesis

The search for criteria to estimate swelling risk and the identification of the mechanisms involved in expansions, related with the presence of gypsum and anhydrite in the rock mass, has been conducted along two ideas: the collection of case records showing the presence or absence of swelling phenomena in tunnels in sulphated formations in Central Europe and in Spain; and the detailed field investigation of the recent experiences of swelling problems in Lilla tunnel and heave of the Pont de Candí Bridge. Investigations in Lilla and Pont de Candí have led to a modification of some commonly accepted swelling mechanisms in sulphate rocks. Alternative processes have been observed in the field and in the laboratory. It was

thought that understanding their origin may result in better identification criteria, improved designs and in more efficient remedial actions.

The first case, Lilla tunnel, was investigated in detail in research works carried out at the UPC previous to the present Thesis. These works have consisted in a Doctoral Thesis performed by Iván Berdugo (2007), and three Geological Engineering final degree Thesis performed by Daniel Tarragó (2006), Álex Plaza (2008) and Amadeu Deu (2008). In the present Thesis the outcomes of these works have been analysed and reviewed.

Lilla tunnel offered a good opportunity to solve the uncertainty in the development of swelling when anhydrite and gypsum are present. This is a case with excellent data in the tunnel itself but the few information on the rock mass that could be related to the heterogeneous occurrence and intensity of swelling found along the tunnel was limited. A new field investigation has been performed to give some insight, in particular, to the different behaviour observed along the tunnel, but also to the observed fact that the presence of gypsum and anhydrite in the rock mass does not automatically lead to the development of swelling phenomena in tunnelling. The new field investigation consisted in the detailed analysis of two boreholes drilled from the natural ground surface at different locations along Lilla tunnel. One borehole was placed at a position where high expansions were detected and the other one was drilled in a stretch where no significant swelling was observed.

In addition, the behaviour of the tests sections and the performance of the final reinforced circular cross-section in Lilla tunnel, including recent measurements, have been analysed to obtain practical criterion for the design of cross-sections in tunnels with a risk of development of expansions. The fracturing and mineralogy along the length of the tunnel and the rainfall in the area of Lilla tunnel have been taken into account in the analysis.

The second case investigated, the heave of Pont de Candí bridge, was detected recently, some years after the case of Lilla tunnel. The engineers in charge of the viaduct provided the opportunity of defining a wide investigation programme during this Thesis to study and analyse the expansions resulting in the heave being experienced by the bridge. The initial research campaign performed in the area of the bridge was widened in several occasions and the new results were interpreted.

The observed development of swelling deformations in depth in Pont de Candí bridge, challenged the initial explanation for the swelling phenomena related to crystal precipitation

in Lilla. It became clear that evaporation of sulphated water couldn't occur at the deep active expanding layer in Pont de Candí bridge. The field investigations in Pont de Candí provided remarkable information on the development of swelling, and resulted in an alternative interpretation for the mechanism leading to expansions.

A revision of the published work on the precipitation and dissolution of gypsum and anhydrite crystals has been performed. It was concluded that precipitation of gypsum is possible without evaporation when anhydrite is present. Saturation conditions of sulphated groundwater have been also verified by means of simulations of the chemical composition of natural groundwater.

The development of swelling pressures due to crystal growth has been studied under a thermodynamic point of view and provided the estimation of upper boundary values of swelling pressure.

Once the mechanisms involved in expansions were identified, they were formulated and included in the general Thermo-Hydro-Mechanical (THM) framework offered by the available code of the program CODE_BRIGHT (DIT-UPC, 2002) for general THM coupled analysis in porous media. In addition, some modifications of the balance equations had to be done. The literature review performed on crystal growth and the processes of dissolution and precipitation of crystals allowed formulating kinetic equations for describing the precipitation and dissolution of anhydrite and gypsum crystals, taking into account the pressure acting on crystals.

The instrumentation installed in the area of Pont de Candí provided the evolution of heave and deep expansions over time necessary for the simulation of heave of Pont de Candí bridge. The boundary conditions in the rock mass of Pont de Candí bridge have been simulated, as well as the development of expansions.

The real cases of cement stabilized railway track bases and Pallaressos embankments have been analysed to investigate the development of swelling behaviour due to growth of ettringite and thaumasite crystals in artificial soil affected by high sulphate content. A field and laboratory investigation campaign was designed. The laboratory campaign proposed has consisted not only on standard tests. Original procedures for sample testing have been defined in view of the heterogeneity of the material in the cases studied. A literature review on the chemical description of sulphate attack processes and on reported real cases affected by

sulphate attack has been performed. The swelling pressure exerted by the massive expansion of the embankment has been estimated by modelling the heave measured at the surface of the embankments. The chemical interaction at the interface between the cement and the compacted soil has been studied through geochemical calculations.

1.4 Content and organization of the Thesis

The content of the Thesis is organised in nine Chapters as follows:

Chapter 1 constitutes the introductory Chapter of the Thesis and Chapter 9 is the closing one. The main work carried out along the Thesis research is described in Chapters 2 through 8, and partial conclusions derived from the work described in each particular Chapter are presented at the end of them.

Chapter 1 describes the motivation and interest of the Thesis. Then as an introduction for the objectives of the Thesis, the gaps in knowledge related to expansions in sulphated materials are described. The content and organization of the Thesis in Chapters is detailed and the relevant publications derived from the research work performed during the Thesis are presented.

Chapter 2 describes the presence and the main characteristics of sulphated rocks in Central Europe where several tunnels affected by expansions have been reported in the literature. A summary of the expansive behaviour observed in Central Europe is presented. The Chapter includes a review of the calcium formations present in Spain to highlight the wide presence of sulphated rocks existing in Spain and therefore the potential risk of development of swelling affecting infrastructures. The Chapter ends with a description of the current alternatives to design tunnel lining in expansive sulphated rocks.

Chapter 3 describes the extreme expansive phenomena occurred in Lilla tunnel. The geological framework, design and construction of the tunnel is described, as well as the chronology, the characteristics of the expansions observed and the ground properties found during field and laboratory investigations. Some observations made in cores, relevant for the understanding of the mechanisms involved in expansions are also described. Then, the performance of different cross-sections built, including testing sections and the final

reinforced circular cross-section is analysed from the measurements obtained by instrumentation.

Chapter 4 concentrates on the case of heave of Pont de Candí bridge. The design of the bridge; the geological background of the location of Pont de Candí and the geotechnical properties obtained from initial geotechnical field reconnaissance at the bridge design stage and from the new investigations defined once the heave was detected, are described. The field investigation designed to give insight in the development of heave is described and the results are analysed. In-situ tests results and observations found in recovered cores, that provided an explanation of the expansions occurring at depth, are highlighted in the Chapter. The remedial measures performed to counteract the heave and the response of the expanding deep phenomena are described at the end of the Chapter.

The description of swelling mechanisms due to gypsum crystal growth and the analysis of the factors triggering expansions in sulphated materials are collected in Chapter 5. A series of situations and characteristics of the rock mass that may eventually result in, or trigger, severe expansive phenomena are identified from a review done on a number of tunnels crossing gypsum formations in Spain and Central Europe. Also, a detailed analysis of the cores recovered from two boreholes drilled close to the position of Lilla tunnel at two locations experiencing either high or no expansions provided additional information. The explanation of swelling phenomena given by several authors that report expansions in tunnels in Central Europe is reviewed, and a different interpretation of the mechanisms dealing to expansions is suggested in this Chapter. Plausible scenarios for heave and swelling in Pont de Candí bridge and Lilla tunnel are set out.

Chapter 6 describes the studies performed to evaluate theoretically the pressure induced by crystal growth. Relevant aspects are the role of interfacial pressure and pore structure on crystal growth and soil expansion.

Chapter 7 describes the model developed capable of simulating gypsum crystal growth processes and swelling behaviour. The formulation is detailed in Appendices included at the end of the Chapter. The method is applied to the modelling of Pont de Candí bridge heave and expansions at depth. A sensitivity analysis on the model parameters is included in the Chapter.

Chapter 8 concerns the swelling mechanism in sulphated materials induced by ettringite and thaumasite crystals. The Chapter concentrates on the analysis of massive sulphate attack to cement treated railway embankments and track bases made of compacted clay. A review of the phenomena of sulphate attack reported in the literature is summarized. The design of the railway embankments and the initial observed development of damage are described. The research work, and field and laboratory investigations defined to study the problem are presented and the results obtained are analysed. The geochemical calculations performed allow a deeper understanding of the sulphate attack reactions in the treated clay materials. The Chapter describes also the modelling of the heave observed at the embankments, the stress response of the embankment and the pressure exerted against bridge abutments. The remedial measurements performed are briefly summarized.

Chapter 9 points out the main conclusions derived from the research and propose future research work.

1.5 Papers published during the development of the Thesis

The research work carried out in the Thesis has resulted in the following publications:

Journal papers:

Alonso, E. E. and Ramon, A. (2013). Heave of a railway bridge induced by gypsum crystal growth: field observations. *Géotechnique* **63**, No. 9, 707 – 719, [http://dx.doi.org/10.1680/geot.12.P.034]

Ramon, A and Alonso, E. E. (2013). Heave of a railway bridge: modelling gypsum crystal growth. *Géotechnique* **63**, No. 9, 720 – 732, [http://dx.doi.org/10.1680/geot.12.P.035]

Alonso, E.E., Berdugo, I.R. and Ramon, A. (2013). Extreme expansive phenomena in anhydritic-gypsiferous claystone: the case of Lilla tunnel. *Géotechnique* **63** No. 7, 584 – 612, [http://dx.doi.org/10.1680/geot.12.P.143]

Alonso, E. E. and Ramon, A. (2013). Massive sulfate attack to cement-treated railway embankments. *Géotechnique* **63**, No. 10, 857 – 870, [http://dx.doi.org/10.1680/geot.SIP13.P.023]

Chapter of a book:

Alonso, E., Ramon, A. and Berdugo, I. (2011). Túneles en terrenos expansivos. Chapter of the book: *Manual de túneles y obras subterráneas*. pp: 1097-1154. Universidad Politécnica de Madrid (UPM). ISBN: 978-84-96140-36-3 Legal deposit: M. 16.764-2011.

Papers published in Conferences, Symposiums and Workshops:

Alonso, E. E., Berdugo I., R., Tarragó, D. & Ramon, A. (2007). Tunnelling in sulphate claystones. Invited Lecture. *Proc. 14th European Conference on Soil Mechanics and Geothecnical Engineering, Madrid*, **1**, 103–122.

Ramon, A., Alonso, E.E. and Romero, E. (2008). Grain size effects on Rockfill constitutive Behaviour. In: *Proceedings of the I European Conference on Unsaturated Soils, Durham 2008*, 341-347.

Ramon, A. (2008). Mecanismos de expansión de rocas yesíferas y su influencia sobre las excavaciones. Diploma of Advanced Studies, UPC. Barcelona.

Ramon, A. (2008) Expansive phenomena in tunnels through anhydritic-gypsiferous claystones. Lessons learned from a case study. In: *Proceedings of the 19th European Young Geotechnical Engineers' Conference (EYGEC), Györ*, 268-276.

Ramon, A, Olivella, S and Alonso, E.E. (2009). Swelling of a gypsiferous claystone and its modelling, In: *Proceedings of the 17th International Conference on Soil Mechanics and Geotechnical Engineering, Alexandrie*, **1**, 730-733.

Ramon, A., Alonso, E. and Olivella, S. (2009). Modelo hidro-mecánico acoplado de expansión por cristalización. In: *Proceedings of the Métodos Numéricos en Ingeniería 2009, Barcelona*, 185-186.

Alonso, E. and Ramon, A. (2009). Interacciones hidrodinámicas y químicas en el comportamiento y patología de terraplenes. In: *"Terraplenes y pedraplenes en carreteras y ferrocarriles"*, 1-40. Chapter of the course syllabus "Terraplenes y pedraplenes en carreteras y ferrocarriles", organized by Instituto técnico de la vialidad y del transporte (INTEVÍA), Madrid.

Ramon, A. (2010) Modelling of deep foundation heave induced by crystal growth. *Alert Workshop 2010, Aussois*, 1-2.

Alonso, E. and Ramon, A. (2010). Fenómenos de expansión en estribos. Chapter of the course syllabus "*Muros, Estribos y Transiciones*" organized by Instituto técnico de la vialidad y del transporte (INTEVÍA), Barcelona, 1-49.

Alonso, E. and Ramon. A. (2011). El túnel de Lilla. Invited lecture In: *Túneles en terrenos salinos y expansivos. Barcelona*, 57-88. Aula Paymacotas – UPC.

Ramon, A. and Alonso, E. (2011). Heave of a piled foundation on a sulphated claystone. In: *Proceedings of the 15th European conference on soil mechanics and geotechnical engineering: geotechnics of hard soils, weak rocks, Athens*, 909 - 914. IOS Press, ISBN 978-1-60750-800-7.

Ramon, A and Alonso, E. (2011). Gypsum crystal growth in tunnels. In: *Harmonising Rock Engineering and the Environment: 12th ISRM International Congress on Rock Mechanics. Beijing*, 1797 - 1802. CRC Press. Taylor & Francies Group.

Ramon, A and Alonso, E. (2011). Hinchamiento en túneles por crecimiento de cristales y su modelación. In: *Proceedings of the "Jornada de recerca i innovació a l'Escola de Camins: resum de les ponències", Escola de Camins. Barcelona*, 1-4.

Sauter, S., Alonso, E.E. and Ramon, A. (2012). Efecto de la expansión profunda sobre cimentaciones por pilotes. In: *Proceedings of the 9º Simposio nacional de Ingeniería Geotécnica. Cimentaciones y excavaciones profundas, Sevilla*, 385-397.

Ramon, A. and Alonso, E. E. (2012). Thaumasite and ettringite massive crystal growth in two railway embankments. In: *Proceedings of the workshop CRYSPOM* III. Crystallization in porous media, 57-58. Extended abstract.

Alonso, E. E. and Ramon, A. (2012). Gypsum crystal growth under bridge foundations. In: *Proceedings of the workshop CRYSPOM III. Crystallization in porous media*, 17-18. Extended abstract.

Ramon, A.; Alonso, E."Crystal growth under bridge foundations". In: *W(H)YDOC 12: 4th International Workshop of Young Doctors in Geomechanics, Paris,*. 61 - 66. 2012.

Ramon, A.; Alonso, E. E. (2013). Modelling swelling behavior of anhydritic clayey rocks. In: *Proceedings of the 3rd International Symposium on Computational Geomechanics : COMGEO III : Krakow, Poland, 2013*. 348 - 358. International Centre for Computational Engineering.

Ramon, A.; Alonso, E. E. (2013). Analysis of ettringite attack to stabilized railway bases and embankments. In: *Proceedings of the 18th International Conference on Soil Mechanics*

and Geotechnical Engineering: Challenges and Innovations in Geotechnics: Actes du 18e Congrès International de Mécanique des Sols et de Géotechnique: Défis et Innovations en Géotechnique, Paris, 785 - 788.

Ramon, A.; Alonso, E. E. (2013). Coupled hydro-chemo-mechanical modelling of a foundation heave due to gypsum crystal growth. In: *Computational Methods for Coupled Problems in Science and Engineering V: Proceedings of the V International Conference on Computational Methods for Coupled Problems in Science and Engineering held in Ibiza, Spain 17-19 June 2013*, 1 - 2. International Center for Numerical Methods in Engineering (CIMNE). Extended abstract.

Ramon, A.; Alonso, E. (2013). "Modelling crystal growth". In: *Proceedings of the 5th Workshop of CODE-BRIGHT Users*, 1 - 4.

Ramon, A. & Alonso, E.E. (2014) Crystal Growth and Soil Expansion: The Role of Interfacial Pressure and Pore Structure. In: *Unsaturated soils: Research & Applications (UNSAT 2014)*, Sydney, 875-881.

Ramon, A. & Alonso, E. (2014). Modelling swelling phenomena in Lilla tunnel. Extended abstract. In: *Proceedings of The 4th international workshop on crystallization in porous media (CRYSPOM IV), Amsterdam*, 47. Abstract.

CHAPTER 2

Sulphated rocks in Central Europe and Spain and tunnel experience

This Chapter describes the main formations from Central Europe known for their capability to develop severe swelling phenomena affecting tunnels. The expansive behaviour in those formations containing sulphate species is presented and compared with expanding behaviour in other swelling materials. Later, the main calcium sulphated formations in Spain are reviewed to demonstrate that coming across an excavation in a sulphated formation that may be affected by expansions is a real possibility in Spain. The experience gained from tunnelling in Central Europe and from the case of Lilla tunnel in Spain is summarized.

2.1 Introduction

Tunnels excavated in anhydritic-gypsiferous claystones have often experienced severe swelling phenomena. Within Europe, Triassic sulphate rocks found in Baden-Württemberg (Germany) and in Jura Mountains (Switzerland) have been repeatedly mentioned when gypsum-related swelling problems in tunnels have been reported. Recent contributions to the

study of swelling in tunnels crossing these materials have been made by Kovari & Descoeudres, 2001; Amstad & Kovari, 2001; Wittke, 2006 and Anagnostou, 2010.

Gypsum-rock formations are also common in other countries and, in particular, in extensive regions of Spain. However, the number of reported cases of swelling in Spain up to now is substantially lower than in Central Europe. This was substantiated by a review of tunnels in sulphated formations showing the presence and absence of swelling behaviour that will be described in Chapter 5. A recent case has been Lilla tunnel excavated through the Lower Ebro Basin, an evaporitic deposit. Another recent case is the Albertia tunnel built close to Vitoria in the high-speed railway Madrid-Valladolid-Norte in Spain. It crosses highly tectonized sulphated rocks containing gypsum and anhydrite with a sedimentary origin (Lower Cretaceous). Moderate expansions were recorded during its construction.

Once the tunnel is built, the tunnel operation has to cope with the swelling pressures and deformations affecting the tunnel. The design of the tunnel lining can be performed according to the principles of resisting or/and yielding support taking into account the intensity of the expected expansive phenomenon, the possible limitations associated with the difficulty to build a lining stiff enough to support the expected pressures, and the limitations derived from the operation of the tunnel (railway or road tunnel).

The swelling behaviour in sulphated rocks in Central Europe and Spain is not limited to tunnels. Expansions involving stratums of anhydrite formations have been reported recently in relation with the surface heave experienced in the historic town of Staufen in Germany (Sass & Burbaum, 2010) and in the French town of Lochwiller. The heave of a railway bridge located in Spain, Pont de Candí viaduct, is another case of different nature compared with tunnels affected by expansions. This case will be described in detail later in Chapter 4.

The present Chapter starts with a short description and a summary of main data concerning swelling phenomena reported in tunnels excavated in Central Europe. Then, the characteristics of sulphate rock formations in Spain are described. Finally, this Chapter concludes with the analysis of the alternatives to select tunnel lining at the design stage or during repairing works. This analysis is based on the experience obtained in tunnels affected by expansions crossing sulphated claystone in Central Europe and in the field investigations performed in circular testing sections during the investigation of the expansion affecting Lilla tunnel.

2.2 Expansive sulphated rocks in Central Europe

This section will describe the Triassic sulphate-bearing rocks from Baden-Württemberg and Jura Mountains and its expansive behaviour.

2.2.1 The Anhydritgruppe and the Gipskeuper

Most tunnels in Baden-Württemberg (South-western Germany) and Jura Mountains (Northeastern Switzerland) affected by severe expansive phenomena have been excavated through Triassic hard rocks from the Anhydritgruppe (Middle Muschelkalk) and the Gipskeuper (Middle Keuper) with a high content in sulphates. Both materials are heterogeneous mixtures of anhydrite and gypsum in a hard clayey matrix. Images of these materials and their mean mineralogical composition are presented in Figure 2.1 and Table 2.1, respectively.

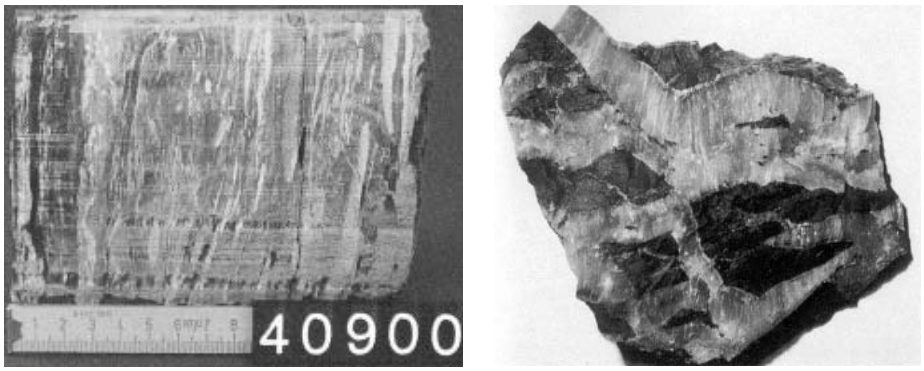

(a) (b)

Figure 2.1. Undisturbed samples from (a) the Anhydritgruppe (Middle Muschelkalk) (Madsen & Nüesch, 1990), and (b) the Gipskeuper (Middle Keuper) (Amstad & Kovári, 2001)

Table 2.1. Mean mineralogical composition properties of the Anhydritgruppe and the Gipskeuper

Material	**Mineralogical composition (%)**					
	A	G	C	CO_3	Q	F
Anhydritgruppe	45 90	1 4	2 50	1 25	1 15	1 5
Gipskeuper	30 75	1 20	5 20	0 20	5 20	1 5

A: anhydrite, G: gypsum, C: clay, CO3: carbonates, Q: quartz, F: Feldspars

The Anhydritgruppe mainly consists of evaporites (gypsum, anhydrite and halite) and dolomite. On the other hand, the Gipskeuper is a sequence ranging from clays and silts to dolomitic marls showing a wide range of colours. Red to violet sediments indicate oxidizing environments while grey to greenish sediments corresponds to reducing environments. Evaporation of saline sea water led to the formation of anhydrite, gypsum and halite pseudomorph crystals (Aigner, 1990).

In Baden-Württemberg a distinction is made between two different geological levels associated with the Middle Gipskeuper: (i) the upper leached gypsiferous level and (ii) the unleached anhydritic level. This distinction is illustrated in Figure 2.2 using the case of Wagenburg North tunnel (Stuttgart) as reference. Above the unleached anhydritic level, the anhydrite has been converted into gypsum in geological times. In the leached gypsiferous level, the gypsum has been dissolved and transported away by the groundwater (Wittke, 2000). Prommersberger & Kuhnhenn (1989) point out that the rock shows very limited stability problems when opening a cavity in the leached zone. On the other hand, below the anhydritic level the rock can be considered essentially impervious. The material is compact and of sufficient stability for tunnel excavation.

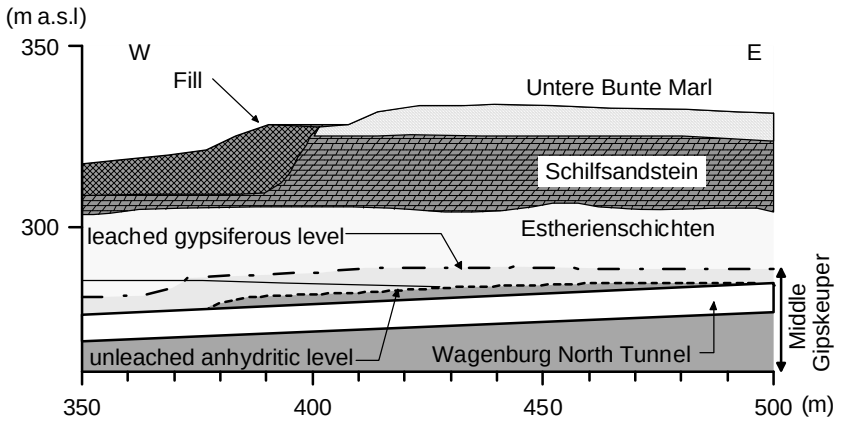

Figure 2.2. Geological longitudinal section of Wagenburg North tunnel in Stuttgart (Nagel, 1986; Paul & Wichter, 1996 and Amstad & Kovári, 2001)

Information related with chemical composition of groundwater in tunnels excavated in the Anhydritgruppe and the Gipskeuper is not complete. Some data of sulphate content have been reported by Amstad & Kovári (2001), but only regarding to the possibility of sulphate attack to concrete. Isolated values of sulphate content in water from Belchen tunnel, built in Jura Mountains and affected by expansions, were reported by Grob (1972) and Werder (1989). The occurrence of macroconstituents as calcium, magnesium, sodium and potassium -which may

have an essential role in the interaction between sulphated waters and sulphate-bearing rocks-, is, in general, not reported in the German and the Swiss literature on the subject. Values of sulphate content reported by some authors are presented in Table 2.2.

Table 2.2. Sulphate content in groundwater from some tunnels excavated in the Gipskeuper and the Anhydritgruppe (extracted from Amstad & Kovari, 2001)

Tunnel	SO_4 (ppm)	Reference
Weinsberg	up to 1500	Gremminger & Spang (1978)
Kappelesberg	1957 - 2755	Krause & Wurm (1975)
Adler	2990	Chiaverio & Hürzele (1996)
Belchen	up to 6000	Grob (1972)
Belchen	1290	Werder (1989)
Freudenstein	up to 5600	Berner (1991)
Engelberg Base	> 8600	Kuhnhenn et al. (1979)

Expansive clay minerals, particularly corrensite, are isolated components of the host clayey matrix in the Gipskeuper in Baden-Württemberg (Götz, 1972; Henke, 1976; Lippmann, 1976). Corrensite is a 1:1 regular interstratification of trioctahedral chlorite and trioctahedral smectite, also called “swelling chlorite”; however, illite and chlorite are also present in the Gipskeuper as illustrated in Figure 2.3. In general, non-expansive clays have been detected as principal clay matrix components in many tunnels excavated through the Anhydritgruppe and the Gipskeuper [i.e. Adler, Belchen, Hauenstein and Sissach tunnels (Grob, 1972, 1976; Madsen et al., 1995; Nüesch et al., 1995; Hauber, 1996; Nüesch and Ko, 2000); Kappelesberg tunnel (Krause, 1976; Kurz and Spang, 1984); Freudenstein tunnel (Kirschke, 1987; Kirschke et al., 1991)].

2.2.2 Expansive behaviour of the Anhydritgruppe and the Gipskeuper

In general, swelling in gypsiferous-anhydritic claystones far exceeds the expansivity threshold of most hard soils and rocks, which are well-known because of their high expansive potential.

Figure 2.4 shows the magnitude of extreme heave and swelling pressures measured during construction and operation in some tunnels from Baden-Württemberg and Jura Mountains.

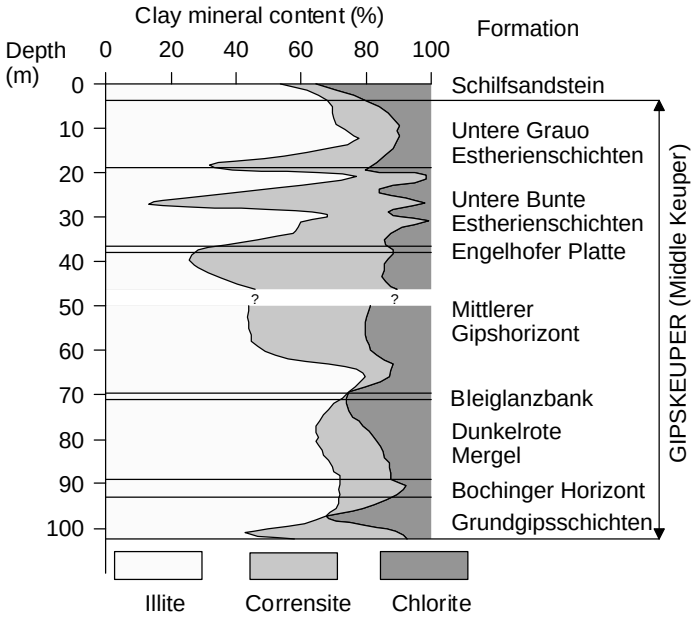

Figure 2.3. Lithology and composition of clay matrix of the Gipskeuper in Baden-Württemberg (modified after Schlenker, 1971)

The distinction between sulphate claystones and other expansive clayey materials facilitates a first assessment of the complex phenomena studied in this Thesis. Figure 2.4 points out that under similar conditions of construction and operation, heave and swelling pressures in sulphate claystones could be one order in magnitude greater than in expansive clayey materials.

Swelling in tunnels excavated in sulphate rocks evolves at high rates and, in some cases, a limit value for displacements or pressures cannot be clearly defined. This situation is illustrated in Figure 2.5 using long-term observations in some tunnels and test galleries from Baden-Württemberg and Jura Mountains. Some laboratory observations reveal the same behaviour in undisturbed samples of sulphate claystones. Figure 2.6 illustrates this aspect by means of a comparison between the typical swelling behaviour of some expansive rocks (Esna shale, Al-Qatif shale and Opalinus clay) -characterized by a clear limit for both swelling strain and swelling pressure-, and the non-asymptotic swelling response of samples from the Gipskeuper and the Anhydritgruppe.

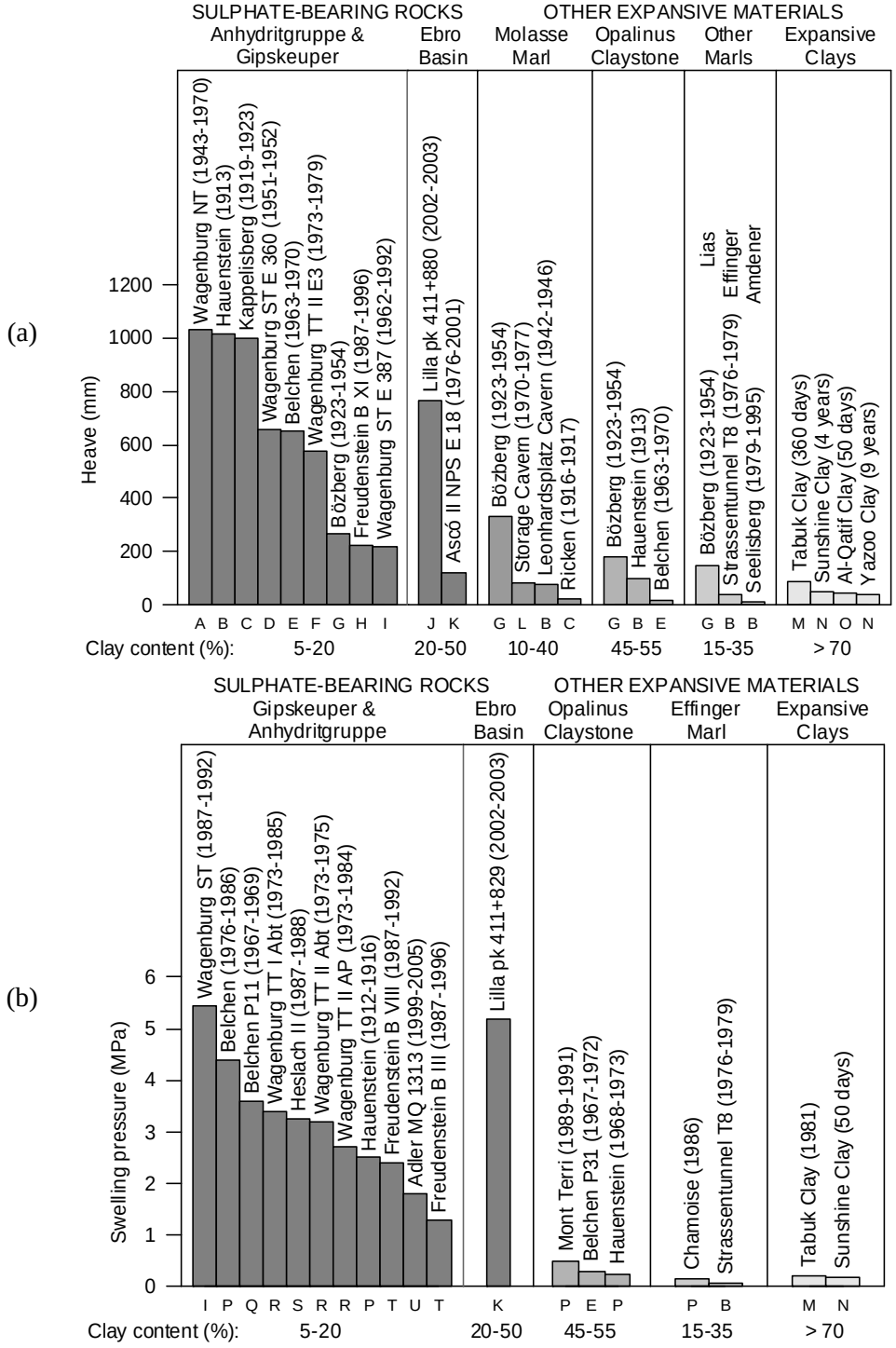

Figure 2.4. Extreme expansive phenomena in tunnels, caverns, deep excavations and foundations in swelling rocks and soils, compiled in Berdugo, 2007: (A) Krause (1976), (B) Amstad & Kovári (2001), (C) Einstein (1979), (D) Krause& Wurm (1975), (E) Grob (1972), (F) Nagel (1986), (G) Grob (1976), (H) Wittke-Gattermann (1998), (I) Paul & Wichter (1996), (J) Alonso et al (2004), (K) Berdugo et al (2006), (L) Bischoff & Hagmann (1977), (M) Dhowian (1984), (N) Young (2004), (O) Abduljauwad et al (1998), (P) Steiner (1993), (Q) Huder & Amberg (1970), (R) Wichter (1985), (S) Wittke (2000), (T) Fecker (1992), (U) Noher et al (2006)

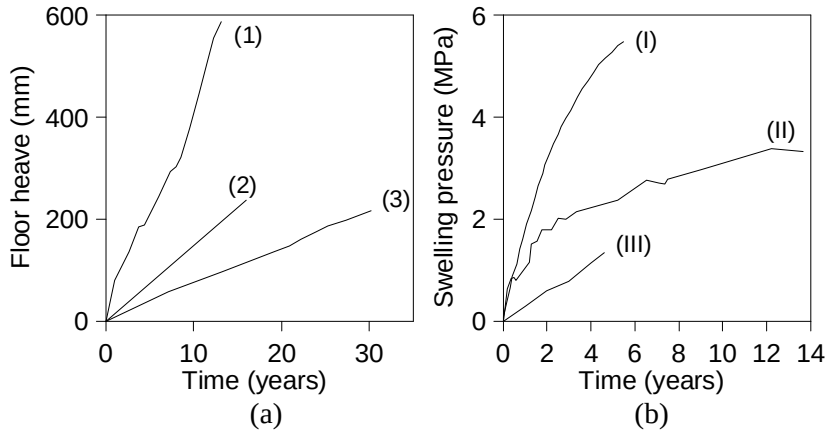

Figure 2.5. Floor heave and swelling pressure evolution in tunnels excavated in swelling rocks, compiled in Berdugo, 2007: (a): (1) Wagenburg NT E 391 -Gipskeuper- (Nagel, 1986), (2) Bözberg -Anhydritgruppe- (Grob, 1976), (3) Wagenburg ST E 387 -Gipskeuper- (Paul & Wichter (1996); (b): (I) Wagenburg ST E 409 -Gipskeuper- (Paul & Wichter,1996), (II) Wagenburg TT I -Gipskeuper- (Wichter, 1985), (III) Freudenstein TG Block VIII -Gipskeuper- (Fecker, 1992)

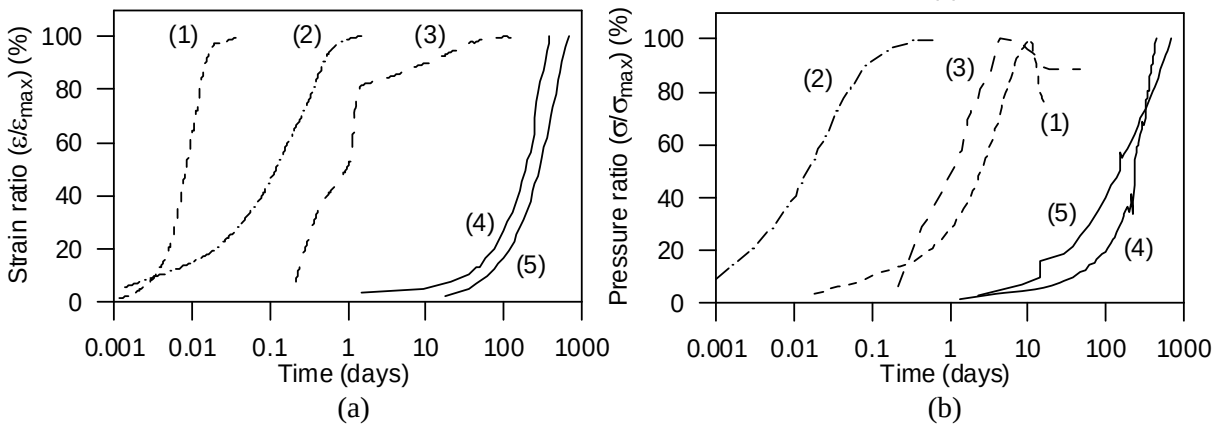

Figure 2.6. Examples of (a) swelling strain and (b) swelling pressure evolution over time (both are normalized with respect to the maximum value) for swelling rocks obtained in laboratory tests, compiled in Berdugo, 2007: (1) Esna shale (Wüst & Mclane, 2000), (2) Al-Qatif shale (Abduljauwad et al, 1998), (3) Opalinus clay (Grob, 1976), (4) Gipskeuper (Madsen et al, 1995), (5) Anhydritegruppe (Madsen & Nüesch, 1990)

2.3 A review of main calcium sulphated formations in Spain

Calcium sulphate rocks occur in extensive zones of the Iberian Peninsula and Balearic Islands as outcrops and buried formations. According to Riba & Macau (1962) gypsiferous rocks outcrop in 7.2 % of the Spanish territory, and they are mainly located in the eastern part of the country (Figure 2.7). This is, certainly, a very large area of the territory in surface; however

the extension is greater in depth. Taking into account buried formations -particularly the materials from the Keuper-, the relevance of calcium sulphate rocks in the infrastructures of Spain increases substantially. In fact, tunnelling works in Spain affect sulphate formations relatively often. Therefore, a proper knowledge of main characteristics of these formations is essential to evaluate their behaviour in tunnels.

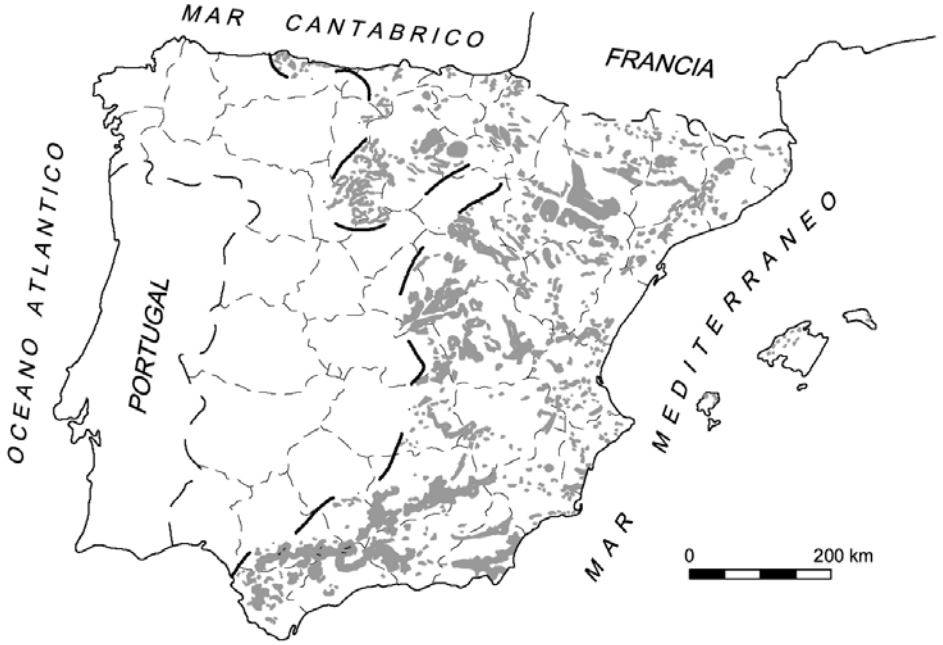

Figure 2.7. Schematic distribution of gypsiferous outcrops in Spain, including materials from the Triassic to the Neogene (Riba & Macau, 1962)

Calcium sulphate formations in the Iberian Peninsula were originated basically during two geological periods clearly differentiated: the Triassic and the Tertiary. In both cases calcium sulphate appears in two different lithologies: (i) evaporitic, or (ii) veins in claystones, mudstones, marls or micro-carbonates. Specifically, calcium sulphate is present under two different minerals: anhydrite ($CaSO_4$) -at certain depth-, and gypsum ($CaSO_4 \cdot 2H_2O$) -usually in outcrops-.

Several theories explain the dehydration-hydration cycle of gypsum-anhydrite during diagenesis and exhumation of sediments. According to Murray (1964) the gypsum-anhydrite division commonly occurs at depths of 400-450 m in the diagenesis phase of the cycle, and at depths of 150-100 m in the exhumation phase. Exhumation of anhydrite formations is often related with erosion or tectonic processes. During these events anhydrite is transformed into

gypsum (secondary gypsum), under isovolumetric conditions (Ortí, 1977; Ortí et al., 1989). According to this author, most of gypsum outcrops in Spain prior to the Pliocene are secondary gypsum.

Gypsum in both Triassic and Tertiary formations is found in certain representative lithofacies: (i) nodular, (ii) massive, (iii) laminated (mm) or banded (cm) and (iv) fibrous veins. There are also processes that produce neoformed gypsiferous precipitations from calcium sulphate rich waters stored in perched water tables and aquifers. These are fibrous gypsum units and often fill rock discontinuities. Images illustrating these lithofacies are presented in Figure 2.8 to Figure 2.9.

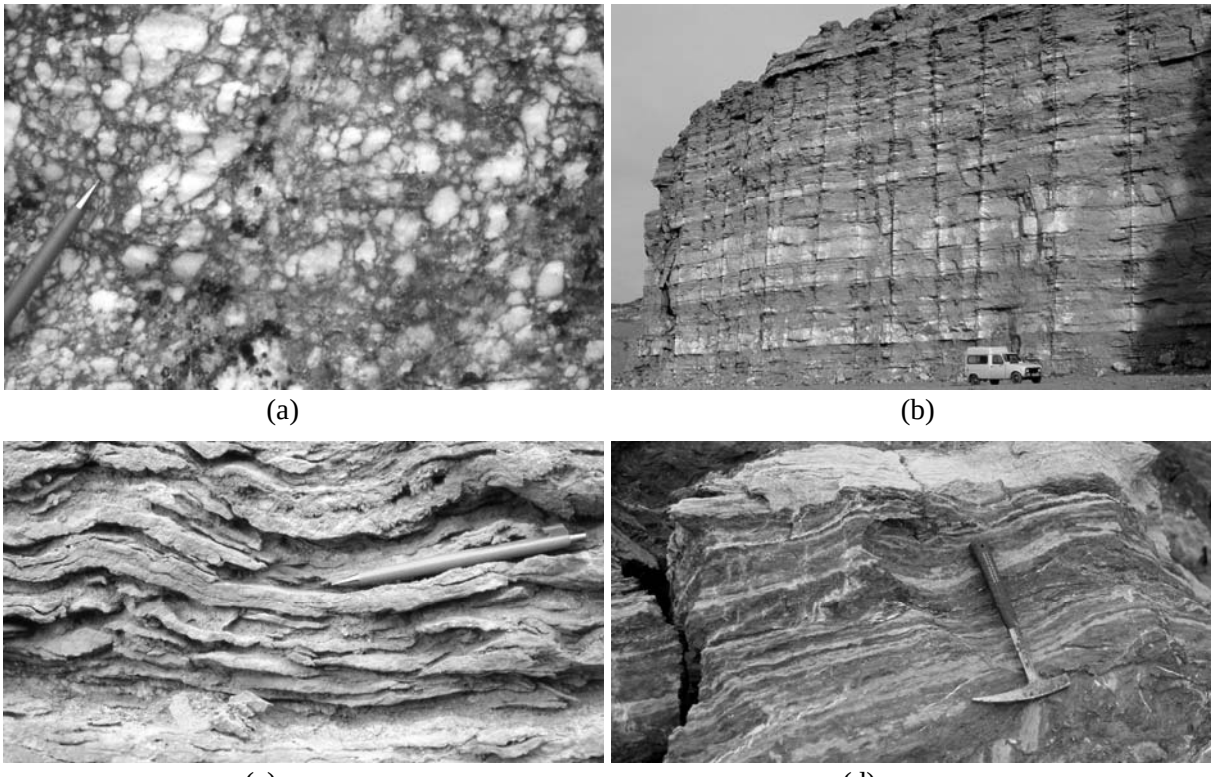

(a) (b)

(c) (d)

Figure 2.8. Lithofacies of gypsum found in sedimentary rocks:(a) Oligocene micronodular gypsum from Sorlada (Navarra, Spain) (Salvany, 1989); (b) Miocene massive gypsum from Villalómez (Burgos, Spain); (c) Miocene laminated gypsum from Los Arcos (Navarra, Spain); (d) Triassic (Keuper) gypsum in bands from the Spanish Pyrenees ((b),(c),(d): J. M. Salvany, personal communication)

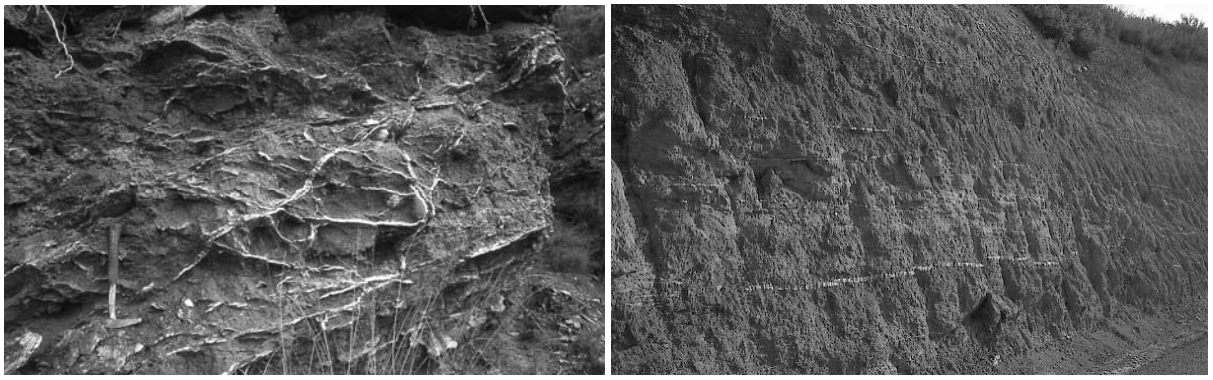

(a) (b)

Figure 2.9. Neoformed fibrous gypsum veins filling discontinuities: (a) Triassic (Keuper) fibrous gypsum veins from the Spanish Pyrenees (Salvany, 1989); (b) Oligocene interbedded fibrous gypsum veins from Ascó (Catalunya, Spain) (O. García, personal communication)

2.3.1 Triassic sulphate-bearing rocks

Figure 2.10 illustrates the distribution of main Triassic sulphate outcrops in the Iberian Peninsula and Balearic Islands in which nine lithostratigraphic units have been defined (IGME (Spanish National Geologic Institute), 1981).

Ibérico, Cantábrico and Pirenaico Triassic outcrops present similar litotypes with only one carbonate layer associated with Muschelkalk facies. The Hespérico Triassic outcrop is formed by a continental facies (red beds) and Mediterranean Triassic outcrops (Catalanides and Valenciano) include Buntsandstein, Muschelkalk and Keuper facies. Finally, the Bético Triassic outcrops (Germanic facies and Alpine facies) has more Triassic types than the rest of outcrops (Pérez, 1991).

Triassic gypsiferous outcrops are usually found in Keuper formations. The reason is that Keuper deposits in Spain often act as “sliding surfaces” in large scale tectonic motions. Consequently, outcrops of Triassic sulphate formations are usually associated with tectonized zones in which water may find easier percolation paths in fractured materials. However, sometimes gypsum, often tectonized, occurs in Bundsandstein (Röt) and Muschelkalk (M-2) formations, as well as in Liassic formations (Early Jurassic).

The preceding observations refer to outcrops of Triassic sulphate rocks that are often represented as thin bands of irregular shape in the map of Figure 2.10. However, the buried formations occupy extensive areas. This is the case of the Keuper unit and one example is

given in Figure 2.11. It shows the contours of equal thickness of the "Levante" Keuper, which does not outcrop in the zone. This material occupies most of the territory of several provinces in Eastern Spain. Similar examples are found in other regions of the Iberian Peninsula, including the Pyrenees.

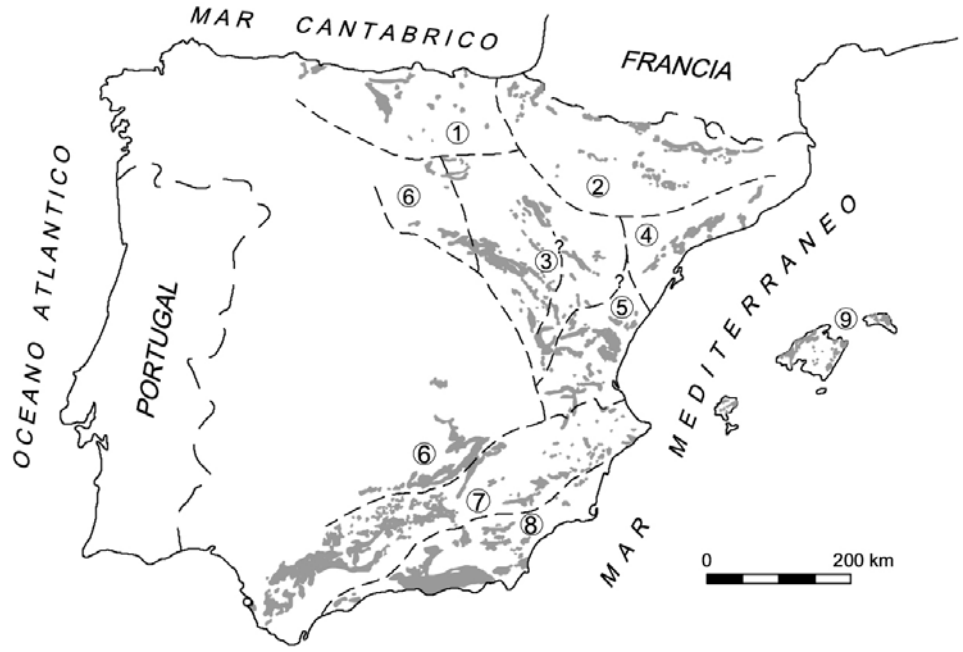

Figure 2.10. Distribution of Triassic outcrops in Spain according to a map published by the IGME (1981). (1) Cantábrico; (2) Pirenaico; (3) Ibérico; Mediterráneo: (4) Catalanides and (5) Valenciano; (6) Hespérico; Bético: (7) Germanic facies and (8) Alpine Facies; and (9) Balear Islands Triassic

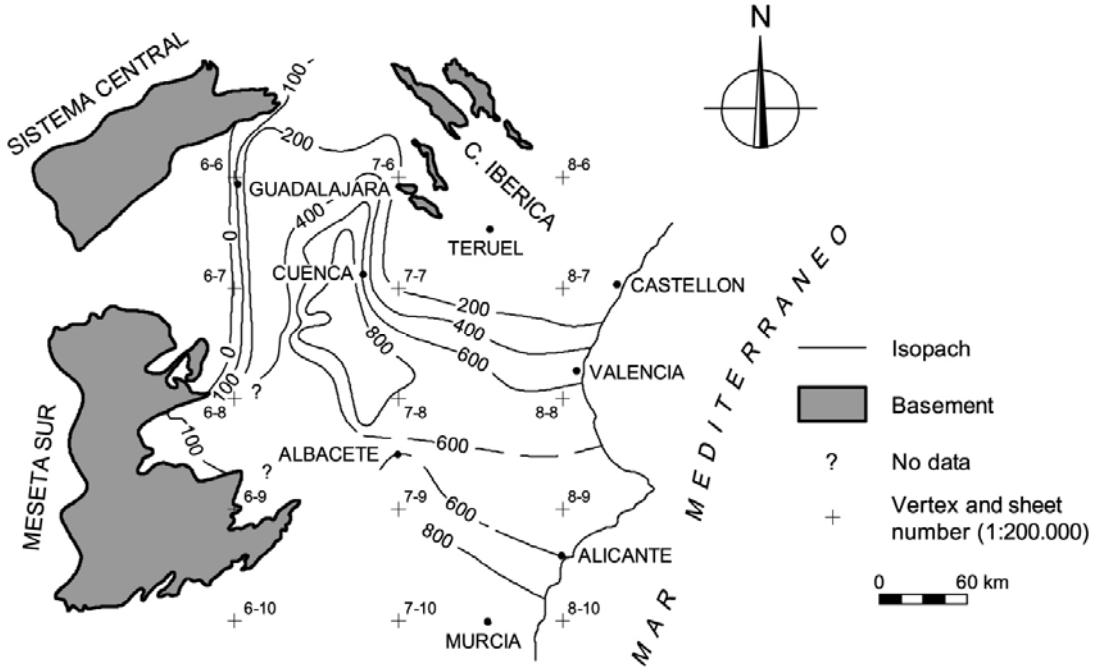

Figure 2.11. Isopachs of the "Levante" Keuper (from de Torres & Sánchez, 1990)

2.3.2 Tertiary sulphate-bearing rocks

Tertiary rocks are mainly found into four basins, which are drained by the four main rivers of the Iberian Peninsula: Duero, Tajo, Guadalquivir and Ebro (Figure 2.12). In Guadalquivir Basin no evaporitic formations are found. Often, these Tertiary basins cover Triassic rocks and were filled with sediments developed during the Alpine orogeny.

The sedimentary formations, from the Eocene to the Miocene, exhibit often outcrops of sulphated rocks. In the Duero Basin, thick layers of Miocene sandstones, marls and mudstones were later covered by gypsum and gypsiferous marls, and finally capped by calcareous levels. Gypsum is frequent found in the Tajo Basin in which Eocene and Miocene deposits are often interbedded with marls frequently tectonized. In particular, Miocene gypsums cover the South-East of Madrid.

The largest evaporite basin is, however, the Ebro Basin. It is bounded by three mountain ranges: Pyrenees, Iberian and Catalanides. Sediments, mainly clayey materials, reach in some locations depths in excess of 4000 m. Figure 2.13 shows a map with the main gypsiferous formations of the Ebro Basin. Two structural aspects explain the distribution of evaporite formations in this basin (Anadón et al., 1985):

- The Pyrenean uplift caused a progressive displacement of the basin axis towards the south. As a result, the youngest Tertiary materials are located to the East of the basin.
- The basement elevation at the Pyrenees tilted the basin and induced a lateral displacement of its lower point.

Two broad classes of Tertiary materials may be distinguished: marine and continental (lacustrine) evaporites (Ortí et al., 2007). This origin is related to the salt content of the parent water, the local climatic conditions and the texture of rocks.

Clays are often mixed with sulphate minerals in most of the above mentioned Triassic and Tertiary basins. They can have two origins. They are either deposited concurrently during the sedimentation process (this is the case of illite and chlorite), or they are neoformed clayey minerals (montmorillonite, paligorskite).

Smectitic clays are found in young Tertiary sediments (they are found in the South of Madrid), but they are seldom present in older Triassic sediments, because smectitic minerals are sensitive to diagenetic modifications (Ayala et al., 1986).

Figure 2.12. Main Tertiary basins in the Iberian Peninsula (modified after Salvany, 1989)

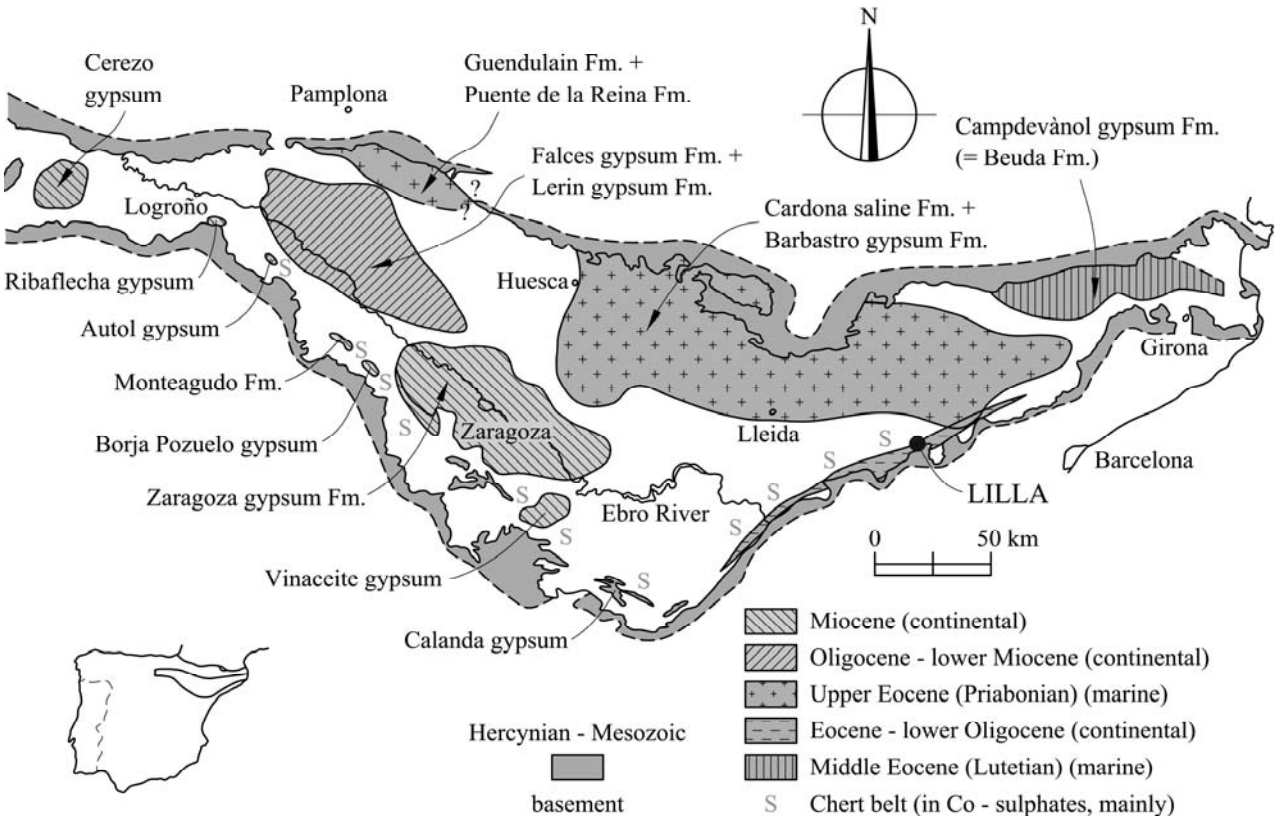

Figure 2.13. Distribution of evaporite formations in the Tertiary Ebro Basin (Ortí et al., 1989), and location of Lilla tunnel

2.3.3 Sulphate-rich waters

The groundwater in both Triassic and Tertiary formations in Spain is highly mineralized. Some cases from the Ebro and the Tajo basins in which deep excavations have been executed

or tunnels are planed were analysed in terms of saturation index for gypsum, SI, using data from different sources (Table 2.3). A water analysis reported by Esteban (1990) was assumed representative of conditions in Ascó II Nuclear Power Station (Lower Ebro Basin). In the case of Tunnel A two water analyses are available, and in the case of Tunnel B a data-base including 23 water analyses is available.

Table 2.3. Chemical composition and properties of groundwater in two Tertiary evaporite deposits from Spain (Berdugo, 2007)

Location	Ebro Basin	Tajo Basin	
	Ascó (1)	Tunnel A (2)	Tunnel B (3)
Constituent	**Concentration (mg/l)**		
Sulphates	2800	3400	43017
Bicarbonates	215	641	256
Carbonates	40	< 0.5	-
Chlorides	25700	6160	88827
Calcium	202	535	1067
Magnesium	568	185	3230
Sodium	13486	3920	69720
Potassium	-	11.5	757
Other properties			
pH	9.27	7.5	7.67
E.C at 20ºC (µS/cm)	59170	16640	-

(1) Esteban (1990), (2) Iberinsa (2006), (3) Sener (2006)

Saturation index for gypsum was calculated at 25ºC (Ascó and Tunnel A), and at temperatures obtained during sampling in the case of Tunnel B. The results of these analyses are presented in Figure 2.14. SI = 0 indicates equilibrium conditions, SI < 0 reflect subsaturation and SI > 0 reflect supersaturation. When equilibrium is not found SI indicates in which direction the process may go: for subsaturation dissolution is expected, and supersaturation suggests precipitation.

Precipitation of calcium sulphate, particularly of gypsum, due to supersaturation of natural sulphate-rich waters is possible as a result of either a fall in temperature, which causes a decrease in gypsum solubility, or the exposition to a ventilated dry environment, which causes water evaporation and, therefore, an increase in calcium sulphate concentration.

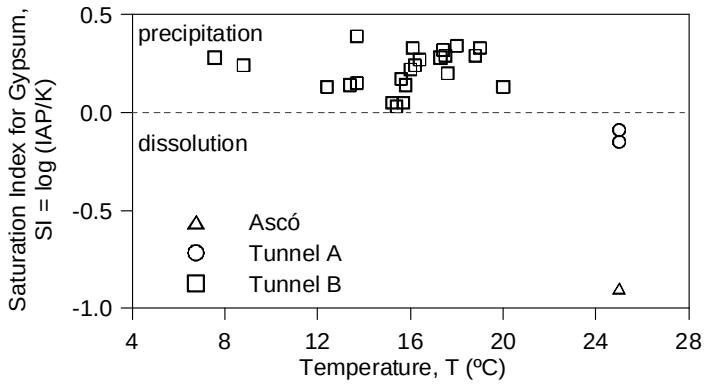

Figure 2.14. Saturation index for gypsum in natural waters from some Spanish evaporite deposits as a function of the temperature (Berdugo, 2007)

2.4 Current alternatives to design tunnel lining

A common characteristic of tunnels affected by swelling problems in sulphate expansive rocks is that heave displacements and damage of structural elements occur at tunnel floor level, and no substantial damage is detected at abutments or crown in the cases reported. Amstad & Kovári (2001) described typical scenarios (summarized in Figure 2.15) that can be originated, alone or in combination, in tunnels affected by either swelling pressures or vertical displacements depending on the geometry of the excavation, the rigidity of the lining, the intensity of the expansion and the overburden stiffness.

There is certain evidence that the swelling displacements and pressures present a heterogeneous distribution along the tunnel length and also across the excavated sections. This seems to be a result of the heterogeneity in the distribution of fractures and in the mineralogical composition in the sulphated claystones. This results in a difficulty to design the cross-section shape and lining in a tunnel having a potential risk of being affected by swelling problems, and also to design repairing works in a tunnel already showing swelling behaviour. Because of this uncertainty there is a risk of overdesigning the lining. The case of Lilla tunnel, described in Chapter 3 illustrates this comment. In some cases the tunnel lining

structure needs to include longitudinal reinforcement, a situation seldom found in conventional practice.

(a) Flexible flat-slab heave

(b) Rigid invert-arch heave and failure

(c) Rigid circular section heave and displacement as rigid body

Figure 2.15. Typical scenarios associated with swelling in tunnels according to Amstad & Kovári, 2001

Several authors have analysed the damage and failure due to swelling phenomena in tunnels crossing Triassic sulphated hard rocks from Medium Keuper (Gipskeuper) and from Muschelkalk (Anhydritgruppe) in Baden-Württemberg (Germany) and Jura Mountains (Switzerland). The works of Kovári & Descoeudres (2001), Amstad & Kovári (2001), Wittke (1990, 2000, 2006), Anagnostou (1993, 2007, 2011), Wittke-Gattermann & Wittke (2004), Anagnostou et al. (2010), Sahores (1962), Grob (1972, 1976), Henke (1976), Kaiser (1976), Krause (1976), Einstein (1979), Wichter (1985, 1991), Nagel (1986), Fecker (1992), Steiner (1993), Paul & Wichter (1996), Madsen et al. (1995), Kovári et al. (1988) and others have provided value information on the expected swelling in anhydritic and gypsiferous hard claystones.

Two alternative strategies to design or repair tunnels exposed to sulphate-related heave have been adopted (Kovári et al., 1988): either the expected pressure against the tunnel lining is resisted; or else some amount of deformation of the ground is allowed, with the purpose of reducing the heaving pressure, at least for a given period of time. These strategies are possible because of the specific nature of the tunnel structure. In fact, once it is properly designed, a closed circular-like structure is able to resist very high swelling-induced pressures.

Tunnels excavated in expansive rocks and soils are often designed following the resisting support principle, which consists in design the lining to resist with a low deformation, the swelling pressures. According to Wittke and his co-workers (1979, 1990, 1998, 2000, 2004, 2005, 2006), the advantage of the design of the resisting lining for tunnels in sulphated rocks is the self-sealing induced by swelling itself around the lining of the tunnel.

The self-sealing is a mechanism linked, among other causes, to crystal growth in porous media, which in the case of sulphated rocks consists in the precipitation of gypsum in relict or induced discontinuities. Wittke-Gattermann & Wittke (2004) and Wittke (2006) suggested that a limit value can be defined for swelling pressure due to self-sealing and, as a consequence, the thickness and the reinforcement of the lining are considerably reduced.

The permanent damage and failure of inverts and tunnel lining designed according to the principle of resisting support, the prevision that a stiff tunnel lining would be unable to resist the expected swelling pressures, and the necessity of achieving close to zero displacements due to tunnel operational requirements in some tunnels (railway tunnels), motivated other design alternatives (Kovári et al. 1988). These alternatives include mainly the use of anchored plates and flexible support systems (Figure 2.16). The design criterion in flexible support system consists in matching the best possible equilibrium between swelling deformations and pressures, in order to limit both the deformation of the structure and the swelling pressure exerted by the rock against the lining. Two alternatives for the flexible support systems have been proposed to reduce the radial pressures due to swelling: the use of a yielding layer of deformable foam in the contact lining-rock and the opening of longitudinal slots in the lining to facilitate convergence.

Three testing sections designed each one following the principle of resisting support, yielding support materialized by a set of springs, or by a thick layer of foam where built in Lilla tunnel. The sections were instrumented with sliding micrometers and pressure cells. The performance of the testing sections is analysed later in Chapter 3.

The classical design of flexible support system is the installation of a deformable zone (usually by means of a foam of plastic material), below the invert of the tunnel (Figure 2.16(c)). A drainage is also included in the design of the yielding zone to avoid the groundwater reaching the rock above the tunnel vault and thus to prevent its swelling (Wittke-Gattermann & Wittke, 2004). In general, the presence of the deformable (yielding) zone compensates the effect of swelling in the rock, leads to a reduction of the swelling pressure developed and, therefore, leads theoretically to a significant reduction of the thickness and reinforcement of the lining of the tunnel compared with the resisting support.

The principle of yielding support was used for the first time in the middle 70's in Buechberg highway tunnel in Eastern Switzerland, and afterwards in the tunnel for the Super Proton

Synchroton at C.E.R.N. in Geneve, (Lombardi, 1979) and Tunnel T8 Biel-Sonceboz in Switzerland, (Kovári et al 1988). In spite of the noticeable benefits related to the use of this system in clayey swelling rocks, experiences in tunnels through sulphate bearing rocks are limited mainly to the cases of Gasstollen Cogefar in Italy, (Amstad & Kovári, 2001), Freudenstein test gallery in Germany, (Kirschke, 1987; Prommesberger & Kuhnhenn, 1989, Fecker, 1992), Freudenstein tunnel (Kovári & Amstad, 1993; Amstad & Kovári, 2001) and Engelberg Base tunnel (Amstad & Kovári, 2001). Testing sections designed according to yielding support made of a 40 cm thick foam layer were built in Lilla tunnel and are analysed later in Chapter 3.

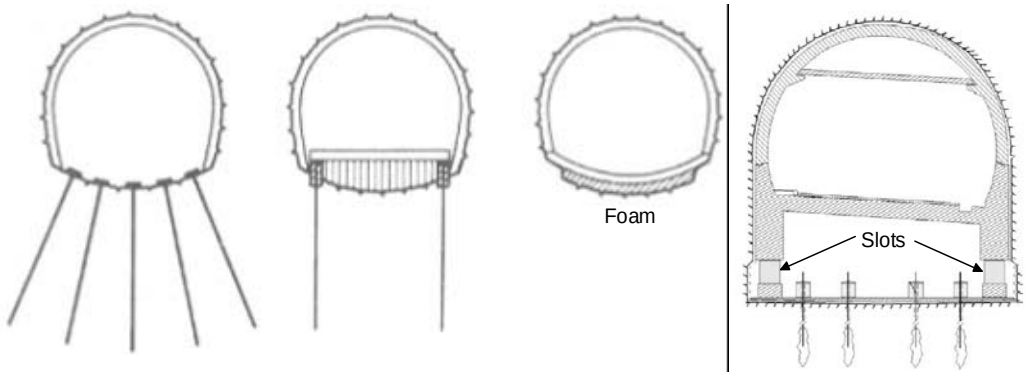

Figure 2.16. Designs of lining in tunnels in rocks (a), (b) and (c): Kovári et al., 1988; (d): Solexperts

Wittke & Wittke (2005) and Wittke (2006) published exhaustive studies (including numerical modelling) on the applicability of both resisting and yielding support systems for tunnel excavation in the Stuttgart 21 project. According to these authors, the fundamental factors that allow selecting the type of support when tunnelling in sulphated rocks are the amount of weathering of the rock of the overburden and the position of the phreatic level. Following these criteria, it is convenient to use resisting support when sound rock exists above tunnel vault; in the opposite cases yielding foam should be used in their opinion.

The second alternative for flexible support consists in the construction of slots and springs at the vault-invert interphase, as shown in Figure 2.16 and Figure 2.17. Information on the performance of slots and springs in tunnels is limited. The documented experiences are limited to Chienberg tunnel in 2006 in Jura Mountains (Thut et al., 2007), which was reinforced by means of highly deformable concrete modules (Solexperts HDC ®), and Lilla

tunnel in the Ebro river basin in Spain, which was reinforced by means of steel springs at one testing section, as described in Chapter 3 .

(a) (b)

Figure 2.17. Example of modular yielding supports (slots and springs) installed in the interface vault-invert of tunnels excavated through swelling rocks: (a) highly deformable concrete springs (Solexperts HDC®) in Chienberg tunnel (Jura Mountains); (b) metallic springs in a circular test section of Lilla tunnel (Lower Ebro Basin) (after Berdugo, 2007)

2.5 Summary

Cases of swelling in tunnels in both hard and soft anhydritic-gypsiferous clayey rocks from Switzerland and Germany have been presented and discussed in order to gain a better understanding of these phenomena and to isolate the most relevant ones. It has been shown that the intensity of the expansive phenomena in sulphated rocks exceeds the swelling phenomena observed in most hard rocks and soils, known for their high expansive potential (i. e. Molasse marls, Opalinus Clay, Tabuk clay, Al-Qatif clay and similar ones). The main phenomenological features of the observed swelling have been summarized, and also a description of the characteristics of the rock mass and groundwater that may have an important role on the expansive response have been highlighted.

Calcium sulphated formations present in Spain have been reviewed and it has been shown that sulphated formations are abundant and therefore these formations may be involved in several infrastructures. Sulphates are common in some geological levels such as Triassic and Mesozoic fine sediments in evaporative environments.

The experience on the design of tunnel lining in tunnels affected by expansions has been summarized. Different alternatives consisting in rigid or flexible support have been presented and the expected behaviour has been analysed.

CHAPTER 3

Extreme expansive phenomena in Lilla tunnel

The study of the expansive phenomena in sulphated claystones is done, in part, through the analysis of the extreme swelling behaviour observed in Lilla tunnel in Spain. The Chapter describes the swelling phenomena affecting the tunnel during construction and subsequent operation. The geology of the site and the performance of alternative support designs are described. Field observations are analysed to identify the causes of the observed swelling. The original horseshoe cross-section was transformed into a circular one and a reinforced concrete lining was built to resist swelling pressures. Long term monitoring of the reinforced tunnel provided valuable data on the evolution of swelling pressures against the lining and on the stresses developed in the resisting structure. The highly heterogeneous distribution of swelling pressures against the lining explains the low strains measured in reinforcement bars despite the very high maximum swelling pressures recorded.

3.1 Introduction

Three tunnels on the high-speed railway from Madrid to Barcelona, excavated in anhydritic-gypsiferous claystone, were affected by extreme expansive phenomena during construction. These tunnels are located in the route of the railway through the Lower Ebro basin, the largest

evaporite deposit in Spain. Table 3.1 provides the main characteristics of the three tunnels (Camp Magré, Lilla and Puig Cabrer), which were located in the vicinity of Montblanc city, province of Tarragona. Camp Magré had a moderate maximum cover -52 m- and was excavated in the upper levels of Eocene claystone, in contact with overlying limestone. It experienced moderate to severe expansions in a short length (200m). The Puig Cabrer tunnel was excavated under higher cover in much older materials (Triassic rocks). It crossed a short stretch of sulphated claystone and also experienced moderate swelling. The strongest and most damaging heave was recorded in the Lilla tunnel, entirely excavated in Eocene sulphated formations under an intermediate cover (90-110 m on average). First expansions were detected in the tunnel floor flat-slabs immediately after building. These expansions were quickly followed by generalised distortions in longitudinal drainage systems and, finally, by local failures of flat-slabs. The Lilla tunnel was selected to carry out a full-scale swelling study. Laboratory tests and in situ measurements were undertaken to gain knowledge on the swelling mechanisms and to evaluate the efficiency of alternative support designs. The performance of instrumented test sections built with resisting or yielding supports was monitored.

Table 3.1. Data on the three tunnels experiencing swelling phenomena

Tunnel	**Length (m)**	**Maximum cover (m)**	**Excavated cross-section (m^2)**	**Observations**
Camp Magré	954	52	140	Excavated in upper levels of Eocene anhydritic claystone
Lilla	2034	110	117	Cover in Eocene anhydritic claystone: 10-70 m
Puig Cabrer	607	191	137	Excavated in Triassic rocks (limestone, marls and sulphated claystone)

Expansions in Lilla tunnel occurred at floor level without observable swelling signs in the abutments and crown. Heave evolved at high rates and, often, a limiting value for either floor heave or pressures could not be clearly defined. This phenomenology is well documented in the literature, particularly in tunnels excavated through the Gipskeuper in Baden-Württemberg (Germany) and the Jura Mountains (Switzerland). Contributions by Steiner (1993), Amstad &

Kovári (2001), Kovári & Descoeudres (2001), Wittke (2006), Anagnostou (2007) and Anagnostou et al. (2010) summarise these cases and suggest procedures for the analysis and design of tunnels in sulphate-bearing rocks.

Differences in composition between anhydritic-gypsiferous claystone from the Gipskeuper and the Lower Ebro Basin are notorious and significant. The former are hard Triassic materials containing anhydrite and expansive clay minerals, specifically corrensite (Schlenker, 1971; Götz, 1972; Henke, 1976; Lippmann, 1976; Jordan & Nüesch, 1989). The latter, on the contrary, are soft rocks from the Tertiary age in which anhydrite occurs only in nodular lithofacies and the clayey matrix is composed by non-expansive clays, mainly illite and paligorskite (Salvany, 1989; Salvany, personal communication, 2007; Esteban, 1990). In both environments the groundwater is highly mineralised, with calcium (Ca^{2+}) and sulphate ($SO4^{2-}$) as the main dissolved ions (Grob, 1972; Werder, 1989; Esteban, 1990; Amstad & Kovári, 2001; Alonso & Berdugo, 2005).

This Chapter concentrates on Lilla tunnel and describes one of the most extreme cases of heave and swelling pressures developed in connection with tunnel construction. Besides the data provided by geotechnical investigations and monitoring of the tunnel initially excavated, the results of large scale wetting tests performed in three enlarged circular test sections built inside the original tunnel will be reported. In addition, once the entire tunnel was converted into a cylindrical heavily reinforced structure, measurements of swelling pressures against the lining as well as strains (and stresses) measured in steel reinforcing bars make it possible to evaluate the response of the lining during the first 8 years of operation of the railway line.

3.2 Geology

Lilla tunnel, running in a North-South direction, is located on the eastern side of the Tertiary Lower Ebro Basin (Figure 2.12 and Figure 2.13) in Catalunya, very close to the limit imposed to the basin by the Hercinian-Mesozoic basement. The proximity of the basin limit and an illustration of the local tectonism are given in Figure 3.1. The Eocene claystone formation is folded and compressed by the thrust exerted by Triassic and Palaeozoic rocks.

The longitudinal geological section of Lilla tunnel is given in Figure 3.2(a). Figure 3.2 integrates additional information which will be described later. Tunnelling involved mainly anhydritic-gypsiferous early Eocene claystone. This material occurs as a horizontally-oriented

monotonic series of brown claystone with nodular anhydrite and an intricate system of cross-shaped moderately dipping fibrous gypsum veins (Figure 3.3(a)). Locally, grey alabastrine gypsum occurs in subhorizontal strips within the host clayey matrix. A singular aspect is the existence of a persistent system of low-angle slickensided surfaces (Figure 3.3(b)). They are explained by tectonic events that affected the rock formation during the Bartonian uplift.

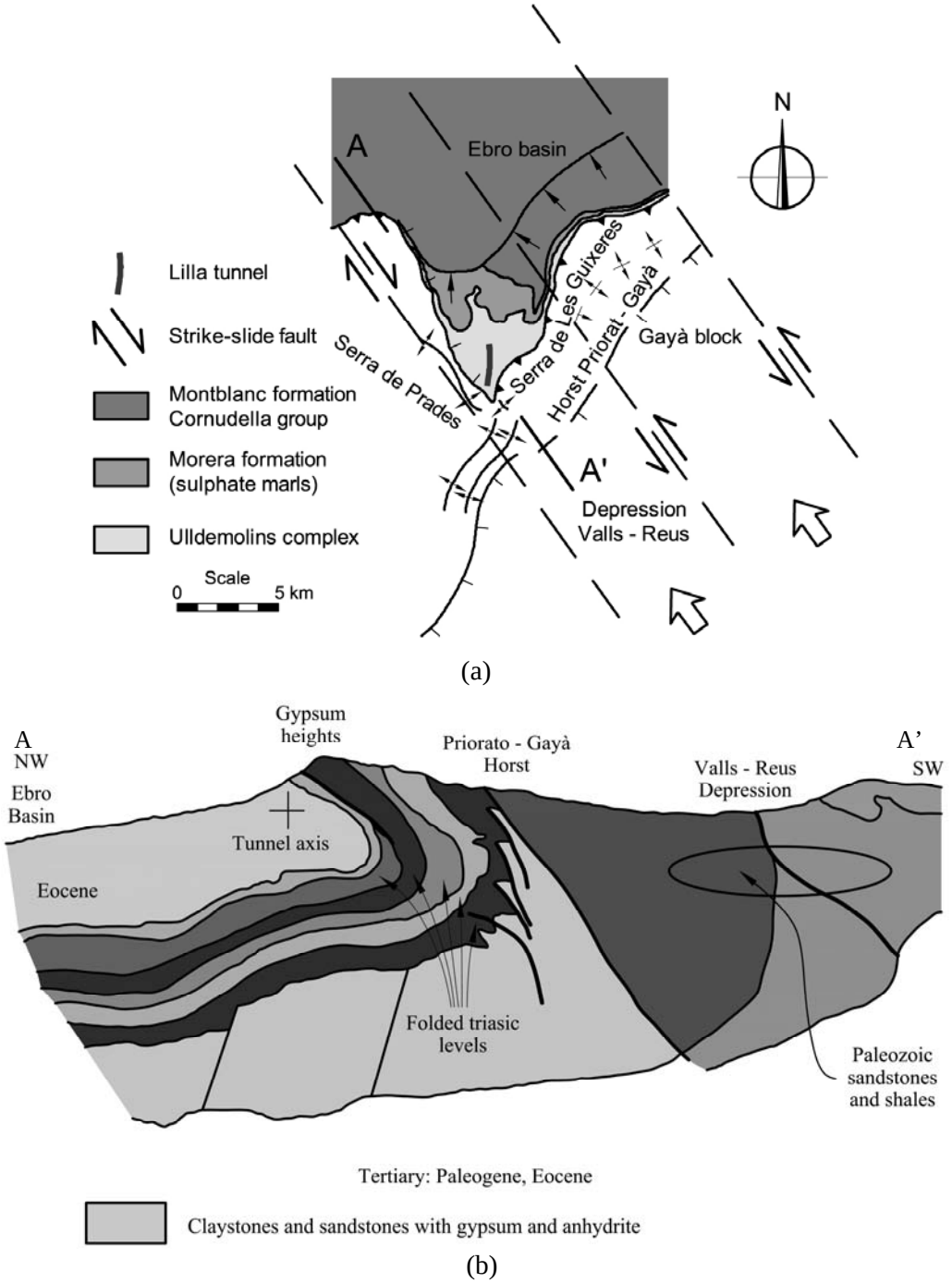

Figure 3.1. Simplified model of regional tectonics and representative cross-section at the site of Lilla and Camp Magré tunnels (based on Julivert, 1954): (a) plan view; (b) representative cross-section

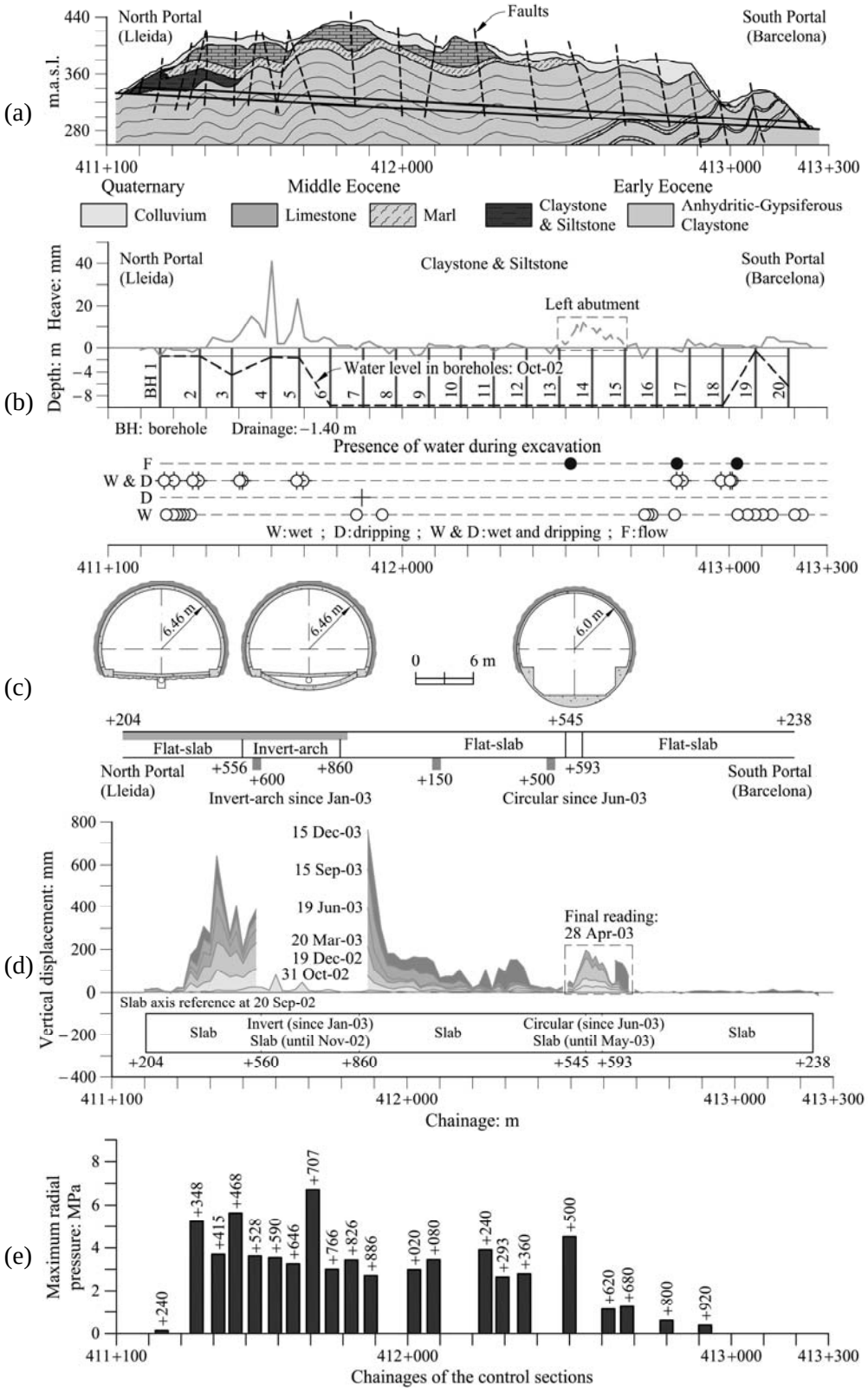

Figure 3.2. Longitudinal section of Lilla tunnel: (a) geology; (b) profile of floor heave in October 2002 and water conditions detected during tunnel excavation; (c) initial cross-section (horseshoe shape) and testing sections; (d) evolution of heave displacements of the flat-slab between October 2002 and December 2003; (e) maximum radial pressures recorded in the period from January 2005 to Dec. 2011

The slickensided surfaces are believed to have played a decisive role in triggering the expansive phenomena which damaged the tunnel. The reason is that the stress change associated with tunnel excavation is then capable of opening the discontinuities allowing the flow of water and the precipitation of gypsum crystals in a mechanism discussed later in more detail in Chapter 5. Figure 3.2(a) also shows the position of faults identified during head excavation.

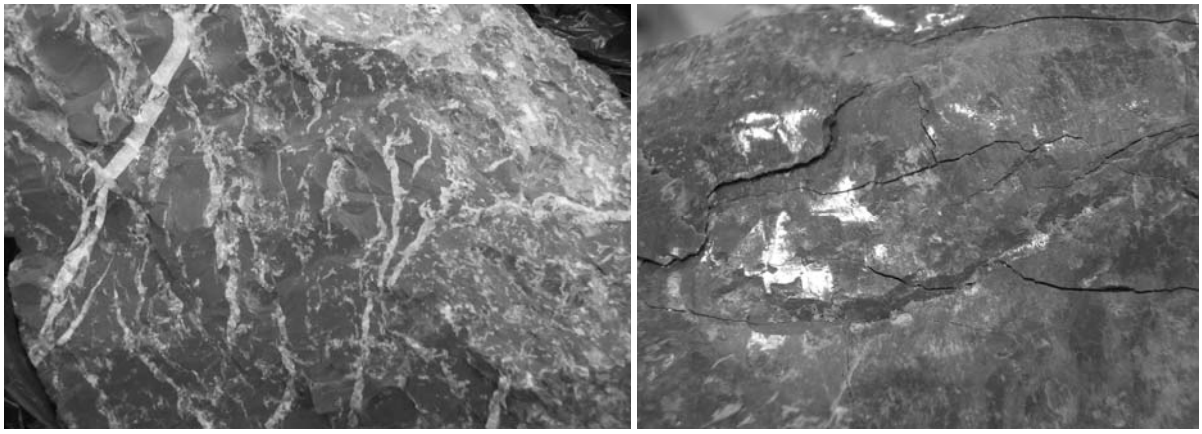

(a) (b)

Figure 3.3. Details of the claystone formation: (a) gypsum veins in the clay matrix; (b) slickenside

3.3 Design and construction

Lilla tunnel has a length of 2034 m and the overburden varies between 32 m and 110 m. It originally had a conventional horseshoe cross-section (117.3 m^2) (Figure 3.4). The primary support elements were designed by means of a Convergence-Confinement method (Panet, 1995). Construction followed the methodology of the new Austrian tunnelling method (NATM). A light immediate support (sprayed concrete) was systematically applied. Sprayed concrete, rock bolts and steel arch ribs (HEB 160) in zones of low rock quality, were used for support. The final lining consisted of 300 mm thick cast in place unreinforced concrete (characteristic unconfined strength: f_{ck} = 25 MPa). A 300 mm thick flat-slab of unreinforced concrete (f_{ck} = 20 MPa) provided some bracing to tunnel abutments at floor level of the initial horseshoe cross-sectional shape of the tunnel. No specific precautions were taken regarding swelling phenomena.

Excavation was carried out mainly by drill and blast from both portals, dividing the section into top heading excavation and subsequent benching. However, mechanised excavation and

mixed systems (roadheaders and hammers) were also used. Heterogeneous rock strength in the excavation face was frequent, sometimes exhibiting a competent lower part of the head and an upper part partially weathered that prevented the systematic use of blast. In some weak zones percussion of hammers was not necessary and a simple hammer dragging was sufficient to excavate the face.

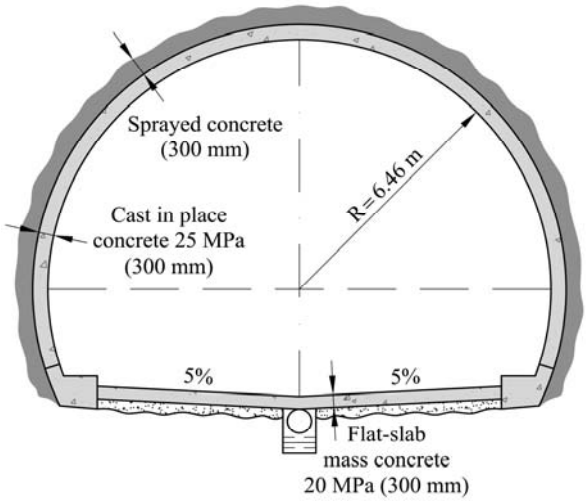

Figure 3.4. Initial representative cross-section of Lilla tunnel

Claystone strength was reported to be heterogeneous along the excavation, from relatively weak stretches, excavated mechanically, to hard formations requiring drill and blast excavation. Unconfined compression strength was determined in cores recovered in boreholes performed from the tunnel floor at different locations. Continuous extensometers and piezometers were installed in these boreholes. Strength is represented in Figure 3.5 in terms of water content. Low water content values (w = 1-2%) correspond to void ratios in the range e = 0.027-0.054. Higher w values (4-5%) are found in samples having e = 0.11- 0.135. The strength drops fast with increasing water content. These results provide an indication of the weathering susceptibility of Lilla claystone. Moderately or non-cemented claystone is frequently reported to exhibit a similar sensitivity to water content changes. The shotcrete layer applied immediately after excavation was aimed at maintaining the original water content of the claystone.

In addition, swelling pressure tests were performed in oedometer cells in recovered cores. Tests were performed following a protocol described in ASTM D3877/80 (ASTM, 2008). Recorded swelling pressures for undisturbed and remoulded samples are plotted in Figure 3.6 in terms of water content. No definite correlation with initial water content was found.

Swelling pressures are small if compared with recorded field pressures. Doubts on the initial conditions of the tested cores exist. An unexpected drying of cores before testing may explain the recorded swelling pressures as a result of clay hydration. However, being the first available information on swelling pressures, they provided a criterion to design the instrumented temporary curved invert described in the next section.

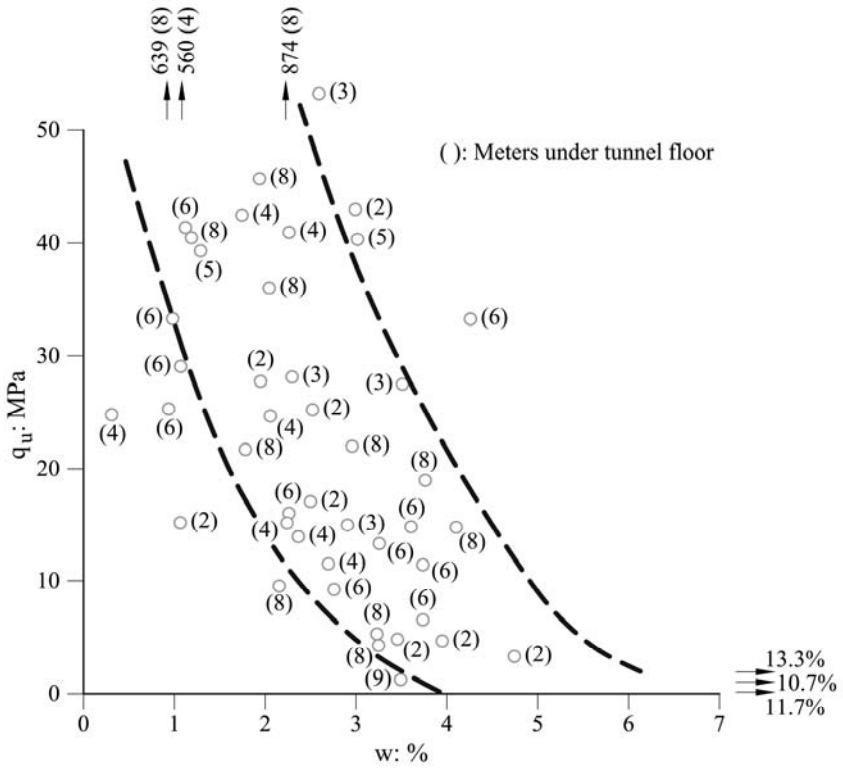

Figure 3.5. Unconfined compressive strength measured in cores recovered in boreholes drilled from the tunnel floor

No face stability incidents were reported. A central drainage was installed at the time of concreting the floor slab. In general, the excavation was carried out under dry conditions. Water leakage into the tunnel was detected in some locations (Figure 3.2(b)). Significant water flow was reported only in the vicinity of the south portal. The inflow was linked to isolated failures connecting colluviums with the excavation as well as with a change in stratification. Waterproofing of the excavated section was limited to portals. A geotextile of 500 g/m2 was placed over a 1.5 mm thick polyvinyl chloride (PVC) sheet located between the support and the lining. The longitudinal drainage system was made of a PVC collector (diameter = 500 mm) located 1.4 m below the floor. Underneath, a 200 mm gravel filter layer was extended. Water coming from the vault was collected in box-type manifolds uniformly distributed along the tunnel floor.

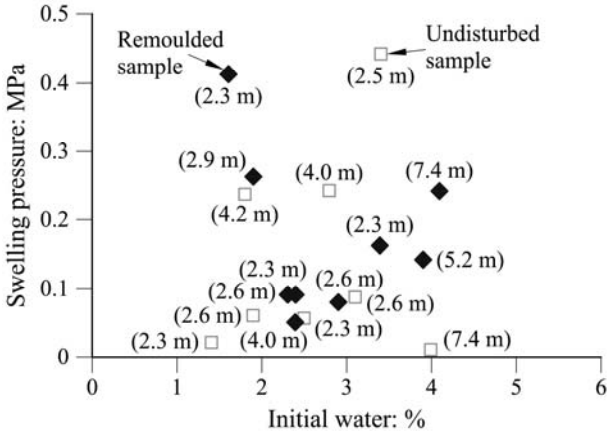

Figure 3.6. Swelling pressure measured in samples recovered in borings drilled from tunnel floor in October 2002. The chemical composition of water used during the tests is unknown. Test protocol: UNE 103 602:1996. Depth of sampling below the flat-slab is indicated between parenthesis

Convergence displacements measured during the heading stage were in general very low and only sections close to the north portal (chainage 411 + 217 to 411 + 258) exhibited small movements in vertical and horizontal directions, in the range from 20 to 30 mm, with a clear tendency towards stabilisation after 30 days. On the basis of visual observations expansive phenomena and, in particular; floor heave, were not observed during construction.

3.4 Expansive phenomena and ground properties

The bench was excavated only after the head construction was completed in February 2002. Afterward, the initial flat-slab was constructed only in a short stretch of 158.8 m between stations 411+203.5 and 411+362.3. Therefore the unprotected (unlined) floor was exposed to tunnel environmental conditions (e.g. wetting and drying cycles imposed by both the construction works and the natural ventilation) for a few months. Floor heave was first detected in September 2002 at chainages 411+598, 411+685 and 412+540, just after the flat-slab was completed and during construction of the lining. The low values of horizontal relative displacements and the absence of fissures in the shotcrete and the lining indicated that the abutments and the crown were not affected by ground expansion.

Figure 3.2(b) summarises the conditions in the tunnel one month after floor heave was detected for the first time. When floor heave started the longitudinal drainage was already completed. At that time the longitudinal drainage tube was already finished. A partial drainage of the foundation material can be expected. However some isolated strong floor

heave was probably capable of damaging the drainage tube which could lead to local water accumulation.

Heave reached maximum values within the first kilometre of the northern side of the tunnel. Figure 3.2(b) also provides an indication of the water conditions met during excavation. The southern part of the tunnel, where some water flow into the tunnel was recorded, was not affected by floor heave. Later, when boreholes were drilled from the floor, without the addition of any water, in order to investigate the swelling phenomena, the water level in the borings before the installation of instrumentation, was recorded. In the cases where the borings remained dry, the depth of water in Figure 3.2(b) is marked at -10 m. Shallow water levels (with respect to the tunnel floor) were recorded in a 600 m long stretch of tunnel, immediate to the North portal. In this part of the tunnel heave was developing at the fastest rate. A shallow water level was also measured in the vicinity of the south portal in a part of the tunnel which did not experience any measurable floor heave.

Heave of the floor slab evolved rapidly and it soon became clear that the adopted resisting cross-section was unable to cope with the observed swelling phenomena. An alternative cross-section was required and, as a first step towards its design an investigation of ground conditions was set out. It was also decided to build a reinforced curved invert in a 300 m long stretch of the tunnel where heave rate reached maximum values. Stress cells were installed at the concrete-claystone interface to measure swelling pressures. The invert was designed as a temporary structure to gain information on the swelling potential of the ground and it was designed for a swelling pressure of 0.5 MPa which may be considered moderate in view of the values recorded later.

In addition, boreholes 15 m long with continuous core recovery were drilled along the tunnel floor. Some of them were equipped with high precision “sliding micrometer” extensometers (Kovári and Amstad, 1982). They were arranged, in groups of three, in several cross-sections along the tunnel. Vibrating wire piezometers were also installed in the same monitoring sections, at varying depths.

It was also decided to investigate the performance of a circular cross-section, which would require the excavation of the tunnel invert. The design approach was to build three cylindrical stretches inside the tunnel and to test them at full scale. The ring structures were equipped with load cells at the concrete-ground interface and the lower section was flooded during the

entire period of measurements making sure that, by means of holes drilled through the lining, water arrived freely to the claystone. The purpose of these tests was to approximate the worst expected swelling conditions with a view of designing the final cross-section properly.

The investigation therefore offered the possibility of comparing three widely different cross-sections within relatively short distances and common expansive ground conditions: an unreinforced flat-slab, a moderately reinforced curved invert and a circular massive lining under three supporting conditions: full support and two different yielding support conditions (Kovári et al, 1988). The position of the different support conditions along the tunnel is given in Figure 3.2(c). The response of the three types of support will be analysed in the next sections.

Table 3.2 provides a mineralogical description of the undisturbed claystone. The table summarises X-ray diffraction analysis of small samples from cores taken in vertical borings drilled from the tunnel floor in the northern part of the tunnel. The clay matrix (illite and paligorskite) dominates the composition. Anhydrite is also present in a substantial proportion. Gypsum is also present but in small percentages. The table does not provide an accurate description of the complexity of the formation. Some samples were found to be pure anhydrite, in others anhydrite was absent and dolomite was dominant. Smectite was never detected, however. Therefore, clay related swelling was disregarded as a possible explanation for the observed heave.

More accurate and useful information is provided by a continuous record of properties along a boring performed from the tunnel floor. This is shown in Figure 3.7 for the upper 10 m of a boring located at chainage 411 + 600 in a zone of maximum heave rate. In fact, the plot integrates the results of two nearby borings drilled in the same cross-section at two different times: October 2002 and March 2003. The figure provides information on the variation with depth of water content, specific gravity, total density and gypsum, anhydrite and matrix mineral components. In addition, vertical strains in depth measured in the same location in March and December 2003, are also represented.

The strain record measured in December 2003 provides precise information on the extent of an upper “active” zone where swelling strains are being developed. It has a thickness of 5.5 m. Below, in the stable zone, identification indices of claystone, including mineralogy, remain essentially unchanged. The active zone can also be easily identified by the evolution of water

content and total density. Water content increased in a period of 6 months from values found in the undisturbed formation (2 - 4%) to values in the range 5 - 10%. This is reflected in the parallel decrease in total density.

Table 3.2. Mineralogy and geotechnical indices of undisturbed Lilla claystone

Minerals: relative content	
Quartz: %	2 – 7
Dolomite: %	11 – 13
Anhydrite: %	13 – 28
Gypsum: %	0 – 7
Clay (Illite and Paligorskite): %	51 – 67
Physical and mechanical indices	
Specific unit weight	2.82 – 2.90
Water content: %	0.5 – 4.5
Total density: Mg/m^3	2.40 – 2.86
Unconfined compressive strength: MPa	17 – 170

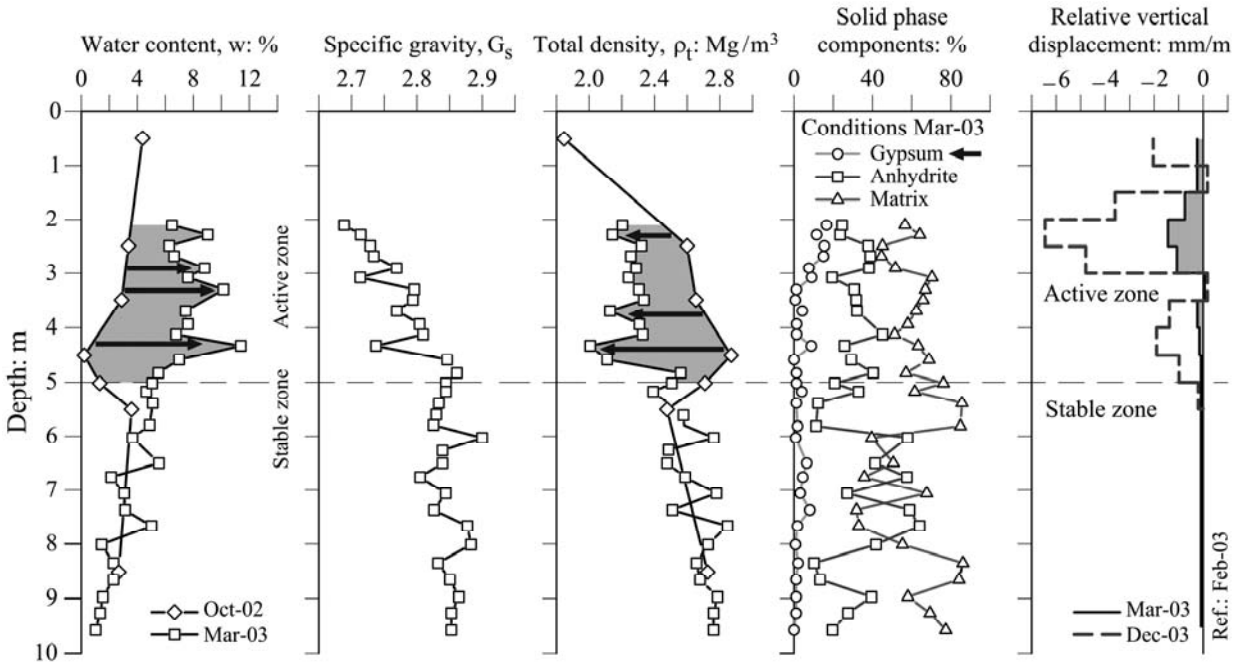

Figure 3.7. Geotechnical and mineralogical characterization of the rock at the chainage 411 + 600 (invert-arch) and vertical displacements measured by the sliding micrometer installed in the axis

The plot of variation of gypsum content with depth is very significant. Within the stable zone gypsum content is low to very low. Above the lower limit of the active zone the gypsum content increases progressively to values of 15-18% in the upper part. Anhydrite maintains a high concentration (25-50%) throughout the vertical profile although low concentrations seem to predominate in the active zone. The plot suggests that within the active zone gypsum content has increased at the expense of anhydrite. Interestingly, the occurrence of anhydrite in the rock was unnoticed at the design stage and all sulphate minerals were assumed to be gypsum (San Dimas, 2002).

Water content is a measure of the degradation of the rock and some relation between water content and sulphate content, in the sense of increasing sulphate content with water content could be expected. This is not apparent in Figure 3.8 although Figure 3.7 shows an increase in gypsum solid content in the upper levels of the active layer, characterised also by a significant increase in water content.

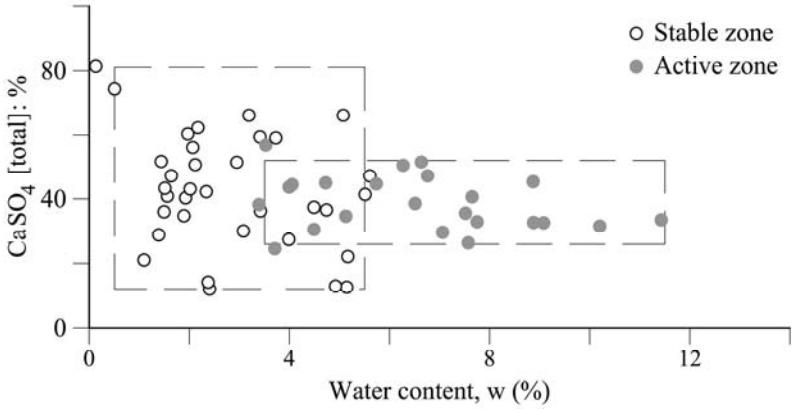

Figure 3.8. Variation of total sulphate content with water content within the stable and active zones

3.5 Crystal growth in the active zone

The material recovered from boreholes performed from Lilla tunnel floor was studied in detail. In this section some observations made in cores extracted from the active zone under Lilla tunnel are reviewed. They provide useful information to understand the mechanisms involved in the swelling phenomenon described in Chapter 5.

Cores recovered from the active zone under the Lilla tunnel show the growth of small gypsum crystals in several geometrical arrangements. Some photographs have been collected in Figure 3.9 to Figure 3.13. Figure 3.9 shows thin monoclinic gypsum crystals in a claystone

discontinuity crossing a core recovered from a depth of 4.2 m, inside the active zone identified at chainage 411 + 600, below the invert testing section. Figure 3.10 shows monoclinic gypsum crystals apparently developing along a discontinuity. Gypsum crystals were also found to group in “rosettes” as shown in Figure 3.11. The core in this case was recovered 20 cm below the core in Figure 3.9. On occasions rosettes were found to cover rock discontinuities almost completely, as shown in Figure 3.12. Rosettes, when confined between two planar claystone surfaces, also exhibited two planar boundaries (Figure 3.13). The impression is that rosettes, in their growing, were pushing apart the two planar surfaces forming the claystone discontinuity.

Figure 3.9. Thin gypsum needles observed in a claystone discontinuity in a core recovered from depth 4.2 m at chainage 411 + 600

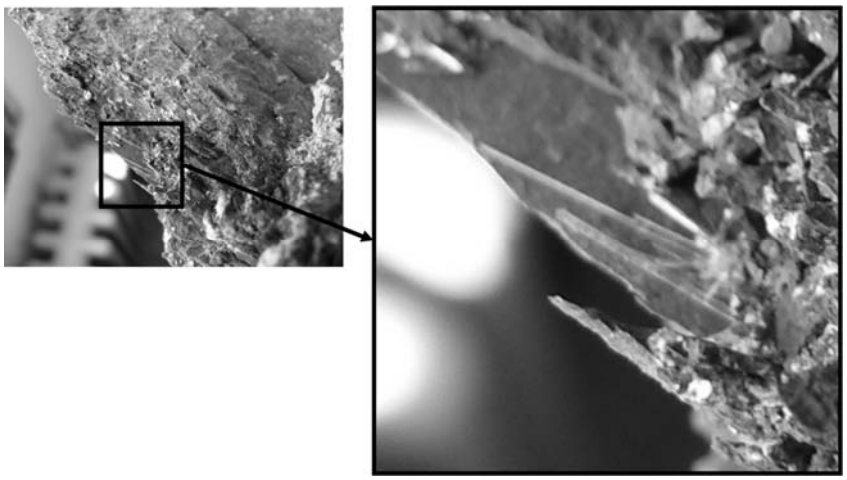

Figure 3.10. Gypsum needles growing in a discontinuity of the claystone

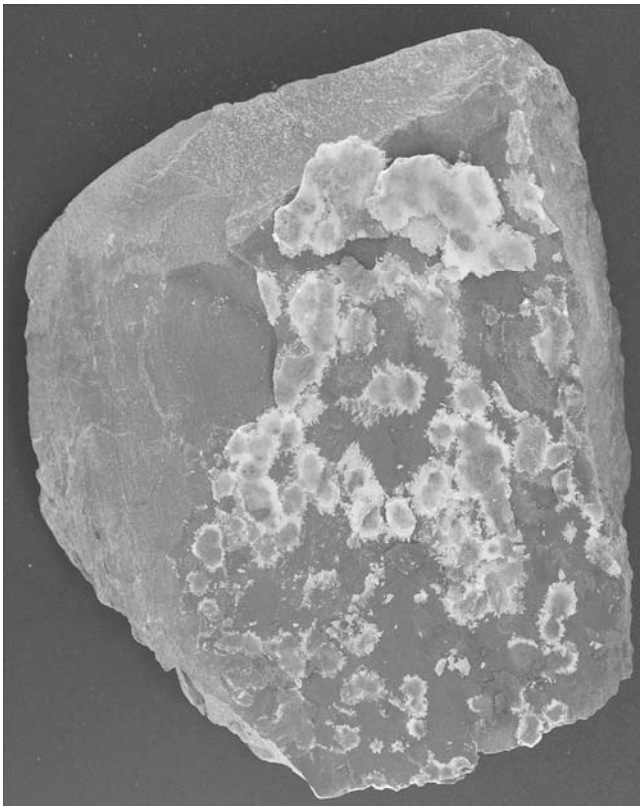

Figure 3.11. Gypsum “rosettes” observed in a claystone discontinuity in a core recovered from depth 4.4 m at chainage 411 + 600

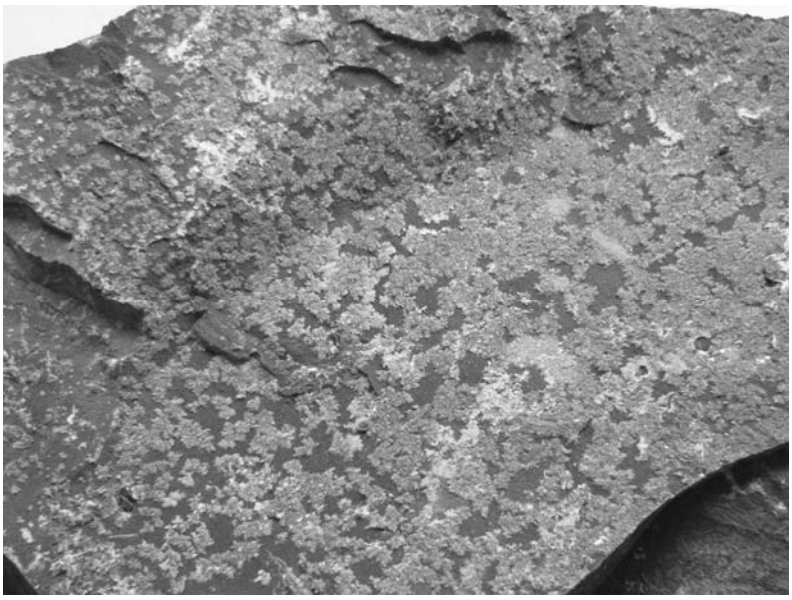

Figure 3.12. Gypsum “rosettes” covering a discontinuity

Figure 3.13. Detail of a planar gypsum “rosette” deposited in a claystone discontinuity

3.6 Performance of flat-slab floor

In March 2003, six months after the initial detection of floor heave and two weeks after a moderate rain, a strong heave, which badly damaged the concrete slab, was detected at chainage 411 + 880 (Figure 1.1). The intense heave was attributed to the uncontrolled presence of water on the tunnel floor. It was also observed that the central longitudinal drainage tube was damaged and interrupted at some points. The average heave rate explaining the displacements observed in Figure 1.1 is close to 2 mm/day.

In general, heave affecting the flat-slab evolved systematically at high rates, without any indication of stabilisation. This is shown in Figure 3.14, which indicates approximately constant heave rates varying between 1.2 and 2 mm/day for a few monitored points. In December 2003, heave displacements in the range 513-763 mm were measured at chainages (411 + 420, 411 + 880 and 411 + 900). Sliding micrometer measurements during ten months of monitoring -from February 2003 to December 2003- allowed the identification of an active upper zone, 4 m thick (but somewhat thicker under the tunnel axis), within the foundation claystone, below the flat-slab, in which expansions accumulated with time (Figure 3.15). The thickness of this active zone remained basically unchanged during the monitoring programme. In this figure a circular section that completes the circumference defining the tunnel vault has

been sketched. The figure suggests that the extension of the active zone may be related to the tunnel diameter. One of the arguments favouring the design of a new circular section as shown in Figure 3.15 was that the necessary excavation would remove the active zone and the heave phenomena would be circumvented. Unfortunately the foundation claystone reacted in a different manner, as described below.

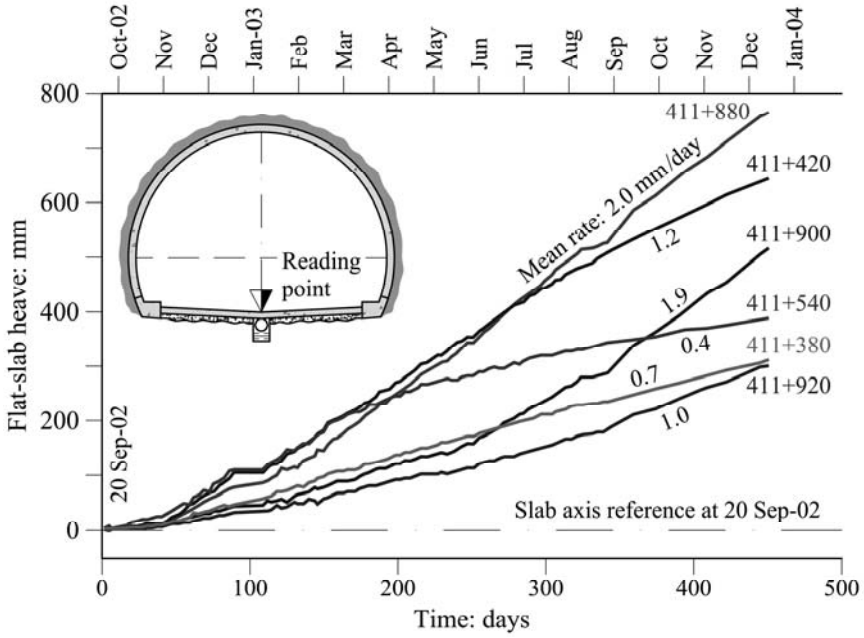

Figure 3.14. Evolution of the floor heave between September 2002 and December 2003 in the indicated tunnel sections with flat-slab

Thirteen months after the first levelling of the tunnel floor, measured heave evolved in the manner indicated in Figure 3.2(d). The 300 m long zone close to the northern portal exhibiting small, but noticeable, displacements corresponds to the position of the curved invert, which was cast in place in January 2003. The curved invert was very efficient in reducing further floor heave.

The maximum displacement recorded (800 mm) is very large, among the highest reported in tunnels built in Gipskeuper formations in Central Europe (Wichter, 1985; Nagel; 1986; Fecker, 1992; Paul & Wichter, 1996; Paul & Walter, 2004; Kovári, & Chiaverio, 2007; Steiner et al., 2011) as can be observed in Figure 2.4(a). The heave intensity decreased towards the southern portal. A 400 m long stretch, immediate to the south portal, did not exhibit any swelling. However, geological conditions were reported to be similar along the entire tunnel. This apparent inconsistency will be discussed in Chapter 5.

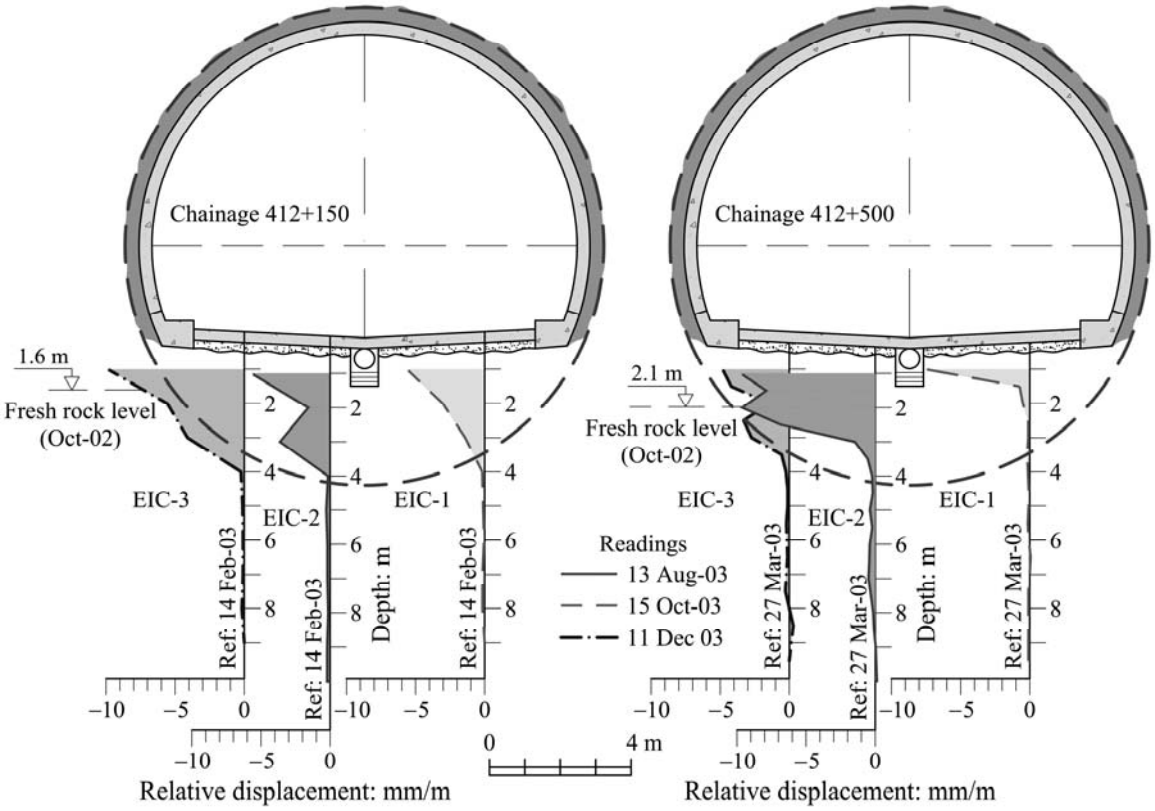

Figure 3.15. Relationship between the depth of the active zone below test sections with flat-slab and the maximum radius of excavation.

3.7 Performance of curved invert

Figure 3.16 shows the design of the curved invert built in January 2003 between chainages 411 + 556 and 411 + 860. It has a moderate curvature and it was anchored in the two longitudinal concrete massifs supporting the abutments. The invert was designed to resist a swelling pressure of 0.5 MPa. This was close to the maximum value recorded in a swelling pressure test performed on an undisturbed sample recovered in October 2002 from a depth of 2.50 m below the floor slab at chainage 411+480, which is located in a very active swelling zone (see Figure 3.6). The curved invert was installed in two stretches: the first one located between chainages 411 + 556 and 411 + 750 (194 m long) and the second one between chainages 411 + 750 and 411 + 860 (110 m long). The reason was to test the performance of two different invert thicknesses: 400 mm in the first case and 600 mm in the second case.

Measured heave rates reduced by more than one order of magnitude but they did not show any indication of slowing in the measuring period of 320 days (Figure 3.17). At chainage 411 + 663 a maximum heave of 27 mm was measured 10 months after invert construction. In this

position, the mean heave rate was 0.1 mm/day. Therefore, despite the invert's ability to reduce the heave, the invert did not provide a rigid reaction and the measured pressures against it cannot be considered "swelling pressures", a concept which implies no volumetric deformations. Measured pressures against the invert will be smaller than the pressures against a support designed on the basis of a resistance principle (no yielding).

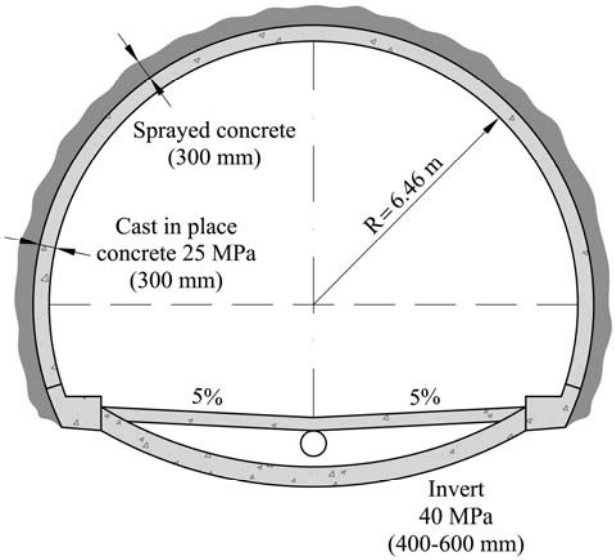

Figure 3.16. Design of invert

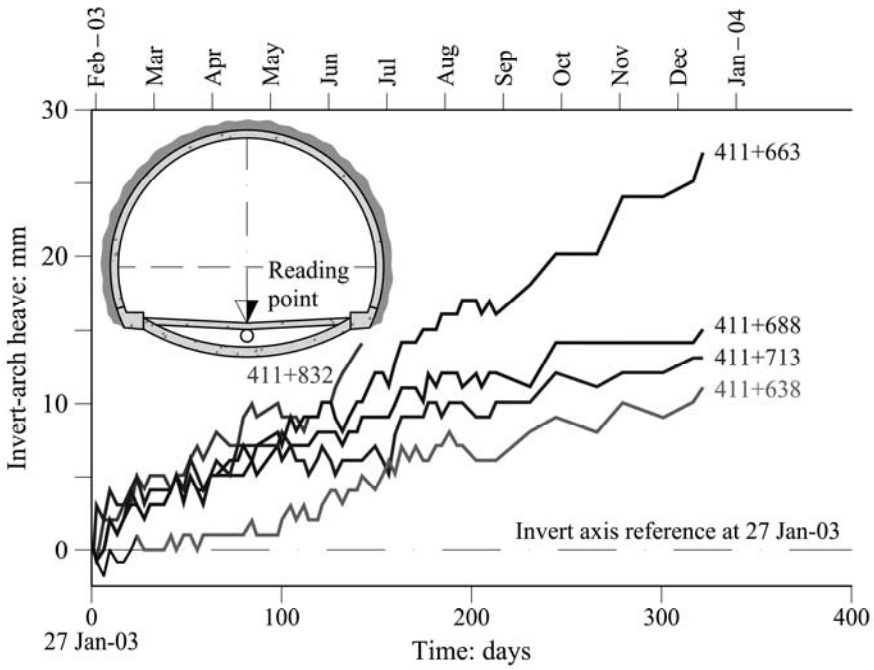

Figure 3.17. Evolution of floor heave between January and December 2003 in test sections with invert

Figure 3.18 indicates the longitudinal and transverse variation of pressure, at the end of the measuring period (December 2003), recorded in the measuring cells. Maximum values are

close to 5 MPa but the distribution in a cross-section as well as along the tunnel is very irregular. At a given cross-section the supporting action of tunnel abutments leads to higher pressures than the values measured in the more deformable central position. The measured heave of points on the floor is also given.

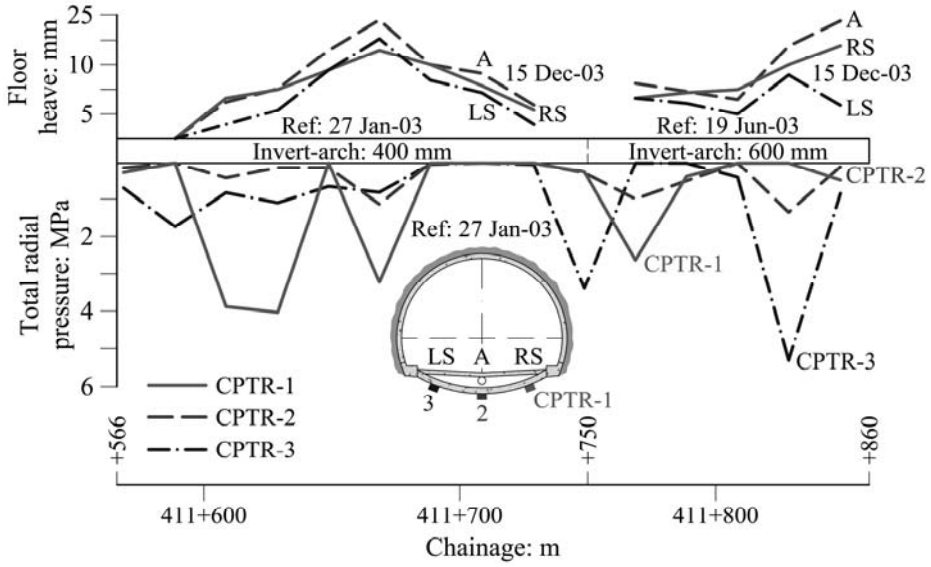

Figure 3.18. Pressures against stress cells and heave measured in the tunnel invert test sections during the period January-December, 2003

Stress cells were regularly measured during 600 days. The pressure-time plots (Figure 3.19) show a general trend towards stabilisation in a natural time scale. However, several cells in Figure 3.19 maintained an increasing rate of pressure development at the end of the measuring period. The effect of the invert thickness was not apparent in the measured contact stresses.

Sliding micrometers were also installed under the invert at chainage 411 + 600 (invert thickness: 400 mm). Total strains recorded in the period February-December 2003 are given in Figure 3.20. An active zone has again developed despite the confinement offered by the curved invert. Instrument EIC-1, close to one abutment, measured some compression in the upper part, a result to be expected under increased confinement. The thickness of the active zone has now reached values close to 6 m under the invert at the tunnel axis. It appears that the moderate excavation required to install the invert has contributed to extending the initial active zone, which was confined roughly inside the circular section also indicated in Figure 3.20.

Vibrating-wire pore water pressure sensors were installed at depths of 2 m and 5 m below the invert at chainage 411 + 600 inside the active layer. They reacted fast (Figure 3.21) and a

water level close to the invert-claystone interface was measured. The quick stabilisation of piezometric levels is an indication of a high permeability in the claystone within the active zone.

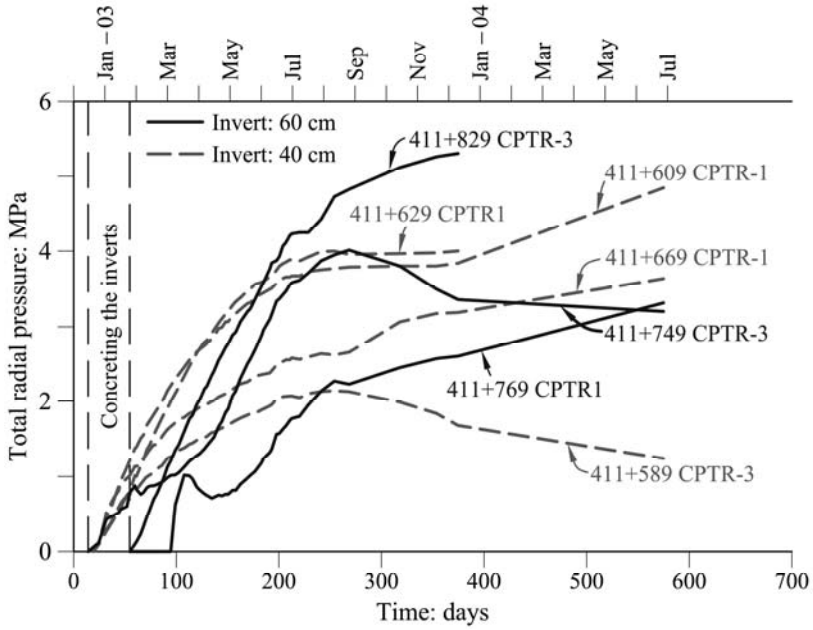

Figure 3.19. Development over time of swelling pressure recorded by some stress cells under invert

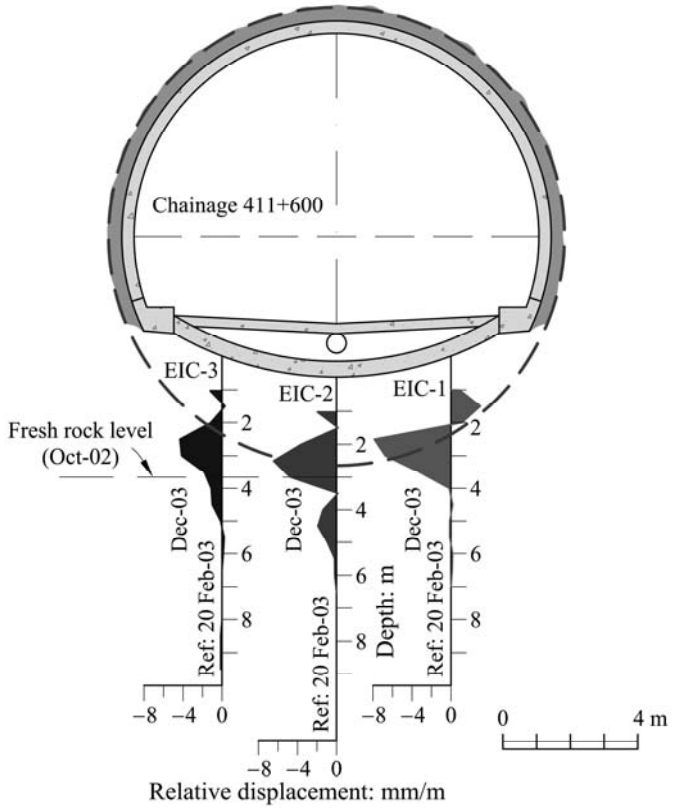

Figure 3.20. Sliding micrometers readings below the test section 411 + 600 with invert-arch of 400 mm; recorded strains in the period February-December 2003.

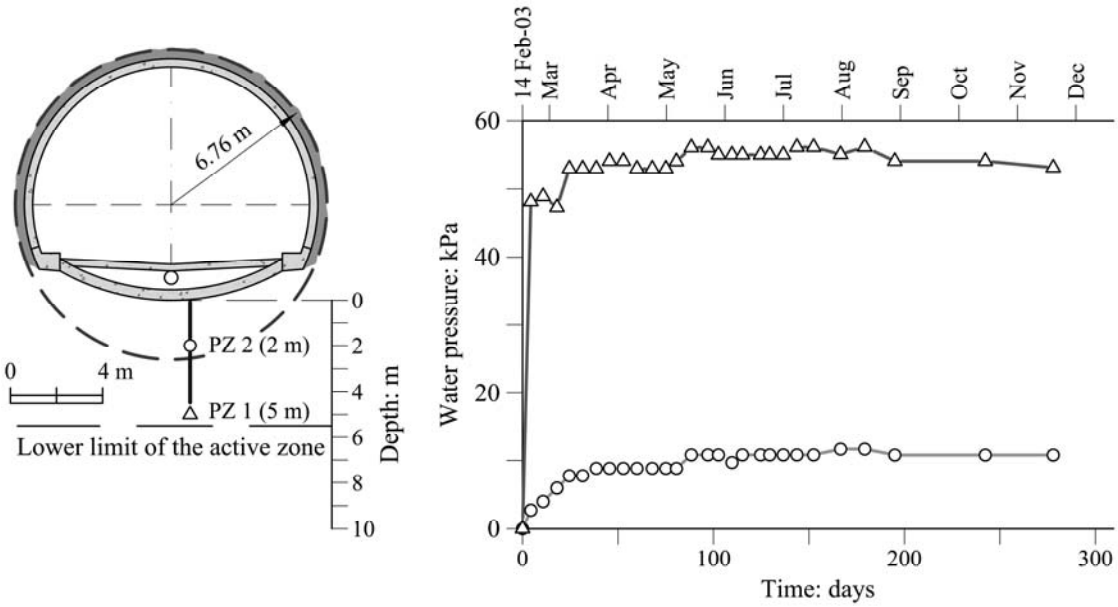

Figure 3.21. Piezometer readings in the test section 411 + 600 (invert-arch 400 mm thick)

3.8 Performance of circular testing sections

Three circular testing sections were built into the tunnel in the position shown in Figure 3.2(c) (chainages 412 + 543 to 412 + 593). The tunnel floor had to be excavated to complete the circular geometry. Each one of the sections was intended to test a design criterion: a resisting support in which the rigid concrete lining reacts against the excavated rock (chainages 412+543 to 412+565), a yielding support, composed by a set of springs (Figure 3.22(b) and Figure 2.17) (chainages 412+571 to 412+581), allowing for the shortening of the tunnel lining under the circumferential load imposed by the ground swelling and a second yielding support below the invert, built by means of a 40 cm thick foam layer (chainages 412+583 to 412+593). Figure 3.22 shows details of the three designs. It was also accepted that the most critical conditions would be met if the rock under the invert could be artificially wetted.

The circular geometry involved a maximum excavation of 4 m under the original flat-slab. It was argued that a positive aspect of this excavation was the removal of a large proportion of the active zone which had developed under the original horizontal slab floor. In addition to the structural advantage of a circular cross-section, the swelling activity would be reduced. In all three sections a careful mechanical excavation was carried out to minimise further rock damage.

Resisting support Yielding support

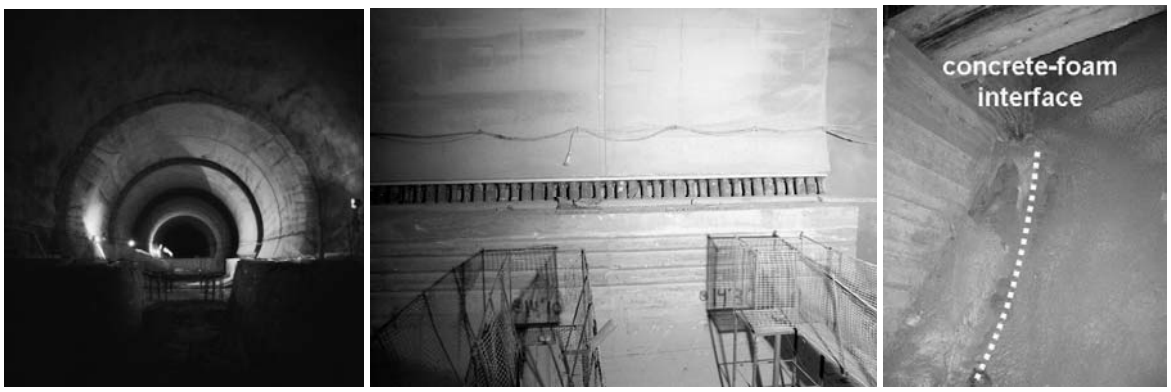

(a) (b) (c)

Figure 3.22. Circular test sections with resisting and yielding supports: (a) rigid section; (b) section with springs; (c) section with foam

The three circular sections were built between May and August 2003. Vertical holes, drilled through the concrete lining (Figure 3.23) allowed the free passage of water when the tunnel sections were partially inundated. The water used in the test was natural groundwater collected in the tunnel area. The composition of this water is given in Table 3.3. The sulphate concentration of this water is high, but it does not reach saturation conditions which, for a temperature of 15ºC is 2.03 g/l of calcium sulphate in the case of equilibrium in the presence of gypsum and 3.2 g/l of calcium sulphate in the presence of anhydrite.

Sliding micrometers and pressure cells were also installed to monitor the performance of the three sections. A pervious geotextile mat was also placed at the rock - concrete contact, connected to the wetting holes, to facilitate a regular distribution of water on the rock surface.

Flooding was initiated on 19 September 2003. A shallow free water level was maintained in the tunnel sections for 30 days. Then, the water was removed. Monitoring of instruments lasted an additional period of 400 days. Figure 3.24 provides the main results. The figure also shows the instrumentation layout which was installed in a centred cross-section of each one of the three designs tested: Five pressure cells at the concrete-rock interface (or concrete-foam in one of the yielding support designs) and two vertical micrometers, 12 m long.

The pressure cells of the full support case immediately reached a maintained rate of pressure increase. Interestingly, the rise in pressure was previous to the flooding stage, which, on the other hand, did not have any apparent influence on the rate of increase of pressure. As expected, pressure records on the two cases of yielding support exhibited much lower

pressure values, especially in the case of springs. In the yielding sections the pressure rise started soon after the pressure cells were in operation and reached, in some cases, a limiting value. However, some of the cells also recorded a linear increase of stress with time, which lasted for the entire testing period.

Table 3.3. Chemical composition of the groundwater used in the flooding test. Chainage 412 + 552; date 23 September 2003; water temperature 18.2 ºC

Macroconstituent	**Concentration: mg/l**
Sulphates (SO_4^{2-})	1072.60
Bicarbonates (HCO^{3-})	278.35
Chlorides (Cl^{1-})	68.84
Nitrates (NO_3^{1-})	4.15
Calcium (Ca^{2+})	398.57
Magnesium (Mg^{2+})	67.25
Sodium (Na^{1+})	66.00
Potassium (K^{1+})	15.40
pH	7.74
Electrical Conductivity at 20ºC: $\mu S / cm$	2002

Extensometer records indicated that a new active zone had developed under the invert of the circular sections. Extensometers under the foam section could not be monitored, however. The active zone reached a thickness varying between 4 and 6 m, a thickness also found in the flat and curved invert sections. Plots showing the swelling strains measured at varying depths within the active layer are given in Figure 3.25. Data from the resisting support and the yielding support (spring) are combined in the same figure. Strains increase fast initially and then the increase progressively slows down, although no indication of an asymptotic trend towards stabilisation is observed. Swelling rates are higher in the yielding support case, which is an important piece of information for the establishment of criteria for the design of the tunnel support, discussed in the next section.

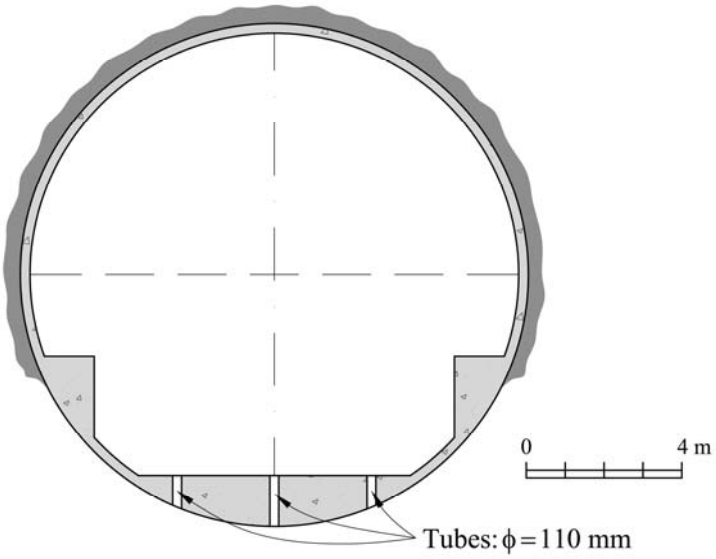

(a)

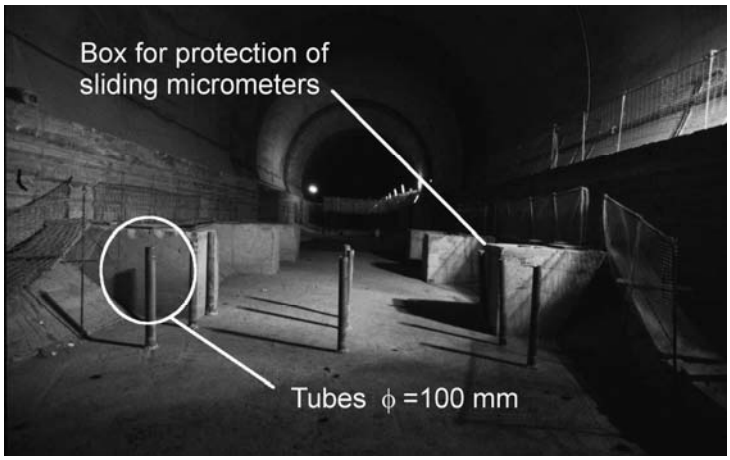

(b)

(c)

Figure 3.23. Details of the system for the flooding test in circular sections with resisting and yielding supports: (a) design of cross-section and boreholes to allow wetting the rock; (b) test section before the start of test; (c) flooded test section

3.9 Tunnel reinforcement

Despite the smaller short term swelling pressures recorded in the yielding support designs, their long term performance was not so clear. The larger deformations allowed by the yielding support solutions could induce an additional damage to the rock in the active layer, possibly leading to an enhanced swelling activity. A circular lining based on the resistance principle was therefore selected and a reinforced circular cross-section was adopted for the entire tunnel. It was also appreciated that it guarantees a minimum risk of rail track displacements.

The new reinforced concrete tube was to be built inside the original horseshoe shaped section. A design swelling pressure of 4.5 MPa was also adopted. This pressure was close to the maximum recorded in loading cells monitoring the ground reaction against the invert testing section (Figure 3.19).

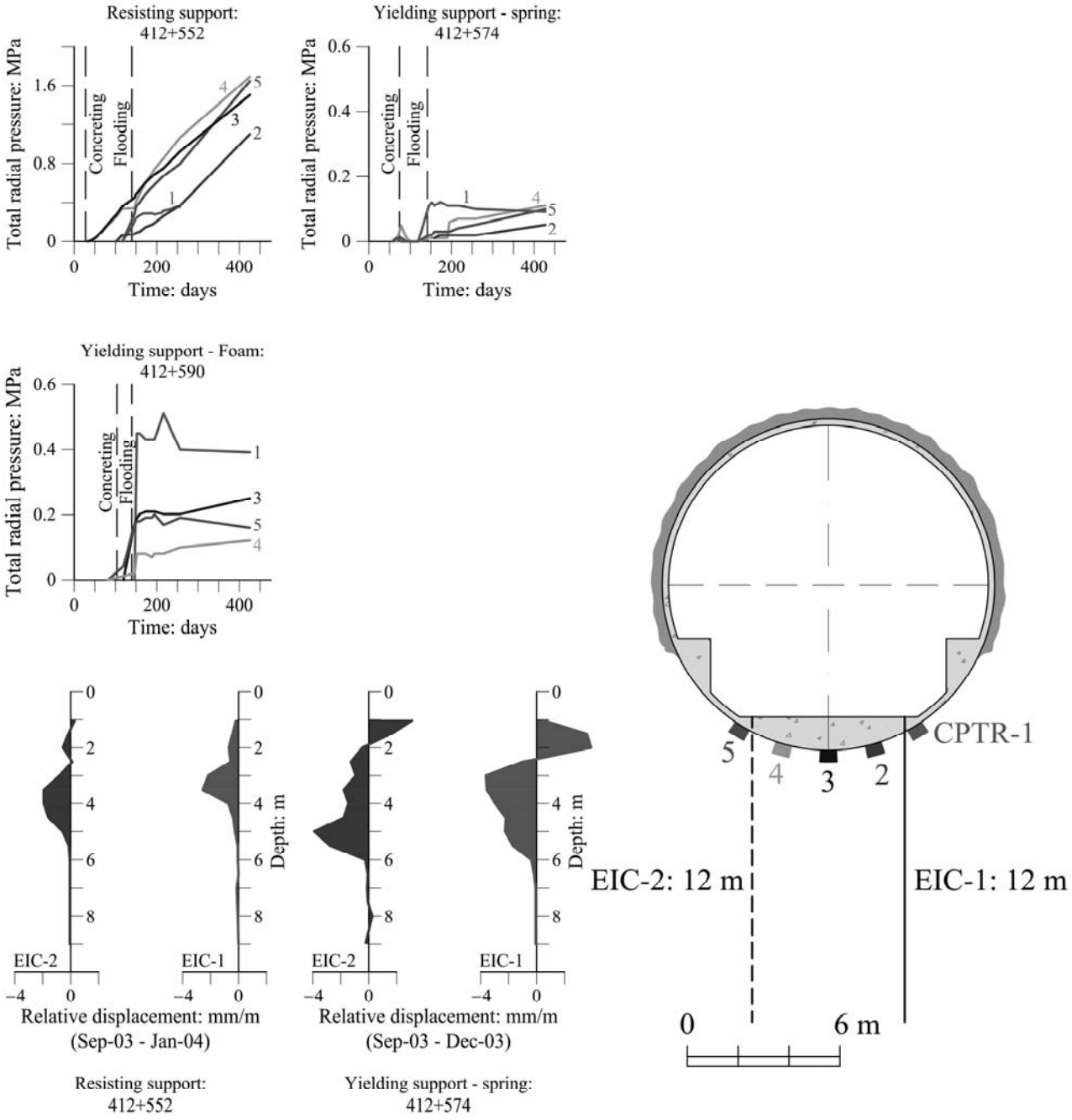

Figure 3.24. Total radial pressures against inverts and sliding micrometers readings in circular test sections

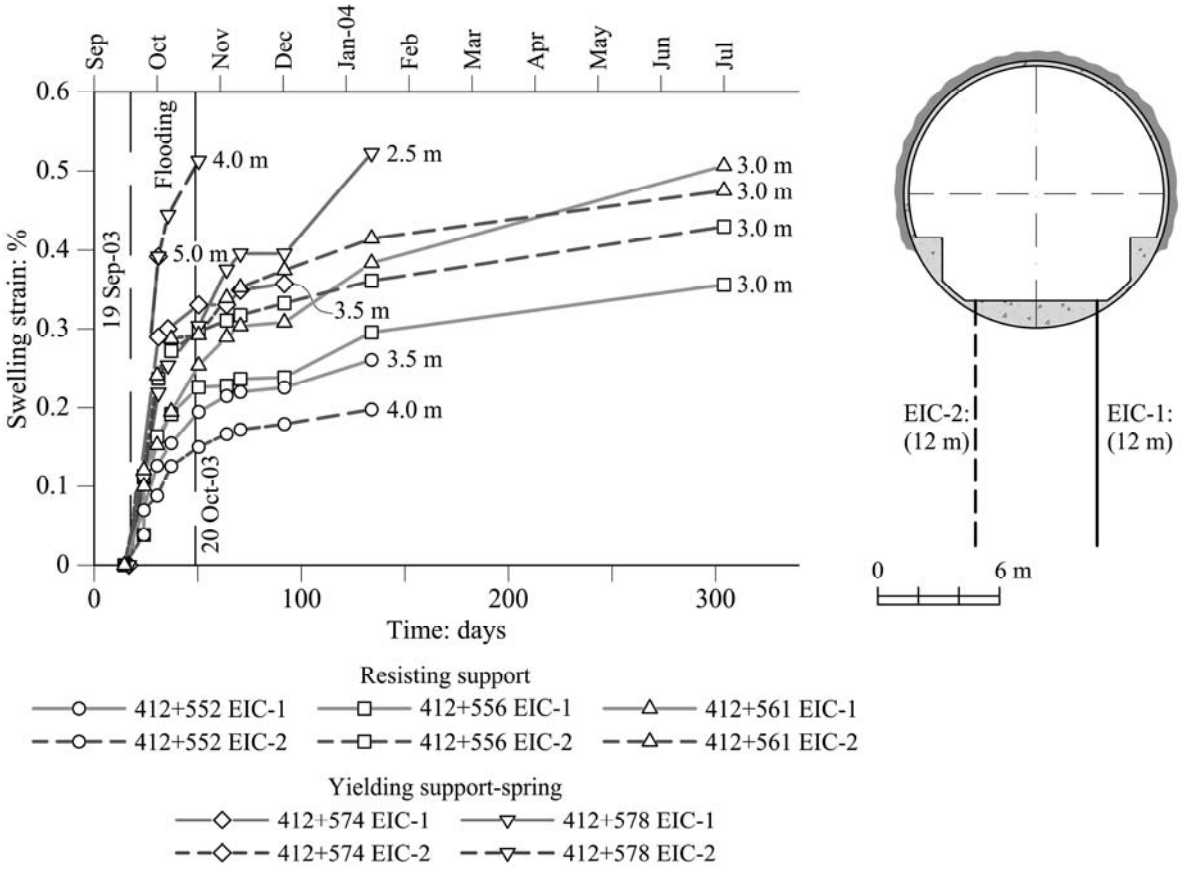

Figure 3.25. Swelling strains in the expansive zone below circular test sections. Results are given for a reference depth, indicated for each of the plotted curves, and describe the strain measured in a 1 m interval (see inset)

The circular structure was calculated under two-dimensional plane strain conditions. A non-uniform distribution of pressure against the tube would induce some combination of bending moments, circumferential and shear loading. The conservative criterion adopted to define the tube thickness and its reinforcement was to select a critical length of pressure application against the external surface of the tube leading to the maximum amount of reinforcement. The ring was analysed as a circular frame supported by radial and tangential springs representing the existing tunnel support and the ground. Calculations were made with the help of a Finite Element program. Radial and tangential subgrade coefficients (3.3×10^5 kN/m^3 and 1.1×10^5 kN/m^3 respectively) were proposed by Alonso & Sagaseta (2003) adopting a rock elastic modulus of 250 MPa. The elastic modulus of the claystone matrix was measured in unconfined compression tests equipped with strain gages glued to samples. Measured modulus ranged from 8000 to 10000 MPa. However, these are values determined in small samples and it was estimated that the deformation modulus of the rock mass, crossed by

slickensides and fissures, could amount to 20-50% of the matrix modulus. These considerations led to the value of 250 MPa.

Figure 3.26(a) shows the calculated maximum axial load and bending moment in terms of the loading angle α, also shown in the figure. The required steel reinforcement (area of steel over the area of the structural section) is shown in Figure 3.26(b) for a liner thickness of 760 mm, an 80 MPa characteristic strength of concrete (E_c =30000 MPa) and steel grade BS500S (E_s = 210000 MPa). The selection of the high strength concrete was required to cope with the limitations of vault thickness, which in turn derive from the required clearance for the circulation of trains. The maximum reinforcement was found for α = 60º for the action of radial pressures of 4.5 MPa against the invert and 2.5 MPa against the vault (Figure 3.27). These considerations lead to the reinforced section shown in Figure 3.27.

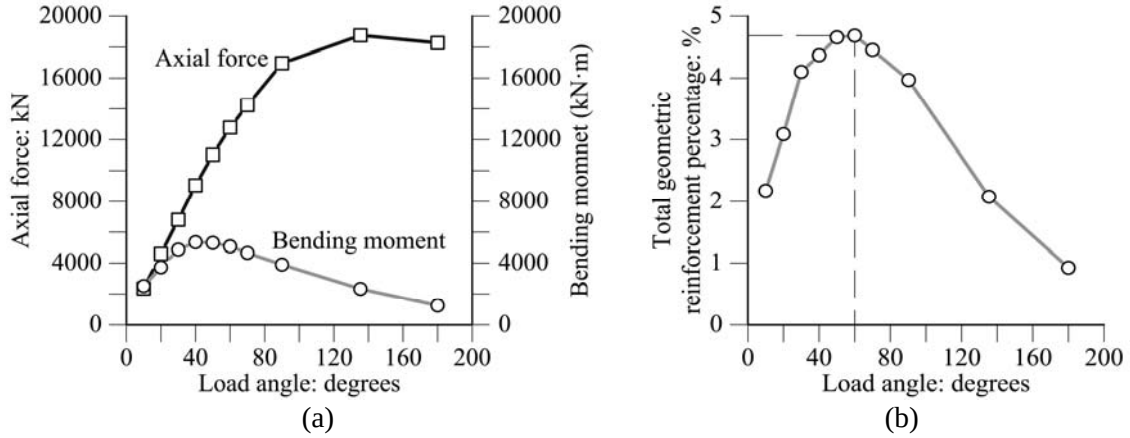

(a) (b)

Figure 3.26. Dependence of (a) the axial force and the bending moment and (b) the total geometric reinforcement on the loading angle (Marí & Pérez, 2003, with permission)

The reinforcement of Lilla tunnel with the new circular resisting support was carried out between July 2004 and October 2005. The construction was divided into two main stages: (i) excavation and construction of the invert; and (ii) lining of the vault. Due to the existence of the original flat-slab along an important stretch of the tunnel -as well as stretches with invert-arches and circular sections-, it was necessary to guarantee the stability of existing vault supports and linings before the demolition of the tunnel floor by means of the installation of rock bolts in abutments. Once the abutments were anchored, the tunnel floor was demolished.

In order to minimise the damage of the rock as a result of excavations, the circular section was excavated using pneumatic hammers and roadheaders. Excavated stretches were sealed by means of a steel fibre reinforced shotcrete installed to limit changes in water content of the

rock and to guarantee the temporary support of the excavation. The tunnel was not waterproofed. The new circular lining was concreted directly against the initial 300 mm lining. Therefore no geotextile or impervious membrane was placed at the interface between the initial lining and the added reinforced tunnel. Two contractors worked on the reinforcement, one from each portal. One of them decided to build the steel reinforcement frames outside the tunnel in modules, 2.4 m long, and then transport them through the tunnel using gantry cranes, before concreting. The other contractor decided to build the reinforcement "in situ". Both achieved a similar performance and speed of construction.

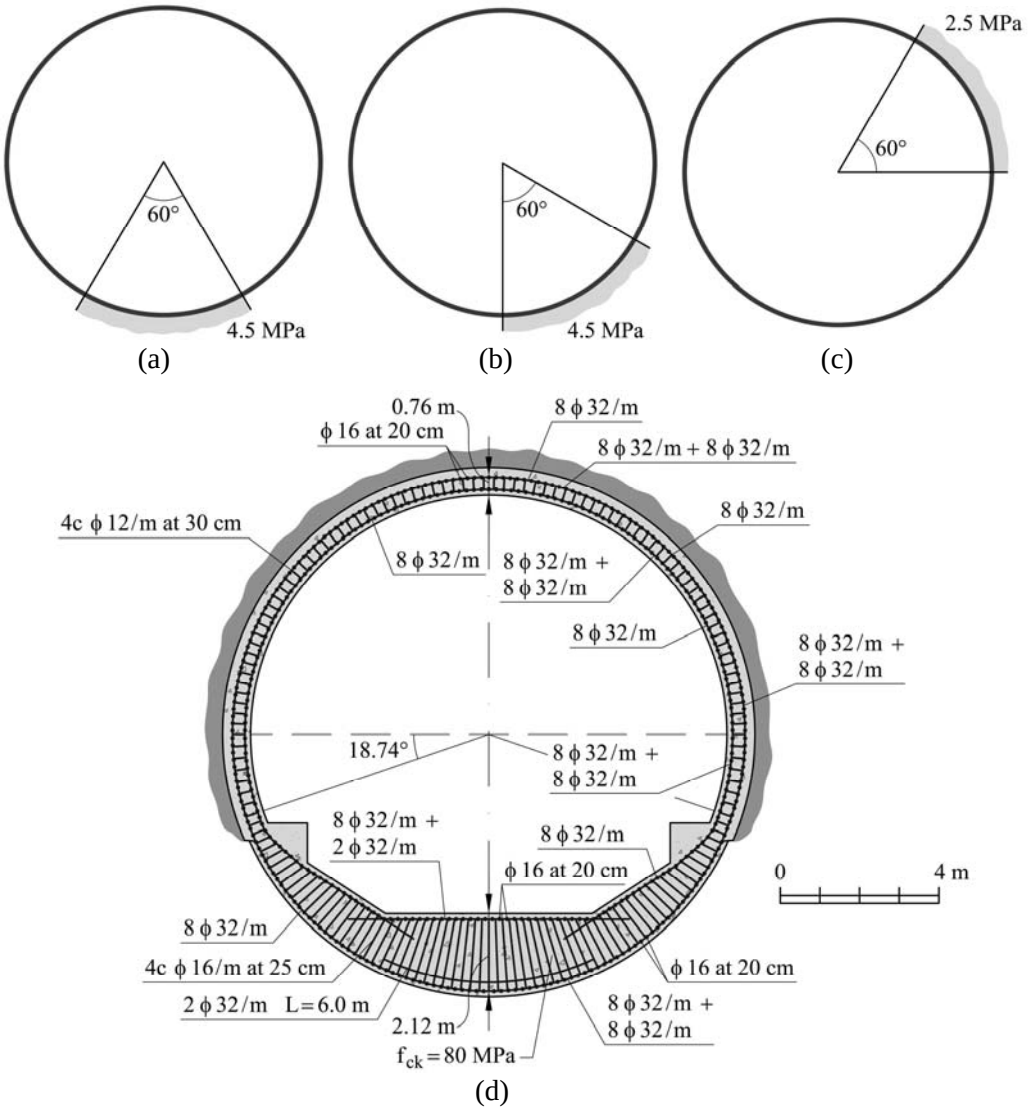

Figure 3.27. Details of the tunnel geometry and reinforcement: (a) – (c): design hypothesis (Marí & Pérez, 2003, with permission); (d) installed reinforcement (ADIF, 2006, with permission)

The circular section was reinforced with two layers of 8 bars per metre (dia..= 32 mm) (Figure 3.27). In addition, shear frames and longitudinal bars were also installed. The weight of steel

reinforcement amounted to 10 t/m of tunnel length. Circumferential reinforcement reached 128 cm^2/m in vault and 257cm^2/m in invert. An image illustrating the tunnel reinforcement is given in Figure 3.28.

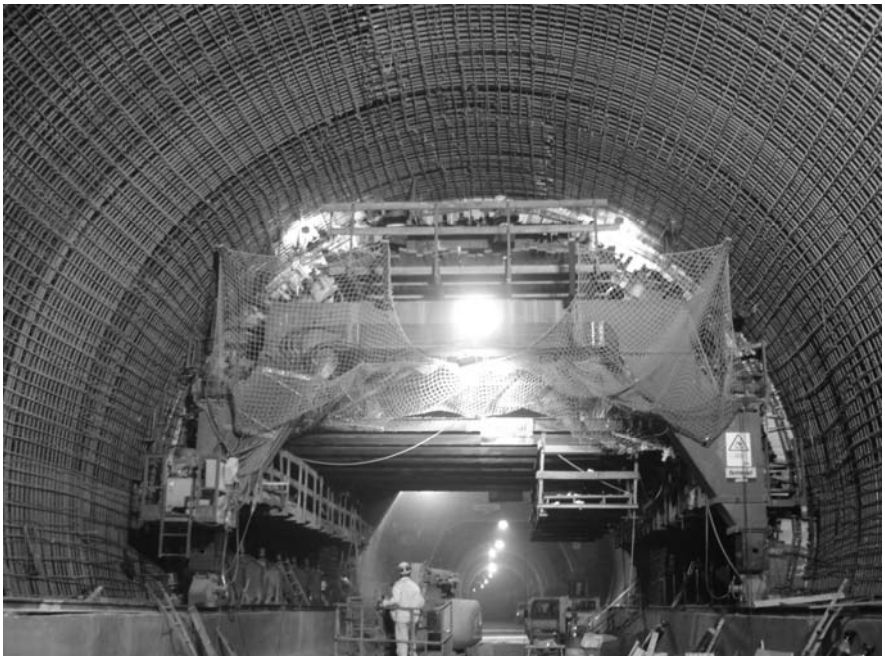

Figure 3.28. Steel reinforcement in vault and abutments of Lilla tunnel

3.10 Performance of reinforced tunnel

The reinforced tunnel was instrumented in order to measure the evolution of total radial pressures at the rock-lining interface and the straining of the steel reinforcement. A few radial pressure cells and vibrating wire strainmeters were installed in the vault (Figure 3.29) but most of the instrumentation was concentrated at the invert (Figure 3.29 and Figure 3.30).

Twenty one cross-sections were instrumented along the tunnel. Significant swelling stresses developed in the northern part of the tunnel, from chainage 411 + 240 to chainage 412 + 700. The southern part of the tunnel, from chainage 412 + 700 to the southern portal was only slightly loaded by swelling pressures. The reason for this behaviour is discussed later in the Chapter 5. Maximum swelling pressures recorded by the total pressure cells in the period 2005-2011 are plotted in Figure 3.2(e), they were recorded in cells installed at the invert, and maximum stresses measured in the steel reinforcement are indicated in Figure 3.31. The measured response of the tunnel is now discussed in more detail.

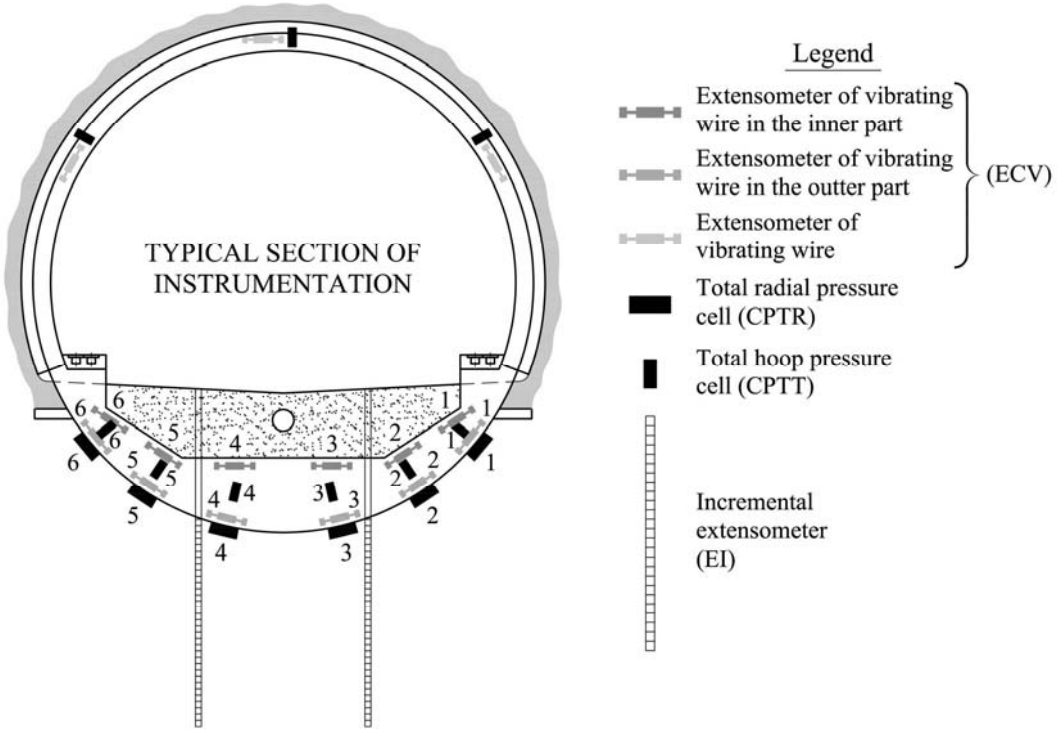

Figure 3.29. Typical instrumented section of reinforced tunnel with instruments in vault and invert

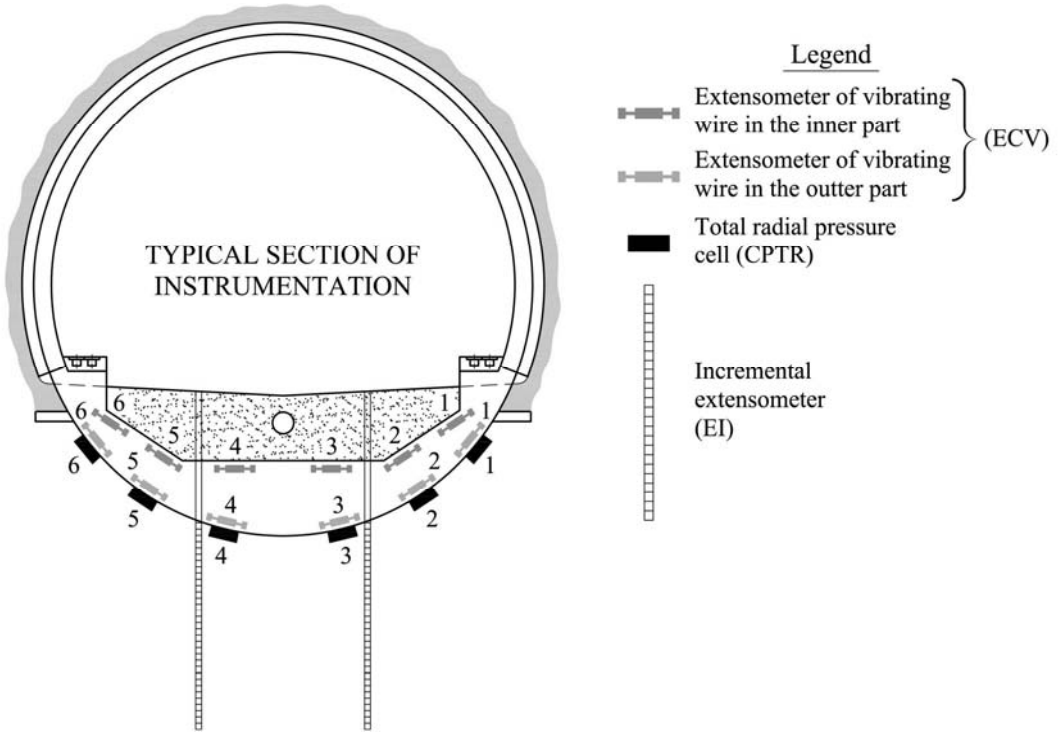

Figure 3.30. Typical instrumented section of reinforced tunnel with instruments installed only in invert

Pressure-time records measured at seven cross-sections, covering the period 2005 - 2011, are plotted in Figure 3.32 to Figure 3.38. They provide a summary of the observed behaviour. Recorded stresses in reinforcement bars are also given. In two cases (Figure 3.37 and Figure

3.38), measured hoop stresses in the concrete lining, recorded in pressure cells oriented radially, are also given. The figures provide the location of sensors.

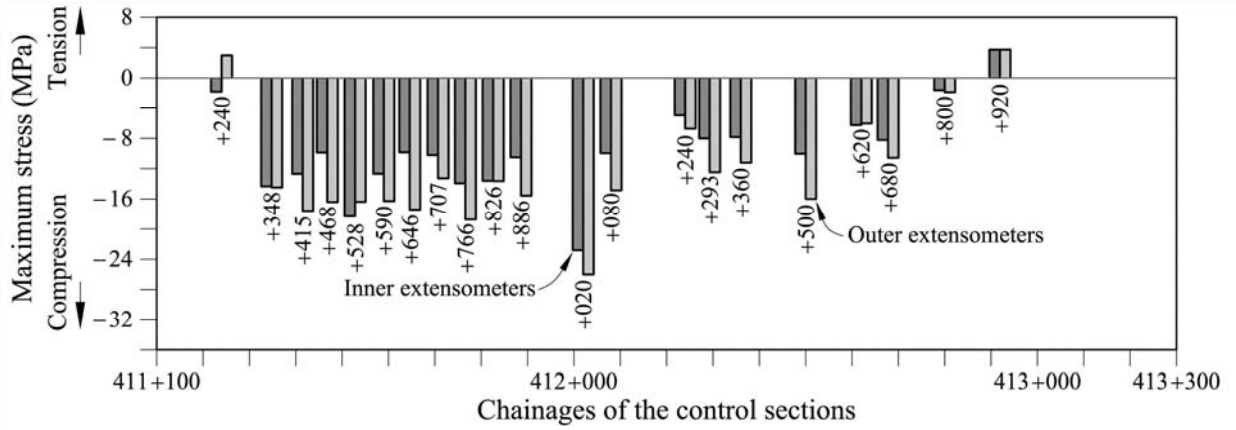

Figure 3.31. Maximum stresses in reinforcement recorded in the period from Jan. 2005 to Dec. 2011

Several radial pressure records show a sudden increase in pressure around May 2005. This behaviour seems to be related to the concreting of the vault, which was performed once the entire circular tunnel invert had been built. The vault closed the circular section and offered a strong resistance to swelling which resulted in a rapid increase in recorded pressures. A second systematic increase in pressure was recorded in October 2006. No structural changes had taken place in the tunnel since the conclusion of the works in June 2005. The reactivation may be a response to a transient change to hydrogeological conditions. In fact, heavy rains were recorded in the area in September and October 2006. Rainfall peak intensity reached a value of 55.6 (l/m^2)/day, the highest value recorded in a six-year period (Figure 3.39).

In some cases the pressure records show a levelling of the pressure after a few years of continuous increase. However, some of them show a significant increase in pressure with time at the end of the measuring period represented in the figures. For instance, pressures in two loading cells at chainage 411 + 826 increase at a rate of 70 kPa/month. Maximum recorded values stay in the range from 5 to 6.7 MPa, but the records indicate that these values tend to be essentially stabilised.

However, the most significant result is the extreme variability of recorded radial pressures in a given section. This is well illustrated, for instance, in the pressure records measured in sections at chainages 411 + 348, 411 + 468 and 411 + 707: One pressure cell may register values in excess of 5 MPa, while the remaining cells in the section, closely located, register very low or even no pressures. This general result is illustrated in the plots given in Figure

3.40. Even if some recording errors may be accepted for pressure cells in contact with the natural claystone and also acknowledging that six loading cells installed in a given cross-section, at the invert, do not provide a continuous distribution of pressures, it is clear that the ground response is fundamentally different from the loading assumptions made at the design stage of the circular reinforcement. This is so not only because of the variability in the transversal direction, but also for the expected variability in the longitudinal direction. The implications are positive because the built massive reinforced concrete tube is well prepared to resist a three-dimensional heterogeneous distribution of "point loads" on its outer boundary.

In fact, Figure 3.32(b), Figure 3.33(b), Figure 3.34(b), Figure 3.35(b), Figure 3.36(b), Figure 3.37(d)-Figure 3.37(f) and Figure 3.38(e)-Figure 3.38(g) seem to support this positive conclusion. They provide the stresses calculated at several positions of the reinforcement bars. In the case of invert reinforcement the plots refer either to a reinforcement located close to the outer circular boundary or to a horizontal reinforcement close to the upper boundary of the invert. In almost all cases the measured stresses are compressive stresses. Their value is rather low: maximum values are seldom greater than 13 – 14 MPa. If compatibility of deformations is accepted for the reinforcement bars-concrete interface, stresses in the concrete do not reach 2 MPa, a very small value. Stresses in the vault reinforcement bars are also very small (Figure 3.37 (d) and Figure 3.38 (e)).

Radial stresses against the vault (Figure 3.37(a) and Figure 3.38(a)) and hoop stresses in the concrete (Figure 3.37(c), Figure 3.38(c) and Figure 3.38(d)) were also measured in some cross-sections. Radial pressures against the vault are very small (less than 0.12 MPa), a result which is explained by the likely absence of water in the rock behind the vault. Hoop compression stresses in the vault and invert remain small: Less than 0.5MPa – 2 MPa.

It is concluded that the heavily reinforced high strength concrete circular lining works in compression despite the extremely high swelling pressures recorded in some positions. The structure is capable of transforming the highly heterogeneous swelling pressure distribution into a ring of small compressive stresses. The steel reinforcement is also under compressive stresses at virtually all measuring points. The magnitude of the stresses is small, very far from yielding conditions.

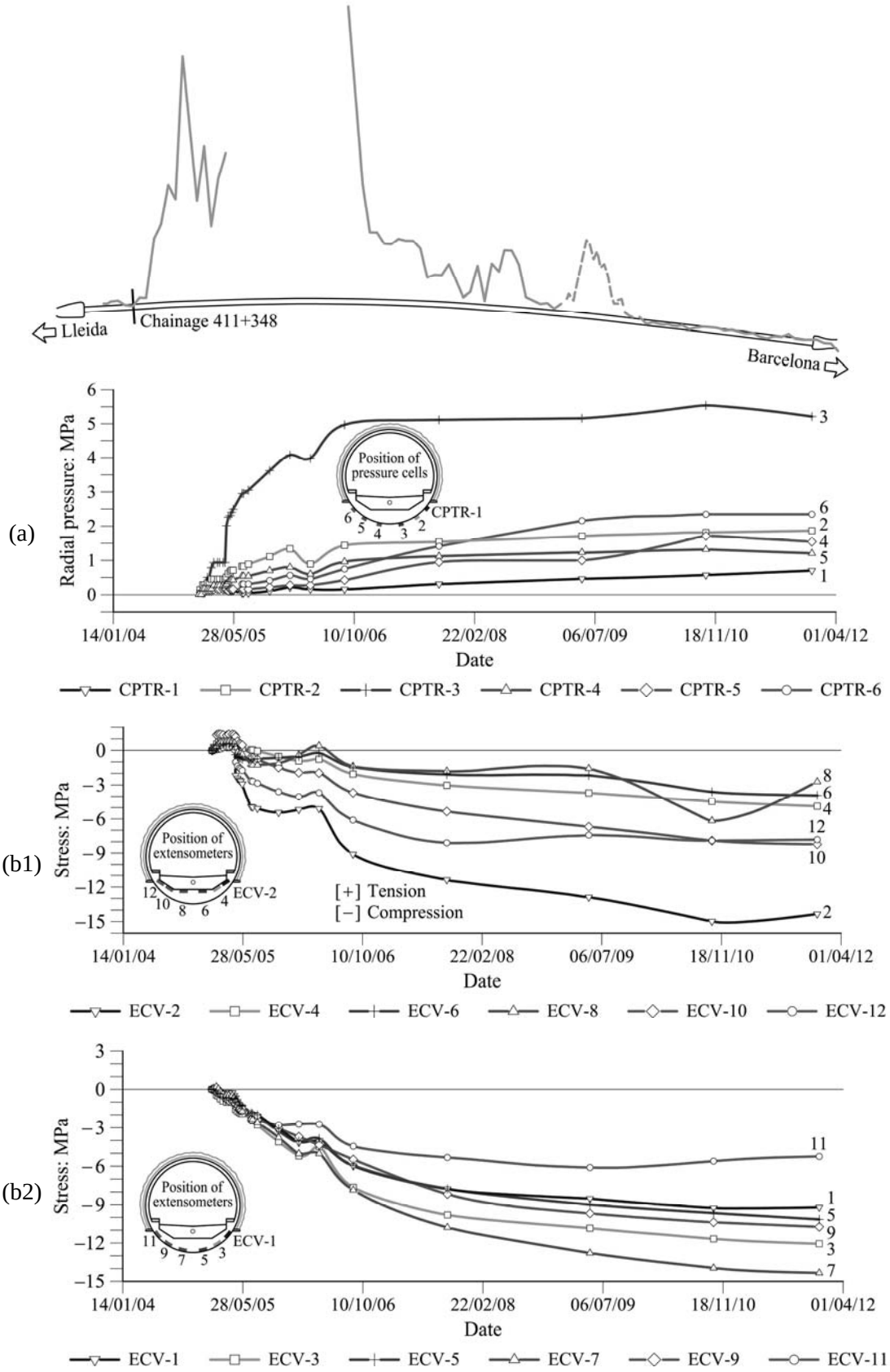

Figure 3.32. Monitoring results of reinforced Lilla tunnel. Chainage 411 + 348 (see also Figure 3.2): (a) pressure cells; (b) stresses in reinforcement

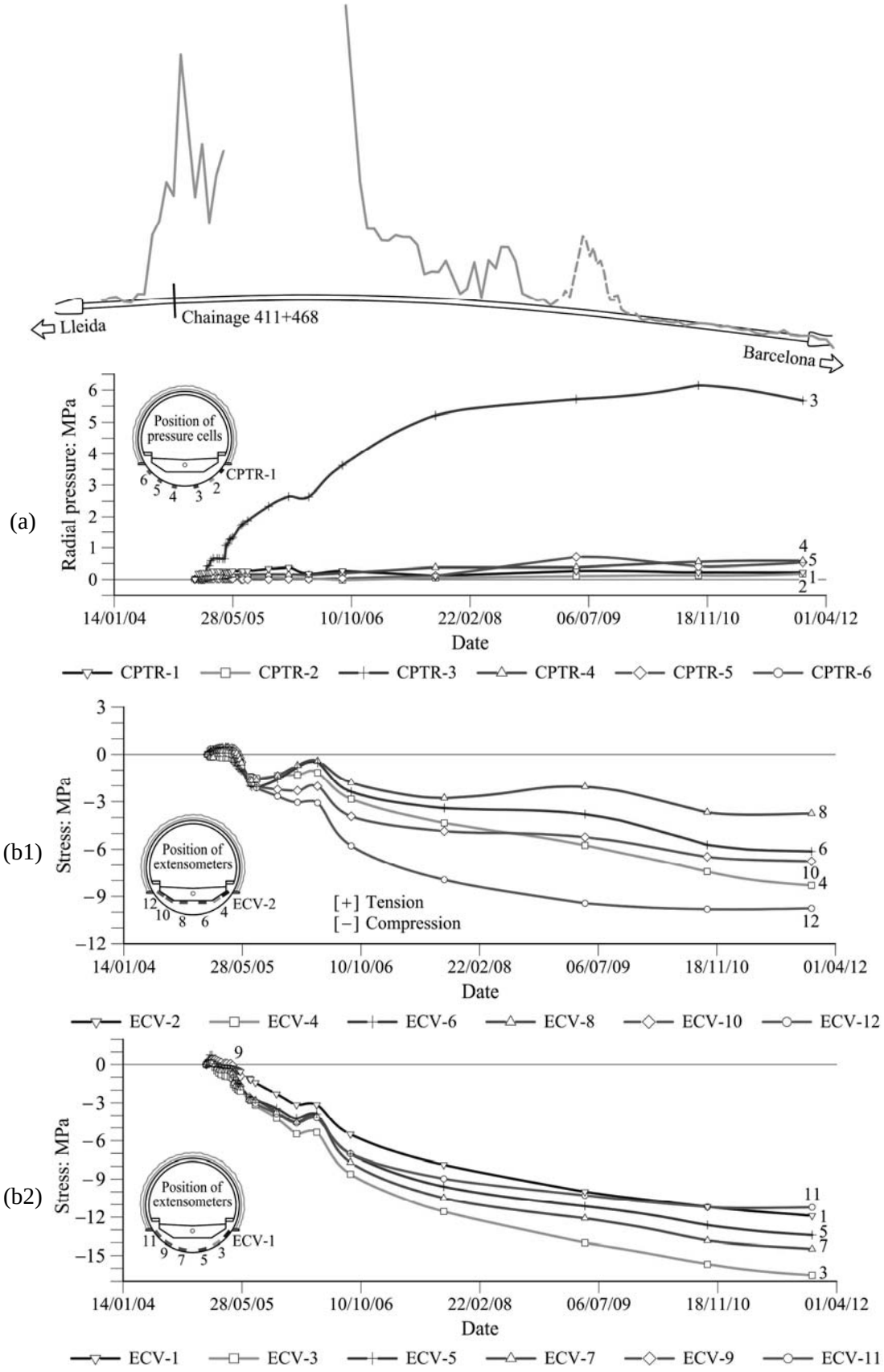

Figure 3.33. Monitoring results of reinforced Lilla tunnel. Chainage 411 + 468 (see also Figure 3.2): (a) pressure cells; (b) stresses in reinforcement

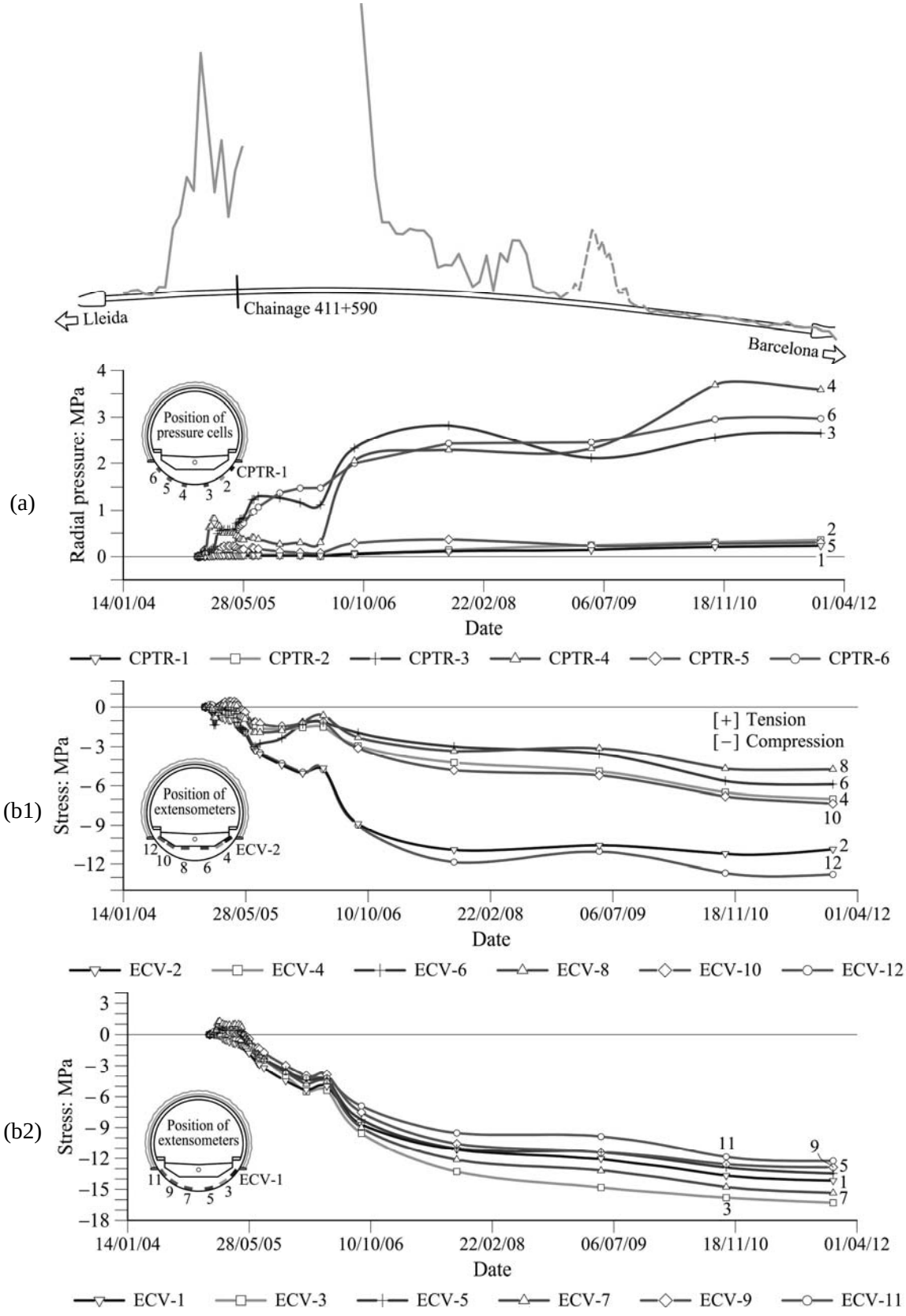

Figure 3.34. Monitoring results of reinforced Lilla tunnel. Chainage 411 + 590 (see also Figure 3.2): (a) pressure cells; (b) stresses in reinforcement

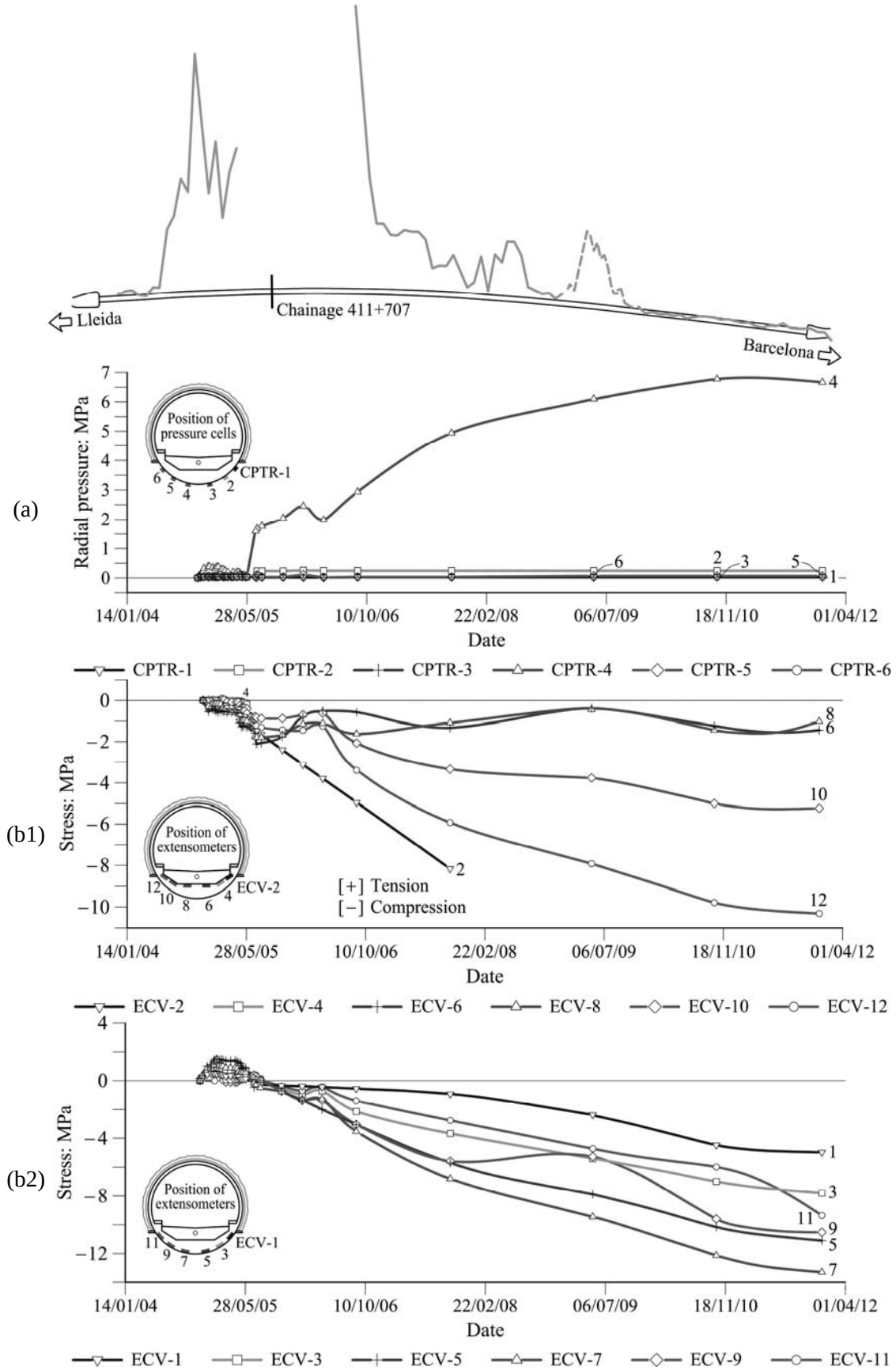

Figure 3.35. Monitoring results of reinforced Lilla tunnel. Chainage 411 + 707 (see also Figure 3.2): (a) pressure cells; (b) stresses in reinforcement

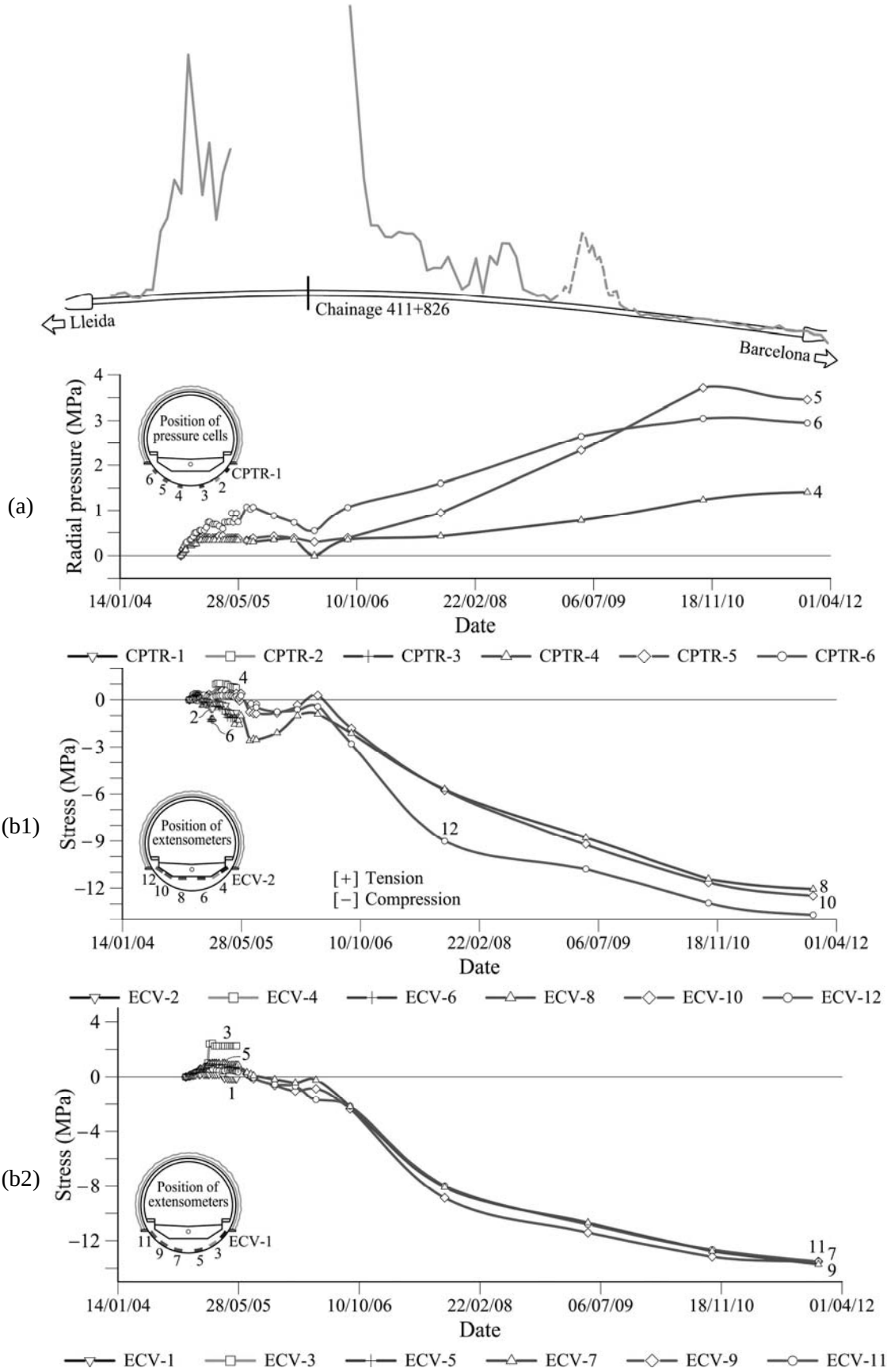

Figure 3.36. Monitoring results of reinforced Lilla tunnel. Chainage 411 + 826 (see also Figure 3.2): (a) pressure cells; (b) stresses in reinforcement

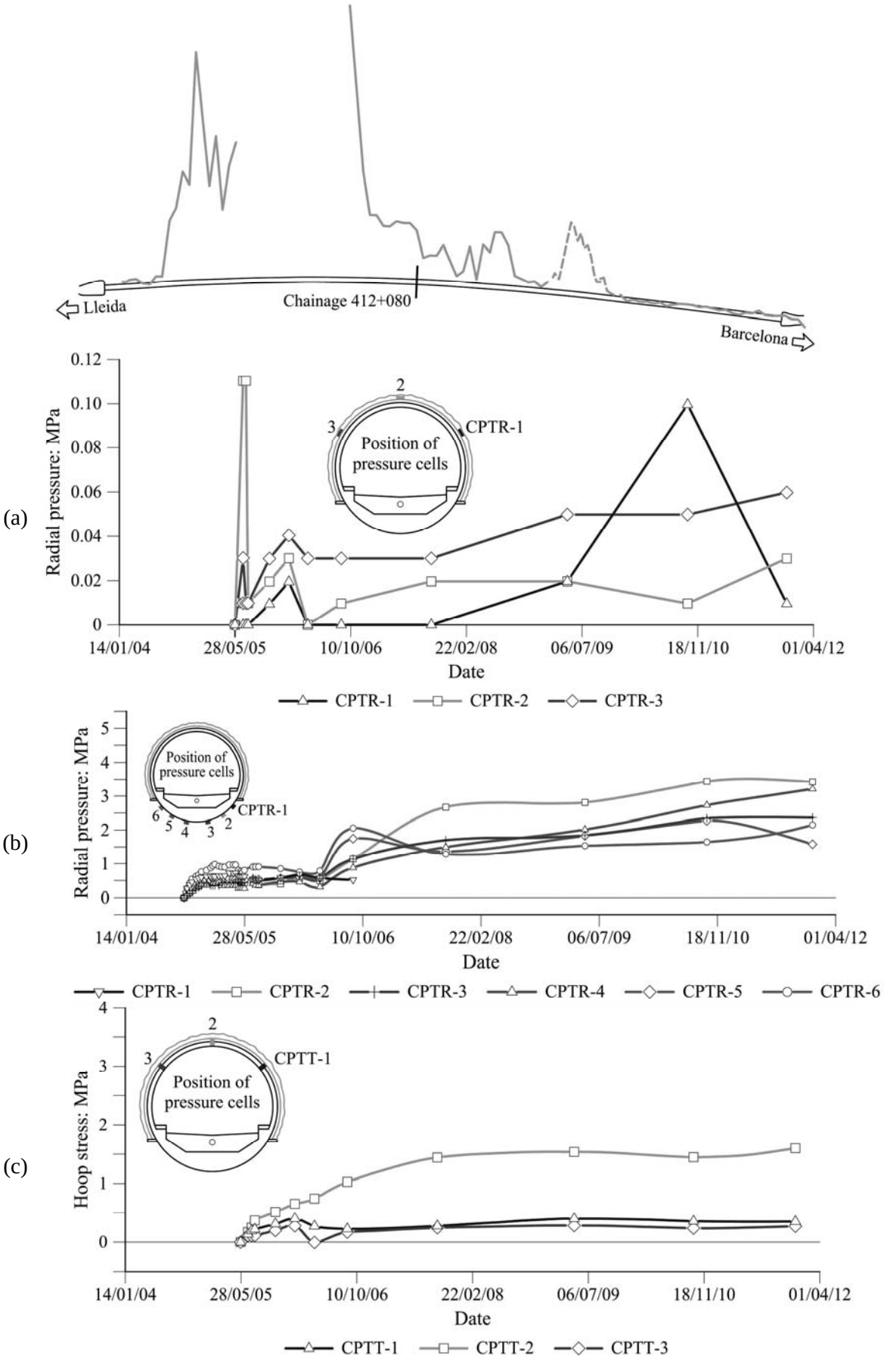
Lleida
Chainage 412+080
Barcelona
(a)
Radial pressure: MPa
0.12
0.10
0.08
0.06
0.04
0.02
0
Position of pressure cells
CPTR-1
2
3
14/01/04
28/05/05
10/10/06
22/02/08
06/07/09
18/11/10
01/04/12
Date
CPTR-1
CPTR-2
CPTR-3
(b)
Radial pressure: MPa
5
4
3
2
1
0
Position of pressure cells
CPTR-1
6
5
4
3
2
14/01/04
28/05/05
10/10/06
22/02/08
06/07/09
18/11/10
01/04/12
Date
CPTR-1
CPTR-2
CPTR-3
CPTR-4
CPTR-5
CPTR-6
(c)
Hoop stress: MPa
4
3
2
1
0
Position of pressure cells
CPTT-1
2
3
14/01/04
28/05/05
10/10/06
22/02/08
06/07/09
18/11/10
01/04/12
Date
CPTT-1
CPTT-2
CPTT-3

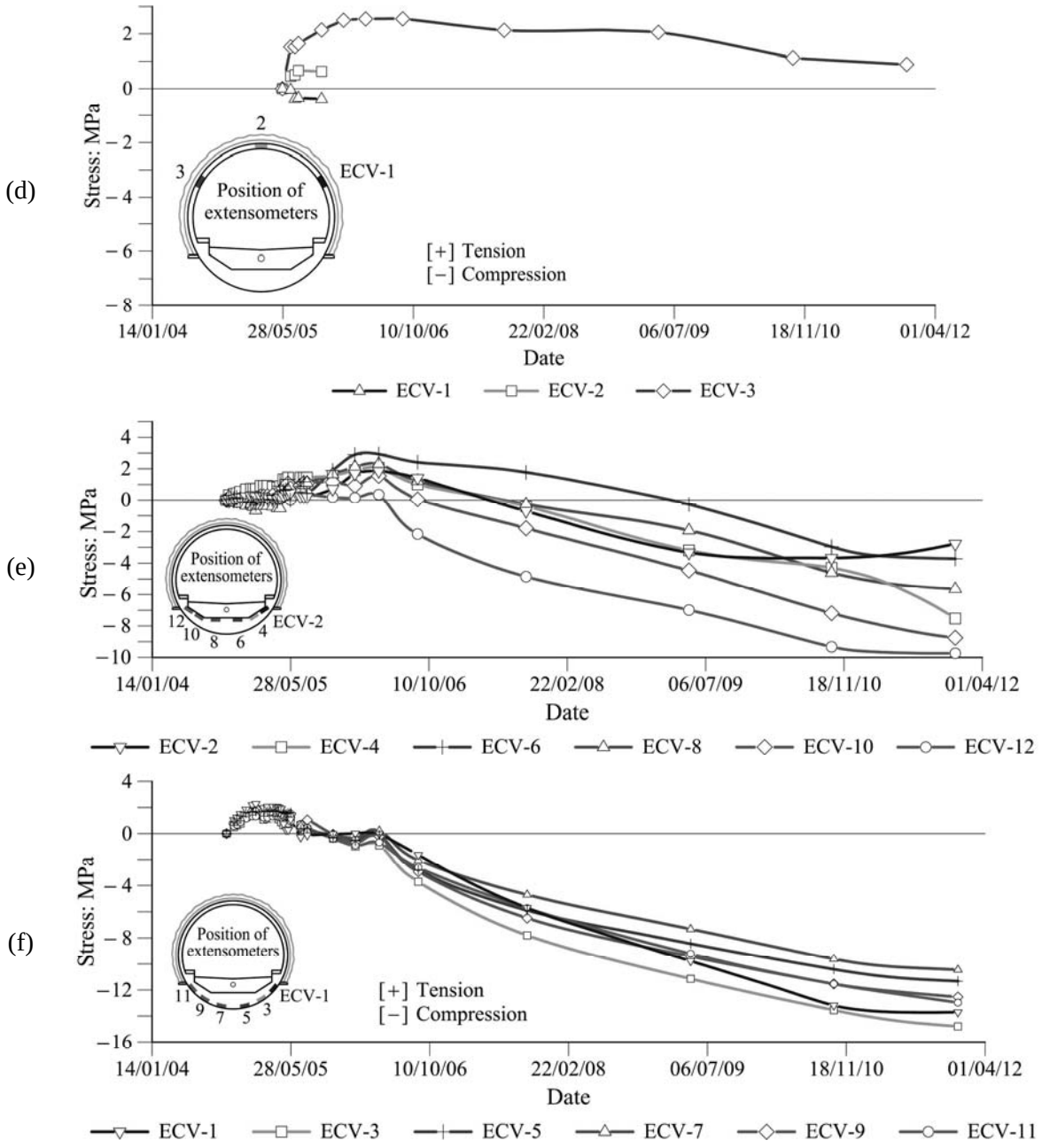

Figure 3.37. Monitoring results of reinforced Lilla tunnel. Chainage 412 + 080 (see also Figure 3.2): (a) radial pressures against vault; (b) radial pressures against invert; (c) hoop stresses in vault; (d) stresses in vault reinforcement; (e) and (f) stresses in invert reinforcement

Levelling of the rail tracks performed routinely since the beginning of the commercial operation of the railway line in February 2008 do not indicate any observable deformation in the Lilla tunnel.

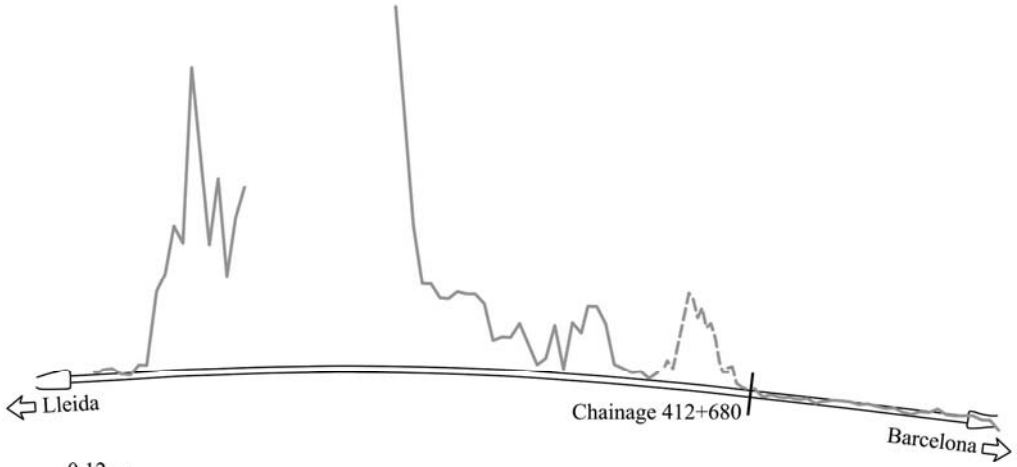
Lleida
Chainage 412+680
Barcelona

(a)

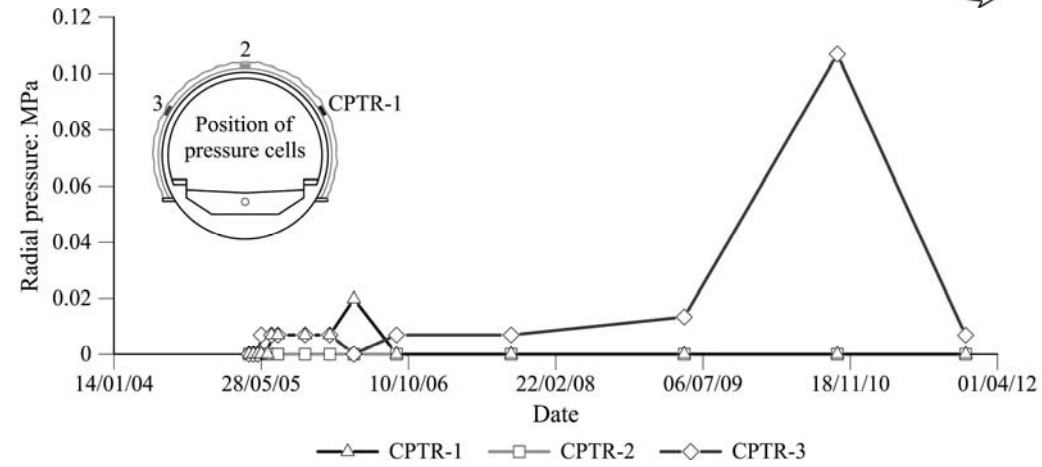
Radial pressure: MPa
0.12
0.10
0.08
0.06
0.04
0.02
0
2
3
CPTR-1
Position of pressure cells
14/01/04
28/05/05
10/10/06
22/02/08
06/07/09
18/11/10
01/04/12
Date
CPTR-1
CPTR-2
CPTR-3

(b)

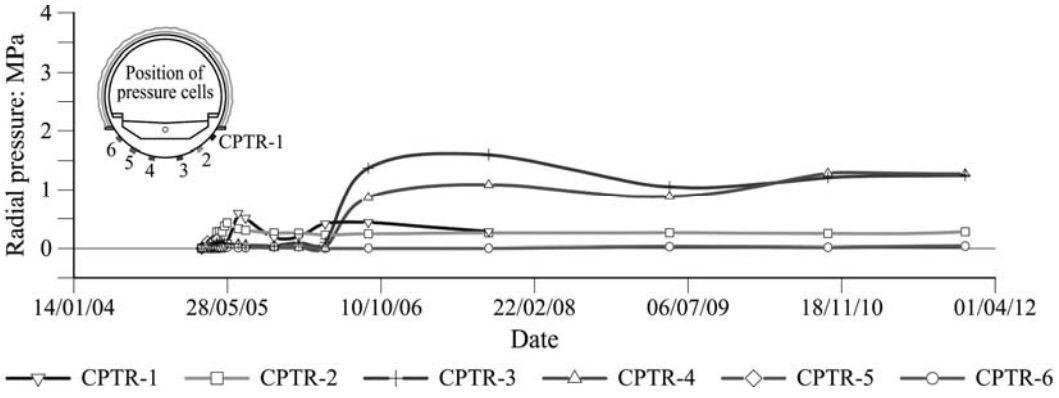
Radial pressure: MPa
4
3
2
1
0
Position of pressure cells
CPTR-1
6
5
4
3
2
14/01/04
28/05/05
10/10/06
22/02/08
06/07/09
18/11/10
01/04/12
Date
CPTR-1
CPTR-2
CPTR-3
CPTR-4
CPTR-5
CPTR-6

(c)

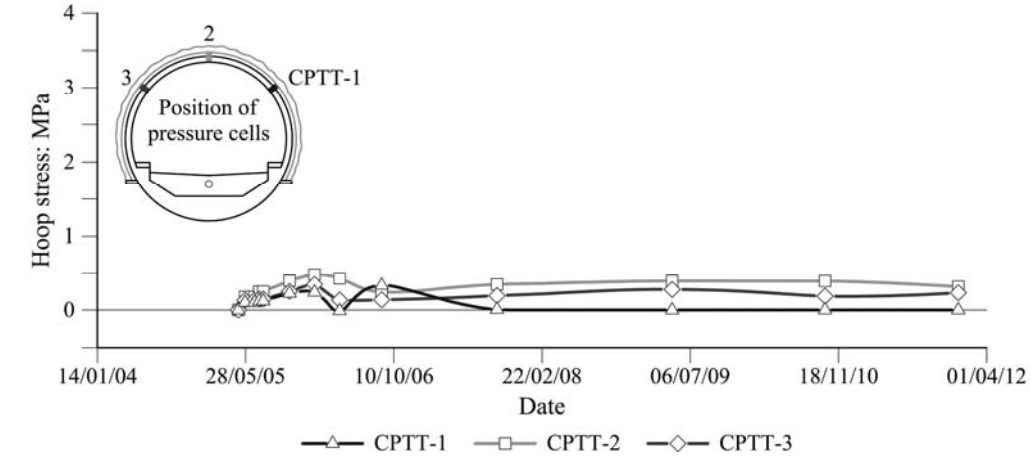
Hoop stress: MPa
4
3
2
1
0
2
3
CPTT-1
Position of pressure cells
14/01/04
28/05/05
10/10/06
22/02/08
06/07/09
18/11/10
01/04/12
Date
CPTT-1
CPTT-2
CPTT-3

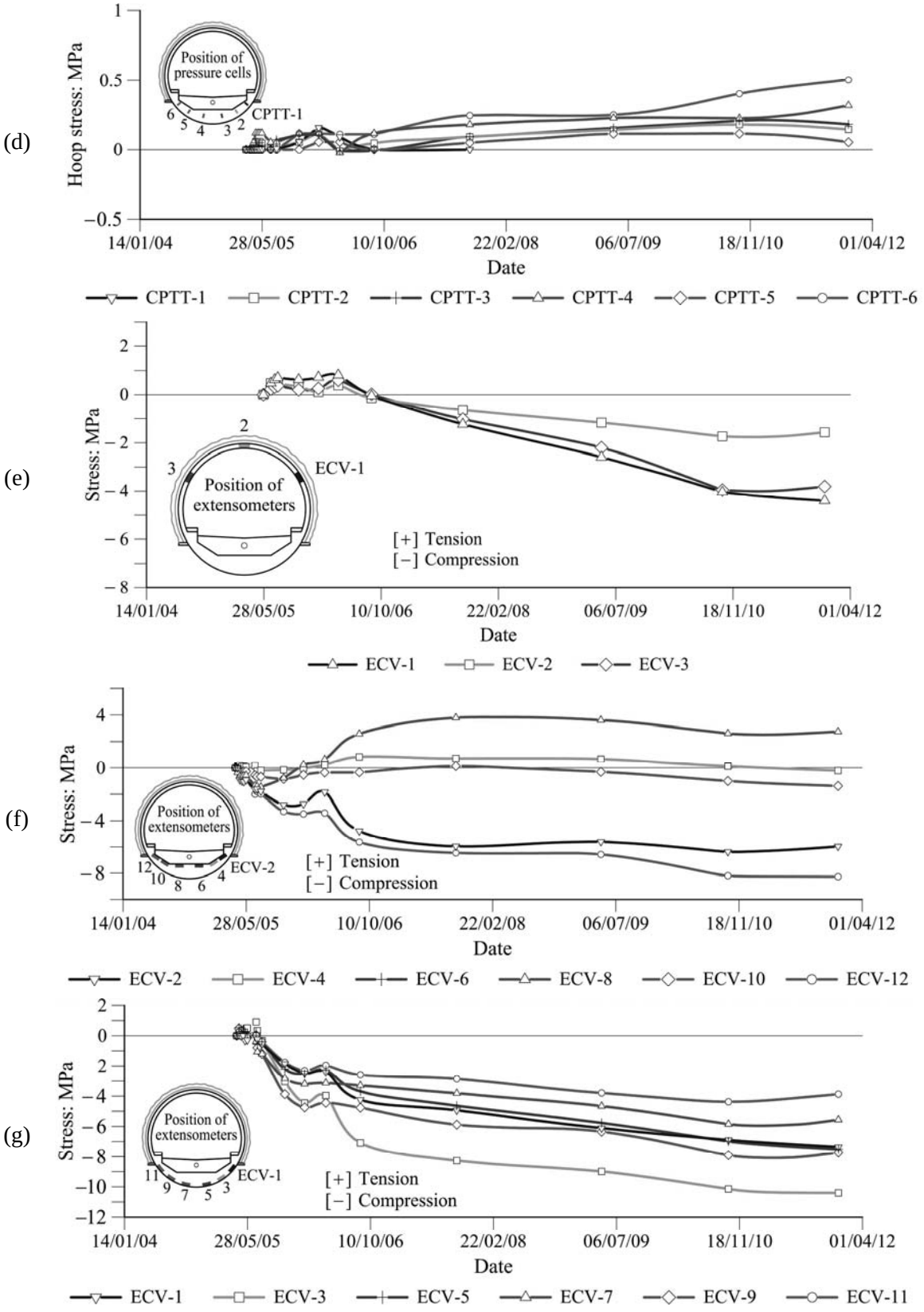

Figure 3.38. Monitoring results of reinforced Lilla tunnel. Chainage 412+680 (see also Figure 3.2): (a) radial pressures against vault; (b) radial pressures against invert; (c) hoop stresses in vault; (d) hoop stresses in the invert; (e) stresses in vault reinforcement; (f) and (g) stresses in invert reinforcement

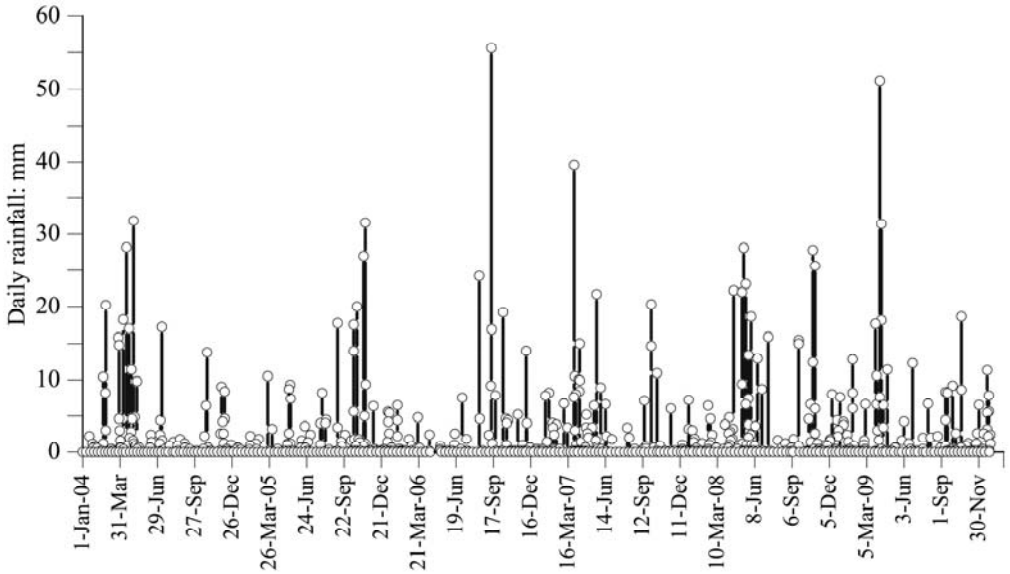

Figure 3.39. Daily rainfall measured in the vicinity of Lilla tunnel during the period January 2004 – January 2010. Data provided by the Servei Meteorològic de Catalunya

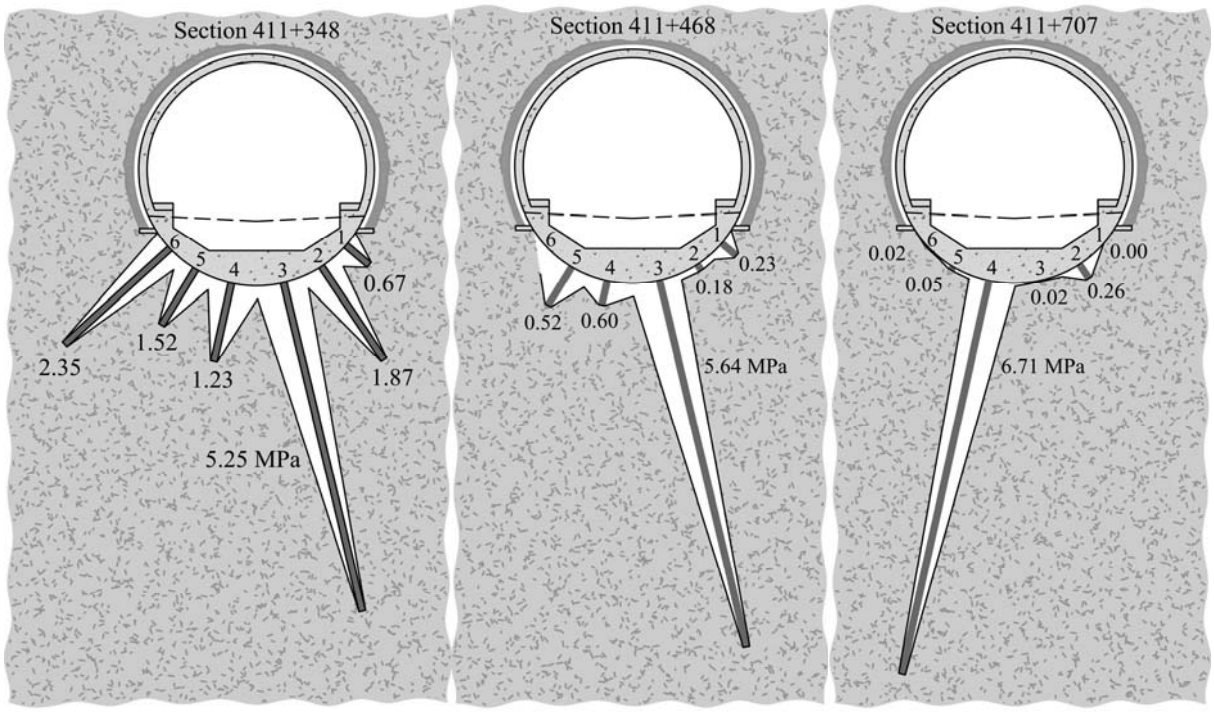

Figure 3.40. Measured distributions of radial pressures in the three sections indicated in Dec. 2011

3.11 Conclusions

The case of Lilla tunnel has provided interesting information on the initiation and characteristics of swelling phenomena in tunnels excavated in anhydritic claystone. The

lessons learned support, in part, existing knowledge and experience gained in Western and Central Europe, as described in references given in the Chapter. The geologic formation involved at Lilla (a Tertiary claystone) is substantially younger than the Triassic evaporitic claystone described in the mentioned references. In general terms, Triassic materials have experienced a more intense tectonic activity than Eocene sediments. Lilla tunnel is located on the border of a large basin (the Ebro basin), which is dominated by horizontal layering. Tertiary evaporitic claystones in the central part of the basin are known to have experienced a limited tectonic activity after deposition. However, the border position of Lilla dramatically changes the situation, which has been illustrated in Figure 3.1. This is an indication of the relevance of internal shearing and damage of sulphated rocks in the development of swelling phenomena triggered by tunnelling (see Chapter 5).

Published field heave records of tunnels may exhibit a very slow development. Berdugo (2007) compared data of heave measurements from different cases. This comparison indicated that Lilla provided one of the fastest rates of development of floor heave and swelling pressures against the invert. Decisions during reconstruction of Lilla tunnel were taken on the basis of observations extending a few years, but the collected experience in other tunnels was also present during the process of reinforcing the tunnel. A few years may be a relatively short time to investigate the swelling process but it is a long time to adopt design decisions for a new high speed railway line. Nevertheless, the field data obtained during the design stage was very relevant for design. For instance, a significant proportion of time records of swelling pressures exhibited trends indicating the proximity of asymptotic swelling pressure values. These records provided invaluable help to establish design criteria which has worked satisfactorily up to date as discussed in some detail in the section devoted to interpret the performance of the reinforced tunnel. Lining stress records reported in the Chapter are 10 years old and they show a stressing far below the design calculations. It can be concluded that the reinforcement design was very conservative but this is a conclusion which could hardly be reached at the time of designing the reinforcement.

The explanation of the swelling mechanisms and the conditions leading and favouring the expanding phenomena in sulphated rocks and in particular in the case of Lilla tunnel are analysed in Chapter 5.

CHAPTER 4

Heave of a railway bridge induced by gypsum crystal growth: Field observations

The investigation on the mechanisms involved in the swelling behaviour reported in several tunnels crossing sulphated formations was extended to another relevant case namely the heave experienced by Pont de Candí railway bridge, located next to Lilla tunnel North Portal.

The central pillars of a bridge belonging to a recently built high-speed railway line experienced an unexpected and continuous heave after the end of construction. Pillars were founded on 3x3 pile groups capped by a rigid slab. The tips of piles supporting the central pillars reached a hard Tertiary anhydritic claystone. Deep extensometers allowed the identification of an active layer, 12-15 m thick, located below the pile tips. Observations in recovered cores suggest also that heave is induced by the growth of gypsum crystals in discontinuities of the anhydritic claystone. No heave was observed in gypsum rich claystones located above the anhydritic layer. Heave rate has been reduced to a small value by the weight added by an embankment 33 m high which partially fills the original valley. The geotechnical investigation campaign, “in situ” tests and field observations are described in this Chapter.

The case will be discussed again later in the Thesis. A hypothesis explaining the role of the bridge construction in the triggering of a dormant heave phenomenon will be described in Chapter 5. In Chapter 7 a model developed to consider the generation of deformations from the precipitation of gypsum crystals will be described in detail and the measured heave in Pont de Candí will be simulated.

4.1 Introduction

Soon after the end of construction, a long railway bridge, founded on large-diameter (1.65 m) bored piles, 20 m long, experienced a sustained heave of its central pillars. Trains are expected to circulate at speeds in excess of 300 km/h over the bridge, and therefore the problem raised by the unexpected heave was of great concern.

The case is believed to be unique, and no reference to similar cases has been found in the literature. The closest case histories have been described in connection with tunnel performance in claystones containing sulphate species, mentioned in previous Chapters. They provided an interesting background for the case described here; however, it was also found that the understanding of the heave phenomena and the modelling capabilities were insufficient to explain the observations of bridge behaviour and to design remedial measures. Recently, a case of damage to an historic town induced by drilling through anhydrite formations, which has some similarities to the case described here, has been reported by Sass & Burbaum (2010). The French town of Lochviller is experiencing also heave which is apparently being related to the development of expansions in an anhydritic stratum.

The chapter starts with a description of the problem. The bridge and its heavy piled foundation will be described, as well as the initial levelling measurements that triggered the alarm. Then, the geology and the geotechnical properties of the foundation soils and rocks will be given. Field observations of the ground heave at the soil surface and at depth will be presented and discussed as well as the results of cross-hole hydraulic tests performed. The basic heave mechanism has been associated with gypsum crystal growth at depth, below the piles tip. The origin of the swelling behaviour is a complex phenomenon, which will be described and supported by field observations and some laboratory tests. The chapter ends by describing some remedial measures adopted to reduce the heave rate experienced by the bridge.

The case is further analysed in Chapter 5 and Chapter 7, which describe a conceptual scenario for the heave mechanism. The problem will be cast in terms of equilibrium and conservation equations in a porous media whose solid component includes inert particles, as well as soluble components (anhydrite and gypsum) able to dissolve or precipitate. Model calculations will be compared with actual field heave records in Pont de Candí.

4.2 Bridge performance

One of the main bridge structures of the recently built Madrid-Barcelona high-speed railway in Spain is the Pont de Candí viaduct (Figure 4.1). It is located between the Camp Magré tunnel and the Lilla tunnel; these tunnels also experienced swelling problems (Alonso et al., 2004, 2007). The bridge was built in the period 2001-2002. The construction of the viaduct finished in July 2002. The bridge deck was set in place by a pushing method. The double railway line is supported by a prestressed continuous trapezoidal concrete box girder, 413 m long, having ten spans (35 m; 8 spans of 43 m; and 34 m), which is anchored in one abutment (Figure 4.2). In plan view the bridge has a constant curvature radius of 7250 m and a longitudinal descendent constant gradient of 1.815% from abutment E1 to E2 (Figure 4.2).

The upper deck is supported by long pillars (pillars P1 to P9); the height of the pillars varies from 11 m to a maximum of 55.9 m in the centre of the valley (pillar P5). The pillars have a rectangular box cross section of 3.5 × 5.9 m at the top. Each of the bridge pillars is supported by a group of 3 × 3 large-diameter (1.65 m) bored piles, 20 m long on average, as shown in the longitudinal profile in Figure 4.3. In pillars P1, P2 and P9, the thickness of the pile cap is 3 m, whereas in pillars P3 to P8, the pile cap thickness is 3.5 m.

Systematic levelling of the railway tracks, carried out by the railway administration immediately after construction, revealed the progressive development of vertical displacements of the viaduct central pillars, especially pillars P5 and P6. Heave profiles plotted in Figure 4.4 for two dates show the pattern of heave, which mainly affected the central pillars. Heave accumulated at rates ranging from 5 to 10 mm/month.

The reason for this anomalous behaviour was not clear. The massive deep foundations of the pillars could hardly experience significant vertical displacements induced by a shallow swelling layer. In fact, the piles were socketed in a rigid stratum of anhydritic claystone, which could resist any swelling strains that might exist along the pile shafts.

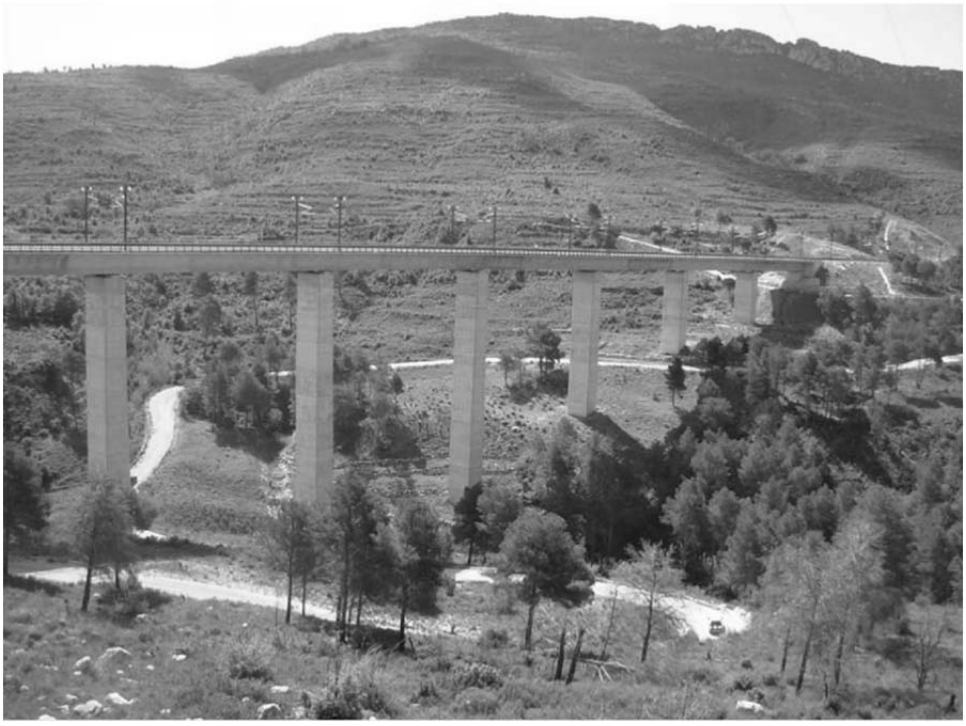

Figure 4.1 The Pont de Candí viaduct in December 2007

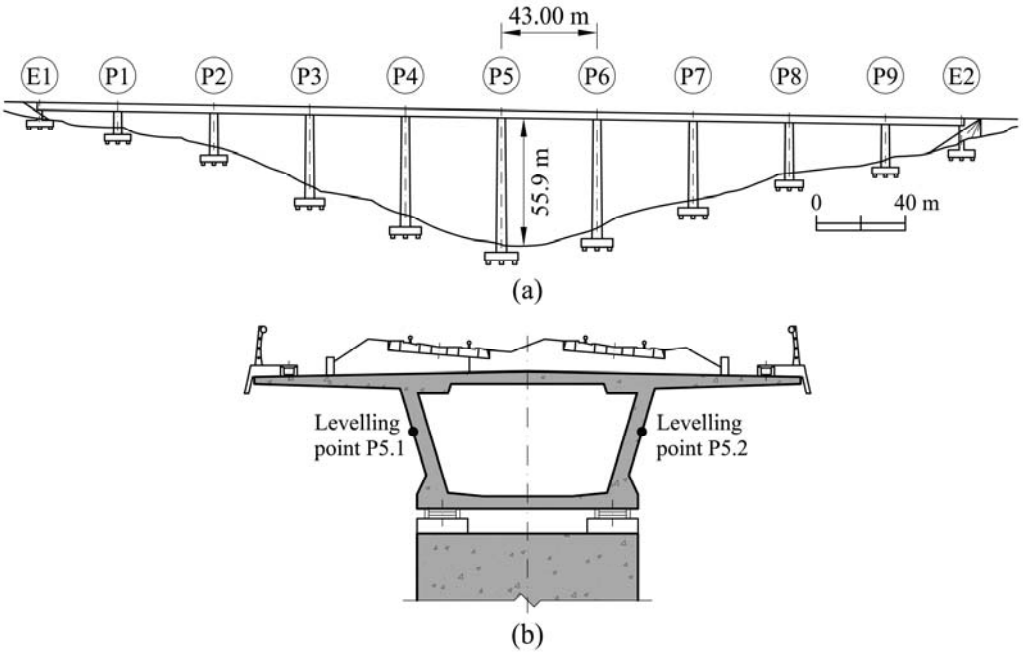

Figure 4.2. Pont de Candí viaduct: (a) longitudinal section; (b) cross-section

Levelling records of the bridge deck indicated that pillars were also experiencing small rotations and not only a vertical displacement. Horizontal displacements in longitudinal and transversal direction were also measured at the top of central pillars (Table 4.1). The deck was supported by means of bearings that were free to move in the longitudinal direction. The observed pillar rotation was a result of the rotation of the pile cap. Table 4.1 indicates that the

distance between pillars P5 and P6, at the deck level, was opening at an average rate of 12 mm/year. However, the bearings restrained the motion in the transversal direction. As a result, the pillar rotations led to a relative motion between deck and pillar, which was resisted by the restraining system of the deck bearings. The support system was close to its strength limit in August 2008.

The progressive heave was compensated at the bridge deck level by shortening the bearing supporting structures. There is a limit to this solution, and it became clear that a geotechnical remedial measure had to be found.

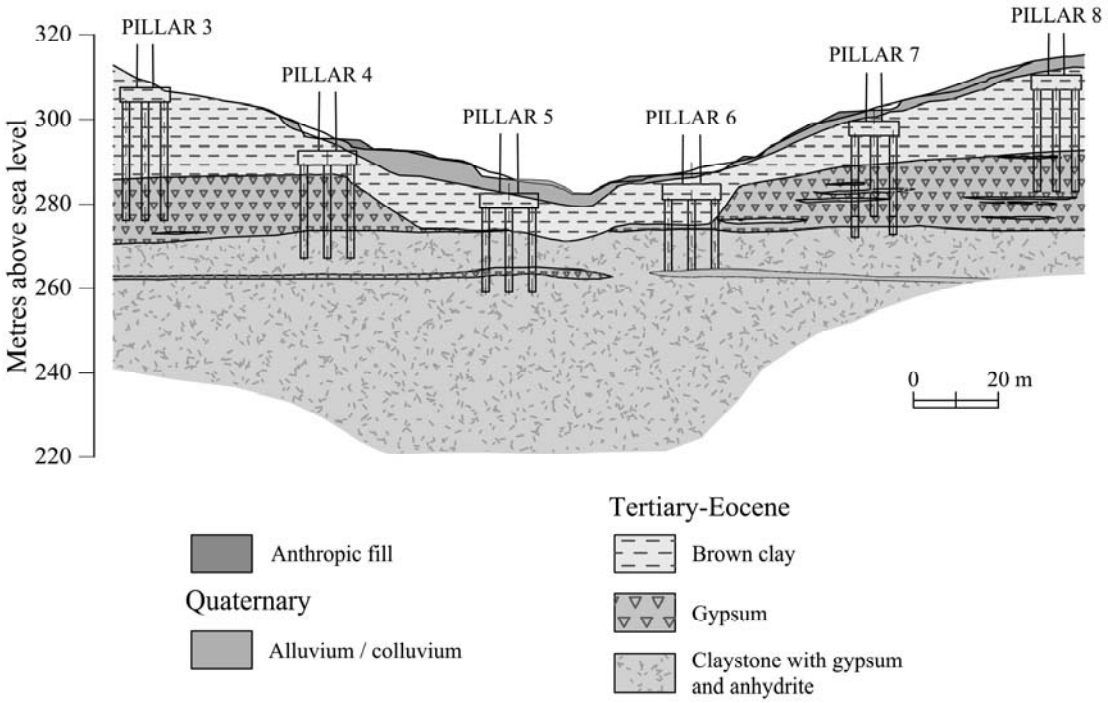

Figure 4.3. Geological profile along Pont de Candí viaduct

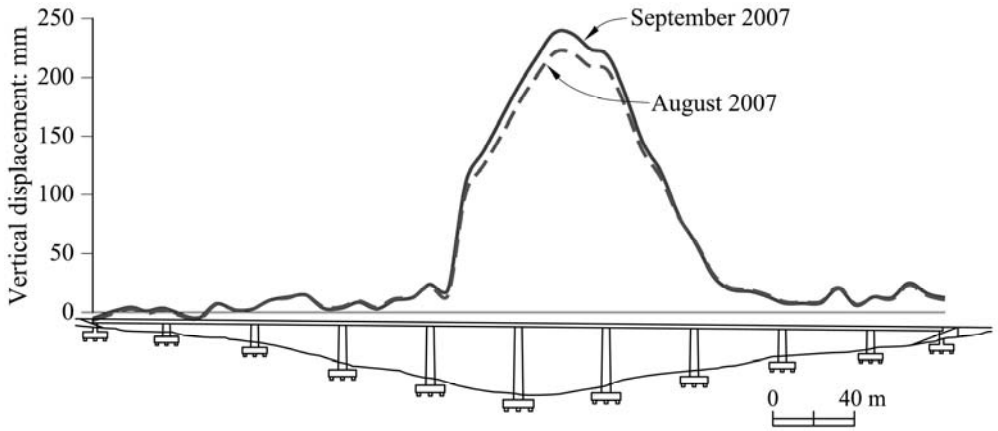

Figure 4.4. Heave profiles in August and September 2007. Initial reading: September 2002

Table 4.1. Measured longitudinal and transversal movements at the top of central pillar for the period September 2002 to August 2007. Positive longitudinal movements follow the direction from abutment E1(North) to E2 (South). Positive transversal displacements go towards the East direction (Figure 4.2).

Measurement point in pillar (Top of pillar, close to deck)	**Longitudinal displacement (cm)**	**Transversal displacement (cm)**
P4	-9.60	5.00
P5	-21.96	6.50
P6	36.70	-2.10
P7	7.30	5.00

4.3 Geological background

The valley crossed by the bridge is located in the eastern boundary of the large Ebro River depression. The valley is the result of intense tectonic action which resulted in faults and folded strata. Sediments belong to old Tertiary formations. Piles were founded on the so-called "Red Formation", which belongs to the lower-medium Eocene. Red claystones, with variable contents of gypsum and anhydrite, dominate the red formation. Thin levels of sandstone, poorly cemented, are also present at the bottom of this formation. At the top, white fibrous veins of gypsum exhibiting a high lateral continuity are found. Often these veins are arranged in a lattice, which is the result of tectonic thrust. Covering these materials and partially filling the paleo-relief, alluvium and colluvium soils of moderate thickness are found. These Quaternary deposits are described as a mixture of a silty and sandy clay matrix, limestone gravels and boulders, which have not experienced long transport distances.

Structurally the valley is located between the Ebro River depression and a mountain range, subparallel to the Mediterranean coast, known as the “Prelitoral” chain. Horst (elevations) and graben (trenches) structures affect Tertiary formations, as well as more ancient rocks. The Pont de Candí valley is the result of intense tectonic action, which resulted in faults crossing the valley and folded claystones.

The geological profile along the bridge established with the help of data provided by the borings performed will now be described in more detail (from top to bottom; refer to Figure 4.3).

4.3.1 Quaternary sediments

A relatively thin mantle of colluvium soils (its average thickness is around 3 m) covers most of the valley slopes and bottom. Its maximum thickness is 6 m, between pillars P4 and P5. The colluvium is a mixture of a low plasticity silty clay matrix and subangular gravels and blocks whose size varies widely from a decimetre- to a meter-based scale. A stream of alluvium soils covers the bottom of the valley. Its composition is similar to the colluvium although blocks tend to be smaller and rounded; the sand/silt content of the fine matrix also increases.

4.3.2 Tertiary formations

An upper brown plastic clay level follows the Quaternary soils. Bridge foundations are entirely located in Tertiary deposits (Figure 4.3). The upper unit of brown plastic clay increases in thickness from the centre of the valley (5–10 m) to the upper levels (up to 25 m at the position of pillars P3 and P8). The non-clay minerals of this clayey formation include gypsum, dolomite, calcite and quartz.

The profile of Figure 4.3 indicates that this clay layer rests directly on the lower claystone substratum in the central part of the valley. However, an intermediate gypsum layer appears under the valley slopes, suggesting a dissolution of gypsum under the valley bottom by running waters before the upper clay unit was deposited.

The gypsum layer, eroded and dissolved in the central part of the valley, has an average thickness of 15 m. Note the abrupt fossilised slopes in this formation between pillars P4 and P5, and between pillars P6 and P7. The gypsum layer is not homogeneous. Interbedded centimetric clay layers are often found. These clay layers exhibit a significant lateral continuity (tens of metres). X-ray diffraction analysis, as well as optical analysis of thin sheets of samples taken from the gypsum unit also reveal the presence of dolomite, calcite and, in some cases, anhydrite.

The lower hard and cemented substratum is the red claystone unit, which provides the name for the entire Tertiary formations. Cement is provided by sulphates and carbonates. Weathering intensity of upper levels is rated as II-III on a scale from I (unweathered) to VI (fully weathered). In a few cores recovered from the central part of the valley a more intense weathering has locally been reported. Gypsum is present in a network of crossing veins.

A continuous horizontal gypsum layer (0.6–2 m thick) at mean absolute elevation 263 m crosses the red claystone. This gypsum layer divides the claystone unit into an upper and a lower level. The gypsum layer was cut by all the borings performed in the area during the successive geotechnical investigations, except for some borings performed on the central part of the valley between pillars P5 and P6. This feature is interpreted as an indication of past dissolution of gypsum by water infiltrating through a fracture or a fault.

The upper claystone level presents high gypsum content. Microscope analysis of thin sections revealed a secondary origin for the gypsum: it was the result of a previous dissolution of anhydrite and a subsequent precipitation of gypsum. Anhydrite was not detected in this upper level. This upper claystone, which has a higher water content (4 - 9%) than the lower unit, will be referred to in the figures as a 'weathered' claystone level, or a gypsiferous claystone.

In sharp contrast, the lower claystone unit below the thin continuous gypsum level has a high anhydrite content, a lower water content (1.2 - 4%) and an increased strength. Pile tips of pillar P5 cross the dividing gypsum level and enter a few metres into the lower anhydritic claystone formation. Piles supporting pillar P6 reach the thin gypsum layer. The remaining pillars of the bridge are founded either on the upper weathered claystone formation (pillars P4 and P7) or in the upper gypsum layer (pillars P3 and P8).

4.4 Geotechnical properties

Preliminary geotechnical investigations aimed at defining the bridge foundation started in October 1999. The first two boreholes were located in both bridge abutments and reached a shallow depth (10 m). It was initially suggested that the bridge pillars should be supported by means of spread footings. An additional site investigation was performed in 2001. The initial geotechnical report at the bridge design stage (1999-2001) was based on 12 boreholes (one per pillar –except for pillar P1, where two borings were drilled– plus two boreholes in abutments). Identification and strength tests (unconfined and triaxial undrained tests), as well as sulphate and carbonate content tests, were conducted on some of the recovered samples.

Reference was made in the geotechnical report to an intense network of fibrous gypsum precipitated in a system of fractures. These fractures were linked with the horst-graben tectonism mentioned before. It was estimated that the network of gypsum veins provided an increased strength of the claystone.

A longitudinal geotechnical profile was developed, and the pile foundation was defined. Piles were conservatively designed on the basis of the undrained strength determined in tests. The unconfined compression strength of samples recovered in the claystone formation was often greater than 10 MPa. In a few cases, values in the range 0.5 – 10 MPa were measured. Pile length was decided to have the pile tip embedded on the gypsum layer (pillars P3 and P8) or in the claystone formation (pillars P4 to P7). The base resistance of the piles was defined by accepting a conservative undrained strength c_u = 0.5 MPa.

Once the levelling of tracks detected the progressive heave of central pillars, new geotechnical investigations were launched in May 2007. A campaign of levelling observations of pillars and readings in continuous vertical extensometers in several locations was carried out. The necessary borings also provided an opportunity to recover undisturbed samples, and to perform some specific tests. Given the nature of the problem there was a specific interest in knowing in more detail the distribution of sulphated species in the successive layers. The degree of fracturing of the deep substratum was also soon identified as a necessary target of the new geotechnical campaign described later.

The presentation and discussion of results obtained are divided into two parts: the results of tests on recovered samples and cores and field monitoring results.

Most of the new boreholes (Figure 4.5) were performed in the vicinity of the central pillars of the viaduct. However, some borings were located upstream and downstream of the central pillars - following the direction of the valley - at distances of 100–130 m from the position of the pillars. In most of the boreholes, a continuous core was recovered. Some of the cores were paraffin coated and sent to the laboratory for testing.

Index properties of the four main Tertiary geological units (upper brown clays, gypsum layer, gypsiferous claystone and anhydritic claystone) are given in Figure 4.6(a), Figure 4.6(b) and Figure 4.6(c), and in Table 4.2 and Table 4.3. Laboratory results of different borings have been collected in plots showing the variation of a given index with depth.

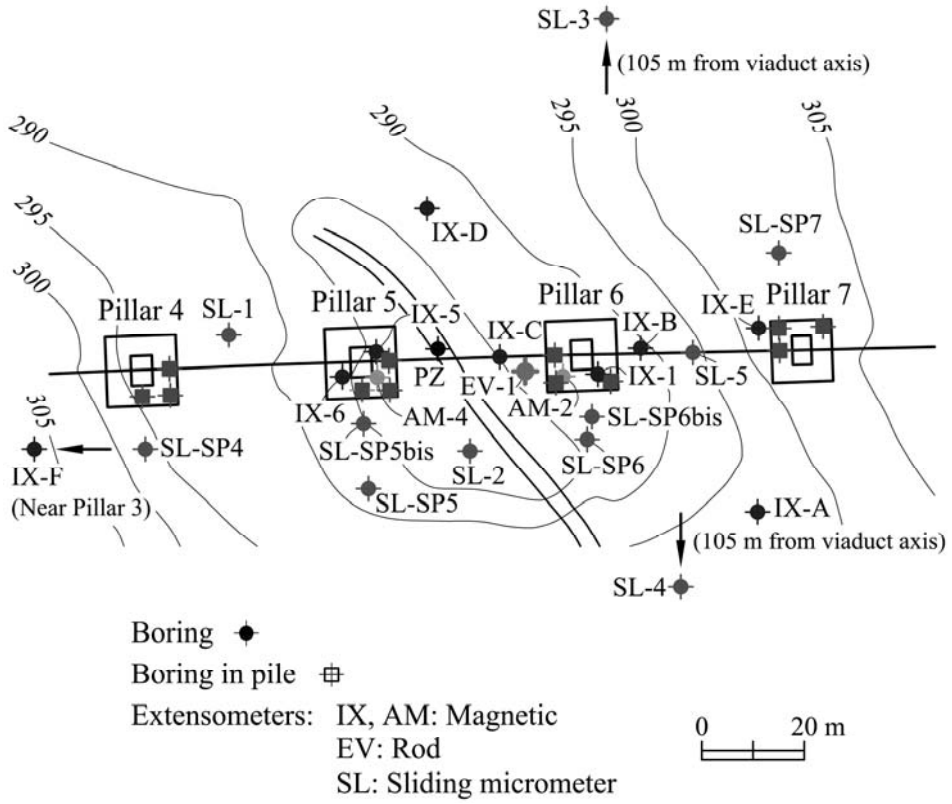

Figure 4.5. Positions of surveying boreholes and deep extensometers

Water content (Figure 4.6(a)) provides a good index to distinguish the different layers. This was determined by heating samples to 60ºC to avoid the dehydration of gypsum, which might distort the results (gypsum dehydrates at slightly more than 100ºC). The hard claystone substratum has a low water content: 4.2%, on average, for the weathered claystone and 2.7%, on average, for the anhydritic claystone. Water content is essentially nil in the gypsum layers. The upper brown clay is a softer material and the water content increases rapidly when moving upwards. These changes are also reflected in the measured dry unit weights shown in Figure 4.6(b).

The degree of saturation was calculated from the measured values of natural unit weight, water content and solid unit weight. The results, which are collected in Figure 4.6(c), show a significant scatter. Values in excess of 100% are an indication of testing errors. Values close to zero are concentrated in elevations where gypsum layers are found. The upper brown clay layer is essentially saturated; however, degrees of saturation consistently lower than 100% are found in the lower claystone layers. This is a significant result, which helps to define a scenario for the observed heave phenomena. Nevertheless, a word of caution should be given here, because at low natural void ratios, small changes in water content result in large changes

in degree of saturation. These minor changes may result from specimen storage and handling in the laboratory.

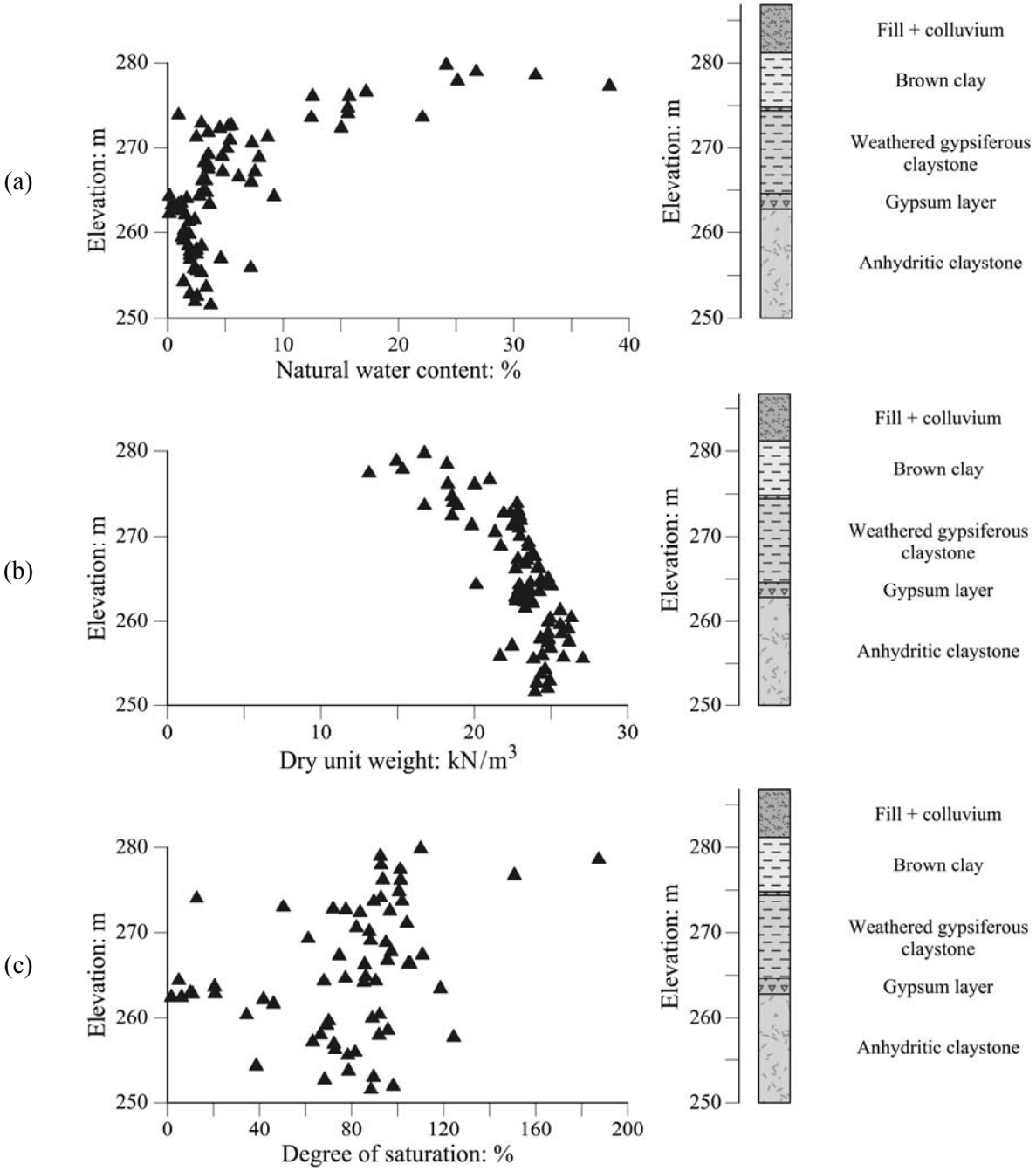

Figure 4.6. Variation of (a) natural water content, (b) dry unit weight and (c) degree of saturation with absolute elevation

Additional identification data are collected in Table 4.2. Mean values and the range of measured indices are given. Almost all the Tertiary materials in the site exhibit a low plasticity. This fact rules out an explanation for the observed heave relying on the hydration

of active clay minerals. The table reinforces also the lack of saturation of the lower red claystone layers.

Table 4.2. Average values and range of index tests for Tertiary formations

Geological formation		**Brown clays**	**Gypsum level**	**Upper red claystone (gypsiferous)**	**Lower red claystone (anhydritic)**
Dry density, ρ_d (g/cm^3)		1.80 (1.31-2.30)	2.41 (2.31-2.51)	2.31 (2.01-2.48)	2.4 (2.17-2.63)
Water content, w (%)		19.8 (11.1-38.2)	-	4.2 (0.3-9.2)	2.7 (1.3-7.2)
Solid specific unit weight, γ_s/γ_w		2.65 (2.57-2.77)	2.63	2.70 (2.60-2.75)	2.70 (2.6-2.8)
Degree of saturation, S_r (%)		~100 (90-100)		78 (5-100)	68 (34-100)
Atterberg limits	w_L (%)	38.7 (30.4-61.1)	-	28.1 (22.1-42.7)	30.5 (23.3-62.7)
	w_p (%)	24.5 (19-40.8)	-	20.1 (14-34.5)	22.4 (17.4-47.6)
	Plasticity index (%)	14.2 (10-20.3)	-	8 (5.6-11)	8.1 (5.2-15.1)
Particle size< 2μm (%)		10.4 (3.2-25.8)	-	7.8 (5-13.4)	6.7 (1.3-13.2)

Mineralogical determinations, as given by quantitative X-ray diffraction analysis, are given in Table 4.3. Estimations based on thin section petrographic analysis were also performed. Observations in thin sections indicated that, in the upper red claystone, residual anhydrite takes the form of inclusions within the gypsum mineral. The gypsum itself was sometimes identified as secondary gypsum (gypsum that results from anhydritic hydration). Secondary gypsum was identified by means of observation in thin sections (anhydritic prismatic pseudomorphs were observed at the edges of isolated secondary gypsum nodules, originally of anhydrite). However, gypsum found in fractures was primary precipitated gypsum mineral.

Table 4.3. Summary of mineralogical analysis (X- ray diffraction and thin sections)

Geological formation	Brown clays	Upper red claystone (gypsiferous)	Lower red claystone (anhydritic)
Gypsum (%)	14	39	16
Anhydrite (%)	0	0	43
Phyllosilicates (%)	12	13	8
Quartz (%)	8	9	4
Feldspar (%)	1	1	0
Calcite (%)	14	1	0
Dolomite (%)	51	36	20

Anhydrite is absent in the upper brown clays and the red gypsum-laden claystone (except for the inclusions mentioned). By contrast, it is the dominant mineral in the lower claystone.

There is a moderate content of clay minerals in all layers. Dolomite is also ubiquitous, and it reaches a maximum concentration in the upper brown clays. The remaining minerals identified (quartz, calcite and feldspars) are present in relatively minor proportions. It turns out that the term "claystone" is not an accurate description in view of the mineral content although it will be maintained for simplicity. The soft rock is essentially a cemented aggregate of sulphate minerals and dolomite, with a low proportion of clay minerals. Concerning phyllosilicates, the following minerals were identified: illite, smectite, chlorite and palygorskite.

4.5 Field observations

4.5.1 Piles and pile caps

In view of the difficulties to find an explanation for the observed upward displacements of the bridge deck, it was decided to investigate the foundation integrity. Attention was initially given to the state of the deep piles in an attempt to find a faulty pile construction. Vertical boreholes were drilled in a position centred with a given pile. The entire pile length was drilled, and concrete cores were recovered. Boreholes also penetrated a few metres into the

natural ground below pile tips (Figure 4.7). Twelve boreholes of this type were drilled in pillars P4, P5, P6 and P7 (three boreholes per pillar).

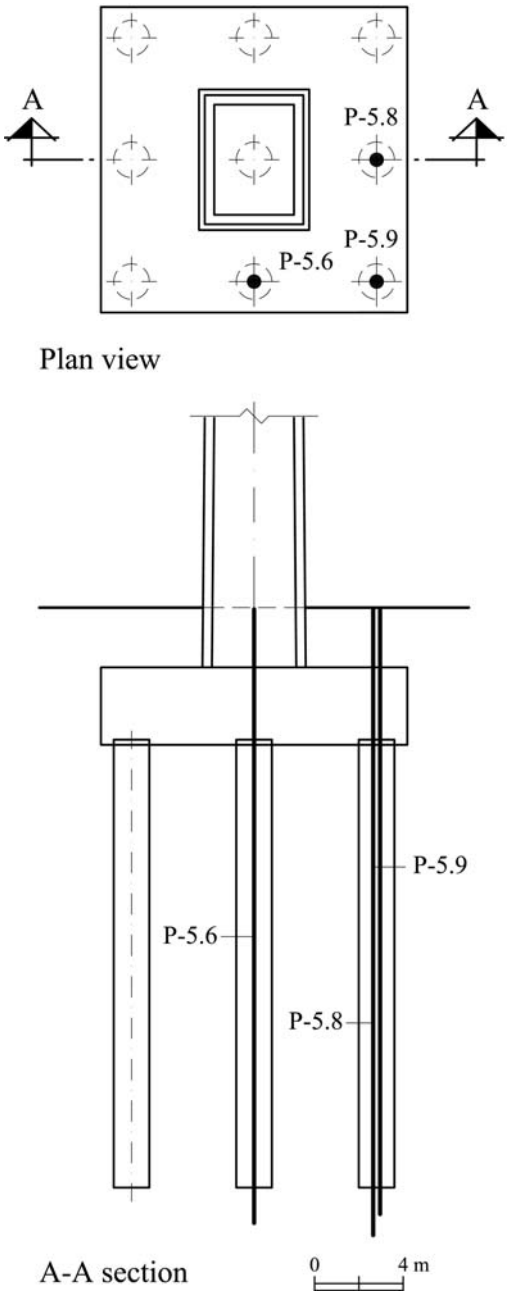

Figure 4.7. Borings drilled through piles of pillar P5

No gaps or cavities were found in any of the boreholes. However, fractures were observed in the cores and also in the walls of the boreholes. Boreholes were inspected by means of a high-resolution acoustic televiewer, a multi-arm caliper and an optical video camera. A crack was often observed at the pile-cap contact plane in most cases. This observation was initially interpreted as an indication of the existence of swelling pressures acting against pile caps. The

swelling pressures would explain the heave of the pillars, the gap created at the pile cap contact and the tensile cracks observed in the pile shafts. The implicit assumption in this explanation, which is illustrated in Figure 4.8(a), is that the piles remained firmly anchored at depths where shafts were excavated in hard claystone.

However, such a high swelling pressure cannot be attributed to the low-plasticity non-active brown clay layer directly in contact with the pile cap. There is an alternative explanation for the cap-pile cracks observed in borings, which is illustrated in Figure 4.8(b). If a non-homogeneous heave displacement of the piles develops, originated below pile tips, a single pile of a group, experiencing the highest heave, would generate a tensile stress in the remaining piles within the group.

Boreholes drilled through the piles were initially filled with water coming from drilling operations. However, once emptied, they all recovered a water level located at approximately 7 m below the surface in piles of P 6 and 16 m in pillar P5. Chemical analysis of the water filling again the boreholes, once emptied after drilling, confirmed that they contained natural ground water. This behaviour was an additional indication of the existence of fractures in the pile's shaft. It was also observed that the speed of water-level recovery in piles belonging to pillars P5 and P6 (those located in the bottom of the valley, and experiencing the greatest heave) was higher than in pillars P4 and P7. These observations may be explained by more severe pile cracking in pillars P5 and P6. A higher permeability of the soil/rock around piles in pillars P5 and P6 would also explain the difference rate of water level recovery.

4.5.2 Water levels

Two open tube piezometers were located in a borehole drilled between pillars P5 and P6 at depths of 14.70 m and 26 m. Water levels in all 12 boreholes drilled through the piles were also measured until stabilisation. Water depth measured in a number of wells located in the bridge area also provided valuable data. In an excavated trench located in the valley bottom, upstream from the bridge alignment, a significant flow rate was observed to enter the trench at a depth of 1.60 m (a second trench, 5 m deep, located downstream from the bridge always remained dry). The set of observations available indicates that a relatively shallow phreatic level, 5 m deep, occupies the lower part of the valley crossed by the bridge. The deep

piezometer also suggests that a deeper water level is found in the weathered claystone at a depth of approximately 14 m below the bottom of the valley.

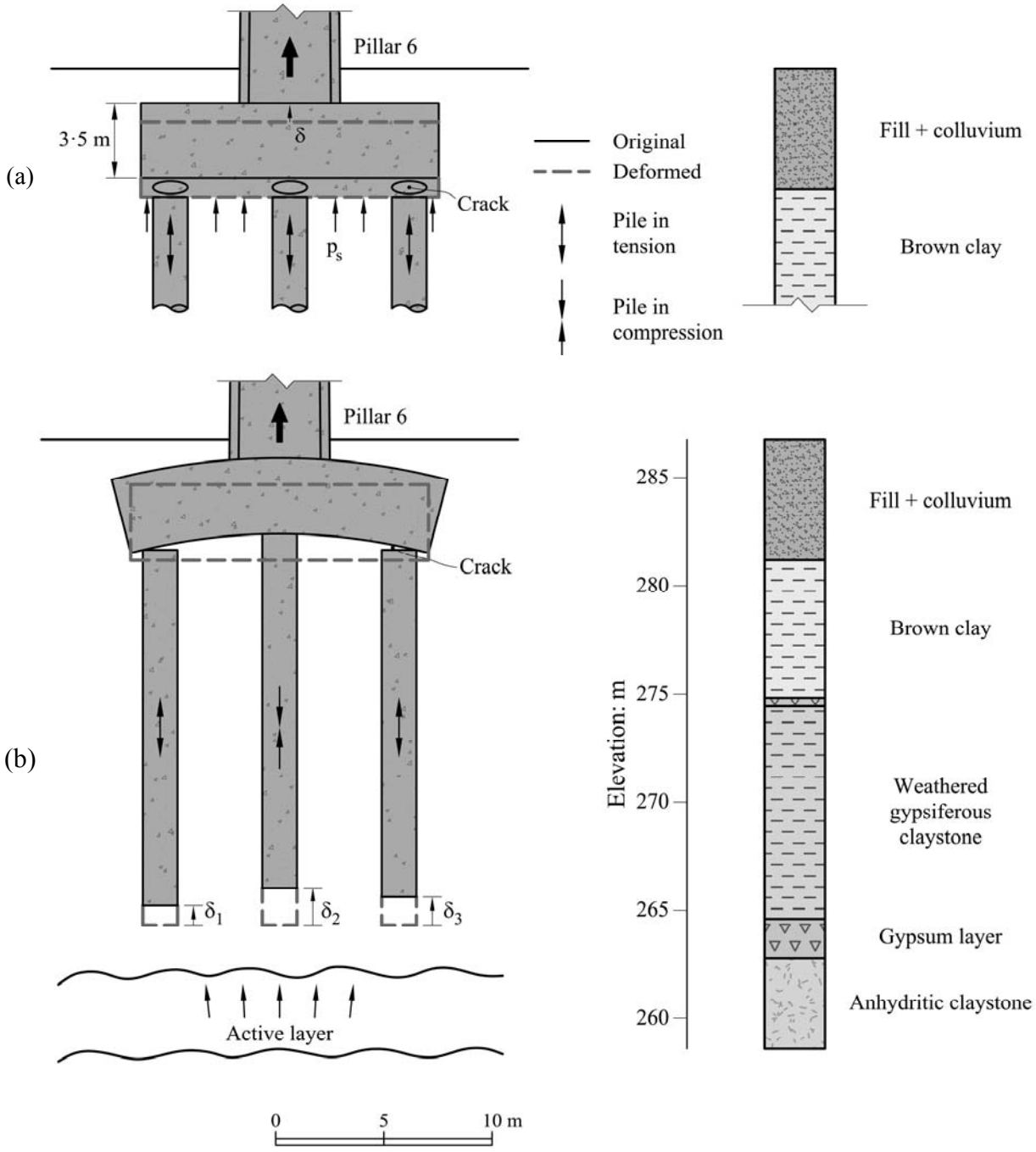

Figure 4.8. Sketches showing two alternative interpretations of foundation-heave interaction. Also shown is the geological profile in the vicinity of pillar P6. (a) Swelling pressure against the pile cap induces tensile strains in piles and lifts the pillar. A crack develops at the pile-cap contact. (b) Piles are pushed upwards because of heave at the deep active zone. Non-uniform heave creates a tensile gap between the cap and piles in most cases

4.5.3 Surface movements

A network of surface topographic marks was installed on the ground surface. The network covers a corridor 200 m wide, centred on the viaduct axis.

Figure 4.9 provides contours of equal vertical displacement at the ground surface measured from 26 November 2007 to 30 April 2008. A maximum value of 44.1 mm of accumulated heave was measured during the first 5 months of monitoring in a topographic mark located 30 m upstream of the viaduct axis, near pillar P5. It corresponds to a heave rate of 8.5 mm/month. During the first 5 monitoring months, significant ground surface heave was measured (9–13mm) at points located 70–90 m far away from the axis of the bridge.

The expanding phenomenon resulted not only in the heave of piles and the viaduct itself, but also in a ground heave. Figure 4.9 also shows the position of levelling marks and bridge pillars; an interpolating program generated the plotted contours. Contours of equal heave may be described as irregular ellipses, whose major axis follows the direction of the valley crossed by the bridge. The centre of these ellipses is not located on the bridge axis, but is displaced in the direction of the slope of the valley bottom. This feature suggests that the natural flow of water in the valley controls the distribution of heave, to some extent.

Heave contours passing through the positions of pillars P3 and P8 mark the limits of observed heave. The geological profile along the bridge axis (Figure 4.3) indicates that the deep foundation of pillars P3 and P8 does not reach the lower claystone formation. In fact, the tip of the foundation piles of these pillars is located within the massive intermediate layer of gypsum. Maximum heave (pillars P5 and P6) is recorded when the pile tips reach the lower anhydritic claystone.

The closure of elliptical heave contours in Figure 4.9 in areas with no direct field information (levelling marks were initially located in a corridor parallel to the bridge direction) is a non-realistic result associated with the “logic” of the interpolation program.

In order to establish better the limits of the heave phenomena in the direction of the valley, additional surface markers were installed in points that followed the direction of the valley upstream and downstream of the bridge location. An additional 9-month period of field measurements provided a more accurate picture of surface heave displacements (Figure 4.10). Contours of equal heave rate measured between 11 July 2008 and 2 April 2009 were very similar to the initial heave displacement contour map given in Figure 4.9.

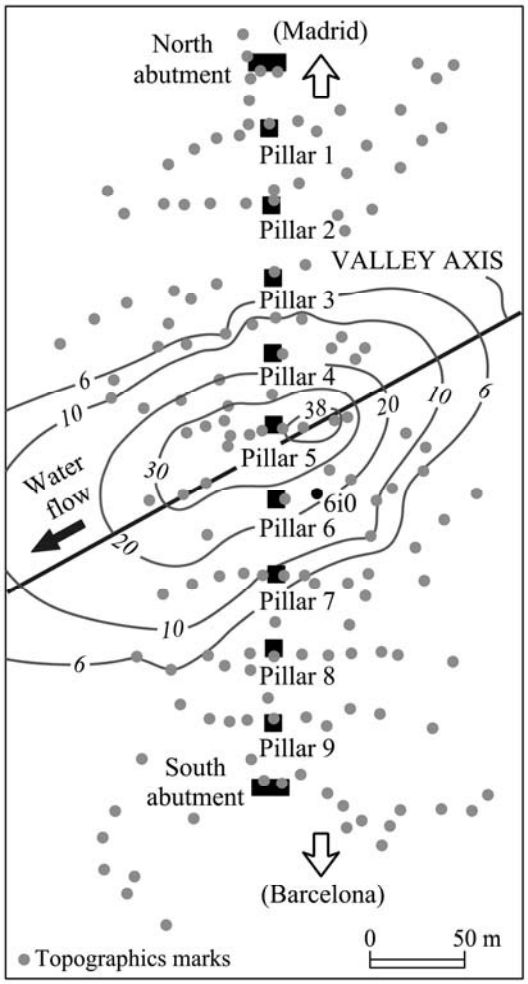

Figure 4.9. Contours of surface heave during the period 26 November 2007 to 30 April 2008

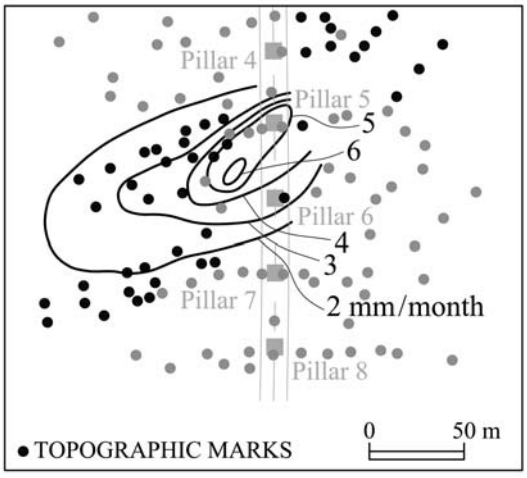

Figure 4.10. Contours of equal rate of heave displacement. Heave rate established in the period 11 July 2008 to 2 April 2009

A cross section of the heave contours given in Figure 4.9, following the bridge direction is plotted in Figure 4.11. It was also found that the pattern of surface heave is similar to the vertical displacements measured at the bridge deck level. Levelling of the pile caps of bridge pillars provided also time plots very similar to the heave records measured on levelling marks located on the ground surface, away from the foundation. This is shown in Figure 4.12 which compares the heave displacements of the pile cap of pillar P6 and the heave recorded in a nearby levelling mark (levelling point 6i0, Figure 4.9).The close agreement suggests that the massive pile foundation has no effect in restraining the surface heave. It is an indication that the origin of heave is located below the level of the pile tips. The deep extensometers, reviewed next, provided the necessary evidence in this regard.

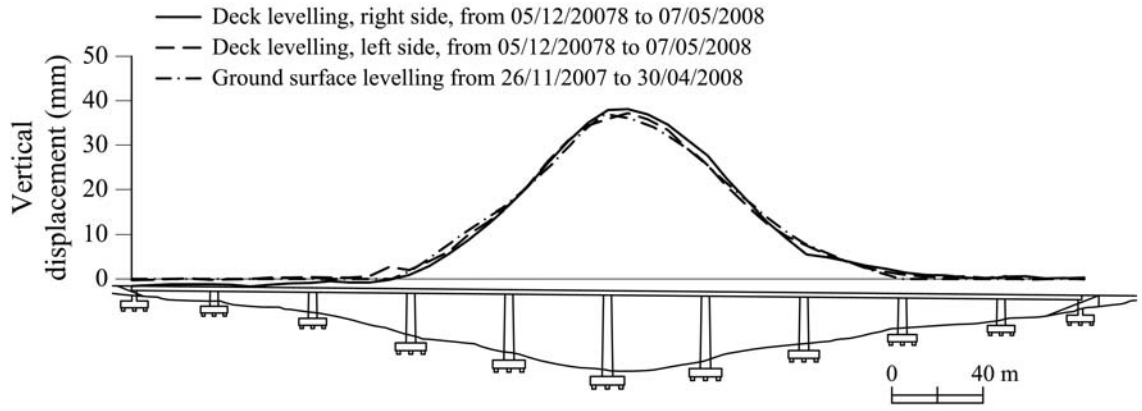

Figure 4.11. Comparison of measured heave displacements of the ground surface and the bridge deck

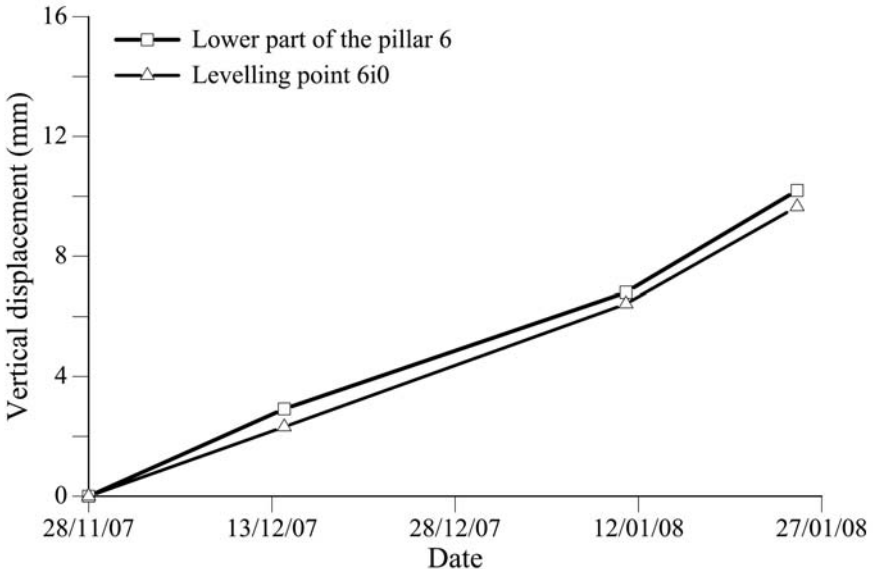

Figure 4.12. Comparison between the measured heave at the lower part of pillar P6 and the measured heave at a point (6i0) on the ground surface near the pile cap of pillar P6 by means of topographic levelling. The position of levelling mark 6i0 is shown in Figure 4.9

4.5.4 Deep extensometers

The deformation of rock at depth in the vicinity of pillars P3 to P7 was investigated by means of rod and continuous extensometers installed in boreholes (magnetic incremental extensometers, rod extensometers and sliding micrometers; Kovári & Amstad, 1982). Data were recorded on a weekly basis. The position of these extensometers is shown in Figure 4.5.

Figure 4.13 shows the recorded vertical strains (mm/m) in extensometer IX-5, located in pillar P5. The borehole was drilled through the pile cap, and penetrated a few metres below the tip of the piles. Swelling strains concentrated below the pile tips, and developed in time without changing the swelling strain pattern. Figure 4.14 shows the recorded swelling strains in extensometer IX-D, located upstream of pillar P5 (Figure 4.5).

Continuous samples were recovered along some of the boreholes drilled for extensometer installation. Gypsum and anhydrite content were determined by means of quantitative X-ray diffraction analysis. The plot of the variation of gypsum and anhydrite content against depth provides interesting information when compared with extensometer readings. This can be seen in Figure 4.13 - Figure 4.15 for extensometers IX-5, IX-D and IX-B. All of them indicate that the development of swelling strains starts when the anhydritic layer is crossed at absolute elevations around 261–265 m. Above this elevation, only gypsum is present. Note also that the gypsum content decreases suddenly within the anhydritic layer from high concentrations to very low values (a few percentage units). Swelling is directly associated with the presence of anhydrite. No swelling is recorded if only gypsum is present.

It is clear that the extensometer lengths, shown in Figure 4.13 - Figure 4.15, were insufficient to cover the whole active layer. Significant swelling strains were measured at the deepest levels of the extensometers. In addition, heave displacements measured at the head of the extensometers (ground surface), by means of conventional levelling, were higher than the integral of vertical relative displacements measured along the extensometer length. This is shown in Figure 4.16 for extensometer IX-5. In view of this inconsistency, which was attributed to an insufficient length of the extensometers, and with the aim of identifying better the position and thickness of the deep active layer, and the swelling intensity of the active layer, a new sliding micrometer was installed in December 2007 between pillars P4 and P5 which reaches a depth of 58 m (SL-1; its position is shown in Figure 4.5); readings are shown in Figure 4.17. This extensometer detects precisely an active layer, 9 m thick, between

elevations 250 and 259. A small straining was also measured at deeper levels (elevations 237–243).

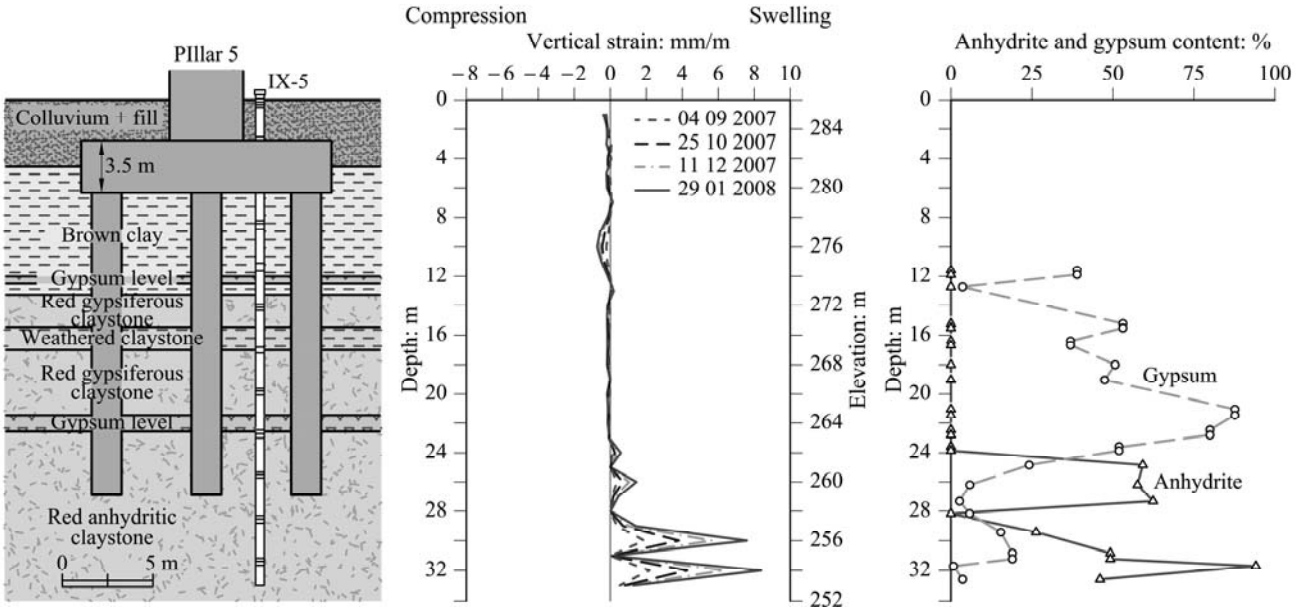

Figure 4.13. Measurements in extensometer IX-5 in the period 4 September 2007 to 29 January 2008, and profiles of anhydrite and gypsum content. Reference measurement from 12 July 2007

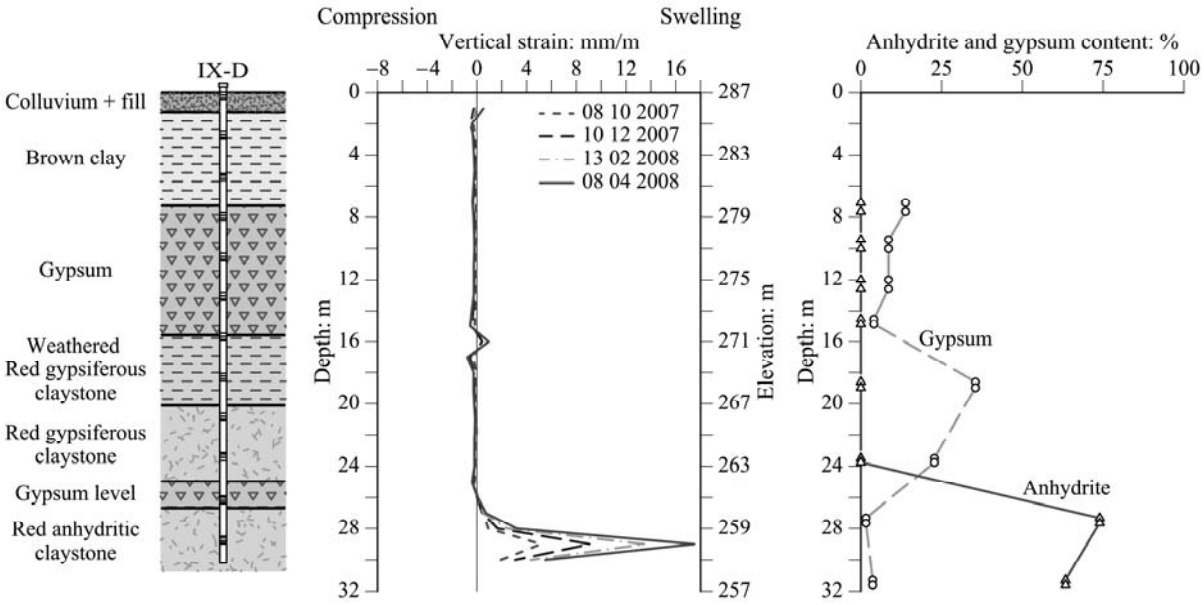

Figure 4.14. Measurements in extensometer IX-D in the period 8 October 2007 to 8 April 2008, and profiles of anhydrite and gypsum content. Reference measurement from 20 June 2007

The set of installed continuous extensometers - even if the information they give concerning the lower boundary of the active zone is not precise - provide enough information to draw the approximate boundaries of the swelling zone (Figure 4.18). Question marks and dotted lines indicate that measured heave at the top of the extensometer exceeds the integral of swelling

strains measured by the extensometer. The uncertain position of the lower boundary is indicated in the figure.

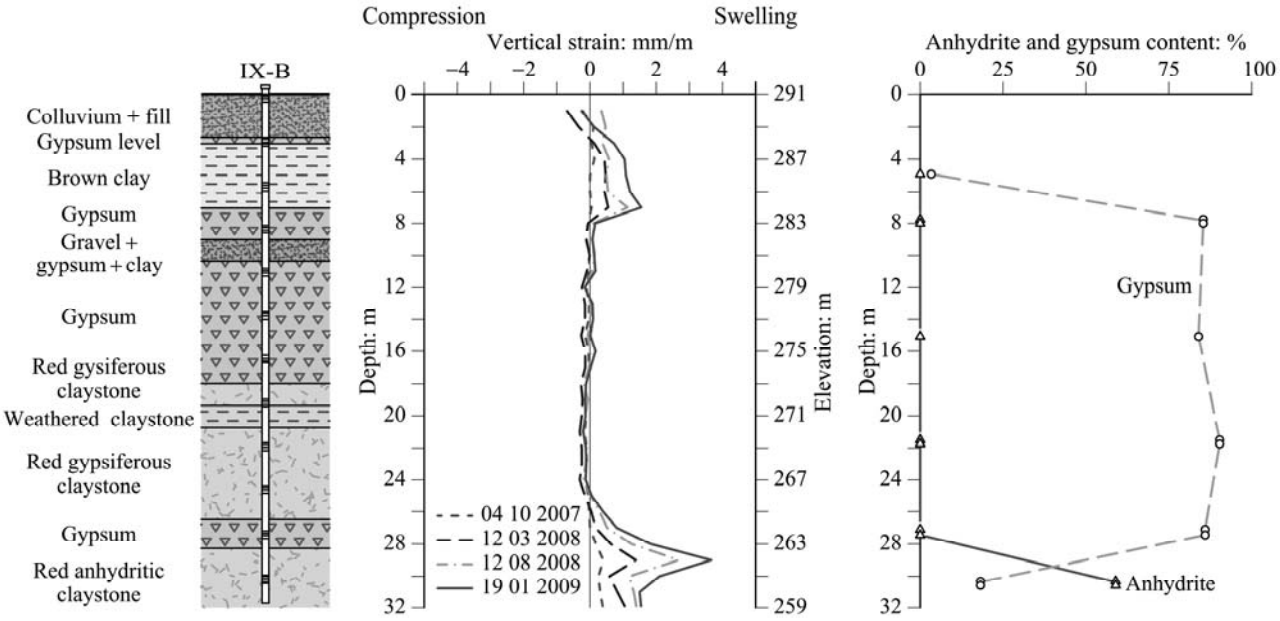

Figure 4.15. Measurements in extensometer IX-B during the period 4 October 2007 to 19 January 2009, and profiles of anhydrite and gypsum content. Reference measurement from 20 June 2007

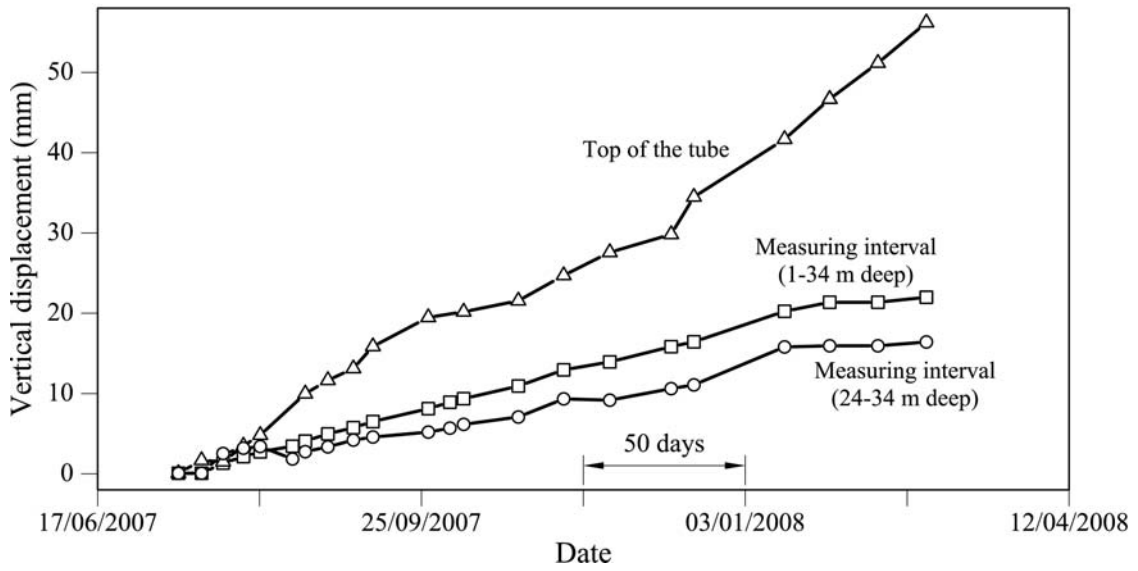

Figure 4.16. Evolution of vertical displacements on extensometer IX-5 (See Figure 4.5). Surface displacements directly measured by topographic levelling (top of the tube) are compared with the sum of extensometer relative displacements at depth

Expansive strains concentrate in a horizontal band, located entirely within the anhydritic claystone. The upper boundary is found approximately centred in elevation 263, which is the

position of the gypsum guide level. The thickness of this band varies between 9 and 15 m. An approximate lower boundary may be located at elevation 250.

Time records of heave displacement show linear trends when plotted on a natural timescale. This is shown in Figure 4.19, which provides the measured vertical displacements of the extensometer surface points, recorded by topographic levelling. Similar linear trends have already been given in Figure 4.12 and Figure 4.16. Long-term linear trends of heave are not expected if hydration of clay minerals is the underlying swelling mechanism. In fact, time records of tunnel heave in sulphated formations exhibit long-term linear trends (Chapter 2 and Chapter 3).

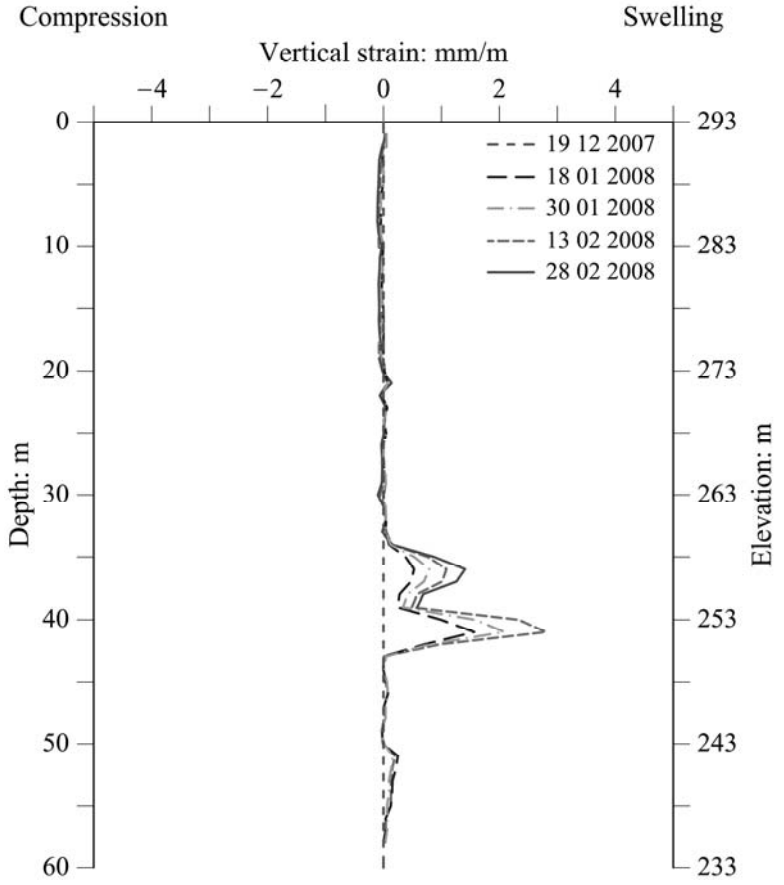

Figure 4.17. Vertical strains measured by sliding micrometer SL-1

4.6 Gypsum precipitation in the active layer

Cores recovered in borings crossing the active zone often showed the presence of gypsum crystals. Two morphologies were observed (Figure 4.20 and Figure 4.21). Crystals partially filling some open discontinuities of the claystone matrix grew as needles (gypsum crystallises

in the monoclinic system) oriented in a direction perpendicular to the plane of the discontinuity (Figure 4.20). Some of the crystals (thin isolated needles) seemed to be very recent. The open discontinuities within the active zone offered an easy route for water flow. Crystal growth was still far from clogging the joint opening in Figure 4.20. The second morphology (Figure 4.21) may be described as a set of thin warped layers of gypsum embedded in the rock matrix.

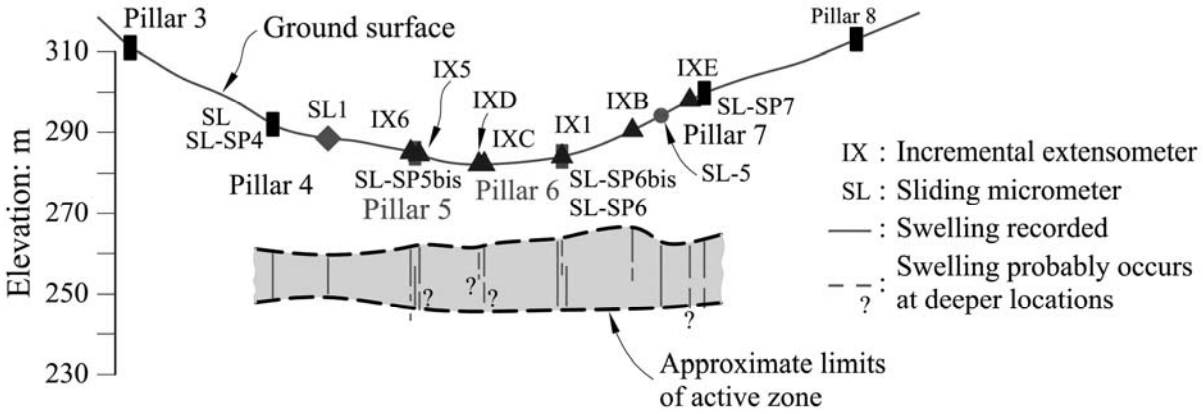

Figure 4.18. Longitudinal section along viaduct between pillars P3 and P8. Positions of sliding micrometers (SL) and incremental extensometers (IX) are shown, plus the location of the active expanding layer

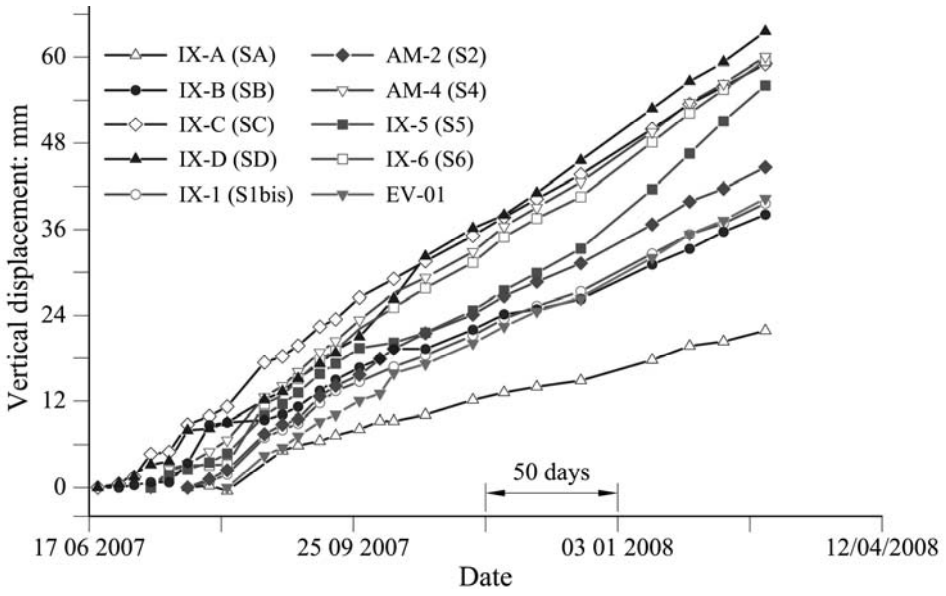

Figure 4.19. Evolution of vertical displacements of cap of extensometers at ground surface, measured by topographic levelling

No direct indisputable evidence of recent crystal growth in discontinuities may be claimed, because the crystal growth process itself was not observed. However, the cores suggest that

water flowing (mainly through discontinuities) is able to dissolve anhydrite and then precipitate gypsum in open spaces (the discontinuities). It is interpreted that the crystal growth acts as a local jack, capable of inducing swelling strains. This phenomenon will be reviewed and analysed in more detail in Chapter 5, in which laboratory observations, fundamentals of gypsum precipitation and additional "in situ" tests will be described.

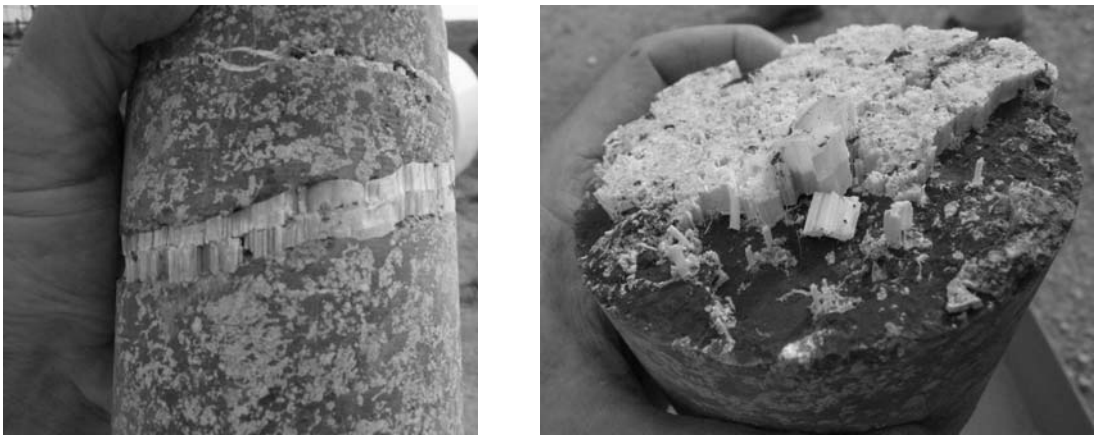

(a) (b)

Figure 4.20. Gypsum crystal growth in needles. Observations in a recovered core from a borehole drilled for hydraulic cross-hole testing at depths corresponding with active layer: (a) image of a gypsum filled vein before opening it; (b) Gypsum crystals form needles partially filling the open vein, once it is opened by hand

Figure 4.21. Laminar gypsum crystal growth developing inside the clay matrix. Observations in a recovered core from a borehole tested during hydraulic cross-hole testing at depths corresponding with active layer

4.7 Hydraulic cross-hole tests

In order to investigate the structure, fracturing and the connectivity of discontinuities in the active expanding layer, a hydraulic cross-hole campaign was performed.

Hydraulic cross-hole tests are performed in boreholes. Boreholes are first divided into isolated sections by means of inflatable packers. During the test, water is pumped or injected in one isolated stretch of one borehole and water pressures are measured in the set of isolated sections of similar nature, both in the "emitting" and in the nearby boreholes. Figure 4.22 shows a scheme of the layout of a typical hydraulic cross-hole test.

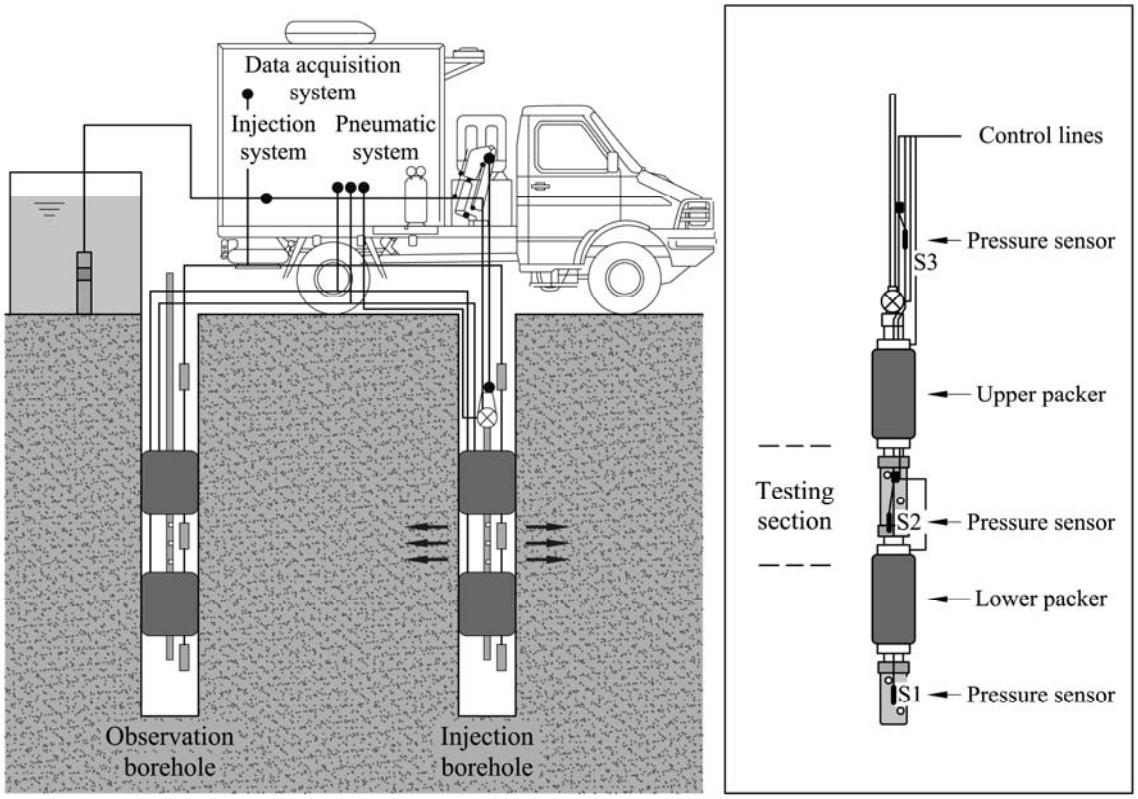

Figure 4.22. Layout and instrumentation used during a hydraulic cross-hole test (AITEMIN, 2009)

Four hydraulic cross-hole tests were performed on three boreholes (S1, S2 and S3), 50 meters long, located downstream and close to pillar P5 (they span from elevations 237 m (end of boring) to 287 m (surface)). Figure 4.23 shows the position of the testing boreholes. Boreholes 116 mm in diameter were drilled with a double-wall core barrel. A continuous string of cores was recovered. Boreholes were located in an area affected by significant heave displacements according to the periodic topographic levelling carried out at the ground surface. The three drilled boreholes define two perpendicular directions, and two testing

distances (4 m and 8 m) (Figure 4.23(b)). This layout allows obtaining the hydraulic characteristics of the rock mass in two directions. As a reference, continuous extensometers in this area indicate the existence of an active layer, 14 m in thickness, which extends from elevations 246 m to 260 m.

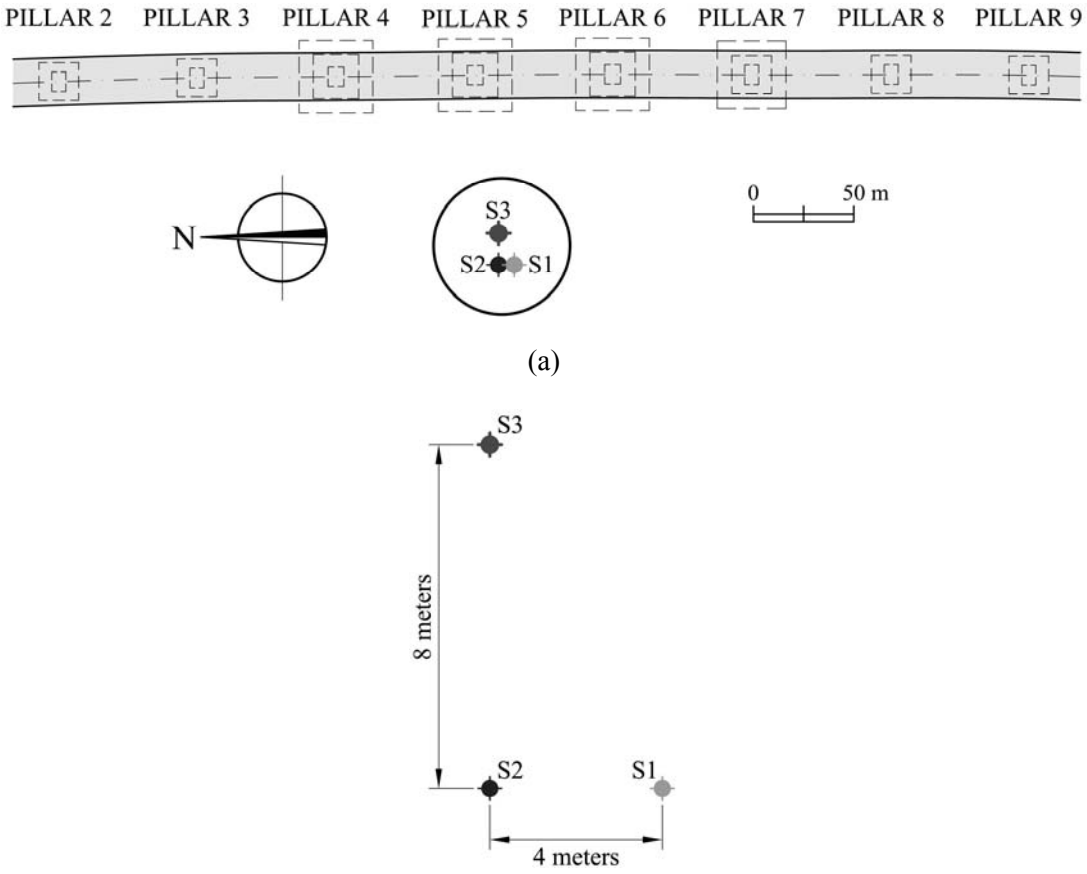

Figure 4.23. (a) Location of boreholes for cross-hole hydraulic testing; (b) layout and distances

The boreholes were lined in the upper 20 m. On each borehole two packers isolated a central section about 7 m in length. Lower and upper sections were also defined; the lower one extended from the end of the borehole to the lower packer, and the upper one extended from the foot of the casing to the upper packer. Four injection tests were performed by injecting water from the central section of borehole S2 while maintaining always its relative distance; packers were lowered in steps for each successive test in order to investigate the response of the claystone at different depths.

A constant flow rate of water was injected in the central section of S2, and water levels were monitored in time in the $3 \times 3 = 9$ sections isolated in the three borings. Pressure-time records

were interpreted by means of backanalysis procedures (AITEMIN, 2009). The analysis provides an estimation of the soil hydraulic conductivity (by dividing the estimated transmissivity by the length of the corresponding borehole section isolated by the pressurised packers).

Of particular relevance for the work reported here are the calculated permeability values. It was found that no hydraulic connection could be established in a vertical direction (pressure changes in boreholes S3 and S1 were essentially recorded in the central section). An average (horizontal) permeability of 2×10^{-6}m/s was calculated at depths varying between 22 m and 34 m (elevations 265–243 m, where the active layer was independently located by extensometers data). Very similar permeability values were found on the two directions tested. The horizontal permeability decreased suddenly at higher depths: it was found to be $1–1.6 \times 10^{-9}$m/s at 33–39 m depth and $3–8 \times 10^{-12}$ m/s at depths of 39–50 m. The high horizontal permeability values measured in the position of the active layers cannot be explained as matrix permeability in a claystone of low porosity.

The measured permeability reflects the existence of open horizontal joints. In fact, the observations of the cores recovered from the boreholes indicated an irregular distribution of fractures. However, the cores presented an increased fracture density at depths of 22.50–35 m. At higher depths the cores were massive again.

Some of the fractures crossing the recovered core exhibited dense deposits of gypsum. One example is given in Figure 4.24. Despite the accumulation of gypsum, channels can be identified. These joints explain a relatively high permeability.

The cross-hole testing campaign provided also a reliable information on the initial water levels within the claystone formation. Before cross-hole testing was started, the water level was measured in the three sections separated by packers, as described above. Once equilibrated, the water levels measured were plotted against the elevation of each one of the sections for each of the three boreholes. The results (Figure 4.25) show a distinct downward vertical gradient in all three boreholes: 0.08 m/m in borehole S2, 0.37 m/m in borehole S1 and 0.60 m/m in borehole S3. These are high values which consistently indicate a vertical flow from an upper aquifer to lower levels. This natural flow is not expected in the bottom of a valley, which is presumably characterised by an upward flow created by higher water heads on the valley slopes.

Figure 4.24. Crystals in a core from a Cross-hole borehole

It is also revealing to check that the piezometric head was similar in all the borings at elevations 243-265 m (active layer), an additional indication of the high permeability of this zone. These are important observations which help to define the heave scenario described in Chapter 5.

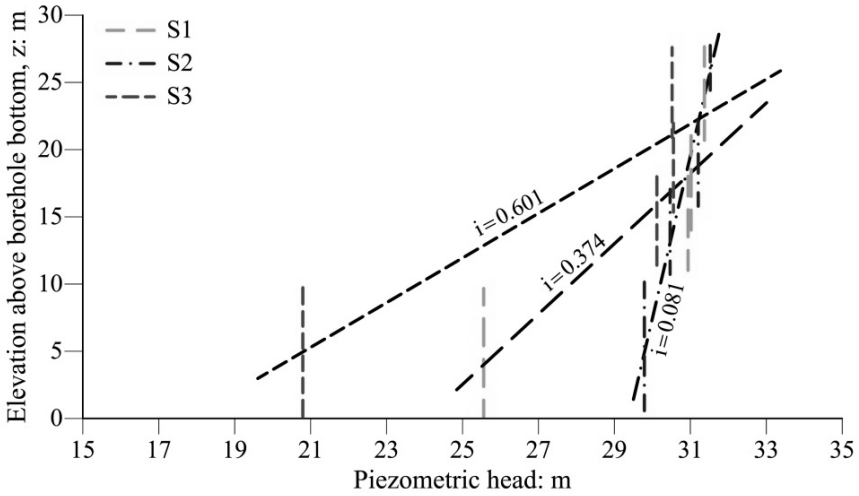

Figure 4.25. Piezometric heads measured during cross-hole testing. Also shown are calculated averages of downwards gradients

4.8 Remedial measures

Remedial measures actually carried out were inspired by the belief that adding weight would reduce the rate of heave and eventually this added stress would be able to eliminate heaving. Therefore an embankment partially filling the valley was designed. It was decided to build the

embankment in two stages: the first would reach a height of 33 m over the lowest elevation of the valley. In the case that the embankment weight was not able to stop displacements, the embankment height would be increased to a maximum height of 48 m over the valley centre.

The first stage of embankment construction (Figure 4.26) was built in the period October 2009 to August 2010. Pillars and the original pile foundation were protected in the manner sketched in the figure. Pillars were embedded in a fill of compacted non-active material, which was bounded by a "ring" of loosely compacted soil to reduce the effect of the embankment deformations on the concrete pillar shafts. In addition, a protective cap founded on deep bored piles installed around the existing original foundation was built to avoid a direct action of the embankment on the original piles. The new piles reached depths similar to the original ones, and therefore their tips were located above the active layer. The new pile cap was not structurally connected to the pillars (a gap of 20 cm was left). Also, the pillars were protected by a double sheet of polyethylene membrane to minimise the friction between them and the surrounding compacted soil. Surface runoff waters were collected and drained away to limit water content changes of the embankment.

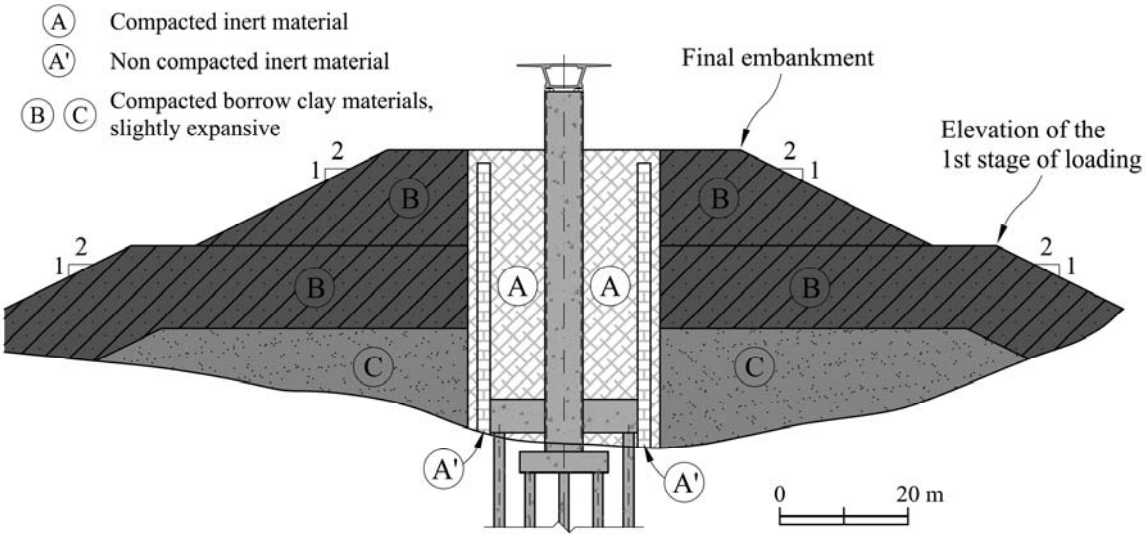

Figure 4.26. Cross-section of embankment

The construction of the embankment slowed the heave rate of the bridge deck (Figure 4.27). However, the expansive activity at depth has not ceased completely. This is shown in Figure 4.28, which shows the strain variation with depth measured by sliding micrometer SL-SP5bis and in Figure 4.29, where the strains in depth measured by sliding micrometer SL-SP-4 are represented (see locations in Figure 4.5). The upper part of the micrometer experiences a

compression as a result of the embankment loading. However, the length of the extensometer crossing the active layer reveals that swelling strains still develop. Compressive strains dominate expansions measured in the recording period shown in Figure 4.28 and in Figure 4.29. Compressive strains of the layers above the active band will eventually vanish some time after the application of embankment loading, and the evolution in time of surface (and pillars) displacement will again be dictated by the expansion of the active layer. This is shown in Figure 4.30, which shows the displacement measured by the sliding micrometer SL-5 (Figure 4.5). The time plot of surface heave (measured total displacement) shows an initial sudden reversal of swelling and a subsequent net settlement, which gradually levels off. Eventually, heave resumes although the heaving rate is now reduced to 1 mm/month, substantially lower than the rate measured before embankment construction (about 7 mm/month on average). The plot also shows that the accumulated heave on the active layer (integrating strains on the depth interval 25 to 40 m) increases at the rate observed on the surface once the transient settlement associated with the embankment construction has ended.

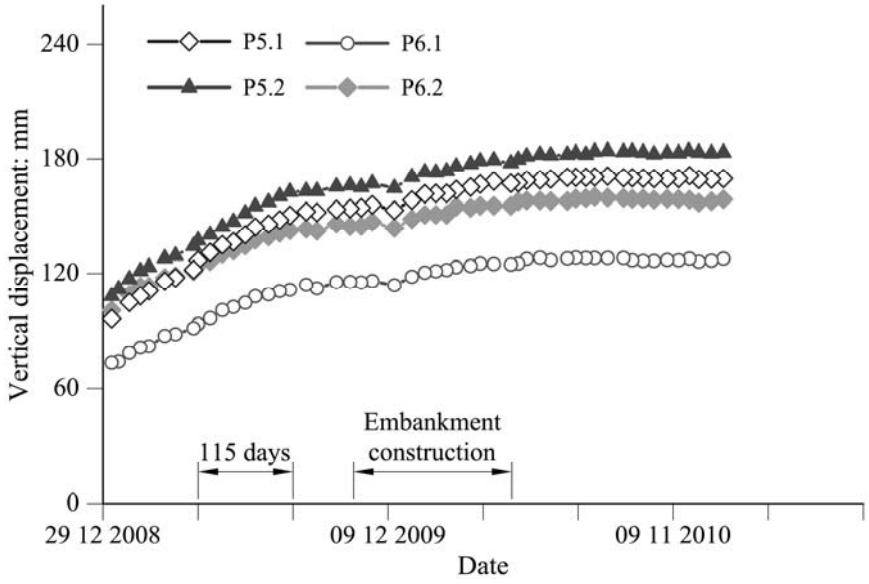

Figure 4.27. Effect of embankment construction on development of vertical displacements of bridge deck. Levelling marks P5.1 and P5.2 are shown in Figure 4.2. Marks P6.1 and P6.2 are similarly located above pillar P6

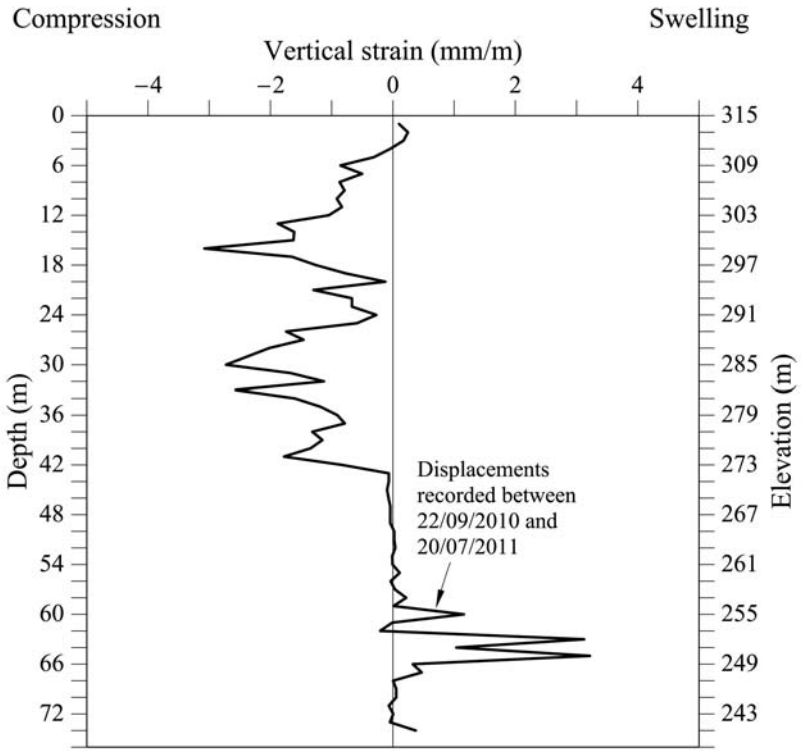

Figure 4.28. Vertical strains measured by sliding micrometer SL-SP5bis (see location in Figure 4.5)

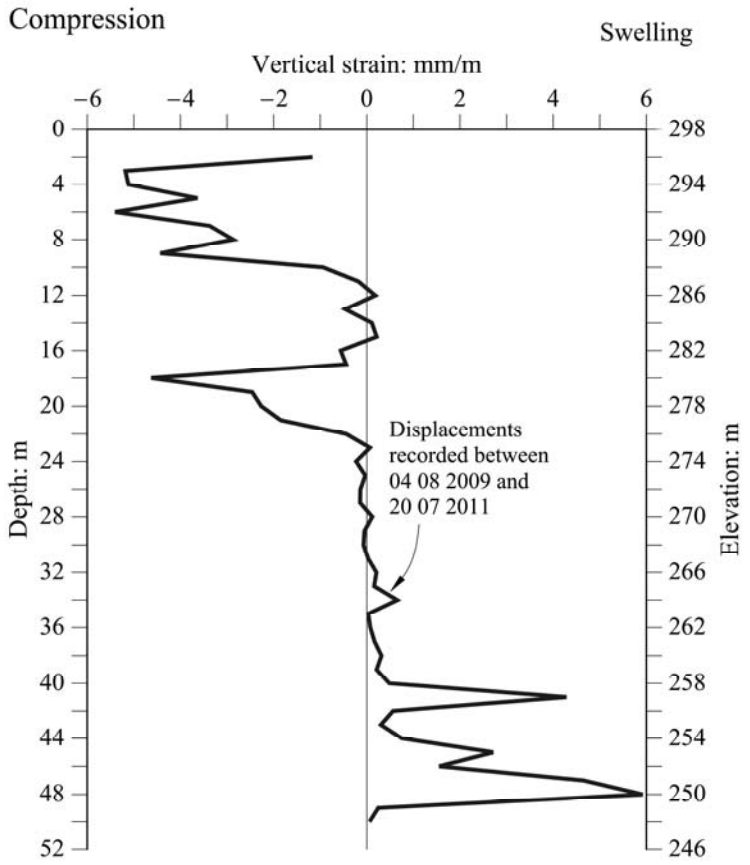

Figure 4.29. Vertical strains measured by sliding micrometer SL-SP-4 (see location in Figure 4.5)

The heave rate measured on pillar P5 has been related to the vertical effective stress acting on the centre of the active layer under pillar P5. Maximum and minimum heave rate values (Figure 4.31), as well as a weighted average (weighting reflects the time interval of each of the measuring records selected) all decrease with applied effective stress. The plot suggests that heave rate may eventually stop if an effective vertical stress of 1.25 MPa is acting on the mid level of the active layer. Reaching this condition would require a small increase of embankment height (approximately 4 m).

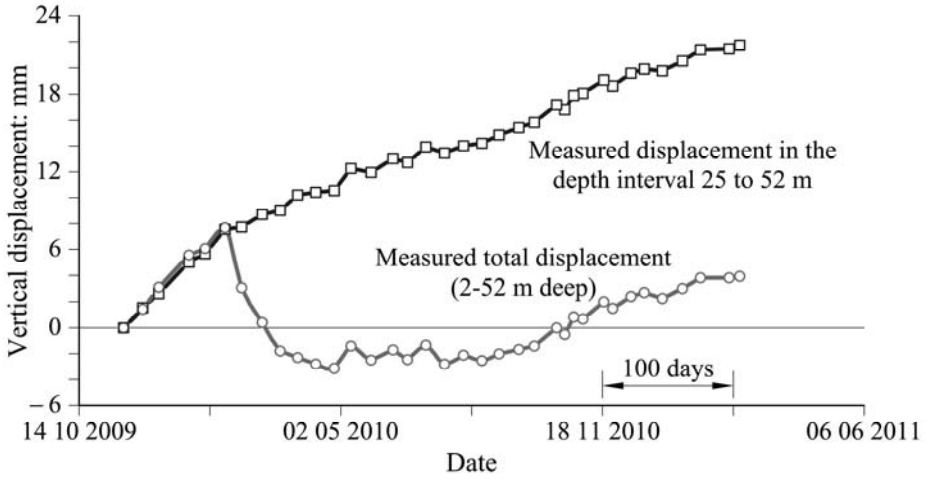

Figure 4.30. Evolution of integral values of vertical strains measured by sliding micrometer SL-5 (see position in Figure 4.5)

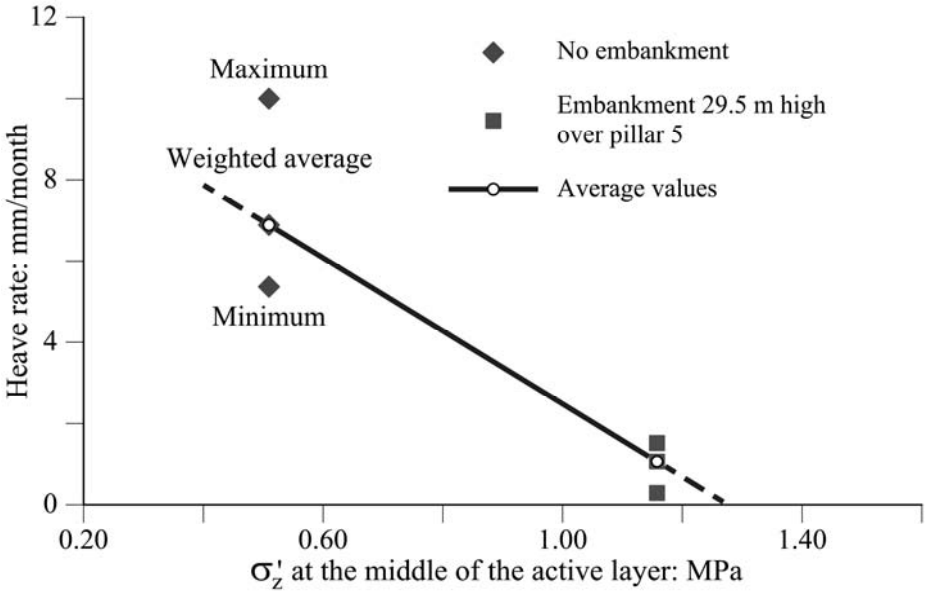

Figure 4.31. Effect of vertical confining stress on the heaving rate measured at the lower part of pillar P5

4.9 Conclusions

The Chapter describes the heave experienced by the central pillars of a railway bridge founded on massive deep pile foundations. Bridge pillars are supported by bored piles 20 m long and 1.65 m in diameter, capped by a rigid concrete slab.

Vertical displacements of the central pillars of the bridge accumulated at an average speed of 7 mm/month before remedial measures. Total vertical displacements of the central pillars have reached values in excess of 370 mm since the end of the bridge construction. These displacements were corrected by modifying the supporting elements of bridge deck. An embankment, 33 m high over the centre of the valley, was built in 2009, in an effort to halt the sustained heave. The effectiveness of the added load was to reduce the recorded heave rate to very small rates, but the long-term performance of the central pillars is still somewhat uncertain.

Field observations and, in particular, the data provided by deep continuous extensometers, indicate that the heave phenomenon originates in a deep active band, 12-15 m thick, located below the tip of the piles. This active band is located entirely within a Tertiary anhydritic-claystone formation. No indication of heave was detected in the upper gypsum-laden Tertiary formations of similar age with very low or non-existing anhydrite content. Piles supporting the central two bridge pillars, where the heave problem is concentrated, reached this lower anhydritic formation. This is not the case for the adjacent pillars, whose deep foundations remained within the gypsum claystones.

The similarities between the vertical displacements measured on the viaduct and the heave measured at the ground surface along the axis of the bridge in the same period of time were in agreement with the fact that the heave of the bridge was due to the swelling layer located below the tip of the piles of the central pillars. A pile group swelling formulation interaction analysis verified that the cracks in the cap-pile contacts observed in borings performed through some piles were the result of the development of a non-homogeneous heave displacement of the piles belonging to a pile group capped by a rigid slab (Sauter et al., 2012).

The observed heave may be also interpreted as a natural phenomenon. This is very unlikely, however, because the heave contours are essentially centred at the position of the pillars and they extend only to relatively small distances in the upstream and downstream directions. A slow natural phenomenon would most probably affect a much larger area.

It is thought that the water percolated from the upper aquifer towards the lower anhydritic claystone as a result of changes induced by the construction of the bridge. The preferred explanation is that drilling of boreholes and the excavation of piles created preferential downward paths. On the other hand, pillars 5 and 6, the ones experiencing the maximum heave, are located in the centre of the valley, suggesting a relationship between the presence of water flow and heave. In addition, the corresponding piles are the only ones crossing the boundary between the upper gypsiferous claystone and the lower anhydritic claystone. This situation also suggests that the heave of the central pillars was essentially due to a downward leakage induced by the construction of piles supporting pillars 5 and 6.

Further observations, namely the presence of newly formed gypsum crystals within the anhydritic layer, suggest that the crystal growth in discontinuities is at the origin of the observed heave. It may also be expected that in the long term, once the anhydrite has been totally dissolved, the flow of water, if it is maintained, will dissolve the gypsum and a settlement (or a karst) will eventually develop.

Anhydrite-gypsum transformation and its impact on tunnels have often been reported. The singularity of the case described in this Chapter lies in the position of a very thick active layer buried deeply under a cover in excess of 25 m and in the limited stress changes introduced by the pile foundation.

The severity and singularity of the case created concern and an active debate on the reasons for the unexpected heave. A plausible explanation, described here, came only after the installation and interpretation of comprehensive instrumentation based mainly on the drilling of deep boring reaching the lower anhydritic claystone. This is why no restrictions were initially applied to the installation of new extensometers or borings for hydraulic cross-hole tests. It was also realised that the existing deep piles continued to be an unavoidable path for downward water flow.

CHAPTER 5

The swelling mechanism due to gypsum crystal growth

The main characteristics of the swelling behaviour of excavations in sulphated claystones affected by expansions have been described in previous chapters. This has been achieved from the analysis of the field observations of real cases suffering expansions related with gypsum crystals, in particular the cases of Lilla tunnel and Pont de Candí bridge. These characteristics were in accordance with the observations recorded in the literature from tunnels affected by swelling and crossing sulphated claystone in central Europe

The mechanisms producing the observed expansions have been reviewed in the Thesis. There was certain evidence that the set of factors involved in the development and triggering of the swelling process were not known precisely. Actually, not all excavations in sulphated rocks develop expansions and, in general, foretelling the potential risk of development of expansions in sulphated rocks on the basis of field investigation is not easy.

This Chapter describes the conditions found in a number of recently built tunnels in Spain, most of them associated with the construction of high speed railway infrastructure. In addition, a field investigation performed in two areas of Lilla tunnel, one experiencing high

swelling and the other without development of expansions is analysed. Some features associated with observed heave (presence of water, tectonics, high sulphate content of natural water) have been isolated. A discussion of the mechanisms leading to field expansion is then made. It was found that long-term swelling in Lilla tunnel and heave in Pont de Candí Bridge were the result of gypsum crystal growth in discontinuities. The classical theory of anhydrite-gypsum transformation is replaced by a mechanism of crystal growth when natural water reaches a condition of supersaturation. The role of the tunnel excavation and bridge construction in the triggering of a dormant heave and swelling phenomenon is explained.

5.1 Introduction

Excavations involving sulphated claystones are not always affected by the development of expansions and, in addition, the prediction of the possible future occurrence of swelling in those materials is a difficult task. A revision of the current mechanisms explaining the swelling behaviour in sulphated rocks and of the field conditions that may lead to expansions in sulphated rocks has been done to try to get some insight into the capabilities to predict the development and the intensity of expansions in sulphated claystone.

The Chapter starts with an analysis of a number of Spanish tunnels and other tunnels in Central Europe crossing gypsiferous-anhydritic formations. The review made allows identifying a series of situations that may eventually result in severe swelling phenomena. Then, a field investigation carried out in the area of Lilla tunnel to give more insight in the field characteristics related to the development of intense or light expansions is presented. Later, the Chapter provides a background on gypsum crystal growth. The classical interpretation for swelling in sulphated format is reviewed and discussed and afterwards an alternative interpretation for the mechanisms causing the observed heave and swelling pressures is described. Then, credible scenarios for the swelling and heave phenomena in Lilla tunnel and Pont de Candí are described according to the interpretation of the phenomena. The Chapter concludes by summarising the lessons learnt from Lilla tunnel and Pont de Candí bridge records and from the review of the cases described in the literature.

5.2 An overview of tunnel behaviour in sulphate formations

Experience indicates that not all tunnels in anhydritic or gypsiferous rocks develop expansive phenomena. However, the reasons for differences in behaviour are not clear.

To examine this important issue, a review of several tunnel projects crossing gypsum formations in Spain has been carried out. Figure 5.1 shows the location of the analysed tunnels, represented on a map of gypsiferous outcrops in Spain (Riba & Macau, 1962). They refer mainly to tunnels in the high speed railway between Madrid and Barcelona.

The following data, which is thought to have some relevance for the swelling phenomena, has been collected: cover, cross section characteristics and presence of invert, waterproofing, excavation process, type of gypsum formation crossed by the tunnel and gypsum lithofacies, occurrence of tectonic activity, occurrence of water, sulphate proportion in the solid phase, sulphate content of groundwater and laboratory data. The geologic and tectonic characteristics of the formations crossed have been completed with data from the 1:50000 geological map from the National Geologic Institute (IGME).

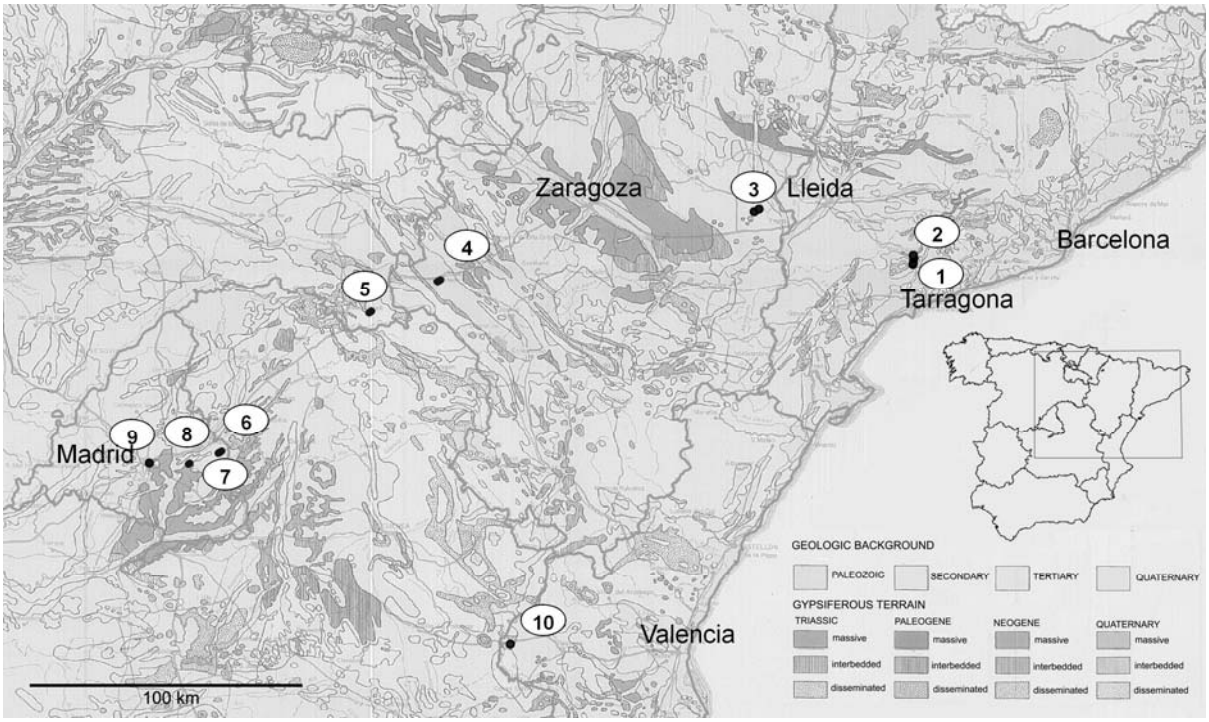

Figure 5.1. Analysed tunnels crossing gypsiferous formations. (1): Lilla tunnel, (2): Camp Magré tunnel, (3): Hechiceras tunnel, (4): Bubierca tunnel, (5): Sagides tunnel, (6): Anchuelo II tunnel, (7): Anchuelo I tunnel, (8): Mejorada de Campo tunnel, (9): South By-pass M-30 tunnel, (10): Villargordo del Cabriel tunnel.

The results of the survey performed are summarized in Table 5.1 and Table 5.2. Some remarks concerning the data should be given: in a significant number of cases the data is based on the tunnel design documents which, in turn, are based on the original geotechnical investigations. Data from the construction period is scarcer (one relevant exception is the Lilla tunnel, described in detail in Chapter 3).

The existence or absence of swelling problems reflects the experience gained during construction, which was made available for this study by persons in charge. Two additional well known cases from the literature are added to the tables, the Swiss tunnels Belchen and Adler (mentioned before in Chapter 2), for comparison purposes. The tables allow extracting a few conclusions:

- In most tunnel projects crossing gypsiferous formations swelling did not develop.
- There is a good correlation between the absence of swelling and water conditions: in most cases water was not present.
- The climate prevailing in some of the locations (semiarid) is the general explanation for the absence of established water tables.

Figure 5.2 shows a cave encountered during the excavation of a hydraulic drift through massive gypsum in Madrid, with no indication of swelling during construction. The main construction problem in this case was the presence of a well-developed network of caverns.

Figure 5.2. Caverns encountered during excavation with open shield through massive gypsum in Madrid.

It is also interesting to realise that waterproofing (by means of PVC sheets) of vault and abutments does not necessarily prevent the development of expansive phenomena. This is shown by the recorded behaviour of Camp Magré tunnel in Tarragona. However, in other cases waterproofing seems to contribute to avoid swelling (this is the case of Bubierca tunnel, which crosses sandstones and lutites from the Buntsandstein, dolomites and dolomitic marls from the Muschelkalk and clays, marls and gypsum from Keuper).

It should be noted that in most of the reported cases waterproofing was installed to capture the water flowing into the tunnel and to drain it in a controlled manner. This was the case of Camp Magré and the waterproofing located on both portals of Lilla tunnel. There was no indication in those cases that waterproofing was designed to avoid swelling problems. In any case, waterproofing of the invert was not attempted in the mentioned tunnels.

One example of geological profile of a tunnel (Villargordo del Cabriel) crossing gypsum formations in Keuper is given in Figure 5.3. In this tunnel the excavation remained essentially dry during construction. Again no gypsum related swelling developed in this tunnel.

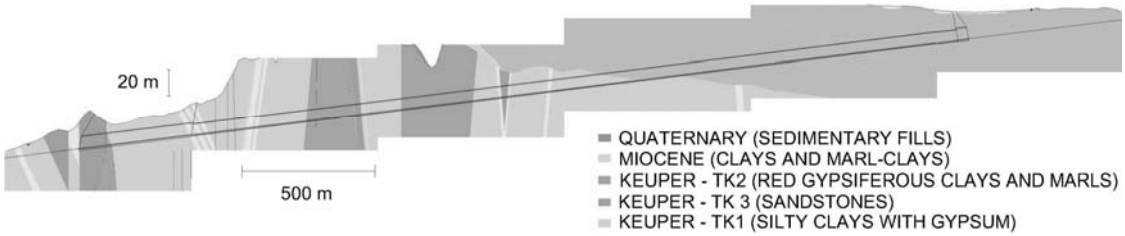

Figure 5.3. Longitudinal geological profile of Villargordo tunnel.

Recent cases where expansive phenomena have been relevant in Spain (Camp Magré and Lilla tunnel belonging to the high speed railway Madrid - Barcelona) indicate a number of additional features which may be of significance to explain the severity of the problem:

- The sulphate proportion (in weight of solid constituents) is high (40%).
- Water has high sulphate content.
- The rock is tectonized (Figure 3.1).

Table 5.1. Main characteristics of tunnels crossing sulphate claystones (Location given in Figure 5.1)

Name of the tunnel	**L (m)**	**Cross-section (m^2)**	**Max. cover (m)**	**Invert**	**Gypsiferous material crossed by tunnel**	**Tunnel length in gypsiferous formations (%)**	**Sulfate content in the rock (%)**	**Sulfate (SO_4) content of groundwater (mg/l)**	**Max. swelling pressure in laboratory tests (kg/cm^2)**
Mejorada del Campo	366	110	38	Yes	Clays interbedded with thin gypsum layers. **M**	70	2.3	2108	1.2
Anchuelo I	817	110	58	Yes	Gypsiferous clays. **M**, **t↓**	90	6	-	-
Anchuelo II	1154	100	42	Yes	Gypsiferous clays **M**, **t↓**	90	6	-	-
Sagides	1731	100	73	Yes	Gypsiferous clays, gypsum with argillaceous layers **Tr**, **t**	50	-	-	-
Bubierca	2433	80	176	Yes	Initial 300 meters: Buntsandstein, Muschelkalk and Keuper (clays, marls and gypsum) **Tr**, **t**	12	-	-	-
Las Hechiceras	2812	110-120	103	Along 660m	Argillaceous marls with interbedded gypsum (cm). **M-O**		0.9	-	- (8% max. swelling strain)
Villargordo	2880	90	87	Yes	Silty clays with gypsum, red gypsiferous clays and marls. **Tr**, **t**	50	0-5	-	0.1-2.35
South By-pass M30 (left roadbed)	4131	177 Circular	60	Yes	(1) Interbedded (cm) gypsum with clays. (2) Massive (m) gypsum. **M**	27	6.8-11.6	174	0.7 max
Camp Magré	954	140	52	No	Early eocenic argillaceous rocks containing anhydrite and gypsum. **E**, **t**	75	40	-	-
Lilla	2034	117	110	No	Early eocenic argillaceous rocks containing anhydrite and gypsum. **E**, **t**	100	40	1783	4.5 max.
Swiss tunnels									
Belchen	3180	85-105		Yes	Gipskeuper. **Tr**, **t**	40		1290-6000	
Adler	5300	124 Circular	130	Yes	Anhydrite and gypsum Keuper. **Tr**, **t**			2990	60 (samples of anhydrite layers)

Legend:
O: Oligocene M: Miocene Tr: Triassic E: Eocene
t↓: Tectonized (low intensity) t: Tectonized

Table 5.2. . Key features related to occurrence of swelling in tunnels crossing sulphate claystones (the location of tunnels is given in Figure 5.1)

Name of the tunnel	Occurrence of water	Waterproofing/ drainage	Excavation process	Gypsum lithofacies	Expansive problems
Mejorada del Campo	Only in a short length (5m)	Geotextile Poliviline sheet	NATM head and bench with a central counterfort. Heavy hammer	▲Crystalline, filling discontinuities	No
Anchuelo I	No	Geotextile	NATM with a central counterfort Boom header	▲Crystalline, specular, gypsiferous cement.	No
Anchuelo II	No	Geotextile	NATM with a central counterfort Boom header	▲Crystalline, specular, gypsiferous cement.	No
Sagides	No	PVC sheet	Head and bench Boom header and explosives	▲ -	No
Bubierca	Yes	Impervious sheet	Head and bench	▲ -	No
Las Hechiceras	Only at west portal	2 mm PVC sheet Geotextile 500g/m^2	NATM Head and bench Boom header	▲Granular, fibrous	No
Villargordo	No	Only in portals	Head and bench Boom header and hammers	▲ -	No
South By-pass M30 (left roadbed)	Possibly	Backfill injection of lining	EP Balance Shield	▲(1) Tabular and nodular (2) Specular or selenite	No
Camp Magré	Yes	In vault and abutments: geotextile of 500g/m^2 and 1.5mm thick PVC sheet	NATM Advance and bench Drill and blast	Fibrous veins and nodules Secondary gypsum, anhydrite	Yes
Lilla	Yes	Restricted to portals: geotextile of 500g/m^2 and 1.5mm thick PVC sheet	NATM Advance and bench Drill and blast	Fibrous veins and nodules Secondary gypsum, anhydrite	Yes
Swiss tunnels					
Belchen	Yes	No in original construction Yes during reconstruction works in 2001-2003	Invert drift+full cross section Half shield and hammers	Fine veins of anhydrite in black marl.	Yes
Adler	Yes	Waterproof seal	TBM		Yes

Legend:
▲: There isn't distinction between gypsum and anhydrite

5.3 Field identification of potential swelling

A very relevant issue in practice is to evaluate the capability of a standard field reconnaissance by means of borings and core recovery to identify the potential for severe swelling phenomena as a result of tunnel construction. Lilla tunnel was designed after a limited field work. However, the subsequent behaviour, the intense monitoring work performed afterwards and the identification of the heave intensity developed along the tunnel opened the possibility of approaching the issue from a different perspective. If a boring is to be performed, from the surface, in a position of strong swelling, what will be encountered? If another boring is performed in a position of no swelling, what would be the differences if compared with the previous boring?

These questions eventually evolved into an interesting research programme performed during the Thesis to contribute to the development of practical criterion from geotechnical investigations. The idea was to drill two borings from the ground surface with continuous core recovery in the position shown in Figure 5.4. Boring B1 was located at chainage 411 + 860, in a position of maximum swelling, at a distance (in plan view) of 25 m from the tunnel side wall. It reached a depth of 130 m. Boring B2 was located at chainage 412 + 825, in a position of no swelling, at a distance (in plan view) of 30 m from the tunnel side wall. It reached a depth of 93 m. The two borings penetrated 10 m below the level of the tunnel invert to reach positions in which the active zones had developed in the nearby tunnel.

Cores were carefully described by an experienced geologist. The description included the following items: the proportion of calcium sulphate (anhydrite or gypsum) in the rock; an estimation of the relative proportions of anhydrite and gypsum; the presence of slickensides, striations, shearing surfaces and discontinuities; and description of the rock matrix material (other than sulphated components). Figure 5.5 shows the estimated proportions of sulphates for the two borings, below the level of the Lilla tunnel invert. In B1 the proportion of sulphates is high: very often it amounts to more than 40% of the core recovery. In B2 the proportion is much lower: it seldom reaches 20%. Moreover, in B1, most of the sulphated mineral is anhydrite. Sheared surfaces were often found in borehole B1, but not so frequently in B2. Two examples from borehole B1 are shown in Figure 5.6. Another feature distinguishing boreholes B1 and B2 was a dominant ratio claystone /sandstone in B1.

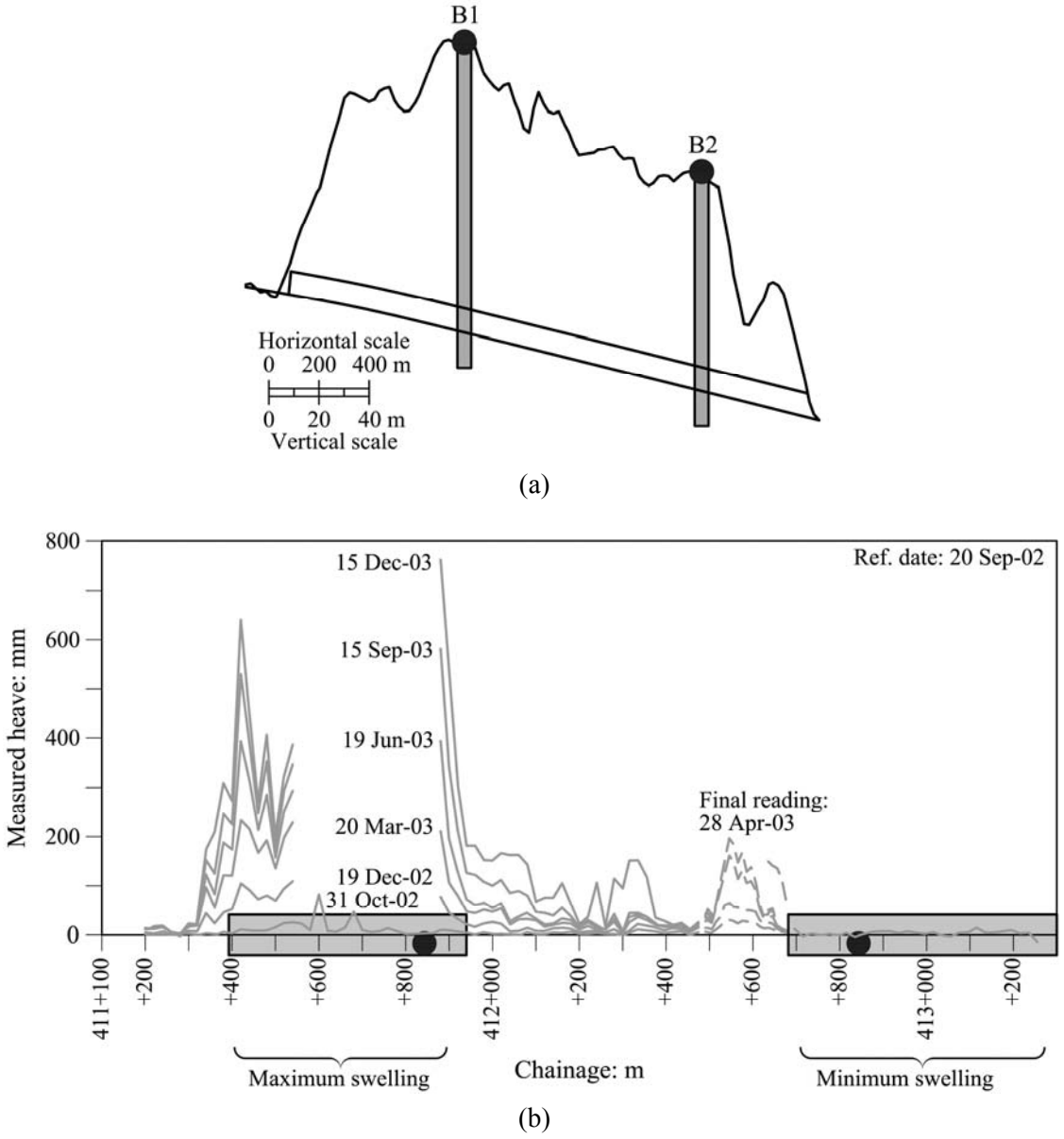

Figure 5.4. (a) position of borings B1 and B2; (b) position marked in swelling profiles

Summarising this information, conditions that favour the development of sulphate-induced heave are a significant proportion of sulphate minerals (specifically anhydrite), certain rock damage (in the case of Lilla the presence of sheared discontinuities) and a significant presence of clay. It is also clear from the nature of the gypsum precipitation that water must be present. The contribution of all these factors is understood except for the presence of clay, whose role remains still somewhat uncertain.

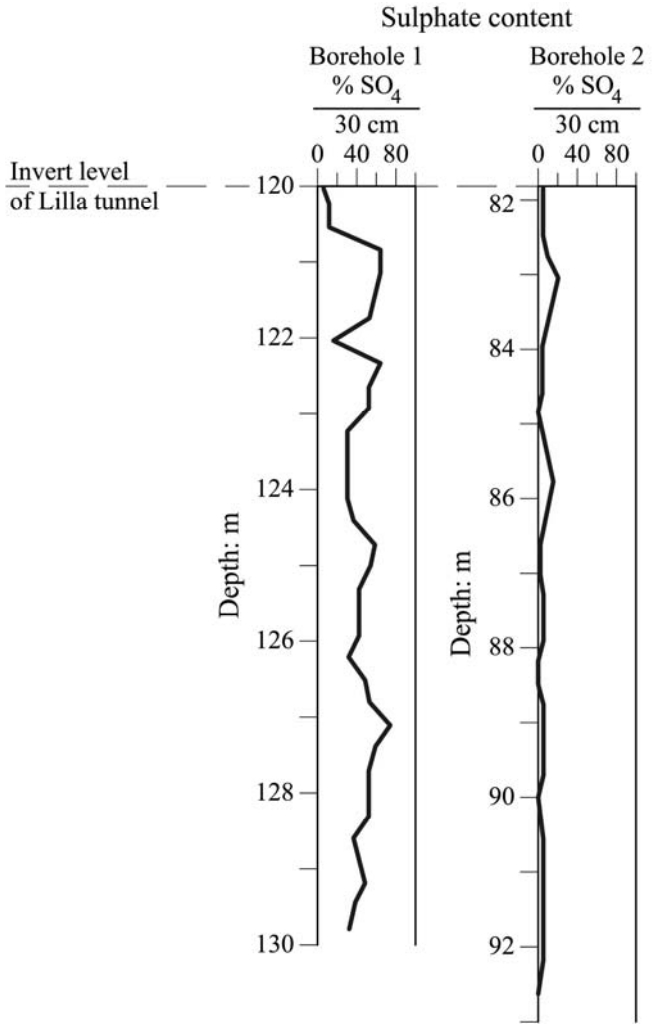

Figure 5.5. Proportion of sulphates in boreholes B1 and B2 below the invert of Lilla tunnel

Figure 5.6. Striated discontinuities found in cores recovered in borehole B1 at depths below the elevation of Lilla tunnel invert

5.4 A classical interpretation for swelling in sulphated formations

Early publications (see below) on swelling phenomena observed in tunnels in central Europe crossing Triassic anhydrite and gypsum formations attribute the observed swelling in sulphated claystones, when the sulphated claystones get into contact with water, to two uncoupled phenomena: a short term "physical" swelling associated with the expansion of clay minerals and a long term "chemical" swelling explained by the transformation of anhydrite into gypsum with a volumetric increase. If the volumetric increase is partially or totally inhibited in either of these mechanisms, then the corresponding swelling pressure is generated. The interdependence of these mechanisms is not clear; however, for some authors the existence of certain "optimum clay content" is assumed necessary to maximize the volumetric effects of the "chemical" swelling. Expansion in non-sulphated claystone (in terms of non-restricted swelling and swelling pressures against linings) was found to be moderate if compared with equivalent data for anhydritic formations. A large number of publications, starting in the sixties of the 20th century describe interesting case histories (Sahores, 1962, Einfalt, 1975, 1979; Einfalt & Götz, 1976; Einstein, 1979, 1996; Wittke & Pierau, 1979; Zanbak & Arthur, 1986; Madsen & Nüesch, 1991; Steiner, 1993; Amstad & Kovári, 2001; Kolymbas, 2005; Wittke, 2006, among others).

The transformation of anhydrite into gypsum is commonly written

$$CaSO_4 + 2H_2O \rightarrow CaSO_4 \cdot 2H_2O \tag{5.1}$$

A calculation of the change in volume when a given mass of anhydrite transforms into gypsum, comparing molar volumes of gypsum (MVg) (density: 2.32g/cm3) and anhydrite (MV_a) (density: 2.96g/cm^3), and taking the anhydrite value as a reference, provides the following theoretical volume increase

$$Volume\ increase = \frac{MV_a - MV_g}{MV_g} = \frac{74.21cm^3 - 46cm^3}{46cm^3} = 61.3\% \tag{5.2}$$

This is a very relevant volumetric expansion which was roughly consistent with the severity of the observed phenomena.

The distinction between the "physical" and "chemical" swelling seems, at first sight, correct. The first mechanism is possible even in the absence of active clay minerals and is characterized by relatively low limiting values for both swelling strain and swelling pressures.

However, the direct transformation of anhydrite into gypsum generating a volumetric increase doesn't seem to be a realistic mechanism. The theoretical volume increase of the gypsum molecule, if compared with the "parent" anhydrite molecule, was challenged as a convincing explanation for the observed volume increase when gypsum precipitates. Several authors (Holliday, 1970; Ortí, 1977; Madsen et al., 1995; Pimentel 2003; Pina, 2009) have concluded that the transformation represented by equation (5.1) is an isovolumetric process in which anhydrite dissolves and then precipitates as secondary gypsum. The excess of hydrated calcium sulphate can be transported in aqueous solution or precipitated in available open spaces of the host rock. On the other hand, recent contributions to the study of epitaxial growth confirm the impossibility of volumetric changes when anhydrite is exposed to sulphate-rich water since gypsum generates a protective thin surface film on the anhydrite (Pina et al., 2000).

Inspections of foundation materials in Wagenburg tunnel and Kappelesberg tunnel during the early 70's confirm the validity of the isovolumetric approach: *«… the original anhydrite has converted almost completely to gypsum in the heaving floors without showing any visible increase in volume. Except for strongly leached sections, the sulphate rocks have remained essentially compact»* (Krause, 1976).

Evidence of transformation of anhydrite into gypsum was not detected in the active zone of Lilla tunnel. On the contrary, it was apparent in several cases that anhydrite nodules were covered either partially or totally by neo-formation gypsum needles configuring a surface able to isolate -and eventually protect-, the material from continuous dissolution. These features can be observed in Figure 5.7 , which illustrates the phenomenon on a sample recovered in May 2005 just below the flat-slab in station 411+880 during the reinforcement tasks of Lilla tunnel. These observations can be explained if epitaxial growth of gypsum on anhydrite is taken into account.

An alternative to the explanation of the "chemical" swelling due to the isovolumetric process of anhydrite-gypsum transformation is the replacement of a host (anhydrite) by a guest (gypsum) crystal inside the rock matrix by means of a simultaneous dissolution-precipitation process. These phenomena were discussed by Nahon & Merino (1997), Fletcher & Merino (2001) and Banerjee & Merino (2011). The replacement is explained as a simultaneous pressure dissolution of the host crystal and a growth of the guest crystal. This replacement

preserves volume and shape in the examples given (which do not include gypsification of anhydrite). However, these transformations require high pressures and temperatures that are not present in the earth surface when dealing with most civil engineering works.

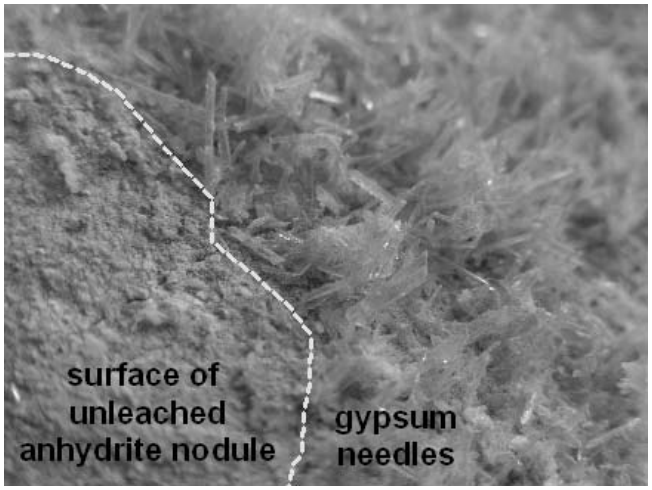

Figure 5.7. Growth of neo-formation gypsum needles on an unleached anhydrite nodule in Lilla tunnel (Alonso, et al., 2007)

It is concluded that the theoretical volume increase associated with reaction (5.1) is not a convincing explanation for the swelling observed in civil works when anhydrite and gypsum are present.

The dependence of the transformation of anhydrite into gypsum on clay content is a hypothesis presented by Madsen and co-workers (Madsen and Nüesch, 1990, 1991; Madsen et al., 1995; Nüesch et al., 1995; Nüesch and Ko, 2000). Based on long–term swelling tests on various materials from the Gipskeuper and other sulphate-bearing units from Switzerland and Austria, these authors postulate that a certain amount of clay is necessary to generate the dissolution of anhydrite and the precipitation of gypsum. Specifically, *«the clay content which in anhydritic marls produces the largest swelling parameters is about 15%»* (Madsen et al., 1995). Actually, the nucleation and growth of gypsum crystals in porous media is dependent on the supersaturation gradient and hence depends on the transport properties of the medium in which crystallization takes place (Prieto et al., 1990; Putnis et al., 1995). In other words, no theoretical bases exist to formulate cause-effect relationships between clay content, dissolution/precipitation of calcium sulphate species, and gypsum growth in porous media.

Establish precise swelling mechanisms in sulphated chaystone is a difficult task because swelling mechanisms are related to the mineralogical composition and structure of the rocks,

and to the chemical composition of groundwater. However, it seems that the triggering factor is related with the degradation of the rocks due to tensional changes and also to wetting and drying processes.

5.5 An alternative interpretation

In the presence of sulphated claystone the swelling phenomenon appeared as a "hydration" phenomenon which could explain the expansion of the clay minerals or the transformation of anhydrite into gypsum. However, the deformations and high pressures developed in sulphated rocks are not directly related with the swelling processes associated with the hydration of clay minerals.

Field observations made when interpreting the swelling experienced by Lilla Tunnel (Chapter 3) and the heave at the area of Pont de Candí Bridge (Chapter 4), a review of the records of the tunnels affected by swelling crossing sulphated claystone in Central Europe and also some laboratory experiments presented below suggest that the origin of the observed swelling and heave is the precipitation of gypsum crystals in discontinuities. It has been observed that the swelling phenomenon in sulphated claystone occurs mainly in structural discontinuities and a common characteristic in the different cases of swelling in sulphated claystone is the presence of neoformation gypsum crystals in open discontinuities located in the active zone where expansions occur (see Figure 5.8 and Figure 5.9). However, crystal growth is far from being a phenomenon associated with hydration. The precipitation of gypsum crystals in discontinuities is a process that requires the presence of water in the host rock to be in contact with the anhydrite mineral. This understanding is the starting point for the analysis developed here.

Gypsum crystals are originated from the precipitation of sulphates in supersaturated water. Therefore, gypsum precipitation requires the presence of water as it has been mentioned before. In an impervious claystone water percolates through discontinuities, either pre-existent, created by the tunnel excavation or developing as a consequence of the crystal growth itself. Then, the existence of fissures or voids is necessary for the precipitation of crystals because they permit water flow, but also they are necessary because, in addition, fissures and voids provide available space where precipitation of crystals can occur, as it will

be discussed later in this Section. Gypsum precipitation also requires conditions leading to calcium sulphate supersaturation.

Two mechanisms leading to supersaturated conditions of groundwater have been explored in connection with field observations in Lilla tunnel and Pont de Candí Bridge: (a) the evaporation of groundwater and (b) the supersaturation conditions created by the presence of anhydrite.

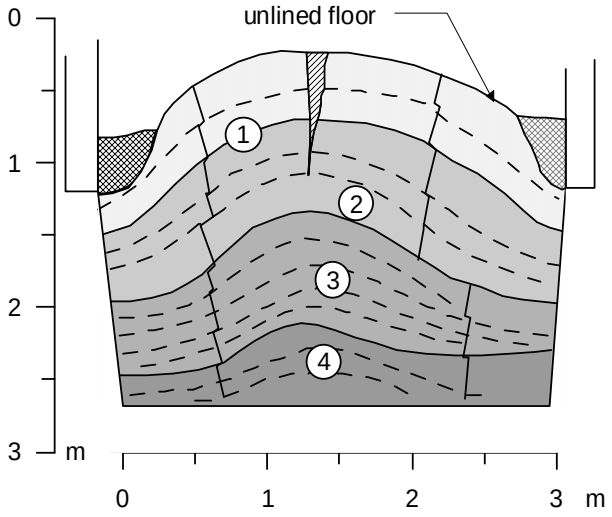

Figure 5.8. Distribution of gypsum crystals along the degraded rock profile in Wagenburg North tunnel according to Krause (1977) and Nagel (1986): (1) segregate-impure gypsum crystals and macrocrystals; (2) segregate-pure gypsum crystals in fine sheets; (3) gypsum macrocrystals and fibrous gypsum; (4) transition between (1) and (2)

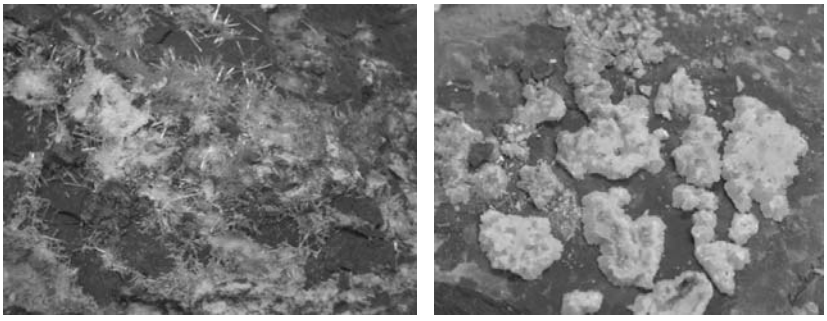

(a) (b)

Figure 5.9.Gypsum crystal growth in fissures found in Lilla tunnel (a) gypsum needles on an open slickenside surface located in the active zone, (b) gypsiferous aggregations in a confined discontinuity located in the lower part of the active zone

Regarding the first mechanism, the presence of the tunnel itself, due to the relative humidity conditions imposed by its atmosphere, with its ventilated environment, favours the evaporation towards the tunnel boundary in the exposed surfaces of the rock.

Figure 5.10 describes a simple laboratory experiment (Oldecop & Alonso, 2012), which illustrates the deformation (and damage) experienced by Lilla claystone when subjected to a flow-evaporation process, leading to the precipitation of gypsum. The test scheme is given in Figure 5.10(a): a rock core (117 cm in diameter, 15.1 cm long) is partially submerged in water (pure water or sulphate saturated water did not make any significant difference). Water is forced to migrate upwards, through the core, by wrapping the outer cylindrical boundary of the core with an impervious cellophane sheet. The evolution of the core with time is shown in Figure 5.10(b) and Figure 5.10(c). Figure 5.10(b) and Figure 5.10(c) show the progressive growth of gypsum crystals in some discontinuities during the test. The process starts at the upper boundary, where the upcoming water evaporates and the dissolved calcium sulphate salt precipitates as gypsum. Joint opening results in a moving evaporation boundary (it penetrates into the core) and the crystal growth process advances in a downward direction, expanding and damaging the claystone. The measured deformations (extracted from periodically controlling sample dimensions) are given in Figure 5.10(d).

This process, namely the precipitation of gypsum in an evaporation boundary (Lilla Tunnel floor), was believed to be the fundamental explanation for the heave observed at Lilla. A description and a model for this mechanism were reported in Alonso & Olivella (2008). However, matching some observed heave displacements of the planar floor slab required a mass of precipitated gypsum much higher than the mass that could be derived from water evaporation, even if no restrictions to vapour transfer through the concrete slabs or lining are assumed. The absence of swelling in crown and walls may also be invoked to question the evaporation mechanism. However, walls and crown, unlike the invert, were soon covered by sprayed concrete. The understanding of the swelling mechanism at the time of tunnel repair was imperfect and swelling was attributed in general terms to the presence of water. This belief led to the inundation of the circular test sections described previously in Chapter 3. However, the case of severe heave of the deep massive foundations of Pont de Candí is a major obstacle to the acceptance of this interpretation. In fact, no evaporation may be assumed to act on the boundaries of the deep active layer, precisely identified immediately below the tips of the foundation piles of pillars P5 and P6.

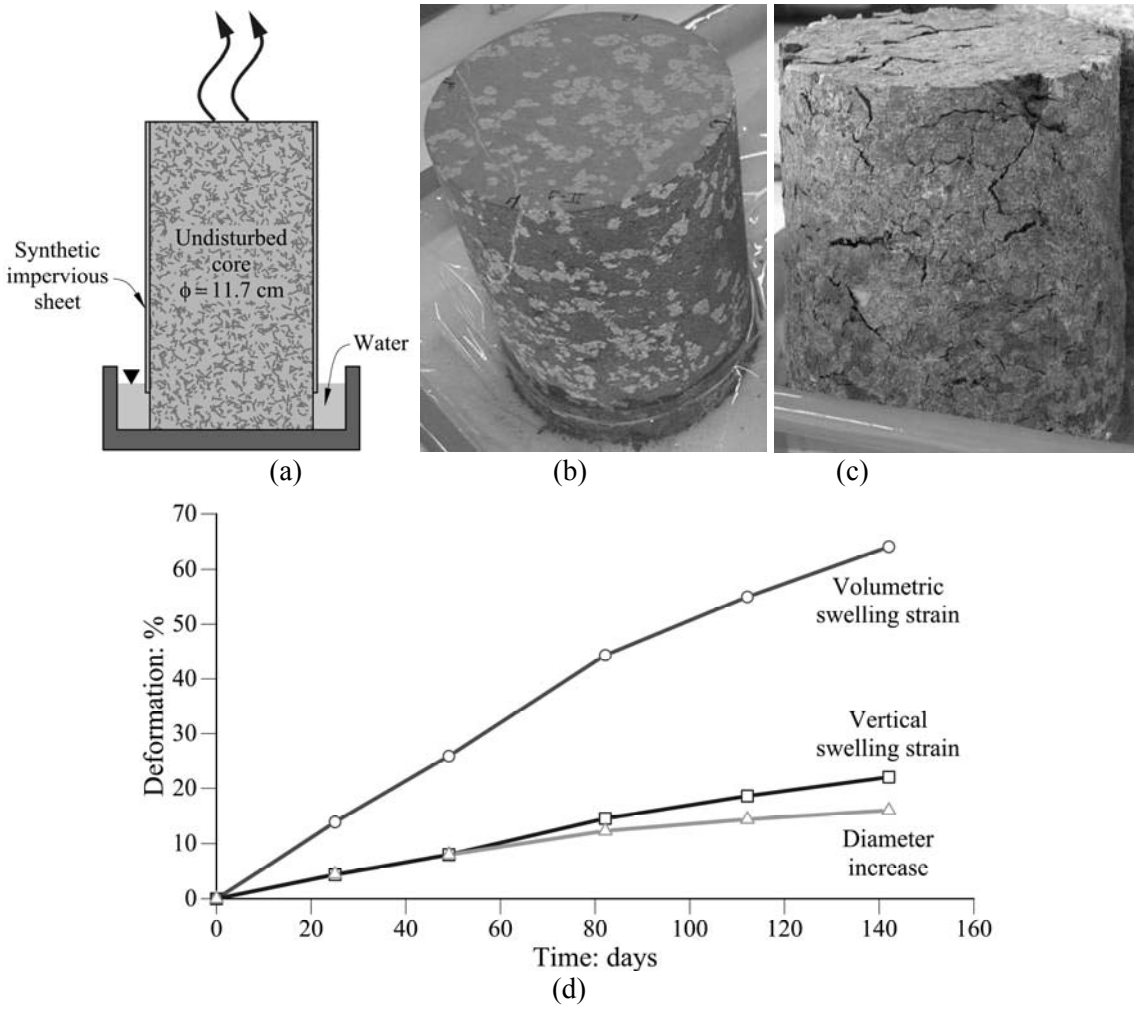

Figure 5.10. Evaporation test on a claystone core: (a) test set-up; (b) initial state of core; (c) core after nearly 5 months of testing; (d) recorded deformation

The second mechanism, the achievement of conditions of supersaturation in calcium sulphate due to the presence of anhydrite, is explained because the solubility of anhydrite ($CaSO_4$) is higher than the solubility of gypsum ($CaSO_4 \cdot H_2O$) at temperatures lower than 56ºC. Consider in Figure 5.11 the equilibrium concentrations of dissolved sulphate in water in the presence of anhydrite and gypsum. For a reference temperature T = 15ºC water in contact with anhydrite is capable of dissolving 3.2 g/l of calcium sulphate. However, the equilibrium concentration in the presence of gypsum decreases to 2.0 g/l. Therefore, water in contact with the anhydritic claystone will tend to dissolve anhydrite until saturation conditions in calcium sulphate with respect to anhydrite are achieved. Then, supersaturation conditions with respect to gypsum will be reached and the excess of dissolved calcium sulphate will tend to precipitate in gypsum crystals. This mechanism has been modelled, for simplified conditions in Oldecop & Alonso (2012) and, in a more general case, in Chapter 7 of this Thesis.

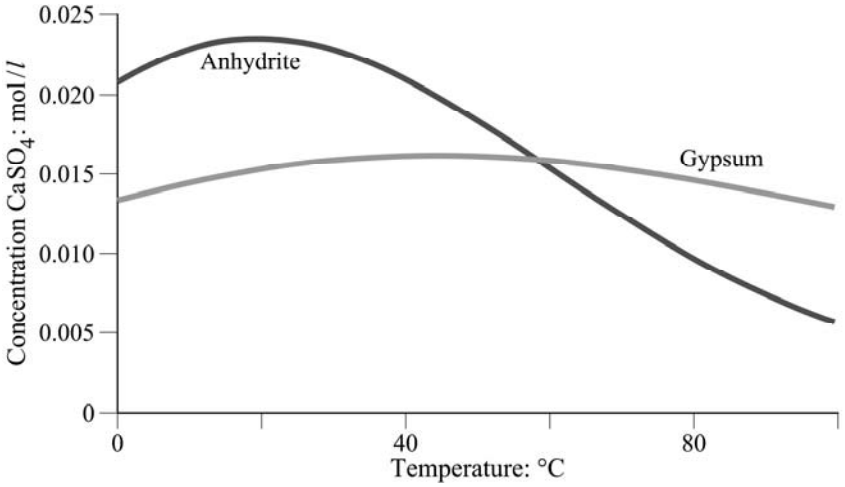

Figure 5.11. Equilibrium concentration of CaSO4 in calcium sulphated water with respect to anhydrite and gypsum. Sulphate concentrations were calculated with the PHREEQC computer program (Parkhurst, 1995; Parkhurst & Appelo, 1999), which simulates chemical reactions in aqueous solutions

Experiments reported by Kontrec et al. (2002) illustrate the transformation of anhydrite into gypsum in aqueous media. They describe the spontaneous precipitation of gypsum from supersaturated solutions in equilibrium with anhydrite, without evaporation. Crystal formation is enhanced by the presence of gypsum crystal seeds; this is a mechanism that may lead, in time, to the transformation of all available anhydrite into gypsum. It requires the presence of water and the transformation involves an intermediate step: the precipitation of gypsum crystals.

This mechanism is potentially more significant (and dangerous) for engineering works than the evaporation-based mechanism illustrated in Figure 5.10. In addition, it is difficult to control, in contrast to the first mechanism. Evaporation requires a boundary exposed to an atmosphere exhibiting a Relative Humidity (which is a measure of the water potential) lower than the water potential on the soil or rock. This is not the case of Pont de Candí deep foundations. Besides, evaporation rates, combined with the relatively low solubility of gypsum (or anhydrite) into water provide, in practice, a small mass of precipitated gypsum. This precipitation concentrates essentially on an evaporation surface and not in a rock volume.

The precipitation of gypsum, via an aqueous solution, in the presence of anhydrite may occur in large volumes (this is the case of Pont de Candí); it does not require evaporation boundaries and in theory the process continues until all the anhydrite precipitates as gypsum. This mechanism is a potentially faster and more intense phenomenon than an evaporation driven

phenomenon. To become active within a claystone formation it requires a number of contributing factors: the presence of anhydrite and the existence of an initial set of fissures or discontinuities, water filled, in contact with anhydrite. A consequence of this interpretation is that small homogeneous samples, tested in the laboratory, may not provide any indication of swelling. In fact, a series of oedometer and triaxial tests performed on Lilla claystone in a classical way (wetting under some confinement), aimed at characterising the observed heave, did not show any significant swelling. Swelling will be controlled not only by the total mass of the precipitated gypsum (which may occur at a distance from the source of anhydrite dissolution), but also by the geometry of precipitated crystals and its interaction with the surrounding soil/rock. Crystals precipitate more easily if some space is available for them. The pores of claystones provide an extremely reduced space, and water flow is essentially restrained through them. But joints provide a more favourable environment for crystal growth: the "open" space increases dramatically, along with the flow rate.

Scherer (1999), discussing the growth of crystals in pores stresses that cracks and pits are sites which favour the nucleation of crystals. Charola et al (2007) in their review of gypsum crystallization and its effect in the deterioration of natural stones refers to observations of gypsum crystal growth in natural pores. They also stress the tendency of gypsum to accumulate and to generate internal stresses in the rock, which enhances deterioration. They also mention the size of crystals as observed through microscopy and mention values in the range of microns. Measured pore sizes of undamaged Lilla claystone are in the range of a few nanometres (Pineda, 2012). However cracks, slickensides and fissures have sizes many orders of magnitude larger (10000nm = 10microns). These defects seem more able to "attract" gypsum crystallization because of their shape and size. In crystallization experiments reported by Oldecop and Alonso (2012) and also shown in Figure 5.10 of the present Chapter it was observed that gypsum crystals started to grow in pre-existing discontinuities of the rock. The void ratio determined in the active zone below the invert of Lilla tunnel, excavated in the same material, was found to increase substantially after the high swelling experienced. In other words, gypsum growth did not fill all the available pores. Instead, observations suggested that it created an increase in porosity.

Therefore, there is certain evidence that in the materials investigated here gypsum crystals may precipitate in fractures. A conceptual representation of this interpretation of gypsum crystals precipitating and growing in fractures from supersaturated water due to the previous

dissolution of anhydrite is illustrated in Figure 5.12. In practice, the supersaturation is achieved when water flowing through discontinuities dissolves anhydrite. The process of precipitation of gypsum in discontinuities is thought to push apart the rock mass. That will tend to open the discontinuities and may contribute to generate new ones, generating new surfaces where gypsum can crystallise, depending on the characteristics of the rock mass and the flow and equilibrium conditions of the sulphated water.

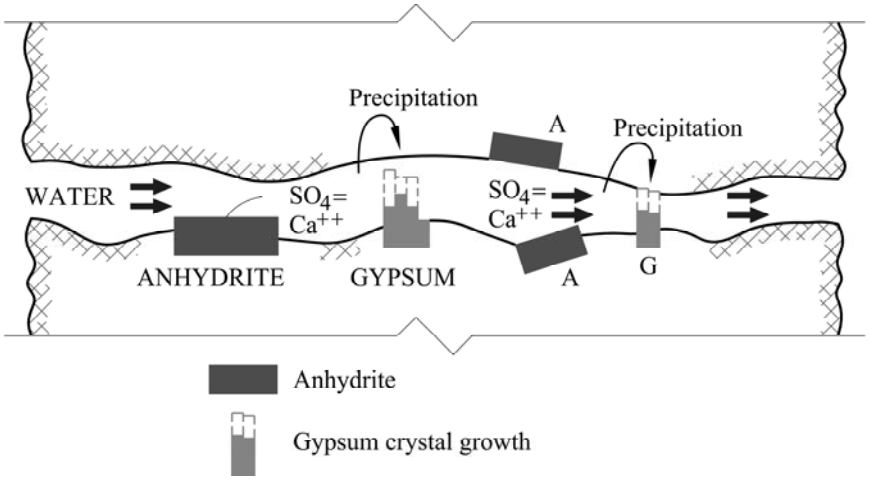

Figure 5.12. Conceptual model for gypsum precipitation

The isolated processes of fracture opening will result in the development of the general swelling phenomenon observed. The different aggregates of crystallized gypsum would act as small hydraulic jacks expanding the mass of the surrounding rock, originating swelling pressures and deformations whose direction and intensity will be controlled by the geometry of fracture families. Apparently, this process would be maintained while crystallisation of gypsum occur, which in turn, is related to the supply of sulphated water.

Experience in tunnels indicates that active zones concentrate under the invert. In horse-shoe tunnel cross-sections, points under the tunnel floor experience the highest stress release after excavation, and therefore the highest risk of opening new or existing discontinuities, inducing an increase on the permeability of the rock mass. In addition, groundwater tends to drain towards the tunnel floor (where collector drains are usually placed). The "drain effect" of the tunnel itself, and the fact that the rock has a high permeability below the floor of the tunnel, produce a concentration of the water below the tunnel floor and allow the triggering of the processes described previously.

These observations bring another difficulty to the observed phenomena in Pont de Candí: since previous fissuring of the claystone rock is a requirement for crystal growth, it was

decided to check if there was evidence of fracturing in the active zone, identified below the piles tip (see Figure 4.18), by means of hydraulic cross-hole tests. The hydraulic cross-hole tests performed has been explained in Chapter 4 and revealed the existence of horizontal hydraulically connected fractures in the active layer which provided the necessary open space for gypsum crystals to grow and also confirmed the presence of circulating water.

The maximum pressure capable of developing during these phenomena is unknown. An upper bound on the crystallization pressure is set in part by the supersaturation of the solution (Scherer 1999). The magnitude of the pressure induced by crystal growth will be analysed later in Chapter 6. In Lilla tunnel, a value close to 7 MPa has been measured in one pressure cell installed between the rock and the lining. This value is one of the highest measured pressure values in similar cases published, in particular in tunnels from Central Europe excavated in sulphated rocks. However, the precise distribution of pressures against the lining of Lilla tunnel is unknown; only values of swelling pressure at a few points were measured. Due to its variability it is difficult to propose specific and reliable distributions of pressures against the lining.

5.6 Heave scenario in Pont de Candí Bridge

The set of "in situ" observations described so far, and laboratory investigations into the precipitation and growth of gypsum crystals, indicate that the initiation of the mechanism requires two main conditions:

- The presence of free water able to dissolve anhydrite.
- The existence of connected voids or fissures to allow the circulation of water. The presence of fissures and defects favours the precipitation of gypsum.

Although not necessary, the pre-existence of some gypsum increases the rate of precipitation (Kontrec et al., 2002).

On the other hand, the scenario for the development of heave should also explain that the main triggering factor was the construction of the bridge.

The favoured explanation is that the lower level of fissured anhydritic claystone received a water inflow as a result of the bridge construction. Borings drilled at the location of each pillar with the purpose of designing the pile foundation connected the upper aquifer with the

lower fractured anhydritic layer in a few isolated locations. Later, pile construction - especially for pillars 5 and 6 - crossed the reference gypsum layer separating the upper gypsum-claystone and the lower anhydrite-claystone (Figure 4.3). Even if the bored piles were filled with concrete, damage induced around the pile shaft during pile construction would allow a vertical transfer of water. Finally, the set of borings drilled later for monitoring and investigation purposes (most of them located in the vicinity of pillars P5 and P6) implied an additional downward water transfer. The water entrance into the horizontal open fractures triggered the swelling phenomena. Figure 5.13 illustrates this scenario.

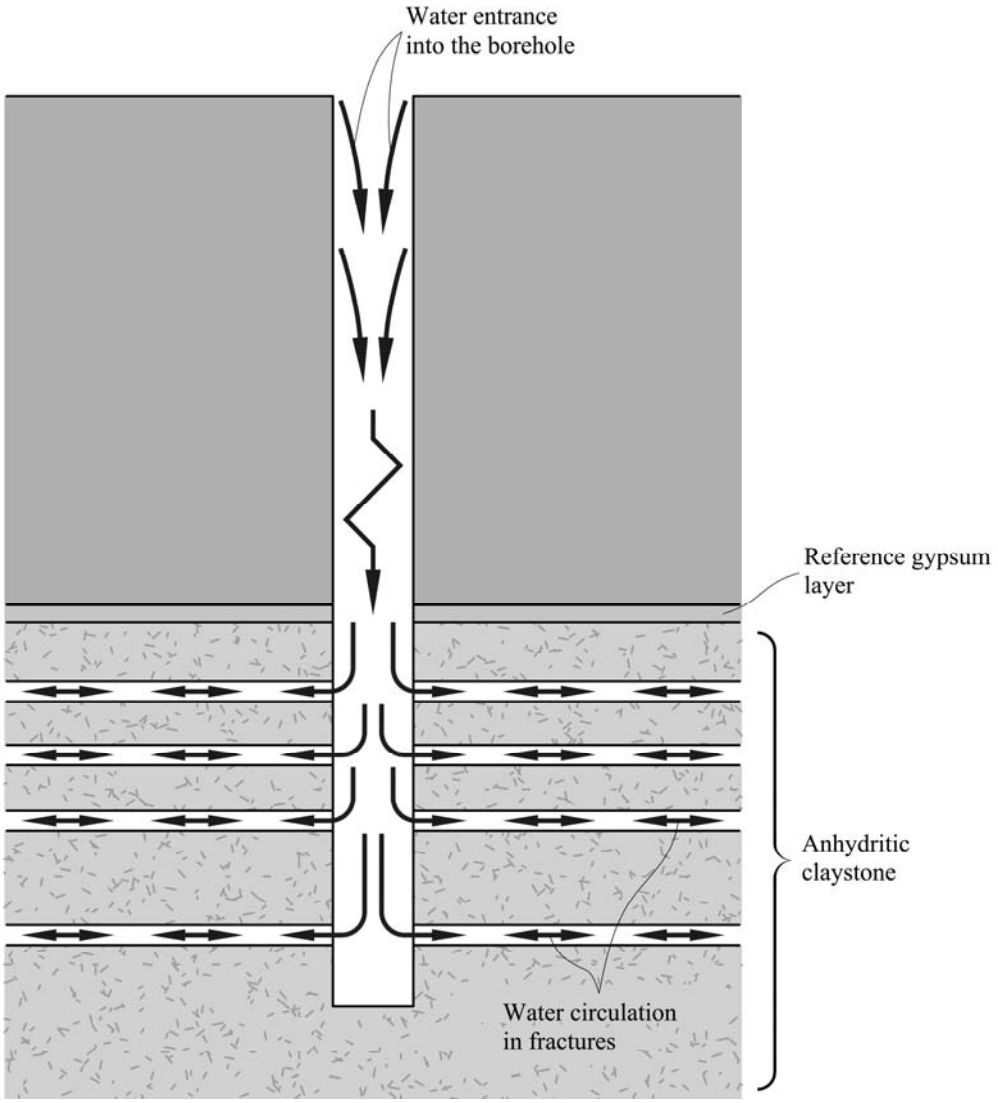

Figure 5.13. Scheme of water access towards the lower fractured sulphated claystone formation from the upper saturated materials

It may be wondered why monitoring boreholes were drilled if they would aggravate the heave phenomenon. However, the reasons for the observed heave had not been agreed upon by the

different parties involved at the time of designing the monitoring programme. In general, no precaution was taken against the drilling of the necessary boreholes; in fact, the scenario described was developed (and supported) later on the basis of the data reported by the monitoring programme.

This hypothesis is also consistent with the heave contours plotted in Figure 4.9 and Figure 4.10. In fact, they show a displacement of the measured surface heave in the expected direction of natural flow in the valley, which also explains why the highest displacements are measured in pillars P5 and P6, whose pile foundations reached the anhydrite.

5.7 Heave scenario in Lilla tunnel

The scenario leading to the heave development in Lilla is conceived as follows: tunnel excavation induced a significant stress release under the horizontal tunnel floor. Blasting also contributed to damage the rock. Existing slickensides facilitated the opening of discontinuities. Groundwater regime in the vicinity of the tunnel was modified by the presence of the tunnel, which acts as a drain. Free water will flow mainly through open fissures under the tunnel invert; then anhydrite exposed in fissures will dissolve and sulphate concentration in water will reach values in equilibrium with anhydrite. This is a super-saturation state for gypsum precipitation. The presence of gypsum crystals will enhance gypsum precipitation. Gypsum crystal growth will contribute to further rock damage and will result in the observed heave and swelling pressures against rigid boundaries such as the tunnel lining.

The next step will be the formulation of a working model at the scale of the field problem, which incorporates the key aspects described.

5.8 Summary of main findings

The swelling mechanism

Expansion is the consequence of gypsum precipitation in rock discontinuities. The precipitated crystals act as local jacks, opening and damaging further the rock. The process is accompanied by a mechanical degradation of the rock and by an increase in water content of the claystone matrix. Gypsum precipitates from water exhibiting a sulphate oversaturation.

This condition is achieved, when anhydrite is present because solubility of anhydrite in pure water, at temperatures in the range 0-56ºC is higher than the solubility of gypsum. Other possible reasons for sulphate oversaturation in water when tunnels are involved, such as the evaporation of groundwater towards tunnel boundaries, are probably of minor significance.

Active zone in tunnels, Lilla tunnel

Expansion concentrates below the tunnel invert. This is a consequence of the natural drainage of the rock mass towards the tunnel invert. Very small swelling pressures have been measured against the vaults and abutment walls. The active zone, which is well identified by continuous extensometers, seems to have a stable dimension (depth) once it has been generated. Expansion accumulates in the initial active zone. The active zone appears to be a direct consequence of the stress release associated with tunnel excavation, which was capable of opening the existing slikensided surfaces and also new discontinuities, allowing the flow of water in discontinuities of the sulphated claystone. The phenomenon of swelling in Lilla was a consequence of a few contributing factors: significant presence of anhydrite, existent or activated discontinuities and the circulation of water. These conditions were present in the highly tectonised Tertiary claystone in Lilla tunnel. The Lilla case shows that relatively small and careful (mechanical) excavations (those required to evolve from a flat floor to a curved invert and then to a full circular geometry) are capable of creating a new active zone. This behaviour is probably enhanced by relatively high K_0 values (not measured in Lilla). Therefore, the active zone is directly related to the damage induced by the excavation. However, the development of swelling also requires the presence of circulating waters. Anagnostou (1992, 1993) describes a model for swelling rock in tunnelling that also expresses the development of swelling strains through an elastoplastic model for the rock behaviour.

Active zone in Pont de Candí bridge

Expansion in the area of Pont de Candí bridge concentrate in an active layer 12-15 m thick located at depths in excess of 25 m. The heave of the central pillars of Pont de Candí Bridge, which are founded on massive deep foundations socketed in sound claystone is a unique case that called for the combination of a few different circumstances to occur: the presence of anhydrite under the piles tip, the existence of a network of fissures within the anhydritic claystone, and a modification of the hydraulic regime of the entire foundation area. The third

circumstance is associated with construction works, and it is believed to be a consequence of the connection of an upper aquifer to the fissured claystone at depth. This connection was made possible by a number of reconnaissance borings but also by the pile construction itself. The circumstances described allowed the circulation of water through the anhydritic level, the dissolution of anhydrie and the precipitation of gypsum crystals in the discontinuities.

Scale effects

Swelling tests on small samples, following methodologies valid for expansive clays, seem not to be suitable to identify expansion phenomena in sulphated rocks. However, Pimentel (2007) has reported high swelling pressures in tests performed on anhydritic claystone. In Lilla claystone the swelling process develops at the scale of the rock mass. Its intensity and spatial distribution depend on the rock structure and, more specifically, on the pattern of joints and shearing surfaces and the intensity of stress changes. A consequence of the definite scale effects is that the expected spatial distribution of swelling and swelling pressures would be as heterogeneous as the rock mass itself. It has been shown that this characteristic behaviour enhances three dimensional effects, which implies beneficial effects on the performance of the tunnel lining.

Yielding versus full support

Yielding support leads to a short term reduction of pressures against tunnel lining. It also allows an increased deformation of the rock and therefore it will lead to associated rock damage. Although no field information is available on the long term behaviour of a yielding support, Lilla final lining was designed as a full support in view of the uncertainties generated by a yielding support design. Full support prevents movements, reduces the expected rock damage and limits the increase in rock permeability making more difficult the percolation of water through discontinuities.

Field reconnaissance

An exercise to predict the swelling potential on the basis of conventional core recovery in reconnaissance borings was performed with the aim of obtaining practical rules to identify conditions likely to result in swelling phenomena during tunnel excavation. The conditions

leading to swelling in the case of the Lilla rock are: a dominant and significant proportion of anhydrite in the rock mass and the presence of internal discontinuities in the rock, identified as slickensides and shearing surfaces with striations. Obviously, water should also be present.

CHAPTER 6

Crystal growth and soil expansion: The role of interfacial pressure and pore structure

Measurements of swelling pressure against the lining of Lilla tunnel at the instrumented cross-sections indicate that the maximum swelling pressure recorded is close to 7 MPa. However, in general the measured maximum values at different cross-sections vary from 5 to 6 MPa. The maximum swelling pressure able to be exerted from swelling sulphated claystone is unknown. The work described in this Chapter was performed to give some insight in that direction. The process of crystal growth requires water because gypsum crystals precipitate from supersaturated solutions of calcium sulphate. The Chapter concentrates on the precipitation of crystal in pores of varying geometry with the purpose of deriving theoretical expressions for the crystal pressure against the (assumed rigid) pore walls. The problem is solved by two complementary approaches: the thermodynamic requirements for the equilibrium of the chemical reaction of precipitation and the consideration of the surface energy at the crystal-solution interface. The phenomenon has strong similarities with other interfaces of interest in unsaturated soil mechanics which are highlighted. The expressions found for the crystal pressure are considered an upper bound for pressures likely to develop "in situ". Several pore geometries and assumptions on the crystal geometric growth, based on

field observations, were analysed. The theoretical pressure derived for cylindrical pores (8.6 MPa) is in reasonable agreement with the maximum recorded swelling pressure against Lilla tunnel (6.7 MPa). The analysis was based on the approach described by Scherer (1999).

6.1 Introduction

The analysis of the severe swelling phenomena that affected Lilla tunnel and Pont de Candí Bridge in Tarragona, Spain showed that expansions were a result of gypsum crystal growth (Chapter 3, 4 and 5). Crystals grew in fractured deep layers in both cases. Instrumentation provided values of sustained heave in time and also values of swelling pressures against the lining of Lilla tunnel.

The reasons for swelling behaviour in Lilla tunnel and Pont de Candí bridge are understood in general terms. However, a more fundamental explanation for the development of swelling pressures is analysed here. Strong similarities exist between the air-water interface in an unsaturated porous media and the interface of the crystal-aqueous solution. The equilibrium of a small crystal under pressure growing from solution is described by means of a psychrometric-type of law which relates the crystal pressure with the curvature of the crystal and the concentration of the aqueous solution at the interface.

The attention is focused on the generation of crystal pressures against the walls of the pores or discontinuities. Estimated values of pressure applied by crystal growth to the rock boundary are compared with swelling pressures measured in Lilla tunnel.

6.2 Crystal growth from aqueous solutions

Crystals precipitate and grow from supersaturated solutions of dissolved salts in water. They dissolve if solute concentration is lower than the limiting concentration for precipitation. Dissolution and precipitation can be described by a simple chemical reaction involving the mineral (or salt), M:

$$1M_c \rightleftharpoons 1M_s \tag{6.1}$$

where M_c refers to the mineral in the solid state, the crystal, and M_s is the dissolved mineral, the solute. Equation (6.1) explains that the number of moles interchanged from the solid and the solution should be equal.

Equilibrium of chemical reactions is approached from the concept of Gibbs free energy of a system with n chemical components at a given temperature, T, and pressure, p: $G(T, p, N_i)$ where N_i is the number of moles of component i of the reaction. A system is in equilibrium if G is minimum ($dG=0$). dG is calculated as

$$dG = \frac{\partial G}{\partial T} dT + \frac{\partial G}{\partial p} dp + \sum_{i=1}^{n} \frac{\partial G}{\partial N_i} dN_i = \\ = -SdT + Vdp + \sum_{i=1}^{n} \mu_i dN_i \tag{6.2}$$

where μ_i is the chemical potential of component i, S is the entropy of the system and V is the volume of the system. At constant pressure and temperature, a chemical reaction will be in equilibrium if

$$dG = \sum_{i=1}^{n} \mu_i dN_i \equiv \sum_{i=1}^{r} \mu_i \nu_i = 0 \tag{6.3}$$

where v_i are the stoichiometric coefficients of the reaction. Applying relation (6.3) to reaction (6.1) results in:

$$1 \cdot \mu_{M_s} - 1 \cdot \mu_{M_c} = 0 \tag{6.4}$$

which explains that the crystal will be in equilibrium in solution if the chemical potentials of crystal and solution are equal.

The chemical potential of a solute having an effective concentration (or activity) a_s is (Langmuir, 1997):

$$\mu_s = \mu_{s,0} + R_g T \ln a_s \tag{6.5}$$

where R_g is the ideal gas constant.

Consider now the crystal. The variation of its chemical potential, in view of Gibbs-Duhem equation can be written (Scherer, 1999):

$$d\mu_c = -S_c dT + \nu_c dp_c \tag{6.6}$$

where S_c and v_c are the molar entropy and the molar volume of the crystal and dp_c is the variation of pressure applied to the crystal. At constant temperature, integration of equation (6.6) results in:

$$\mu_c = \mu_{c,0} + \nu_c (p_c - p_{c,ref}) \tag{6.7}$$

At chemical equilibrium the chemical potentials (6.5) and (6.7) should be equal:

$$\mu_{c,0} + \nu_c (p_c - p_{c,ref}) = \mu_{s,0} + R_g T \ln a_s \tag{6.8}$$

Consider now two states (1 and 2) at equilibrium:

$$\mu_{c,0} + \nu_c (p_{c,1} - p_{c,ref}) = \mu_{s,0} + R_g T \ln a_1 \tag{6.9a}$$

$$\mu_{c,0} + \nu_c (p_{c,2} - p_{c,ref}) = \mu_{s,0} + R_g T \ln a_2 \tag{6.9b}$$

If state 2 is made equal to the reference state ($p_{c,ref}$) equations (6.9a,b) result in:

$$\nu_c (p_{c,1} - p_{c,ref}) = R_g T \ln {a_1}/{a_{ref}} \tag{6.10}$$

Equation (6.10) will be used below to find crystal pressure.

6.3 Crystal pressure

Consider a crystal immersed in a solution of a mineral (activity a_0) which is taken as the reference state. The liquid solution is at pressure p_l. Then, in view of Equation (6.10):

$$p_c = p_l + \frac{R_g T}{\nu_c} \ln \frac{a}{a_0} \tag{6.11}$$

is the necessary pressure applied to the crystal to prevent crystal growth when immersed in a solution with activity a.

Crystal pressure may be approached from another perspective by considering the interfacial energy, γ_{cl}, at the crystal-solution interface. This interfacial energy is conceptually similar to the familiar surface tension at the gas-liquid interfaces. It has the units of force/length and it may be thought also as the energy required to increase in a unit area the contact surface between the two components (crystal and solution).

Following Laplace derivation, a crystal surface, in contact with a solution, having a curvature defined by radii r_1 and r_2 (Figure 6.1) will experience a pressure given by

$$p_c = p_l + \gamma_{cl} \left(\frac{1}{r_1} + \frac{1}{r_2} \right) \tag{6.12}$$

where p_l is the liquid pressure.

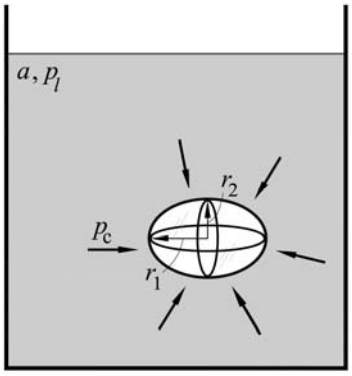

Figure 6.1. A representation of a crystal with a surface curvature defined by r_1 and r_2 immersed in a solution

Equations (11) and (12) provide an explanation for the reference activity a_0. It is the solution activity which prevents the growth of a flat crystal ($r_1=r_2=\infty$). In equation (12) curvature radii are positive when the centre of curvature is located inside the crystal (convex shapes).

Equations (11) and (12) provide an equilibrium relationship between crystal curvature and the activity of the solution in contact with the crystal.

$$p_c - p_l = \gamma_{cl}\left(\frac{1}{r_1}+\frac{1}{r_2}\right) = \frac{R_g T}{\nu_c}\ln\frac{a}{a_0} \tag{6.13}$$

Note that equation (13) is equivalent to the psychrometric relationship for air-water interfaces. The smaller the crystal (low curvature radii), the higher the solution activity able to stop its growth. In other words: a small (spherical) crystal will be more soluble than a (large) flat crystal.

6.4 Crystal growth in pores of rock

When a crystal approaches a solid surface (the wall of a pore or crack) a liquid film of solution remains at the wall-crystal interface (Figure 6.2). Scherer (1999) reports that the thickness of this film is a few nanometres. The liquid film is connected to the solution and its concentration, in equilibrium conditions, will become equal to the solution concentration. Therefore the film allows the growth of the crystal. However the solid wall will oppose crystal growth by repulsive forces. Further analysis of crystal pressures against pore walls requires the consideration of pore geometry.

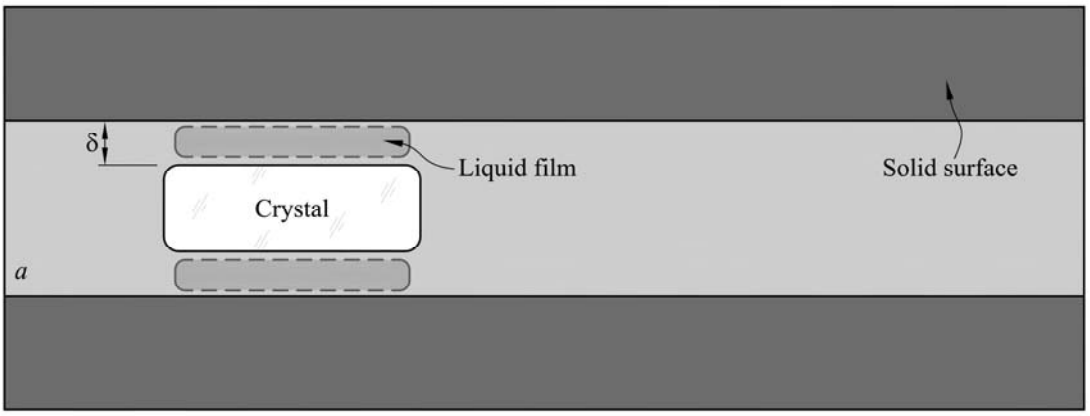

Figure 6.2. A representation of a crystal immersed in a solution approaching a solid surface during its growth

Three geometries will be examined: a cylindrical, a planar joint and a sphere. Connection between the crystal-wall film and the solution liquid is accepted. In the case of a sphere, this is achieved by means of a cylindrical conduct as shown in Figure 6.3(c).

6.4.1 Cylinder (Figure 6.3(a))

A crystal growing in the pore will eventually approach the rock wall. The pore geometry will dictate further growth.

The crystal will grow as a solid cylinder limited by two "caps" which will be assumed to be spherical. From equation (6.13) the solution activity required to prevent crystal growth will be given by

$$a = a_0 \exp\left[\frac{\nu_c \gamma_{cl}\left(\frac{1}{r_1}+\frac{1}{r_2}\right)}{R_g T}\right] \tag{6.14}$$

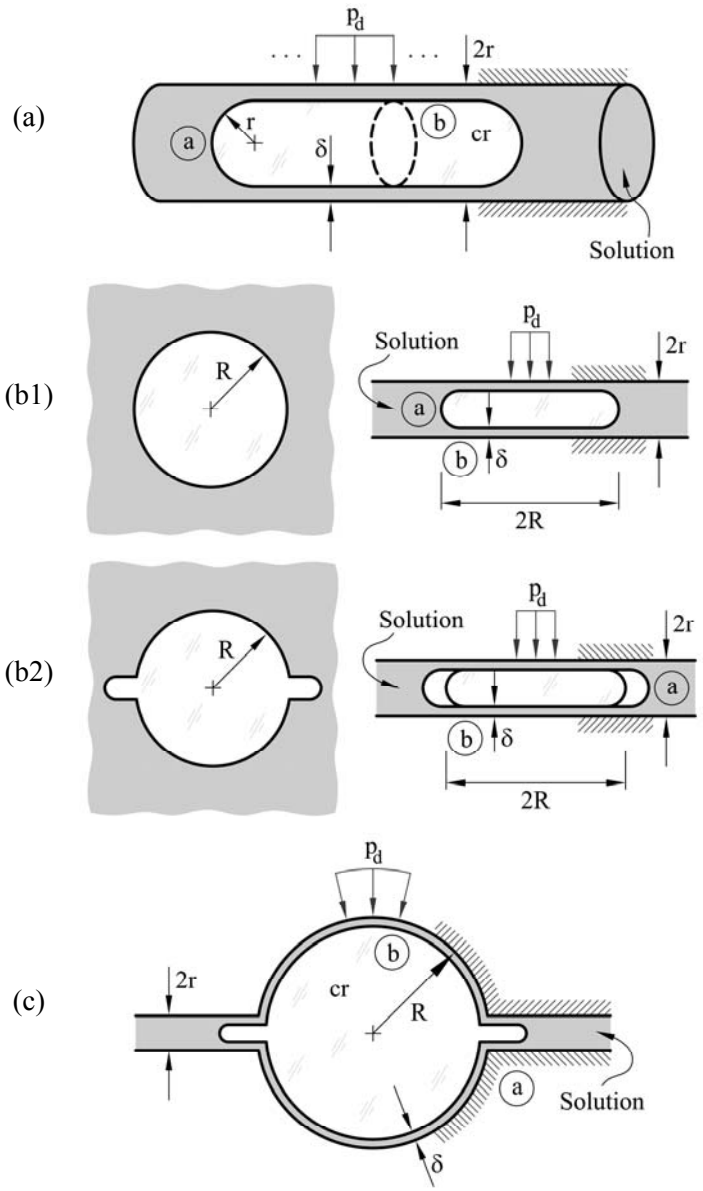

Figure 6.3. Pore geometries: (a) cylinder; (b) planar fissure; (c) sphere

Consider now the zones *a* and *b* of the crystal (spherical "cap" and "long cylinder" respectively). If the film thickness δ is small compared with radius *r*, the curvature in zone *a* will be *2/r* and in zone *b* it will become $1/r + 1/\infty = 1/r$. Therefore, the solution activity capable of preventing the longitudinal growth of the crystal is twice as high of the activity required to grow against the pore walls. If the solution activity reaches the equilibrium value for the spherical cap, the crystal pressure in zone *a* will be given by (equation 6.13):

$$p_{c,a} = p_l + \gamma_{cl}\left(\frac{1}{r_1}+\frac{1}{r_2}\right) = p_l + \gamma_{cl}\frac{2}{r} \tag{6.15}$$

In zone *b*, where the crystal experiences a pressure $p_{c,b}$, the solution activity is the same as in zone *a*. Therefore the following two equations hold:

$$\text{zone } a \quad p_{c,a} - p_l = \frac{R_g T}{\nu_c} \ln \frac{a}{a_0} = \gamma_{cl} \frac{2}{r} \tag{6.16a}$$

$$\text{zone } b \quad p_{c,b} - p_l = \frac{R_g T}{\nu_c} \ln \frac{a}{a_0} \tag{6.16b}$$

therefore $p_{c,a} = p_{c,b}$.

Consider now the Laplace equation for zone *b* ($r_1 = r$; $r_2 = \infty$). A reaction pressure, p_d, modifies the equilibrium

$$p_{c,b} - p_l - p_d = \gamma_{cl} \left(\frac{1}{r_1} + \frac{1}{r_2} \right) = \gamma_{cl} \frac{1}{r} \tag{6.17a}$$

$$p_{c,b} - p_l - p_d = p_{c,a} - p_l - p_d = \gamma_{cl} \frac{1}{r} \tag{6.17b}$$

Therefore in view of (6.15):

$$\gamma_{cl} \frac{2}{r} - p_d = \gamma_{cl} \frac{1}{r} \quad \Rightarrow \quad p_d = \frac{\gamma_{cl}}{r} \tag{6.18}$$

and, taking (16a) into account

$$p_d = \frac{R_g T}{2\nu_c} \ln \frac{a}{a_0} \tag{6.19}$$

Which allows the calculation of crystal growth pressure against the wall of a cylindrical pore if activities *a* and a_0 could be estimated.

6.4.2 Planar fissure (Figure 6.3(b))

Consider the growth of a circular planar crystal in a fissure. In zone *a* of the crystal the curvature radii are *R* and *r* (*r*-δ). Therefore

$$p_{c,a} - p_l = \gamma_{cl} \left(\frac{1}{R} + \frac{1}{r} \right) = \frac{R_g T}{\nu_c} \ln \frac{a}{a_0} \tag{6.20}$$

In the flat surface *b*,

$$p_{c,b} - p_l - p_d = \gamma_{cl} \left(\frac{1}{\infty} + \frac{1}{\infty} \right) = 0 \tag{6.21}$$

Therefore, from (6.20) and (6.21), knowing that $p_{c,a}=p_{c,b}$,

$$\gamma_{cl}\left(\frac{1}{R}+\frac{1}{r}\right)-p_d=0 \tag{6.22a}$$

$$p_d=\gamma_{cl}\left(\frac{1}{R}+\frac{1}{r}\right)\cong\frac{\gamma_{cl}}{r}\cong\frac{R_gT}{\nu_c}\ln\frac{a}{a_0} \tag{6.22b}$$

(if $R >> r$) which is twice as large as the value derived for the cylindrical pore.

It was often found in the field, when opening fissures where gypsum crystals have developed (Figure 3.13) that acicular crystals stem out of a central disk. This geometry is sketched in Figure 6.3(b2). If the tip of these needles is spherical, the following relation holds:

$$p_{c,a}-p_l=\gamma_{cl}\frac{2}{r}=\frac{R_gT}{\nu_c}\ln\frac{a}{a_0} \tag{6.23}$$

In the flat surface *b* equation (21) holds and therefore

$$p_d=\frac{2\gamma_{cl}}{r}=\frac{R_gT}{\nu_c}\ln\frac{a}{a_0} \tag{6.24}$$

which provides an estimation of the swelling pressure against the walls of the fissure. The two conditions shown in Figure 6.3(b) lead to the same crystal pressure against the walls.

6.4.3 Sphere (Figure 6.3(c))

The small cylindrical conduit out of the spherical pore controls the maximum solution activity. Because of its spherical cap it can be written:

$$p_{c,a}-p_l=\gamma_{cl}\frac{2}{r}=\frac{R_gT}{\nu_c}\ln\frac{a}{a_0} \tag{6.25}$$

In zone *b*, the large spherical pore, of radius *R*

$$p_{c,b}-p_l-p_d=\gamma_{cl}\frac{2}{r} \tag{6.26}$$

Therefore

$$p_d=2\gamma_{cl}\left(\frac{1}{r}-\frac{1}{R}\right) \tag{6.27}$$

If *R* is significantly larger than *r*

$$p_d \cong \frac{2\gamma_{cl}}{r} = \frac{R_g T}{v_c} \ln \frac{a}{a_0} \tag{6.28}$$

6.5 Crystallization pressures in anhydritic rocks

The equations given in the preceding section indicate that crystallization pressures may be estimated from pore size (equations 6.18, 6.22 or 6.28) but also if the degree of supersaturation may be estimated. In Lilla tunnel the swelling mechanism is explained by the dissolution of anhydrite until the massif water reaches equilibrium. This water is supersaturated with respect to gypsum.

Consider the pressure against the wall of a cylindrical pore (equation 6.19). The crystal pressure will be given by

$$p_d = \frac{1}{2} \frac{R_g T}{v_{c,gypsum}} \ln \frac{a_{anhydrite}}{a_{gypsum}} = \frac{1}{2} \frac{8.31 \frac{cm^3 MPa}{K\ mol} \cdot 298.15\ K}{74.69\, cm^3/mol} \ln \frac{10^{-4.36}}{10^{-4.58}} = 8.40 MPa \tag{6.29}$$

The values of equilibrium activity for gypsum and anhydrite dissolution considered in Equation 6.29 are taken from the thermodynamic database for PHREEQC (Parkhurst, 1995; Parkhurst & Appelo, 1999).

In the case of crystals growing in planar or spherical discontinuities this pressure duplicates. This is the case of the crystals shown in Figure 6.4. The pore geometry given in Figure 6.3(b) is a simplified model for this type of crystal development.

These estimations are higher than the maximum swelling pressures recorded against the rigid liner of the tunnel (Figure 3.40). This is coherent because the crystal growth is a local phenomenon that takes place in fissures, and the recorded value of pressure in the field is a result of the pressure exerted against the lining by the swelling rock mass, which is not rigid and has an heterogeneous distribution of fissures where crystal growth occurs. But the calculated limiting swelling pressures are not very far away from the maximum “in situ” recorded values, especially in the case of equation (6.29).

6.6 Conclusions

The expected crystallization pressures in a fissured rock have been estimated from some results of chemical thermodynamic equilibrium of solution-precipitation reactions as well as by the implications of the solute-crystal interfacial energy. The general expressions reproduce known results familiar to unsaturated soil mechanics when air-water interface and capillary pressures are analysed.

Simplified pore and crystal geometries allow the calculation of theoretical crystal pressures against the wall of pores. Three cases have been presented. Calculations have been made for solution activities expected in gypsum crystallization when water dissolves anhydrite. The calculated values are above maximum recorded pressures against the liner of Lilla tunnel. However, the estimations are reasonable if one considers the simplified nature of the analysis at the pore scale. The complexity of a rock mass, its deformability and the highly heterogeneous stress field resulting from local zones undergoing crystal growth may explain the discrepancies. The pore-based analysis seems to provide an upper bound to expected crystallization pressures in real cases.

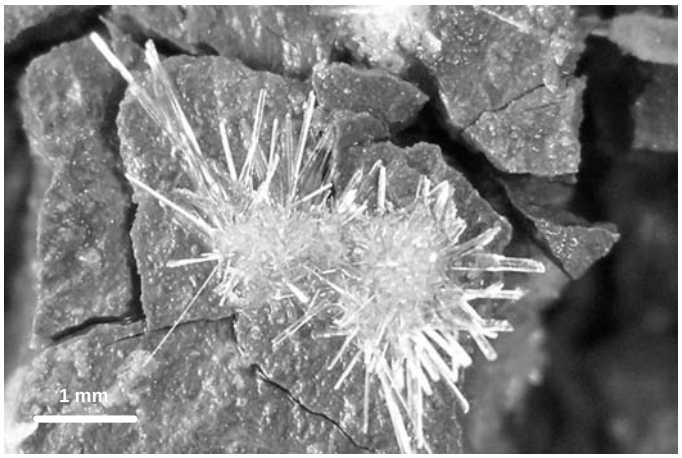

Figure 6.4. Detail of gypsum crystal “rosettes” developing in a discontinuity

CHAPTER 7

Modelling gypsum crystal growth and swelling behaviour. Application to Pont de Candí bridge

The swelling behaviour observed in anhydritic rocks is explained by the precipitation of gypsum crystals in open discontinuities. Gypsum crystals growing in discontinuities contribute to open them and induce deformations or pressures (if the displacements are restrained). A model has been formulated to reproduce the observed expansive behaviour in sulphated rocks. It is described in this Chapter. The model developed integrates a set of balance equations that includes two soluble species (gypsum and anhydrite) in addition to the inert clay minerals, kinetic equations for dissolution and precipitation, mechanical equilibrium, and the effect of precipitated mass on induced volumetric strains. Most of the model parameters are physico-chemical constants, a positive feature that limits the effort to calibrate material constants. The model also keeps track of the solute transport and takes into account the effect of the existing load on crystal growth. As it was described in Chapters 4 and 5, the heave of the central pillars of the railway bridge, founded on large diameter bored piles, is a consequence of gypsum crystal growth in an anhydritic claystone stratum underlying the tip of the piles. The heave mechanism is explained by the presence of circulating water in the fractured anhydritic level. The Chapter also describes a simulation

performed of the heave observed in Pont de Candí Bridge. Model calculations are compared with measured long-term field records of heave. The model is capable of accurate midterm heave prediction at the ground surface and the distribution of vertical strains measured in depth. It also correctly includes the effect of building a surface embankment with the purpose of reducing the heave rate. A sensitivity study is reported to achieve a deeper insight into the phenomena, and to investigate the relevance of a few controlling parameters.

7.1 Introduction

Important heave and swelling phenomena in sulphated claystone is a consequence of gypsum crystallisation in open fissures. Fissures may pre-exist or be induced by crystal growth itself. Once the process is initiated new or more developed fissures may be formed. Crystals precipitate from supersaturated solutions in calcium sulphate, which is a consequence of the presence of anhydrite. In fact, water in chemical equilibrium with anhydrite reaches concentrations that exceed the sulphate saturation conditions for sulphate precipitation. It has also been argued in Chapter 5 that the initial presence of gypsum crystals may play the role of seeds that facilitate the initiation and development of the phenomena.

The Chapter describes first the formulation of a model to reproduce the expansive behaviour in sulphated rocks due to gypsum precipitation developed during the Thesis. Then the model is applied to the conditions prevailing in Pont de Candí bridge and the calculated evolution of heave is compared with actual measurements. The calculated distribution of swelling strains in depth has been compared with recorded strains below piles. A sensitivity analysis performed highlights the relative importance of the contributing factors to the observed heave. The Chapter concludes by summarising the field information necessary for the parameters used in the model, and stressing some open questions.

7.2 A model for gypsum precipitation and heave

Figure 7.1 shows a representative volume of the active layer under the existing total stresses. The precipitation of gypsum in discontinuities will tend to open them and will result in the development of deformations whose direction and intensity will be defined by the distribution of fracture families (Figure 7.1(a) and Figure 7.1(b)).

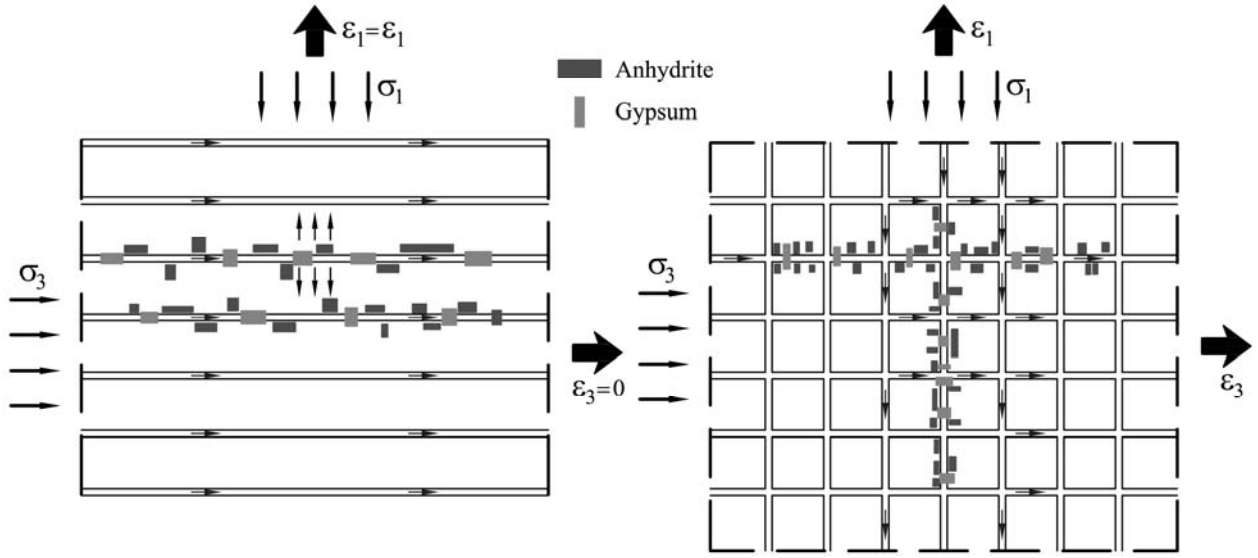

Figure 7.1. A "representative element" of sulphated rock for: (a) swelling in vertical direction; (b) swelling in two directions

The swelling phenomenon is formulated within a general framework of hydro-mechanical analysis for saturated porous media. Some background references for the model, in its "standard" version, are Olivella et al., 1994, 1996; DIT-UPC, 2002 and DETCG, 2010.

However, the material involved in gypsum crystal growth is not a standard medium: the claystone rock includes non-soluble minerals and two minerals (anhydrite and gypsum) that will dissolve and precipitate. Therefore, the solid mass balance equation should include the three solid species. The mass balance equation of inert and salt species should be formulated along with the mass balance of the liquid phase. In addition, the equilibrium equation should take into account that the crystallization of gypsum induces deformations. Also, the model has to keep track of the solute, which in this case is calcium sulphate ($CaSO_4$). Then, a solute balance equation has to be added for the transport of sulphates. The derivation of all the equations is described in detail in the Appendices.

7.3 Mass and momentum equations

The solid skeleton of the soil considered in the present work has been represented in the phase diagram of Figure 7.2. The volume fractions of the soluble species (anhydrite and gypsum) are denoted as anhydrite porosity (ϕ_{anh}) and gypsum porosity (ϕ_{gyp}). Accessible voids are represented by the "open" porosity, ϕ.

The mass balance has to include the three different species of the solid phase: the insoluble clay matrix and other non-sulphate species; the soluble gypsum crystals; and the soluble anhydrite crystals. The mass balance equation for standard soils transforms into three balance equations for the insoluble solids and for the soluble species gypsum and anhydrite:

$$\frac{\partial}{\partial t}\left(\rho_s\left(1-\phi-\phi_{anh}-\phi_{gyp}\right)\right)+\nabla\cdot\left[\left(\rho_s\left(1-\phi-\phi_{anh}-\phi_{gyp}\right)\right)\frac{d\mathbf{u}}{dt}\right]=0 \tag{7.1}$$

$$\frac{\partial\left(\rho_{gyp}\phi_{gyp}\right)}{\partial t}+\nabla\cdot\left[\left(\rho_{gyp}\phi_{gyp}\right)\frac{d\mathbf{u}}{dt}\right]=\frac{dm_{gyp}}{dt} \tag{7.2}$$

$$\frac{\partial\left(\rho_{anh}\phi_{anh}\right)}{\partial t}+\nabla\cdot\left[\left(\rho_{anh}\phi_{anh}\right)\frac{d\mathbf{u}}{dt}\right]=\frac{dm_{anh}}{dt} \tag{7.3}$$

Appendices 1, 2 and 3 provide details of derivations.

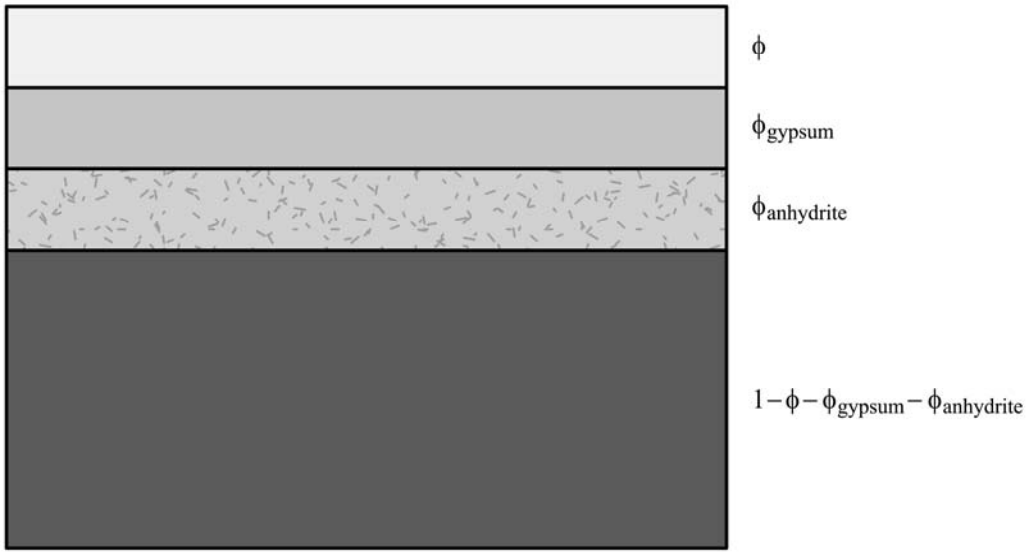

Figure 7.2. Phases and species of anhydritic gypsiferous claystone porous medium

The first equation, equation (7.1), states that the rate of change of mass of insoluble minerals per unit volume must be balanced by the net inflow rate of mass into the reference volume. $\rho_s, \rho_{gyp}, \rho_{anh}$ are the densities of the insoluble minerals, gypsum and anhydrite, and $\boldsymbol{u}$ is the displacement vector field for the porous medium. Acknowledging that gypsum and anhydrite may dissolve or precipitate, a third term, namely the mass rate of precipitation or dissolution of sulphates, should be included in balance equations (7.2) and (7.3).

Combining equations (7.1), (7.2) and (7.3), isolating the rate of change of "true" porosity, ϕ, and taking $\rho_s, \rho_{gyp}, \rho_{anh}$ as constant values results in (Appendix 7.1):

$$\frac{D_s\phi}{Dt} = (1-\phi)\nabla\cdot\left(\frac{d\mathbf{u}}{dt}\right) - \frac{1}{\rho_{gyp}}\frac{dm_{gyp}}{dt} - \frac{1}{\rho_{anh}}\frac{dm_{anh}}{dt} \tag{7.4}$$

where $\frac{D_s(\bullet)}{Dt} = \frac{\partial(\bullet)}{\partial t} + \frac{d\mathbf{u}}{dt}\cdot\nabla(\bullet)$ is the material derivative.

The mass balance equation for the water can be written (
Appendix 7.2) as

$$\phi\frac{D_s\rho_l}{Dt} + \rho_l\frac{D_s\phi}{Dt} + \rho_l\phi\nabla\cdot\left(\frac{d\mathbf{u}}{dt}\right) + \nabla\cdot\left(\rho_l\mathbf{q}_l\right) = f^w \tag{7.5}$$

where ρ_l is the density of the water, $\mathbf{q}_l$ is the flow rate of water, and f^w is any sink or source of water. Gypsum dissolution or precipitation contributes to this term, which is calculated through the mass rate of precipitation and dissolution of gypsum and the stoichiometric relationship (1 kg of gypsum liberates 0.21 kg of water when dissolved). However, the f^w term is negligible in the open system analysed here. The source or sink term refers to the water molecules captured or released by gypsum precipitation or solution. The formulation includes this term. It was later checked with the model that heave rates changed slightly if the source/sink term is eliminated. In other words, the amount of crystalline water and the rates of dissolution and precipitation of gypsum provide a small rate of change of water volume if compared with the rates associated with flow and deformation phenomena.

Consider now the mass balance equation of solute: since, when dissolved, both anhydrite and gypsum originate calcium sulphate, only one solute will be considered. As a result, the balance equation reads (Appendix 7.3)

$$\begin{aligned}&\rho_l\omega_l^m\nabla\cdot\left(\frac{d\mathbf{u}}{dt}\right) + \phi\frac{D_s\left(\rho_l\omega_l^m\right)}{Dt} + \nabla\cdot\left(\rho_l\omega_l^m\mathbf{q}_l - \mathbf{D}\nabla\cdot\omega_l^m\right) = \\ &= -\frac{dm_{gyp}}{dt}\left(1-\frac{\rho_l\omega_l^m}{\rho_{gyp}}\right) - \frac{dm_{anh}}{dt}\left(1-\frac{\rho_l\omega_l^m}{\rho_{anh}}\right)\end{aligned} \tag{7.6}$$

In this equation ω_l^m is the mass fraction of dissolved sulphate in water (the product $\rho_l \omega_l^m$ is the concentration of sulphate in water in units of mass/volume). The term $\mathbf{D}\nabla \cdot \omega_l^m$ accounts for the diffusive rate of flow following a Fick's law. $\mathbf{D}$ is the diffusion coefficient.

The Mass and water balance equations (equations (7.4) and (7.5)) may be combined into a single equation (

Appendix 7.2)

$$\phi \frac{D_s \rho_l}{Dt} + \nabla \cdot \left(\rho_l \mathbf{q}_l \right) = -\rho_l \nabla \cdot \frac{d\mathbf{u}}{dt} - \rho_l \left(-\frac{1}{\rho_{gyp}} \frac{dm_{gyp}}{dt} - \frac{1}{\rho_{anh}} \frac{dm_{anh}}{dt} \right) + f^w = 0 \tag{7.7}$$

where changes in the density of the solid species are neglected.

The equilibrium equation in terms of total stresses

$$\nabla \cdot \boldsymbol{\sigma} + \mathbf{b} = 0 \tag{7.8}$$

where $\boldsymbol{\sigma}$ is the stress tensor and $\mathbf{b}$ is the vector of body forces, completes the set of equations to be solved.

7.4 Precipitation and dissolution of minerals

The rate of precipitation or dissolution of gypsum or anhydrite mass in equations (7.5) and (7.6) needs to be defined by kinetic laws. Kinetic equations express the rate of mass change in terms of the "distance" between the current concentration of a given solute and the concentration for saturated conditions. In terms of mass fractions (ω_l^m), the equations adopted in this work, modified from Lasaga (1984), are:

$$\frac{dm_{gyp}}{dt} = \sigma_c \kappa \xi_{gyp} \phi_{gyp} \left(\left| \left(\frac{\omega_l^m}{\omega_{l_{sat,gyp}}^m (T, p)} \right)^\theta - 1 \right| \right)^\eta \tag{7.9a}$$

$$\frac{dm_{anh}}{dt} = \sigma_c \kappa \xi_{anh} \phi_{anh} \left(\left| \left(\frac{\omega_l^m}{\omega_{l_{sat,anh}}^m (T, p)} \right)^\theta - 1 \right| \right)^\eta \tag{7.9b}$$

where:

$$\xi_{gyp} = \frac{\omega_l^m - \omega_{l_{sat,gyp}}^m}{\left|\omega_l^m - \omega_{l_{sat,gyp}}^m\right|} \tag{7.10a}$$

$$\xi_{gyp} = \frac{\omega_l^m - \omega_{l_{sat,anh}}^m}{\left|\omega_l^m - \omega_{l_{sat,anh}}^m\right|} \tag{7.10b}$$

A quadratic kinetic law (θ = 1; η =2) was adopted for anhydrite dissolution and gypsum precipitation, following experimental results described in Kontrec et al. (2002). In equation (7.9) the mass fractions for saturated solutions of gypsum and anhydrite are made theoretically dependent on the pressure applied to the crystal, p, and temperature, T. Dependence on temperature is well known (Figure 5.11). The effect of stress acting on the crystals (gypsum and anhydrite) is described by Scherer (1999)

$$\omega_{l_{sat}}^m = \omega_{0l_{sat}}^m \exp\left(\frac{p\nu_c}{R_g T}\right) \tag{7.11}$$

where, $\omega_{0l_{sat}}^m$ is the equilibrium mass fraction of dissolved sulphate in water for an unloaded crystal, ν_c is the molar volume of the crystal, R_g is the ideal gas constant, and T is the absolute temperature. Temperature was constant in the case analysed. This is probably the situation in the active region below the pile's tip. The "pressure" on the crystals, $\sigma'_{crystal}$, will be made equal to the effective intergranular stress acting on the solid species

$$p = \sigma'_{crystal} = \frac{\sigma'_z}{1-\phi} \tag{7.12}$$

The effective vertical stress is selected in this case, where swelling strains are essentially vertical. The formula requires three main assumptions: the fractured claystone is assumed to be a saturated granular medium; the effective stress (in the Terzaghi sense) is a measure of intergranular stresses; and all solid constituents receive the same force per unit area (of the solid species). The derivation is given in the Appendix 7.4.

In equation (7.9), σ_c is the specific surface of the species (m^2 of crystal surface/m^3 of medium) and κ is a constant controlling the rate of dissolution/precipitation (kg/s·m^2 of crystal). Finally, the term ξ (equation 7.10) provides a positive or negative sign to the mass

rate of precipitation/dissolution: a negative sign implies dissolution ($\omega_l^m < \omega_{l\ sat}^m$) and a positive sign ($\omega_l^m > \omega_{l\ sat}^m$) implies precipitation.

A significant feature of stress-strain calculations is that precipitation of crystals induces deformations. A first approximation to calculate the imposed deformations is to assume that the precipitated mass results in a volumetric deformation equal to the crystal volume. However, observations in the field (see Figure 7.3, Figure 7.4, Figure 4.20 and 4.21) indicate that new crystals may either occupy part of the volume of an already existent open discontinuity, or else generate additional porosity. A simple approach is to take these effects into account by means of a "swelling" parameter, γ_i, introduced to calculate strain rates (ε_i) from precipitated gypsum mass as follows:

$$\frac{d\varepsilon_i}{dt} = \frac{\gamma_i}{\rho_{gyp}} \frac{dm_{gyp}}{dt} \tag{7.13}$$

where 1 = vertical (*z*), and 2,3 = horizontal (*h*).

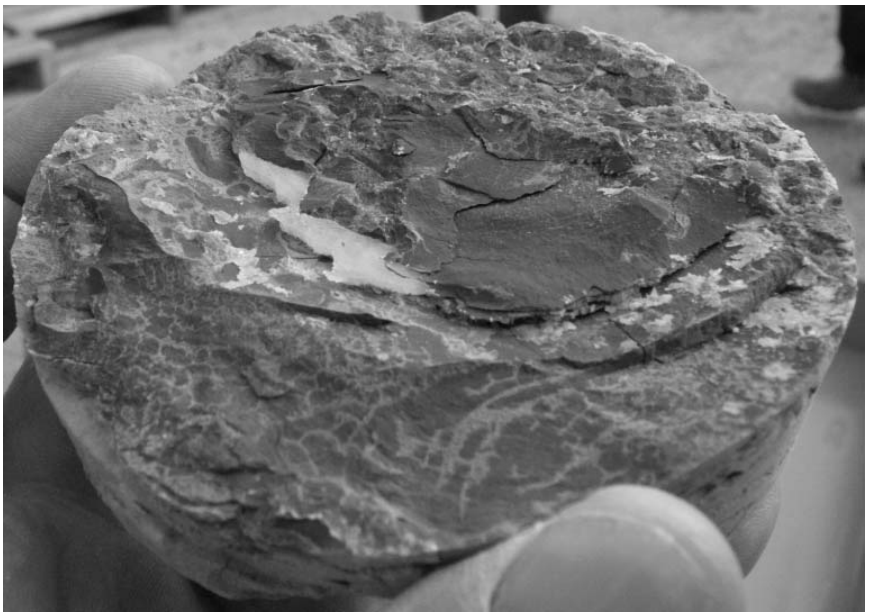

Figure 7.3. Laminar gypsum crystal growth developing inside the clay matrix in a recovered core from a borehole tested during the hydraulic cross-hole tests, at depths corresponding with the active layer

It is reasonable to accept that parameters γ_i depend on the applied effective stress on direction *i*. The higher the effective confining stress, σ_i', the lower the expected volumetric deformation for a given mass of gypsum precipitated. On the other hand, the function $\gamma_i\left(\sigma_i'\right)$

should also include the possibility of a new crystal inducing additional porosity, or partially reducing the existing one. In the second case, subsequent precipitation of gypsum crystals would eventually occupy all the available open space. Under general deformation conditions, γ_i values should also account for the fact that a given volume of precipitated crystal deforms the rock or soil in three directions. The following equations are proposed:

$$\gamma_i = \gamma_{\max} e^{-b\sigma_i'} \text{ for } \sigma_i' > 0 \; ; \; i = 1,\ 2,\ 3 \tag{7.14a}$$

$$\gamma_i = \gamma_{\max} \text{ for } \sigma_i' = 0 ; \; i = 1,\ 2,\ 3 \tag{7.14b}$$

Figure 7.4. Gypsum crystal growth in needles in a recovered core from a borehole drilled for hydraulic cross-hole tests, at depths corresponding to the active layer. Gypsum crystals form needles partially filling the open vein

The maximum value $\gamma_{\max}$ is defined for zero confining stress. It may be suspected that parameters $\gamma_{\max}$ and b will change with spatial direction. A constant value for model parameters $\gamma_{\max}$ and b will be accepted here. Deformation rates induced by gypsum precipitation are treated as imposed volumetric deformations.

All these developments were included into the CODE_BRIGHT Finite Element computer code for thermo-hydro-mechanical analysis of porous media (DETCG, 2010). This program was used in the calculations reported below.

7.5 Heave calculations. Comparison with field data

The simulation performed concerns the central pillar P5 of the bridge, where maximum vertical displacements were recorded (Figure 7.5(a)). A 15 m wide and 55 m long column of foundation material, at pillar P5, was modelled under plane strain conditions. It was further assumed that the foundation material was laterally confined.

The geometrical model, given in Figure 7.5(b), includes the presence of the active layer, 15 m thick, and two stable layers, one above and one below. A phreatic level was located in the position shown in the figure. Following the scheme plotted in Figure 5.13, a horizontal flow was forced in the active layer by adding two inert pervious layers on both sides of the central soil column (Figure 7.5 (b)). A small difference in piezometric head (1 m) between the two lateral layers forces an essentially horizontal flow within the active layer.

The model requires a number of parameters, which have been collected in Table 7.1, under three headings: anhydritic-gypsum transformation, hydraulic parameters and mechanical parameters.

Mass fractions of gypsum and anhydrite for a saturated solution in water are based on a calculation performed with the computer program PHREEQC (Parkurst & Appelo, 1999 and Parkhurst, 1995) which simulates chemical reactions in aqueous solutions. Initial volumetric fractions (porosities) of gypsum and anhydrite in the active layer are approximate average values, which reflect core descriptions made during boring operations.

The rate constant, κ, of kinetic equations has been investigated by a number of authors (Barton & Wilde, 1971; Jeschke et al., 2001; Kontrec et al., 2002). Dissolution is controlled by two processes: a chemical reaction at the crystal surface and a molecular diffusion of dissolved ions through a boundary layer. Therefore, flow conditions around crystals control also the diffusion rate. Laboratory experiments described by the authors mentioned involve tests on crystals in suspension in an agitated aqueous solution or dissolution of crystals adhered to a surface which is rotated in a solution. Following the comprehensive analysis

performed by Jeschke et al (2001) the gypsum dissolution rate parameter is approximately given by κ_{gyp} = 2.23 × 10^{-5}Kg/m^2·s. Experimental results reported by Barton & Wilde (1971) provide a lower value for anhydrite (κ_{anh} = 1.49 × 10^{-5} Kg/m^2·s). However, these authors describe kinetics by mathematical relations which are somewhat different from equation (7.9). As a result, the kinetic coefficient in equation (7.9) could not be estimated reliably from published data based on laboratory tests.

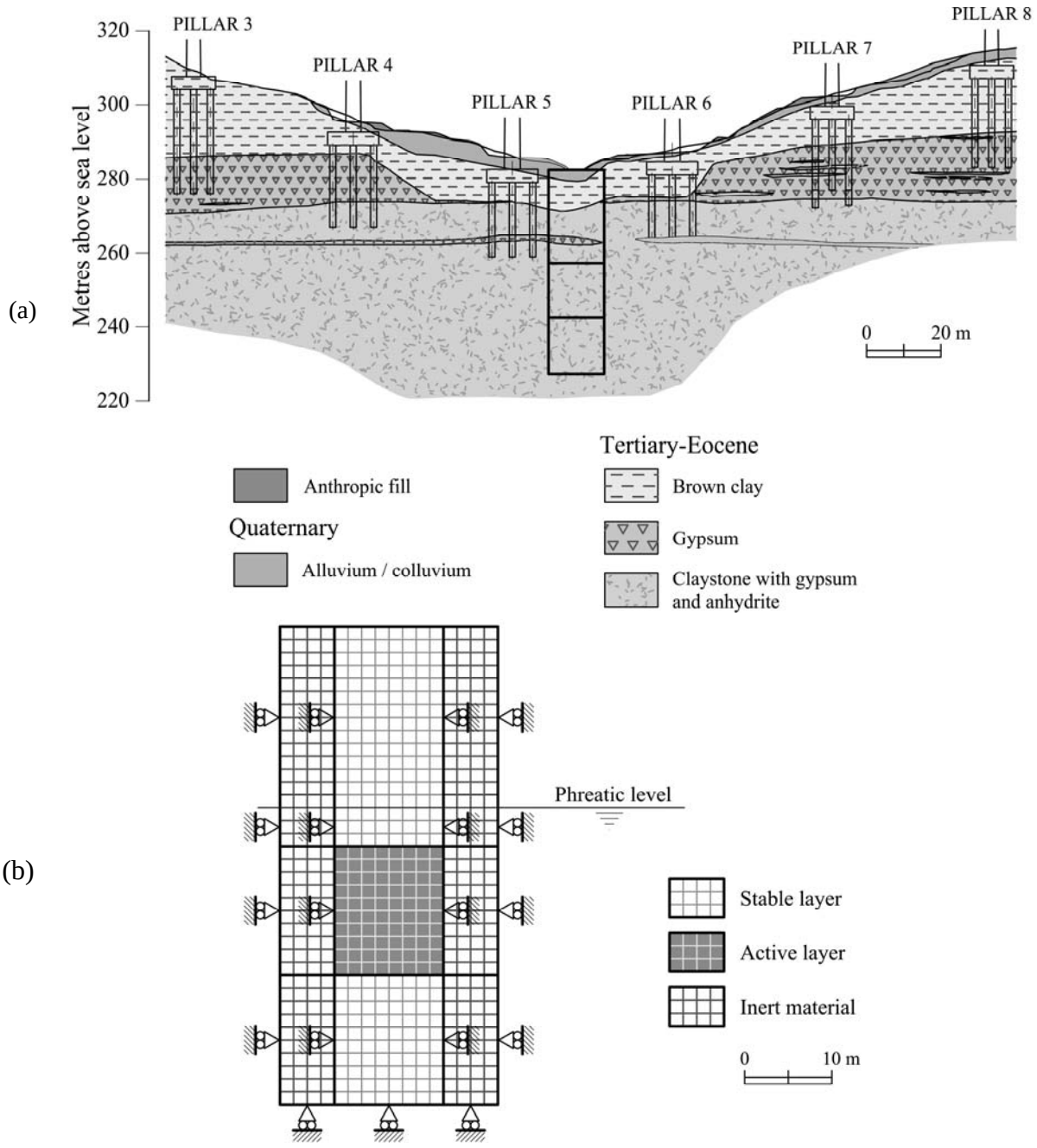

Figure 7.5 (a) Position of column for Finite Element calculations; (b) mesh geometry, materials and boundary conditions

Concerning precipitation, Nancollas et al. (1973) conclude that it is very difficult for anhydrite to precipitate in nature, due to the high activation energy required. Freyer & Voigt (2003) state that precipitation of anhydrite from aqueous solutions is the most difficult one of all phases of calcium sulphate (gypsum, two hemi-hydrates and three anhydrite phases). Below a temperature of 90ºC anhydrite does not precipitate spontaneously. Kontrec et al. (2002) indicate that the dominant precipitation of gypsum occurs spontaneously from highly supersaturated solutions. However, gypsum crystallisation is possible from low supersaturated solutions, provided there are gypsum crystal "seeds" available. The second scenario is likely to prevail in the case described here.

Table 7.1. Model parameters

Anhydrite-gypsum transformation		**Hydraulic**		**Mechanical**	
Parameter	**Value**	**Parameter**	**Value**	**Parameter**	**Value**
Mass fraction of gypsum in water for saturated conditions, no stress applied, $\omega^m_{0l_{sat,gyp}}$	$2.028 \cdot 10^{-3}$	Initial open porosity, ϕ_{ini}	0.09	Elastic parameter, E (MPa)	1000
Mass fraction of anhydrite in water for saturated conditions, no stress applied, $\omega^m_{0l_{sat,anh}}$	$3.187 \cdot 10^{-3}$	Intrinsic permeability K (m^2)	$2 \cdot 10^{-13}$	Poisson's ratio, ν	0.2
Initial gypsum volumetric fraction, ϕ^{gyp}_{ini}	0.2			At rest, earth pressure coefficient, K_0	2
Initial anhydrite volumetric fraction, ϕ^{anh}_{ini}	0.15			Solid specific unit weight, γ_s / γ_w	2.63
Compound kinetic coefficient, $\sigma_c \kappa$ ($kg/m^3 \cdot s$)	$3.5 \cdot 10^{-4}$			Gypsum density, ρ_{gyp} (Mg/m^3)	2.3
Coefficients of kinetic law (10a,b)	$\theta = 1$ $\eta = 2$			Anhydrite density, ρ_{anh} (Mg/m^3)	2.96

It follows from the short review above that the process of anhydrite dissolution and gypsum precipitation is a natural one under the conditions of low stresses and moderate temperatures. It is also consistent with "in situ" observations reported in Chapter 4.

Equation (7.9) indicates that the rate of dissolution/precipitation is governed by the product $\sigma_c \kappa$. Uncertainties in κ are high because of the significant differences between a fractured claystone and the laboratory experiments mentioned. The specific surface σ_c (exposed to free water) is also difficult to estimate in a fractured rock mass. Therefore, the back-analysis of field heave records is better interpreted as providing an estimated value for the compound kinetic parameter, $\kappa\sigma_c$. As a simple choice, a constant value was adopted for gypsum and anhydrite and a value $\kappa\sigma_c$ = 3.5 × 10^{-4} kg/m^3·s was found by matching the field heave records. If further hypotheses are made, κ and σ_c could be isolated. However, not only is the specific surface difficult to estimate, but the dissolution rate reported in some laboratory experiments corresponds to greatly idealised conditions (i.e. isolated anhydrite crystals stirred in a given mass of pure water). "In situ" conditions (a fractured claystone) are far from test set-ups, and the effect of other salts dissolved in groundwater and other solid constituents (clay minerals, for instance) is unknown. Therefore, before further information becomes available, it seems appropriate to maintain the compound coefficient, $\sigma_c \kappa$, as the fundamental rate parameter identified by back-analysis of field records of heave.

Very simple hydraulic and mechanical models were selected because the observed phenomena are not believed to be much affected by them in the observed field behaviour. Two parameters characterise the hydraulic behaviour of the active layer: porosity and permeability. An average value ϕ =0.09 was taken. This value is higher than values measured in some of the recovered cores to account for the open space provided by joints. In the active layer the horizontal intrinsic permeability found in the cross-hole tests described was imposed in the model (K = 2 × 10^{-13} m^2; above and below the active layer permeability was reduced to a lower value, K = 1 × 10^{-16} m^2).

The entire soil/rock column was assumed to be isotropic linear elastic. Initial stresses are given by a geostatic stress in the vertical direction and a horizontal stress given by an at rest pressure coefficient K_0 = 2. The side "auxiliary" columns in Figure 7.5(b) were given a low

elastic modulus to better approximate a free sliding condition in the vertical direction. The swelling phenomenon was activated only in the active layer.

The chemical analysis of water extracted from boreholes crossing the active layer indicated that it was saturated in calcium sulphate salts with respect to gypsum. This condition (ω_l^m = 2.028×10^{-3}) was imposed on the water filling the pores of the active layer.

The assumption made in the model was that (almost) pure water (ω_l^m = 1×10^{-3}) entered the active layer from its left boundary at the position of the active layer. This is an extreme case which may reproduce the inflow of water directly from surface runoff waters (see Figure 5.13). However, the calculation shows that the water entering the active layer rapidly achieves a supersaturated condition as anhydrite is dissolved. There was almost no difference in results when the sulphate concentration of the incoming water was varied between extreme values.

The most uncertain parameters are probably those defining the coefficient γ in equation (7.14a). The selected values $\gamma_{\max}$ = 1, b = 2 result in the $\gamma_z - \sigma_z^{'}$ relationship shown in Figure 7.6. Selecting $\gamma_{\max}$ = 1 implies that no additional swelling, beyond the volume of the precipitated gypsum mass, is considered in the analysis.

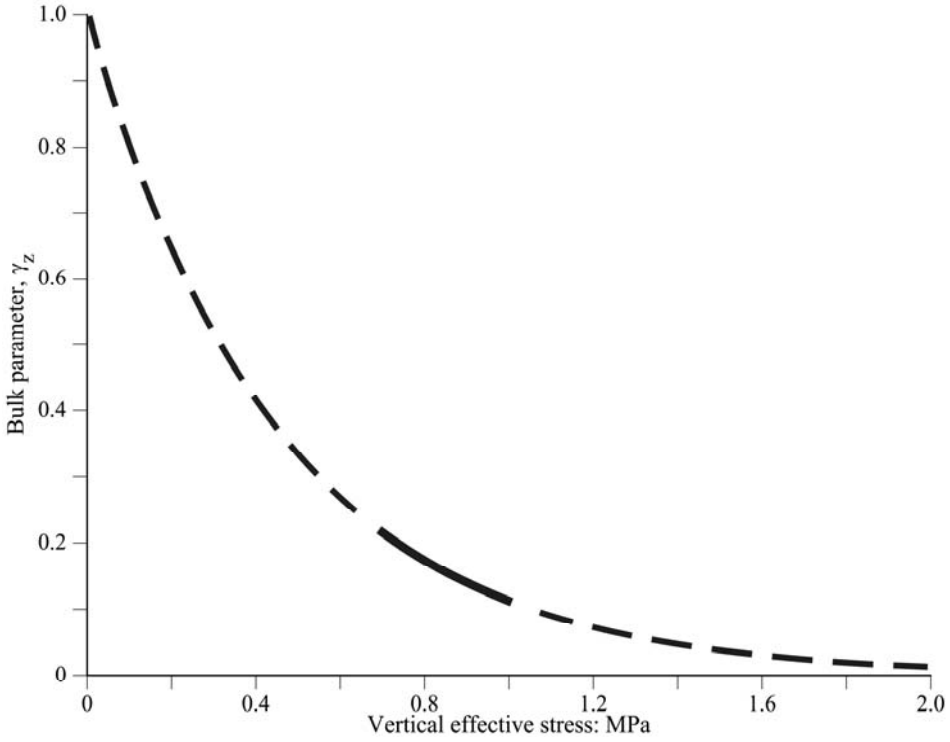

Figure 7.6. Variation of the γ_z with the applied effective vertical stress

Consider first the swelling displacements measured at the top of incremental extensometers IX-5 and IX-6, located in the vicinity of pillar P-5 (the position of these instruments is given in Figure 4.5). An 800-day history of heave displacements is compared with model calculations in Figure 7.7(a). The set of parameters leading to the good fit shown in Figure 7.7(a) is given in Table 7.1, and will be called "base case". The swelling coefficient, γ_z in equation (7.14), takes values varying from 0.11 (deepest point in the active layer) to 0.22 (upper point in the active layer). The range of γ_z values within the active layer is marked in Figure 7.6. These values suggest that a substantial part of the precipitated mass of gypsum occupies the existing void space.

The evolution of calculated vertical strains is given in Figure 7.8. Strains develop in a continuous manner in the active layer, a consequence of the porous model adopted for the claystone porosity.

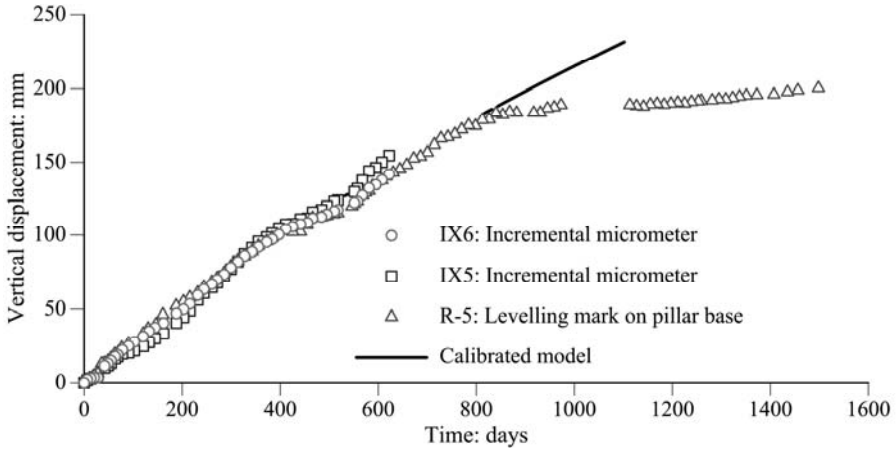

(a)

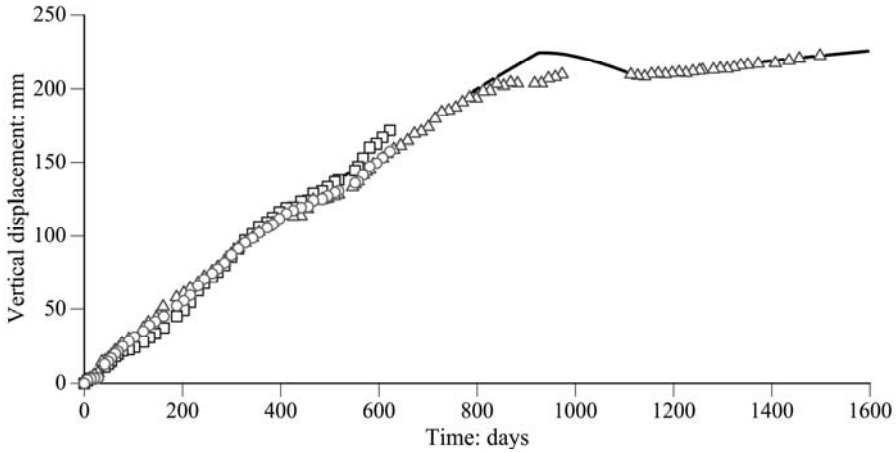

(b)

Figure 7.7. Measured and calculated surface heave: a) model validation for the first 800 days; b) model reaction to construction of surface embankment at t = 924 days

The calculated heave plot in Figure 7.7(a) shows an apparent linear trend of heave with time in natural scale; this is a consequence of the limited time span of the simulation performed. If time is increased (Figure 7.9), there is a progressive decay in the heave rate that eventually stops. Heave development goes in parallel with the depletion of anhydrite content in the active layer (see Figure 7.10). As the anhydrite content (volumetric fraction) decreases, the gypsum content increases in parallel. This is a long term process. The model indicates that if conditions are left unchanged, significant heave rates would develop over a period of 8 years. Once the anhydrite disappears, if hydraulic conditions are maintained, the model predicts a progressive dissolution of gypsum (Figure 7.10).

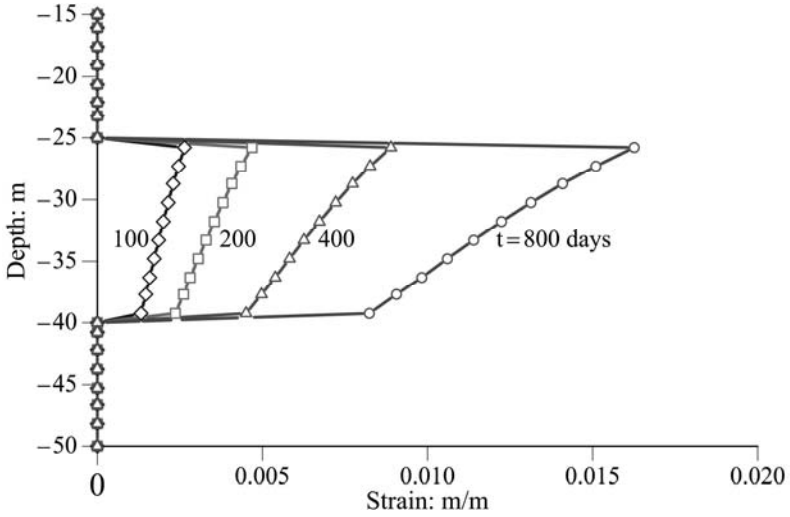

Figure 7.8. Calculated vertical strains in the active layer

The sustained heave rate of the central part of the viaduct experienced a significant reduction when a 29.5 m high embankment over the foundation of pillar P-5 was built on the valley floor (Figure 4.27). Figure 7.7(b) shows the change in swelling rate at t = 924 days when the embankment construction started. The heave record in Figure 7.7 was measured by surface levelling of the base of pillar P-5 and also by levelling the top of the two extensometers located in the vicinity of pillar P-5.

The model reacted in a manner very similar to the actual behaviour, predicting a new rate of swelling very close to the actual values. Model parameters were calibrated on the first part of the swelling record (from t = 0 to t = 800 days). The model also predicts a transient settlement during the embankment ramp loading, which is a consequence of the stiffness assumed for the foundation materials. Field data is scarce during the embankment construction period and this prevents a more accurate analysis of the immediate effect of embankment loading. However,

the heave of the active layer remained at a reduced rate, well defined in subsequent measurements on the pillar surface.

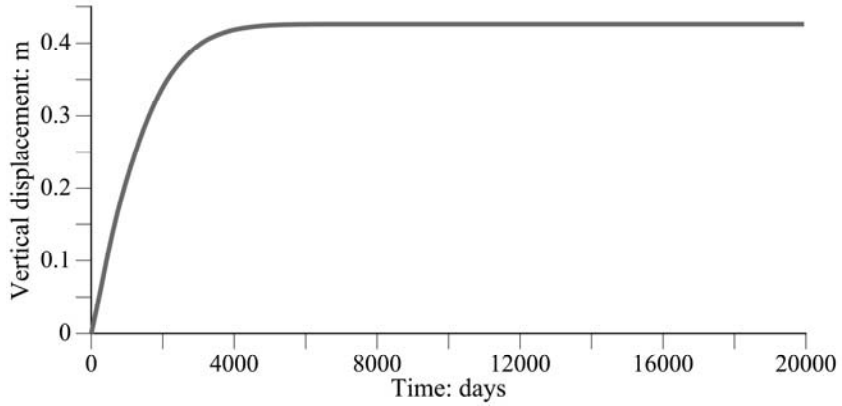

Figure 7.9. Long-term evolution of calculated heave over time

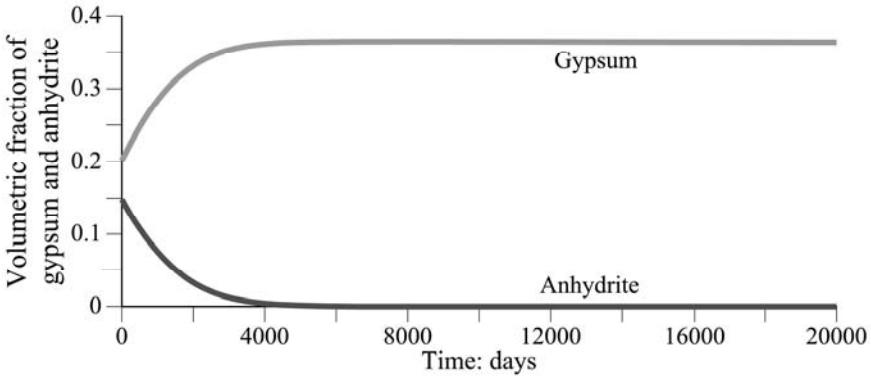

Figure 7.10. Long-term evolution of gypsum and anhydrite volume fractions

7.6 Sensitivity analysis

Further insight into the swelling phenomena and the characteristics of the model developed is gained through a sensitivity analysis on the relative importance of controlling parameters.

The results presented here maintain the parameters of the base case (Table 7.1) except for the parameters defining the effect being investigated. The analysis, in most cases, extends to the first 1600 days, and therefore, it incorporates the embankment loading (except for the cases concerning the effect of applied surface stress on heave development).

7.6.1 Porosity

Changes in porosity modify the water flow rate, which controls the sulphate concentration (Eq. 7.28 in Appendix 7.3), and therefore, the rate of precipitation of gypsum and anhydrite

dissolution. In addition, porosity variations also change the crystal effective stress, which controls anhydrite and gypsum solubility, as well as the swelling coefficient. Despite these cross-effects it turns out that its effect is of relatively minor importance, as illustrated in Figure 7.11. The uncertainty associated with the evaluation of the fissured volume or accessible porosity is therefore quite limited regarding its effect on swelling.

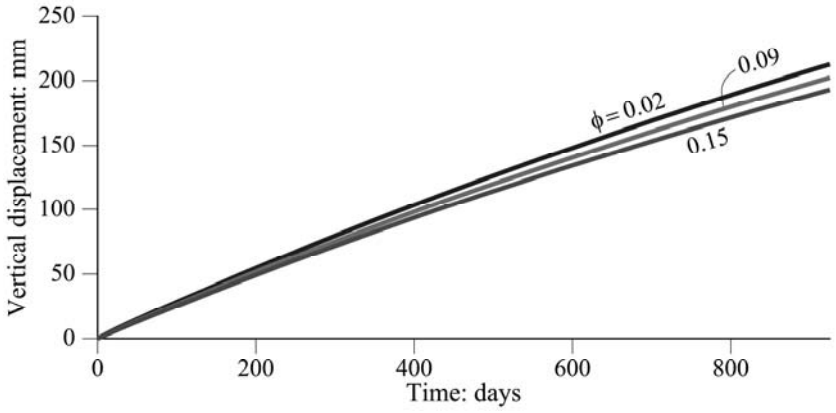

Figure 7.11. Effect of initial porosity on surface heave

7.6.2 Initial volume fractions of gypsum and anhydrite

Volume fractions control rate effects (Eq. 7.9). For instance, equation 7.9a tells that a higher gypsum content results in a higher rate of gypsum precipitation. In other words, increasing the exposed gypsum surface facilitates further gypsum crystallization. The effect of different initial volumetric fractions of gypsum and anhydrite is given in Figure 7.12(a) and Figure 7.12(b). Gypsum volumetric fraction has a small effect (Figure 7.12(a)). However, anhydrite content has a very significant effect on calculated swelling. This result stresses the need for a precise determination of anhydrite content in field investigations.

7.6.3 Equilibrium concentrations

Equilibrium concentrations at saturation are known to depend on temperature and crystal effective stress. The effect of temperature was illustrated in Figure 5.11. The effect of a relatively small change in gypsum and anhydrite values ($\omega^m_{0l_{sat,gyp}}$ from 2.028×10^{-3} to 2.192×10^{-3} and $\omega^m_{0l_{sat,anh}}$ from 3.187×10^{-3} to 2.848×10^{-3}) is shown in Figure 7.13. These concentrations correspond to a change in temperature from 15ºC to 40ºC.

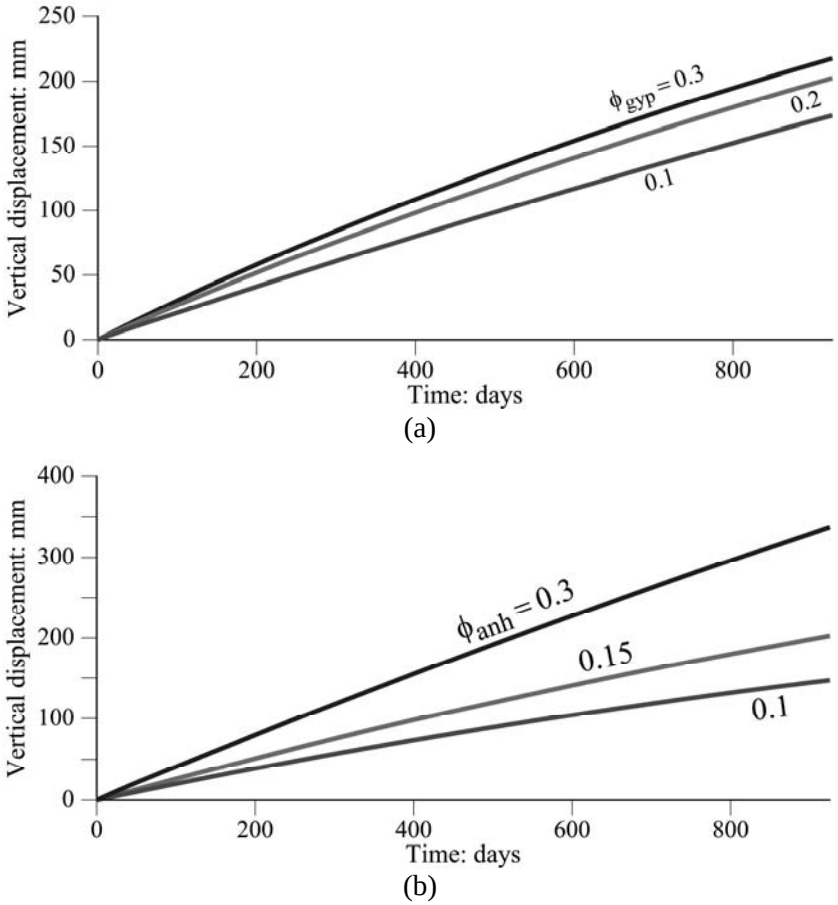

Figure 7.12. Calculated evolution of surface heave. Effect of: (a) gypsum content; (b) anhydrite content

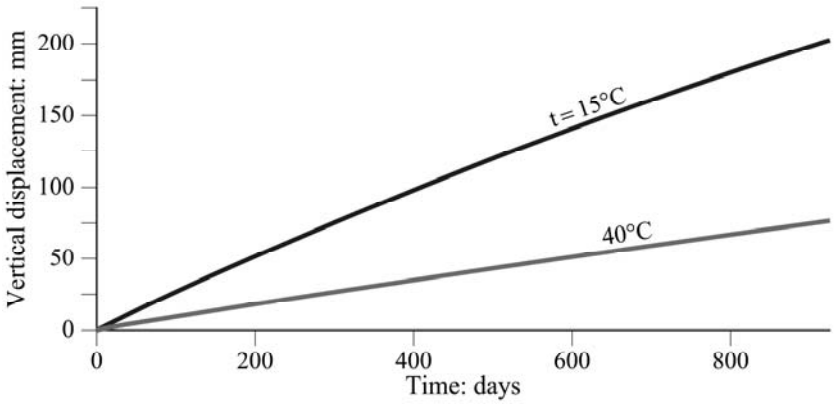

Figure 7.13. Effect of equilibrium concentrations at temperatures 40ºC and 15ºC on calculated heave development

7.6.4 Stress effects

Stress effects are substantial in the developed model for two reasons: they modify the concentration of saturated solutions (Eq. 7.11), and they are expected to modify the swelling

coefficient γ_i (Eq. 7.14). The combined effect is shown in Figure 7.14. Increasing the stress augments the solubility of anhydrite and gypsum. An increased mass of dissolved sulphate is available for gypsum precipitation, but the concentration threshold for precipitation has also increased. The result is shown in the figure: essentially, increasing the stress has a small effect on the development of swelling if only the effect of stress on solubility is accounted for. However, the direct mechanical effect on γ_i reduces the expected heave further. The swelling coefficient dominates stress effects. The three stresses indicated in the plot refer to the initial situation (no load applied on the surface: σ_v = 0), to a 33 m high embankment (σ_v = 0.66 MPa) and to a 48 m high embankment (σ_v = 0.96 MPa).

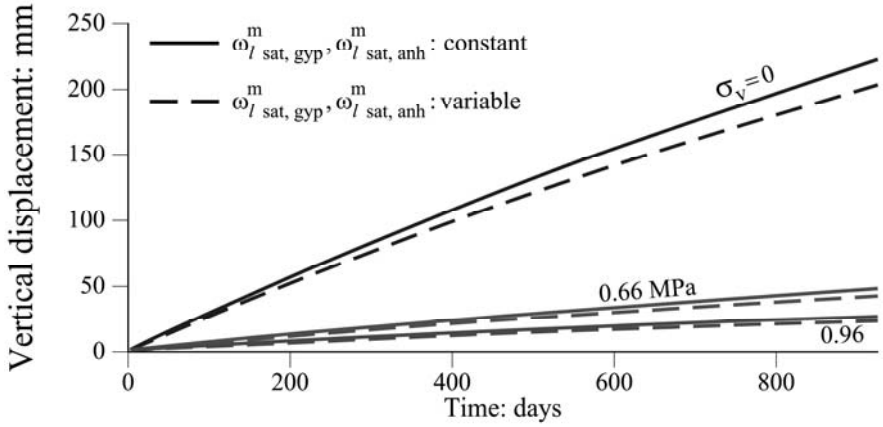

Figure 7.14. Effect of the external vertical stress on calculated vertical heave. The effect of stress on the saturation concentration of anhydrite and gypsum is small. The major effect comes from the "swelling" parameter, γ_i. The curves for σ_v = 0 correspond to the initial situation (no load applied on the surface). The curves for σ_v = 0.66 MPa and 0.96 MPa correspond to 33 m and 48 m high surface embankments

7.6.5 Other effects

Parameters controlling water flow in the active layer (induced gradient, permeability) had a minor effect. Gradient changes result in limited changes in vertical effective stress. Permeability dictates the flow rate, which does not have a direct influence. It affects the time required for the incoming water to reach a saturated concentration of sulphate. But this process is rapid, at least for acceptable permeability values of the anhydritic formation, and

the incoming water saturates shortly after entering the active layer, even if pure water is injected.

The effect of the initial state of stress (K_0) depends on some modelling hypotheses. If swelling strains are activated only in the vertical direction (a hypothesis favoured by the horizontal pattern of discontinuities), the vertical stress controls the calculated swelling, and therefore K_0 has no effect. In the model, K_0 and Poisson's ratio have a definite effect. A change in swelling stresses $\sigma_h^{'}$ implies a change in γ_h, which in turns modifies the calculated horizontal strains needed to compensate the imposed horizontal displacements (zero at the boundary). The calculated horizontal strains result - through the Poisson's effect - in vertical strains that modify the vertical swelling, although this effect is small. A constant Poisson ratio ν = 0.2 was adopted in all calculations.

7.7 A simulation of the distribution of swelling strains in depth

An attempt to reproduce the distribution of swelling strains measured in the active layer has been performed. The same model parameters and geometry defined in the previous sections as a "base case" have been considered in the calculations presented in this section. Gypsum precipitation occurs in open fractures. Measured vertical swelling strains accumulate over time in thin bands inside the active layer (Figure 4.13, Figure 4.14, Figure 4.15, Figure 4.17, Figure 4.28 and Figure 4.29) probably as a result of a relative higher presence of fractures at those depths. These bands, having a higher intensity of fractures, will have more anhydrite in contact with water. The distribution in depth of the initial anhydrite content at depths corresponding to the active layer has been chosen according to the pattern of swelling strains measured near the central pillar P5 (Figure 4.13 and Figure 4.28). The values of initial anhydrite content at different depths have been varied to adjust the calculated vertical displacements to the measured heave in the field (Figure 7.15). Figure 7.16 shows the calculated vertical strains within the active layer. The simulation reproduces the swelling strains measured before the construction of the embankment (Figure 7.16 and Figure 4.13).

The comparison between the calculated heave at the surface of the column and the evolution of the heave measured by topographic levelling at the ground surface level is given in Figure 7.15. The vertical strains due to crystal growth only occur in the active layer and the material located above the active layer is pushed upwards. The calculated vertical displacements

reproduce the field heave records in a four year period of observations. The construction of the embankment was simulated by applying a loading at the upper boundary of the column. The model reacts to embankment construction and the calculated vertical displacement reproduce the field measurements recorded after the "construction" of the embankment (t=924 days in Figure 7.15).

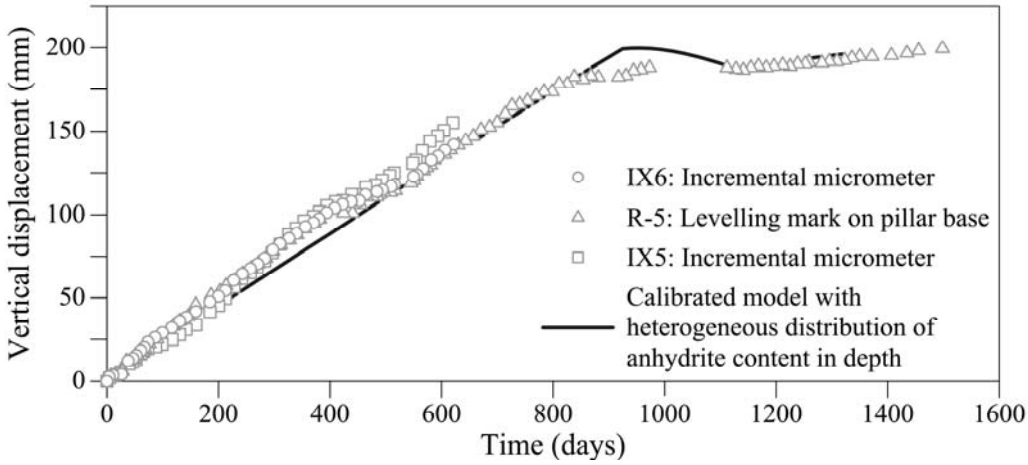

Figure 7.15. Surface heave measured in the field and calculated with non-homogeneous distribution of anhydrite

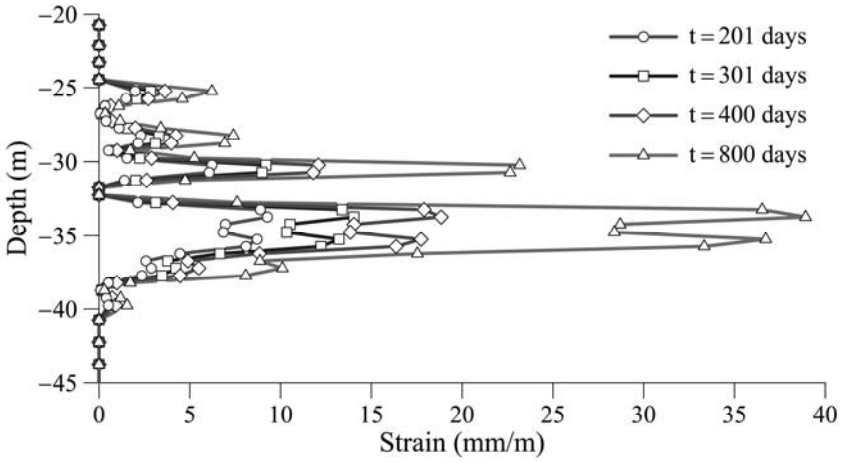

Figure 7.16. Calculated vertical strains in the active layer at different times

Several cases characterized by different embankment heights have been calculated to examine the effect of the increment of load applied at the surface on the vertical calculated strains (Figure 7.17). The model described at the beginning of this section was considered as a "base case". The rates of the vertical displacements calculated after the simulation of the construction of the embankment for different load increments are summarized in Figure 7.18. Actual observations of heave rate (Figure 4.31) compare reasonably well with calculations.

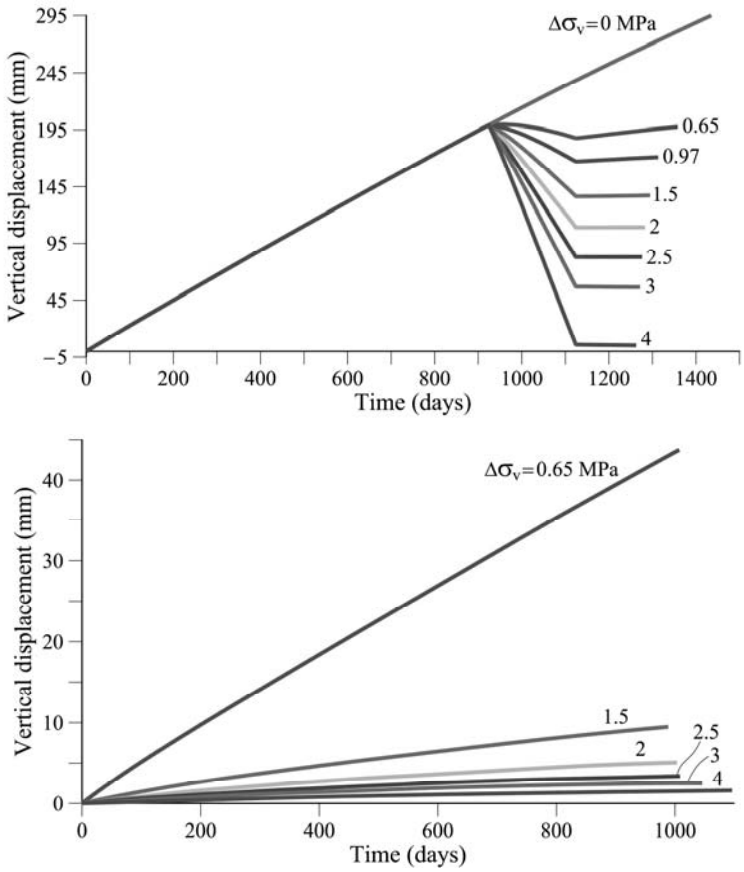

Figure 7.17. Calculated vertical displacements at the natural ground surface

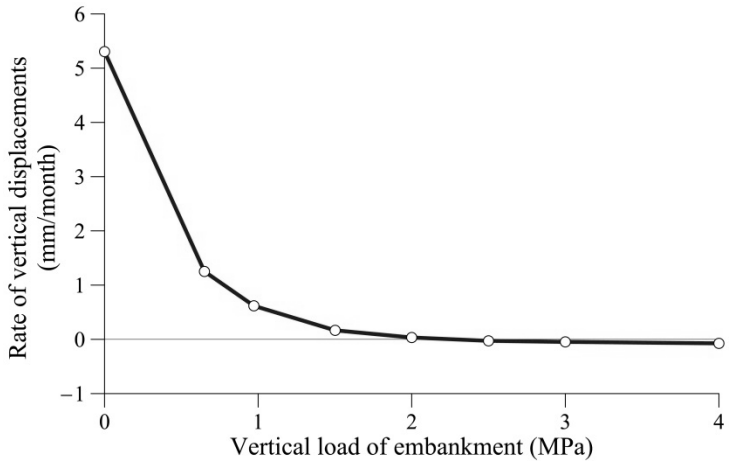

Figure 7.18. Calculated rates of vertical displacements after 70 days of application of vertical load

7.8 Conclusions

The model developed in this Chapter to reproduce the sequence of events responsible for the observed heave abandons the classical explanation of heave associated with direct anhydrite

transformation into gypsum by incorporating two water molecules. The model considers that swelling is a result of gypsum precipitation from supersaturated water due to a previous dissolution of anhydrite.

The model developed remains within a framework of flow-deformation analysis of porous media. The porous media was assumed to be integrated by an insoluble species (inert rock matrix), two soluble species (anhydrite and gypsum) and water. Mass conservation equations have been formulated. They require the knowledge of kinetic equations providing dissolution and precipitation rates of soluble species. They have been taken from some laboratory experiments in aqueous solutions reported in the literature. One important aspect of the model, insufficiently known, is the relationship between precipitated gypsum mass and strain development. An equation relating both variables, depending on stress, has been introduced.

Heave development in the field was shown to be limited to an essentially horizontal active layer, 12-15 m thick. A “column” of soil reproducing the stratigraphic sequence was analysed with the model developed. The model for heave development requires a small number of parameters. Some of them are physico-chemical constants (saturation concentrations of gypsum and anhydrite), while others define the kinetic equations. In the case described, the constant controlling the rate of dissolution or precipitation of anhydrite and gypsum was identified by matching the heave recorded before remedial measures (the construction of the embankment). It is also necessary to know the initial volume fraction of solid gypsum and anhydrite, which should be established by field investigations. The calculated response of the model seems to be consistent with heave records observed over a relatively long period (four years) and the distribution of swelling strains in depth. Once calibrated, the model is able to predict also the effects of adding weight to counteract the foundation heave. Heave would stop when anhydrite content is finally depleted to low values in an asymptotic process. This may take many years in the case analysed. The model also predicts the long-term dissolution of gypsum and therefore an increase of porosity of the active layer if flow conditions do not change. This increase in porosity may eventually lead to a surface settlement.

The sensitivity analysis performed provided additional information on the relative importance of governing parameters. The initial content of anhydrite is a very significant parameter that controls the intensity of expansion. Also significant is the effect of temperature because of its effect on the equilibrium concentrations of gypsum and anhydrite.

Uncertainties remain in some of the assumptions made, especially when trying to relate the basic crystal growth process and its mechanical implications. The dependence of kinetic equations for gypsum and anhydrite precipitation and dissolution on applied stress is not known with certainty.

The entire heave process develops within a fractured soft rock. This medium has been approximated by a porous medium in the model. Probably this is not a serious limitation in the case described but may prove to be too simplified in other cases.

Despite these uncertainties, the model is able to integrate observed experimental information from laboratory and field in a calculation procedure, which does not enter into major inconsistencies.

Appendix 7.1. Derivation of mass balance equation for solids (equation 7.4)

The definition of the material derivative with respect to solid motion is:

$$\frac{D_s(\bullet)}{Dt} = \frac{\partial(\bullet)}{\partial t} + \frac{d\mathbf{u}}{dt} \cdot \nabla(\bullet) \tag{7.15}$$

Using material derivative, equations (7.1), (7.2) and (7.3) of the main text results in:

$$\frac{D_s\varphi}{Dt} + \frac{D_s\varphi_{anhydrite}}{Dt} + \frac{D_s\varphi_{gypsum}}{Dt} = \frac{\left(1-\varphi-\varphi_{anhydrite}-\varphi_{gypsum}\right)}{\rho_s}\frac{D_s\rho_s}{D_t} + \\ + \left(1-\varphi-\varphi_{anhydrite}-\varphi_{gypsum}\right)\nabla\cdot\frac{d\mathbf{u}}{dt} \tag{7.16}$$

$$\frac{D_s\varphi_{gypsum}}{Dt} = -\frac{\varphi_{gypsum}}{\rho_{gypsum}}\frac{D_s\rho_{gypsum}}{Dt} - \varphi_{gypsum}\nabla\cdot\frac{d\mathbf{u}}{dt} + \frac{1}{\rho_{gypsum}}\frac{dm_{gypsum}}{dt} \tag{7.17}$$

$$\frac{D_s\varphi_{anhydrite}}{Dt} = -\frac{\varphi_{anhydrite}}{\rho_{anhydrite}}\frac{D_s\rho_{anhydrite}}{Dt} - \varphi_{anhydrite}\nabla\cdot\frac{d\mathbf{u}}{dt} + \frac{1}{\rho_{anhydrite}}\frac{dm_{anhydrite}}{dt} \tag{7.18}$$

Combining equations (7.16), (7.17) and (7.18) the mass balance equation of solid phase is obtained:

$$\frac{D_s\phi}{Dt} = \left[\frac{\left(1-\phi-\phi_{anh}-\phi_{gyp}\right)}{\rho_s}\frac{D_s\rho_s}{Dt} + \frac{\phi_{anh}}{\rho_{anh}}\frac{D_s\rho_{anh}}{Dt} + \frac{\phi_{gyp}}{\rho_{gyp}}\frac{D_s\rho_{gyp}}{Dt}\right] + \\ + \left(1-\phi\right)\nabla\cdot\frac{d\mathbf{u}}{dt} - \frac{1}{\rho_{gyp}}\frac{dm_{gyp}}{dt} - \frac{1}{\rho_{anh}}\frac{dm_{anh}}{dt} \tag{7.19}$$

When densities are constant it simplifies into:

$$\frac{D_s\phi}{Dt} = (1-\phi)\nabla\cdot\left(\frac{d\mathbf{u}}{dt}\right) - \frac{1}{\rho_{gyp}}\frac{dm_{gyp}}{dt} - \frac{1}{\rho_{anh}}\frac{dm_{anh}}{dt} \tag{7.20}$$

Appendix 7.2. Derivation of mass balance equation for water transfer (equation 7.5 and equation 7.7)

In a saturated regular porous media the mass balance of water is described by Olivella et al. (1994, 1996), DIT-UPC (2002) and DETCG (2010):

$$\frac{\partial}{\partial t}(\rho_l\phi) + \nabla\cdot\left(\mathbf{j}_l^w\right) = f^w \tag{7.21}$$

where, f^w is an external supply of water and $\mathbf{j}_l^w$ is the total mass flux of water, which includes the Darcy component ($\rho_l\mathbf{q}_l$) and the velocity of the solid skeleton ($\rho_l\frac{d\mathbf{u}}{dt}$).

Applying the material derivative equation (7.21) transforms into:

$$\phi\frac{D_s(\rho_l)}{Dt} + \rho_l\frac{D_s\phi}{Dt} + \rho_l\phi\nabla\cdot\left(\frac{d\mathbf{u}}{dt}\right) + \nabla\cdot(\rho_l\mathbf{q}_l) = f^w \tag{7.22}$$

The substitution of variations of porosity in time, from the solid mass balance, in equation (7.22) results in:

$$\begin{aligned}&\phi\frac{D_s(\rho_l)}{Dt} + \rho_l\left[\frac{(1-\phi-\phi_{anh}-\phi_{gyp})}{\rho_s}\frac{D_s\rho_s}{Dt} + \frac{\phi_{anh}}{\rho_{anh}}\frac{D_s\rho_{anh}}{Dt} + \frac{\phi_{gyp}}{\rho_{gyp}}\frac{D_s\rho_{gyp}}{Dt}\right] + \\ &+\rho_l\left(-\frac{1}{\rho_{gyp}}\frac{dm_{gyp}}{dt} - \frac{1}{\rho_{anh}}\frac{dm_{anh}}{dt}\right) + \rho_l\nabla\cdot\frac{d\mathbf{u}}{dt} + \nabla\cdot(\rho_l\mathbf{q}_l) = f^w\end{aligned} \tag{7.23}$$

If changes in solid density are neglected, the mass balance of water results in:

$$\phi\frac{D_s(\rho_l)}{Dt} + \nabla\cdot(\rho_l\mathbf{q}_l) = -\rho_l\nabla\cdot\frac{d\mathbf{u}}{dt} - \rho_l\left(-\frac{1}{\rho_{gyp}}\frac{dm_{gyp}}{dt} - \frac{1}{\rho_{anh}}\frac{dm_{anh}}{dt}\right) + f^w = 0 \tag{7.24}$$

Appendix 7.3: Derivation of solute mass conservation equation (equation 7.6)

Only one species of solute is considered because anhydrite and gypsum crystals dissolve as calcium sulphate.

The balance of solute can be written as follows:

$$\frac{\partial\left(\phi\omega_l^m\rho_l\right)}{\partial t}+\nabla\cdot\left(\rho_l\omega_l^m\mathbf{q}_l-\mathbf{D}\nabla\omega_l^m\right)+\nabla\cdot\left((\phi\omega_l^m\rho_l)\frac{d\mathbf{u}}{dt}\right)=-\frac{dm_{gyp}}{dt}-\frac{dm_{anh}}{dt} \tag{7.25}$$

The first term provides the rate of change of dissolved mass in the saturated open pores. The second term accounts for the advective (Darcy) and diffusive mass flow rates. The third term is the advective mass flow rate induced by the solid motion. The right terms express the solution and precipitation rates of gypsum and anhydrite.

Using the definition of material derivative, the balance of solute equation results in:

$$\begin{aligned}&\rho_l\omega_l^m\frac{D_s\phi}{Dt}+\phi\frac{D_s\left(\rho_l\omega_l^m\right)}{Dt}+\nabla\cdot(\rho_l\omega_l^m\mathbf{q}_l-\mathbf{D}\nabla\omega_l^m)+\phi\left(\rho_l\omega_l^m\right)\nabla\cdot\left(\frac{d\mathbf{u}}{dt}\right)=\\&=-\frac{dm_{gyp}}{dt}-\frac{dm_{anh}}{dt}\end{aligned} \tag{7.26}$$

Variations of porosity in time given by the solid mass balance are substituted in equation (7.26):

$$\begin{aligned}&\rho_l\omega_l^m\left[\frac{\left(1-\phi-\phi_{anh}-\phi_{gyp}\right)}{\rho_s}\frac{D_s\rho_s}{Dt}+\frac{\phi_{anh}}{\rho_{anh}}\frac{D_s\rho_{anh}}{Dt}+\frac{\phi_{gyp}}{\rho_{gyp}}\frac{D_s\rho_{gyp}}{Dt}\right]+\rho_l\omega_l^m\left(\nabla\cdot\frac{d\mathbf{u}}{dt}\right)+\\&\frac{D_s\left(\rho_l\omega_l^m\right)}{Dt}\phi+\nabla\cdot(\rho_l\omega_l^m\mathbf{q}_l-\mathbf{D}\nabla\omega_l^m)=-\frac{dm_{gyp}}{dt}\left(1-\frac{\rho_l\omega_l^m}{\rho_{gyp}}\right)-\frac{dm_{anh}}{dt}\left(1-\frac{\rho_l\omega_l^m}{\rho_{anh}}\right)\end{aligned} \tag{7.27}$$

If the changes in porosity are neglected the mass balance of solute becomes:

$$\begin{aligned}&\rho_l\omega_l^m\nabla\cdot\left(\frac{d\mathbf{u}}{dt}\right)+\phi\frac{D_s\left(\rho_l\omega_l^m\right)}{Dt}+\nabla\cdot\left(\rho_l\omega_l^m\mathbf{q}_l-\mathbf{D}\nabla\cdot\omega_l^m\right)=\\&=-\frac{dm_{gyp}}{dt}\left(1-\frac{\rho_l\omega_l^m}{\rho_{gyp}}\right)-\frac{dm_{anh}}{dt}\left(1-\frac{\rho_l\omega_l^m}{\rho_{anh}}\right)\end{aligned} \tag{7.28}$$

Appendix 7.4. Derivation of the equation of the pressure acting on crystals (equation 7.12)

Expression $\sigma'_{z\ anhydrite\ grains}=\frac{\sigma'_z}{1-\phi}$ is derived as follows:

The first hypothesis is that the effective stress in the fractured and porous rock analysed is a measure of intergranular forces, z refers to the vertical direction:

$$\sigma'_z = \frac{\sum F_{z,intergranular}}{A_T} \tag{7.29}$$

The preceding one-dimensional simplified expression provides the effective stress acting normal to a reference area A_T

The objective is to find the stress acting on the particles. Therefore,

$$\sigma'_{z\ anhydrite\ grains} = \frac{\sum F_{z,anhydrite\ grains}}{A_{anhydrite}} = \frac{\sum F_{z,intergranular} - \sum F_{z,no\ anhydrite\ grains}}{A_{anhydrite}} \tag{7.30}$$

where:

$$A_{anhydrite} = A_{total} - A_{pores} - A_{no\ ahydrite\ grains} \tag{7.31}$$

It is accepted that the porosity may be expressed as area ratios:

$$\phi = \frac{A_{pores}}{A_{total}} \quad , \quad \phi \cdot A_{total} = A_{pores} \tag{7.32}$$

Equations (7.29), (7.30) and (7.31) allow transforming equation (7.32) into:

$$\sigma'_{z\ anhydrite\ grains} = \frac{\sigma'_z \cdot A_{total} - \sum F_{z,no\ anhydrite\ grains}}{A_{total} - \phi \cdot A_{total} - A_{no\ anhydrite}} \tag{7.33}$$

A second assumption, namely that stresses that receive the solid grains (being anhydrite or not) are all equal, allows writing:

$$\sigma'_{z\ solid\ grains} = \sigma'_{z\ intergranular} = \sigma'_{z\ anhydrite\ grains} \tag{7.34}$$

Then:

$$\sigma'_{z\,anhydrite\ grains} = \frac{\sigma'_z \cdot A_{total} - \sigma'_{z\ anhydrite\ grains} \cdot A_{no\ anhydrite\ grains}}{A_{total} - \phi \cdot A_{total} - A_{no\ anhydrite}} \tag{7.35}$$

Isolating $\sigma'_{z\ anhydrite\ grains}$ from equation 7.35 provides

$$\sigma'_{anhydrite\ grains} = \frac{\sigma'_z}{1-\phi} \tag{7.38}$$

CHAPTER 8

Analysis of massive sulphate attack to cement treated railway embankments and track bases

Expansions in soils due to crystal growth can also occur as a result of sulphate attack to cement or lime treated clayey compacted soil containing sulphates. This expanding process involves the growth of crystals of ettringite and thaumasite minerals within the cement or lime treated soil.

Cuts and fills are common in engineering works. Embankments and fills made of compacted marls with gypsum are built when infrastructures are performed in gypsiferous rocks. Transition embankments treated with cementitious materials in the vicinity of a more rigid structure is a common practice. Therefore the risk of sulphate attack to compacted sulphated clay materials in engineering works has to be taken into account when sulphated formations are involved.

The expanding phenomenon related to sulphate attack has been reported in the literature mainly in a number of cases involving compacted road bases and sub-bases stabilised with cement or lime. The comparison of different cases of treated compacted bases affected by sulphate attack indicates that the existence of water is indispensable in the development of

expansions. This is in agreement with the set of chemical reactions taking place for the formation of the minerals causing expansions, which involve dissolution and precipitation processes and that are presented at the Appendix of this Chapter.

Two cases of massive sulphate attack to cement treated embankments and track base in a high-speed railway line have been analysed in this Chapter to study the expanding phenomena induced by ettringite and thaumasite crystal growth in compacted sulphated soils treated with cement. In the first case, two access embankments to a railway bridge experienced a continuous and severe heave shortly after construction. Vertical displacements reached 120 mm in a 2 year period. The embankments were designed, by including soil-cement treated transition wedges. A grid of 10 m deep jet-grouting columns was also built with the purpose of stabilising the embankments. Instead, a sustained swelling deformation, which extended to depths of 8-10 m, was activated. In the second case a compacted cement treated soil was placed over a rigid concrete caisson. The treated layer, 1.5 m thick, expanded at a continuous rate of 0.9-1.3 mm/month. In both cases the compacted soil was low-plasticity clayey material with a variable percentage of gypsum. The embankments and the track base suffered a massive ettringite-thaumasite attack which was triggered by the simultaneous presence of cement, clay, sulphates and an external supply of water (rain). Ettringite and thaumasite crystals were found within the expanding levels.

The Chapter summarises the experience on sulphate attack described in the literature, describes the field extensometer and inclinometer records, the long term laboratory tests performed, some mineralogical observations and the reactions leading to the growth of expansive crystals. It presents the modelling of the chemical evolution at the interface between a compacted sulphated clayey soil and a cement material. Also a model which simulates the measured heave in the embankments was developed. Forces acting against the bridge, which was seriously damaged, were estimated. Solutions adopted to remediate the created problems are briefly described.

8.1 Introduction

Cement attack by sulphates is a well-known mechanism of degradation of concrete and mortars made of Portland cement. The phenomenon is well-known in general terms. Portland cement has a dominant content (60–70%) of calcium oxide (CaO), a significant proportion

(20–25%) of silica (SiO_2), a small proportion (2–6%) of aluminium and iron oxides (Al_2O_3, Fe_2O_3) and sulphate (in the form of gypsum: $CaSO_4 \cdot 2H_2O$) (1–5%). Gypsum is added to retard the paste setting.

Sulphate attack of a hardened cement paste leads to the development of ettringite, a hydrated sulphate of calcium and aluminium. This mineral crystallises in bundles of elongated filaments which retain a high proportion of water molecules in its crystalline structure. The source of the attack is often described as being either "internal" (when the cement itself has excessive sulphate content) or "external" (when water carrying sulphate ions enters into contact with the hardened cement). The development of ettringite implies a destruction of the strength of the cement paste and a substantial swelling. The external attack progresses as an advancing front from the surface exposed to the sulphated water. Aluminium oxides are reduced to a minimum in sulphate resistant cements. In the absence of aluminium, ettringite does not develop. Another mineral, thaumasite, also develops as a consequence of sulphate attack. It is a hydrated sulphate of calcium and silicon. It may crystallise from ettringite by means of an isomorphous substitution of aluminium by silicon.

Cement and lime treated soils are often used to stabilise road bases and sub-bases. When the soil has some proportion of gypsum, or the treated soil is exposed to sulphated waters, a similar attack resulting in loss of strength and significant heave has often been reported (Sherwood, 1962; Mitchell & Dermatas, 1992; Snedker, 1996; Rajasekaran et al., 1997; Puppala et al., 2003; Rajasekaran, 2005). Some of these studies discuss the minimum sulphate content that triggers the attack. Most of the papers point out that sulphate contents in excess of 0.5–1% (concentration of soluble sulphate in water, by weight) result in ettringite formation and soil swelling.

However, lower threshold values (0.3%) have also been identified (Mitchell & Dermatas, 1992; Snedker, 1996). It appears that the loss of strength of the treated soil and associated swell is related to the sulphate content. Sherwood (1962) described an unconfined compressive strength reduction of 24% of treated soil when the sulphate content was as low as 0.25%.

Unlike "pure" cement mixtures or concrete, treated soils usually contain a certain proportion of clay minerals, which are a source of aluminium and silicon ions. In fact, the highly basic environment (pH in excess of 12) created by the hydration of cement's calcium oxide is

capable of dissolving the clay minerals and releasing Al and Si atoms, ready to be integrated into ettringite and thaumasite molecules. The implication is that sulphate resistant cements, low in aluminium oxides do not necessarily guarantee the prevention of sulphate attack in treated soils. However, Puppala et al. (2003) report the good performance of sulphate resistant cement in stabilising soft and expansive clays with high sulphate content.

Most of the geotechnical literature on sulphate attack concerns the stabilisation of compacted road bases and sub-bases. In those cases the treatment is applied to relatively thin layers, and the sulphate attack results in surface heave and reduction of soil strength. In contrast, the two cases affected by sulphate attack described here concern larger soil masses: an entire railway embankment and a 1.5 m thick treated layer in a railway track base in a high speed railway line. The induced swelling strains resulted not only in a surface heave but also in very high and unexpected forces against bridge abutments in the case of the embankments, which caused significant structural damage.

The chapter first describes the two affected embankments, located on both sides of a bridge built recently for a high-speed railway line. Field measurements in the embankments area, once the heave was first identified, will be described, as well as the properties of the compacted material used in the construction of embankments. Then the case of the affected base stretch located close to the embankments is explained. Sulphate attack will be described in some detail, relying on some specific tests performed and on some geochemical calculations analysing the chemical evolution of an interface between a cement treated body and a compacted soil. This chemical modelling will be also presented. The embankment swelling was modelled, and an estimation of pressures developed against the bridge abutment was made. Finally, the costly remedial measures are briefly described. The case is probably an extreme case of sulphate attack to a large engineering structure and highlights the severity of the phenomenon, which may develop when several contributory factors cooperate to create a critical and dangerous situation.

8.2 Design and construction of embankments

Not far from the location of Pont de Candí Bridge, a 196 m long bridge, Pallaressos Bridge, which also belongs to the high-speed railway link between Madrid and Barcelona, was built in the province of Tarragona, Spain, in 2004. Figure 8.1 shows the plan view and a

longitudinal section of the bridge. Each one of the seven bridge spans was structurally resolved by two parallel box girder beams resting isostatically on the pillars. A continuous, cast in situ slab was extended over prefabricated slabs placed over the girder beams. Rails were supported by a ballast layer on top of the continuous concrete slab. Figure 8.2 shows a photograph of one of the embankments, the abutment and the bridge.

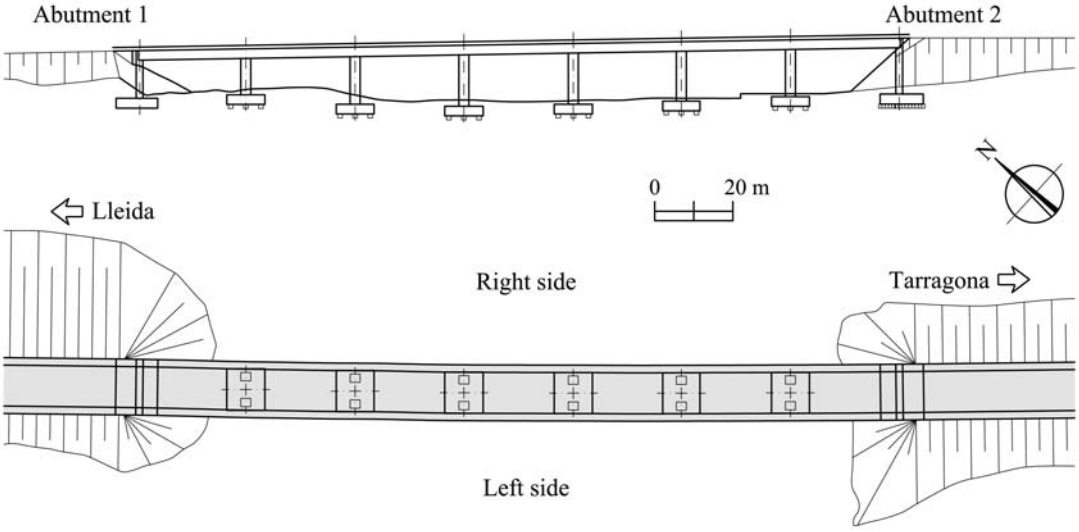

Figure 8.1. Longitudinal profile and plan view of Pallaressos Bridge and embankments

Figure 8.2. Pallaressos embankment, Lleida side. The excavated pathway on the embankment side was made to the allow access of drilling machines for the installation of measuring instruments

Bridge pillars were founded on excavated piles. The two abutments, of similar design and dimensions, were directly founded on a hard marl of Tertiary age. They limit the two embankments shown in the figure, which reached a maximum height of 18 m in the proximity of the abutments. The thickness of the approaching embankment decreased progressively away from the bridge abutments. The internal design of the embankments is shown, in

longitudinal section, in Figure 8.3. Transition wedges of increasing stiffness were designed to ensure a smooth transition from the compacted soil to the rigid bridge structure when train approaches the stiff bridge abutments. The wedge closest to the abutment was specified as a cement-soil mixture. The embankment material was previously excavated in a Miocene natural formation: a sequence of claystones with some proportion of gypsum veins and interstratified sandstone layers. Some selected soil was used also as a rail track sub-base.

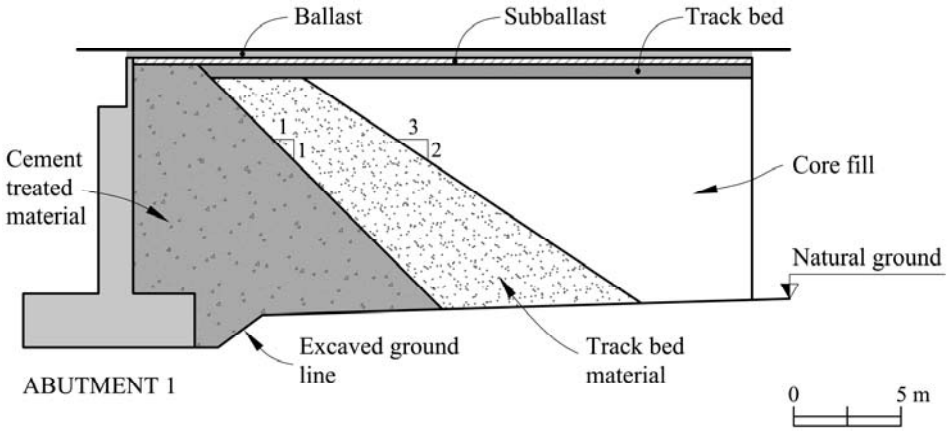

Figure 8.3. Design of the embankment

Once the railway line was in operation, rail levelling started on a routine basis. Results of this levelling for two dates: 13 December 2005 and 3 April 2006 are shown in Figure 8.4. The levelling performed in April 2006 shows two distinct swelling peaks in the position of the two abutments. No significant settlement or heave was detected along the bridge itself. Data in Figure 8.4 show a maximum heave of 12–16 mm with respect to the initial levelling. Maximum heave rate, comparing the two successive levellings, is about 4.0–4.5 mm/month.

Countermeasures were adopted and the rail tracks were levelled periodically by adjusting the thickness of the ballast layer. Since no signs of a reduction in heave rate were noticed, geotechnical investigations were commissioned. A difficulty for all the subsequent field activities was the need to keep the railway line in full operation.

Samples taken in the first borings drilled through the two embankments indicated that the cement-treated soil was rather weak and prone to disintegration. It was also difficult to identify the expected geometry of wedges as shown in Figure 8.3. These findings were probably the reason behind the decision to reinforce again the embankments, in October 2006, by means of 1.5 m diameter jet-grouting columns, which were arranged in the manner shown in Figure 8.5.

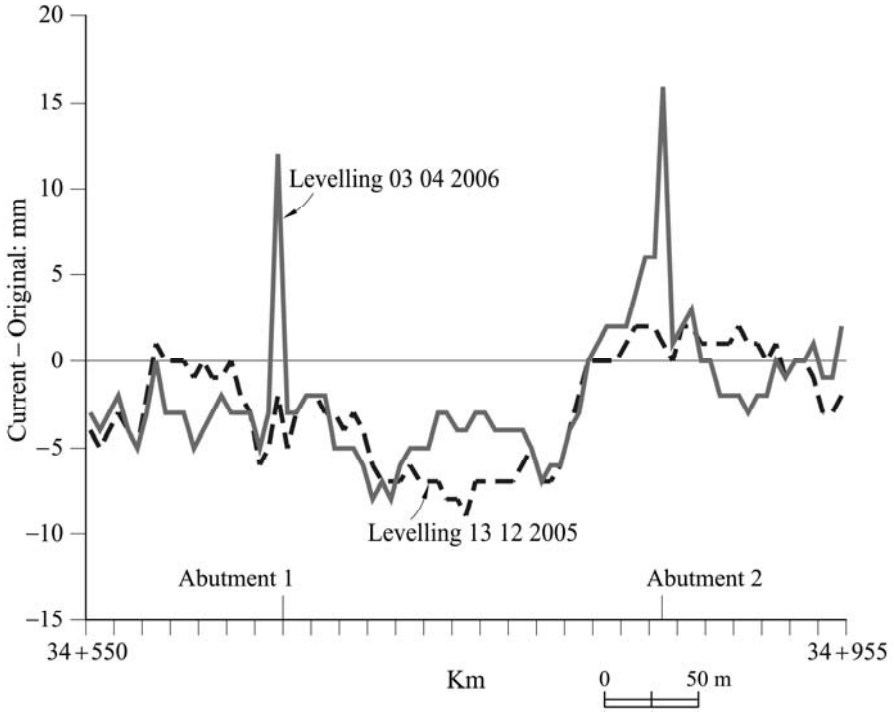

Figure 8.4. Rail levelling after construction

The central part of the embankment was treated. Columns reached a depth of 10 m in the vicinity of the abutment. The length and density of the columns were reduced as the distance to the abutment increased. The transition zone was extended in both embankments to an overall length of 30 m.

One year after finishing jet-grouting treatment, at the end of 2007, embankment heave was again detected, and track profiling, by modifying the ballast cushion, had to start again. In May 2008 a surface-topographic survey provided precise information on the evolution of heave. It was found that the embankment heave had resumed and measured heave rates (4.2 mm/month, 5.7 mm/month and 6.5 mm/month in different positions) were even higher than the values first observed when the problem was initially detected. Field monitoring and soil testing were thereafter increased.

8.3 Field observations in Pallaressos embankments

Additional surface-topographic marks were installed on the top of the embankments. They covered a length of 35 m in the Lleida (1) embankment (Figure 8.6) and 45 m in the Tarragona (2) embankment. Surface horizontal displacements were measured in the transverse and longitudinal embankment directions. Figure 8.7 provides the measurements of horizontal

and vertical surface movements in one of the abutments from 2 March 2009 to 19 April 2010. The records indicated that significant horizontal movements were developing in the transverse direction. An accumulated horizontal transverse movement of 150 mm was measured during the first 17.8 months of monitoring at topographic mark PR-1.5, located 10 m away from the Lleida abutment structure. An accumulated heave of 59 mm was measured at PR-1.5 during the same period.

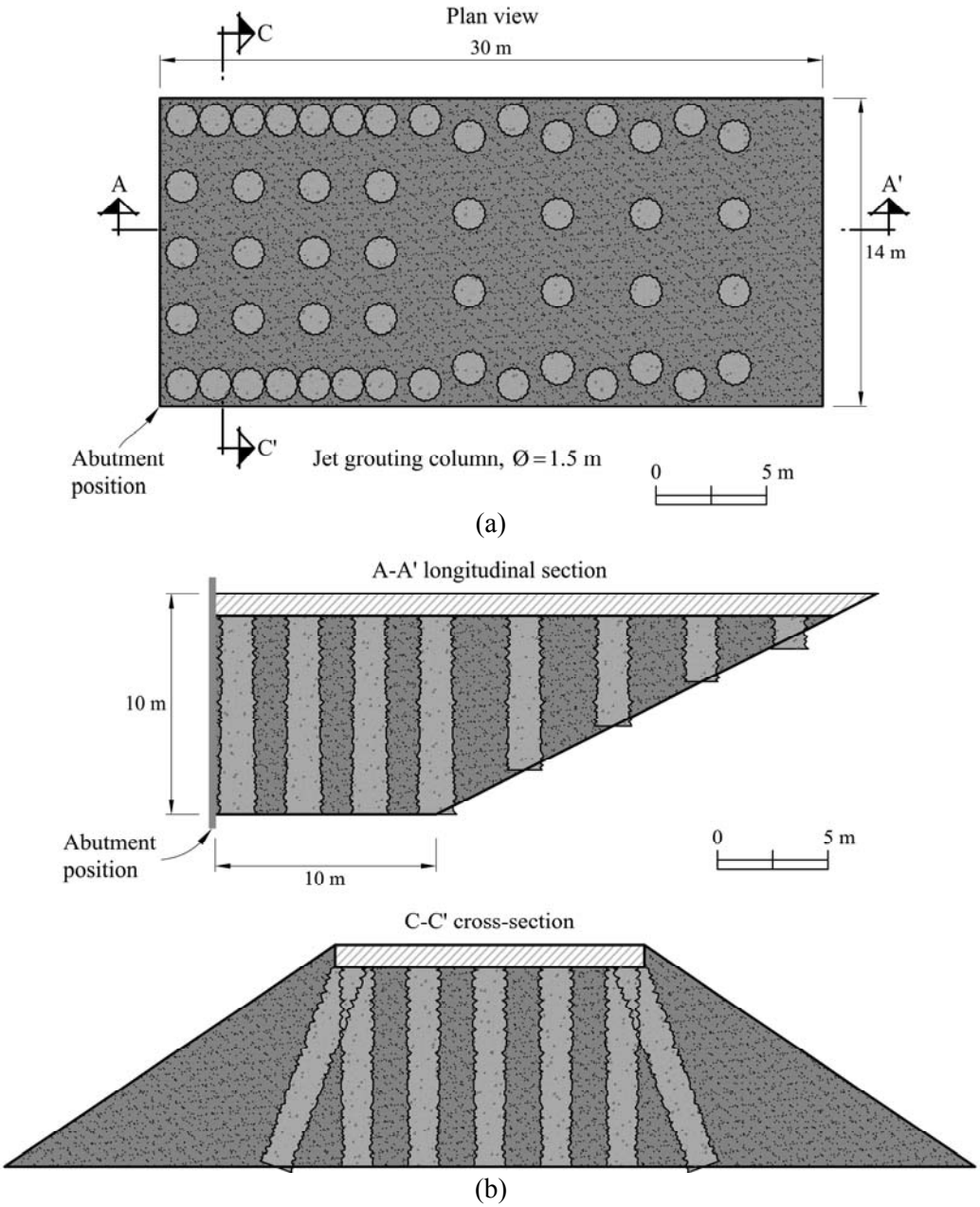

Figure 8.5. Jet-grouting treatment of embankments. (a) Position of columns in plan view; (b) longitudinal and cross-sections

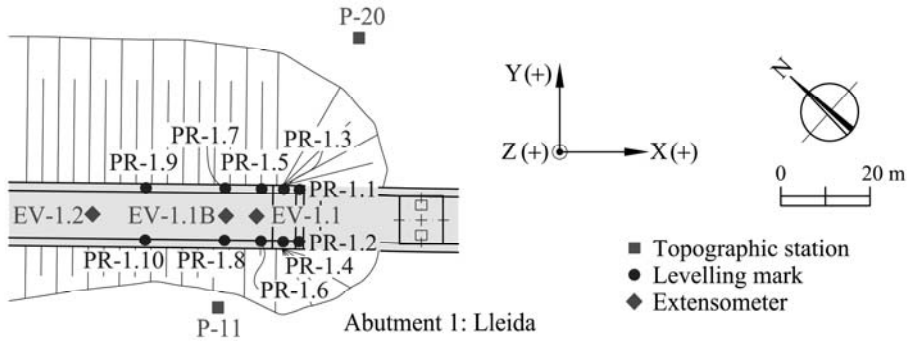

Figure 8.6. Position of surveying topographic stations, levelling marks and continuous extensometers in Lleida embankment

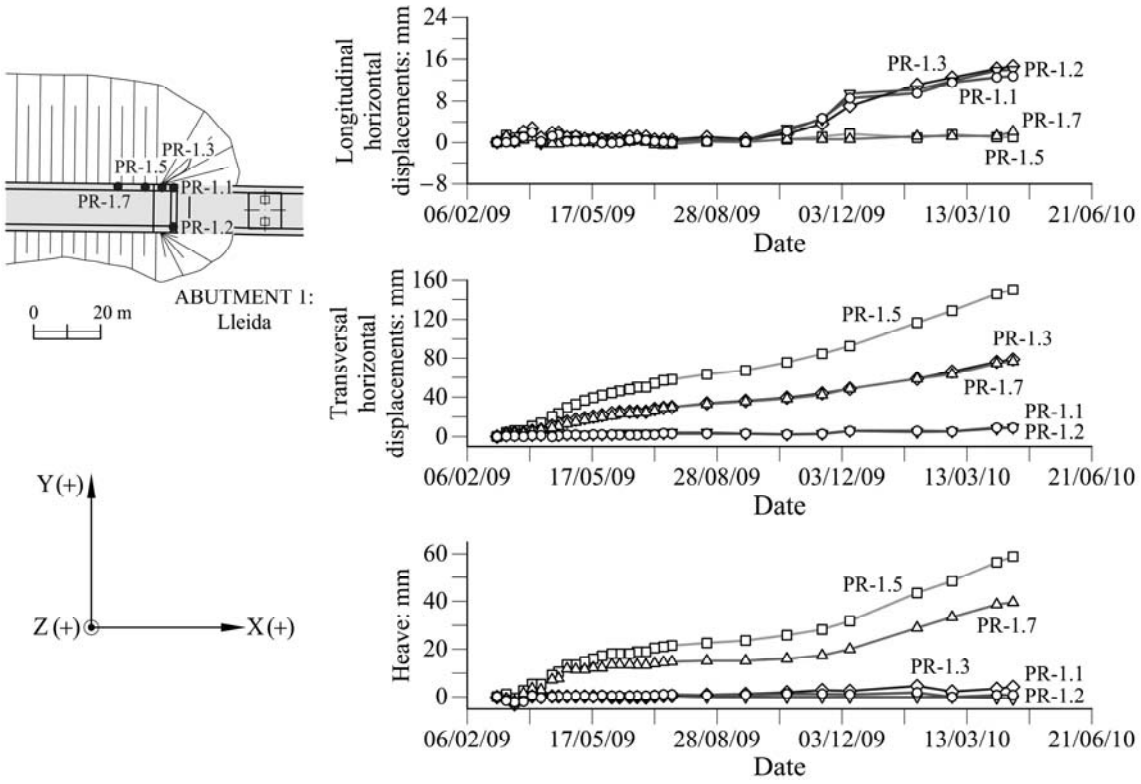

Figure 8.7. Evolution over time of movements measured on the embankments surface. Movements along three perpendicular directions were monitored by topographic surveillance

The distribution of surface heave along distance is shown in Figure 8.8 for Abutment 1 an in Figure 8.9 for Abutment 2. The maximum heave occurred at a distance of 10-13 m from the abutments. At further distances the displacement decreased progressively. At distances in excess of 30 m to the abutment no movements were detected. The transverse horizontal movements followed the same pattern. The maximum transverse horizontal movements were measured at the same points where the maximum heave was recorded.

Both embankments exhibited a similar behaviour. The topographic monitoring also allowed to measure horizontal movements along the longitudinal direction of the embankments. Points displaced towards the bridge abutment. Longitudinal displacements were substantially lower than the displacements recorded in the other two directions. However, displacements reaching 22 mm towards the abutment structure were measured during 17.8 months in topographic marks installed along the first 10 m from the abutment. The smaller displacements recorded in the longitudinal direction are explained by the confinement applied by the abutment and the bridge structure on one side, and by the rest of the embankment on the opposite side.

Topographic stations and levelling marks were also installed outside the embankments, on the natural ground, but no movements were recorded.

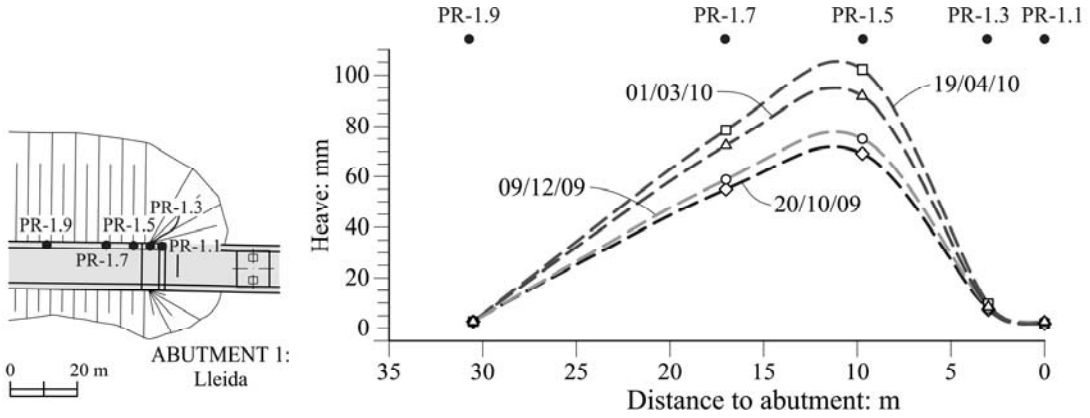

Figure 8.8. Distribution of heave magnitude at embankment 1, measured by topographic levelling, on the embankment surface plotted against the distance between the levelling mark and the abutment. Initial measurement: 26 May 2008

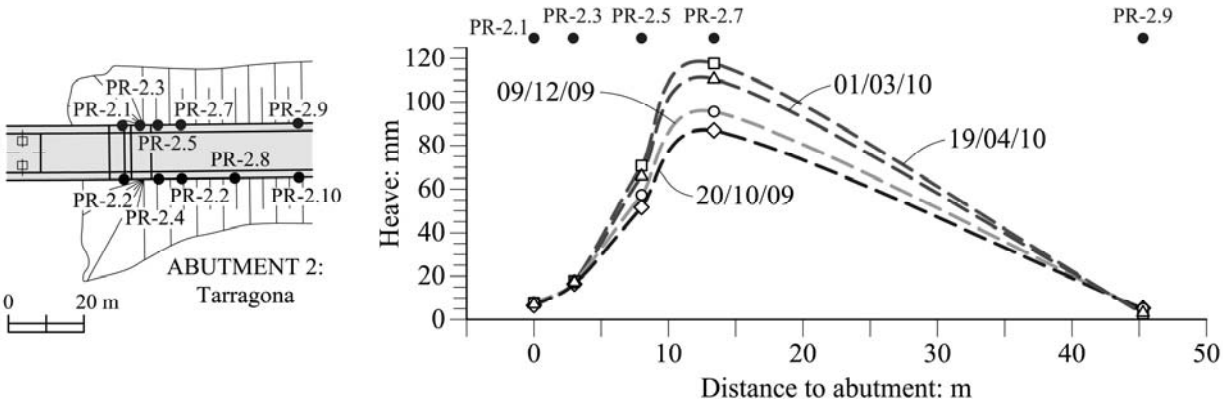

Figure 8.9. Distribution of heave magnitude at embankment 2, measured by topographic levelling, on the embankment surface plotted against the distance between the levelling mark and the abutment. Initial measurement 26 May 2008

The evolution of vertical displacements over time at some points of both embankments is shown in Figure 8.10. The rate of vertical displacements has not been constant in time. The average rates of heave, obtained by means of different measurement procedures, have been plotted in Figure 8.11. The first estimation of heave rate corresponds to rail levelling which was available in 2006. Despite the variability of results, the plot shows that the heave rate has increased from values around 2-4 mm/month in 2006 to heave rates varying from 2.5 to 7.5 mm/month in 2008. Figure 8.10 also provides the total accumulated rainfall. A relation between the evolution of heave and the rainfall events can be identified. Heave rate accelerates in periods immediately following significant rainfall events.

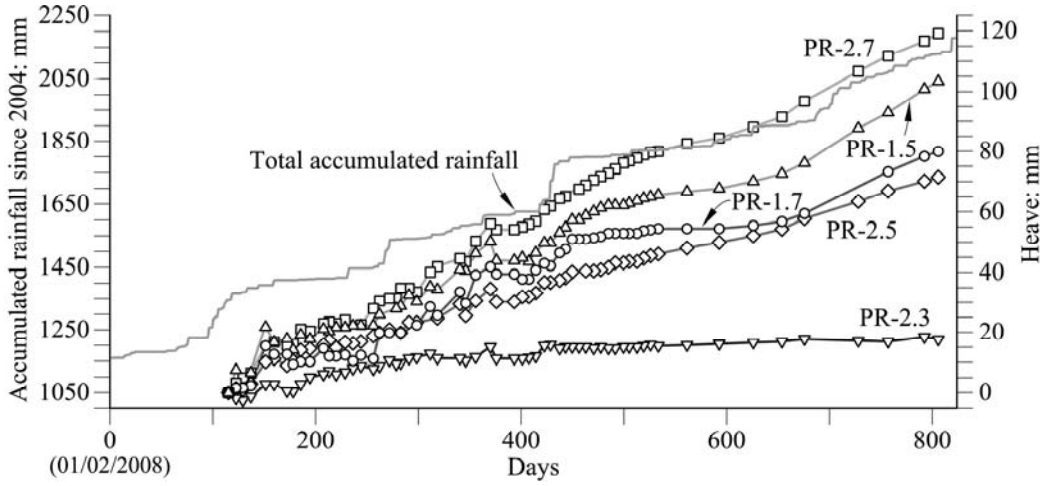

Figure 8.10. Evolution of vertical displacements over time, measured at some levelling marks of both embankments and total accumulated rainfall recorded near the bridge. Rainfall data provided by the Servei Meteorològic de Catalunya

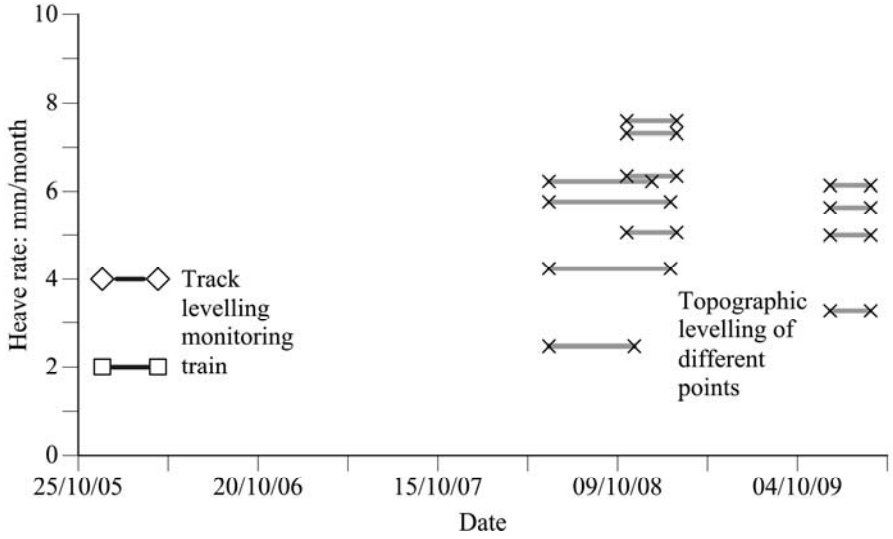

Figure 8.11. Average heave rates of the embankment at different periods of time

Inclinometer records showed that the horizontal movements were developing in depth. Some results are shown in Figure 8.12. The horizontal displacements decreased gradually along the first 8-10 m of boring. Horizontal movements at positions deeper than 13-14 m were not significant. This behaviour was also observed in other inclinometers. Inclinometers measured a horizontal movement about 9-12 mm in the transverse direction from 31 October 2008 to 16 January 2009. Those horizontal movements indicated that the embankment was also swelling in a lateral direction.

Vertical deformation of embankments was investigated by means of continuous extensometers (sliding micrometers, Kóvari and Amstad, 1982) installed in boreholes. Data were recorded on a monthly basis. The positions of the extensometers installed in the Lleida embankment are shown in Figure 8.6. Continuous extensometers with lengths varying from 18 to 48 m were installed in each embankment at distances of 8, 13 and 40 m from the abutments. Measured swelling strains concentrated at the first 8 m. Smaller compressive strains were recorded in the lower part of the embankments (Figure 8.13). Strain records maintained the pattern of vertical variations over time (Figure 8.13). The upper "active" level did not progress downwards. Micrometers installed at a distance of 40 m from abutments recorded only a small compression.

The integral of strains along depth, measured in micrometers, was found to be consistently very close to the surface displacements measured in topographic marks. A continuous extensometer was also installed in natural ground at the centre of the valley to check whether any source of movements, other than the deformation of the embankments, was present in this case. No vertical displacements were measured by this instrument. The substratum was also shown as unstrained in all the sliding micrometers installed.

The results described indicate the three-dimensional nature of the deformation of embankments as a result of an internal volumetric swelling. A significant result was the reduced longitudinal deformation, which implied that high horizontal loads could be acting against the abutments, and therefore, against the bridge itself. These forces were probably symmetrical, acting on both sides of the bridge. In fact, an inspection of the bridge structure revealed the existence of fissures and spalling damage at the contact between the abutment and bridge structural elements (Figure 8.14). The development of swelling in the embankment also induced significant damage to the communications and drainage conduits on the top of

the embankments, near the abutments. A displacement of the abutment structure towards the bridge was noticed “de visu”. This unforeseen horizontal loading against the bridge prompted a thorough inspection of the structure and the adoption of various repairs which are not described here. An interesting observation, which shows the effect of two opposite forces acting on both sides of the bridge, is the pattern of bending induced cracking on the lower part of the pillars, which is sketched in Figure 8.15.

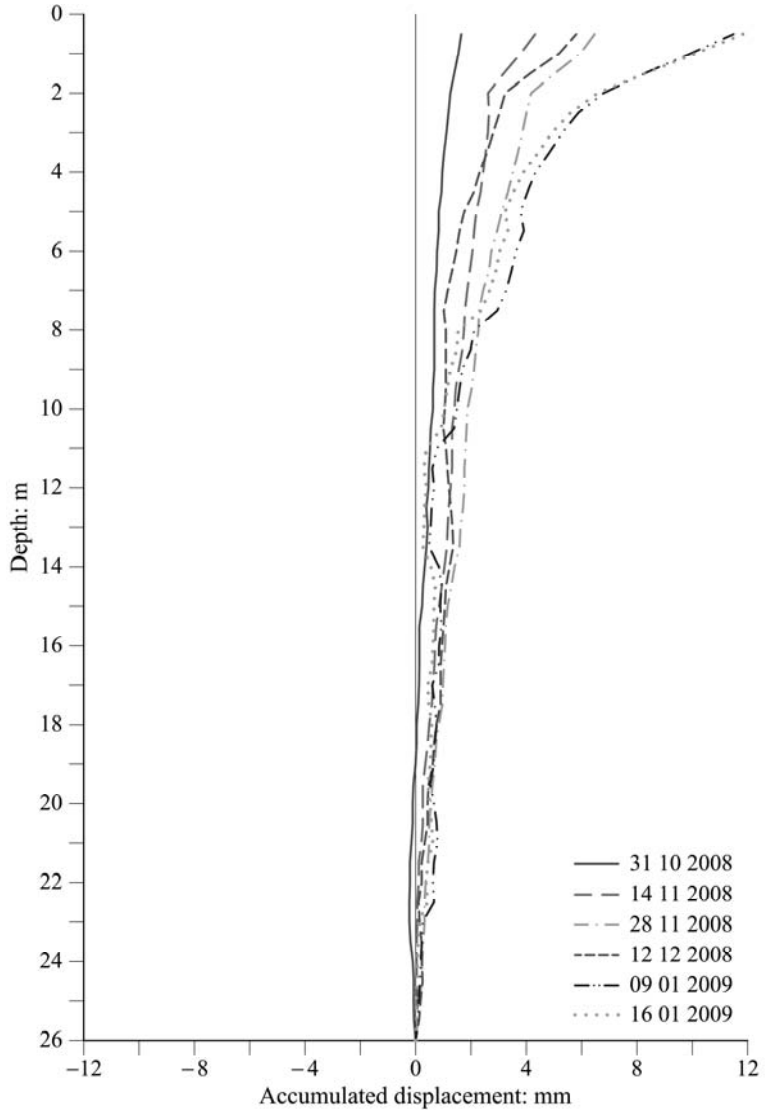

Figure 8.12. Accumulated displacements measured at inclinometer I1T in Tarragona embankment. Initial measurement 25 October 2008

There was also a concern about the possibility of strong passive stresses developing on the upper part of the embankments, in the longitudinal direction. A passive failure could result in a risk of rail distortions. An analysis of the stress state inside the embankments, reported

below, was performed. First, the geotechnical properties of the embankment materials will be described.

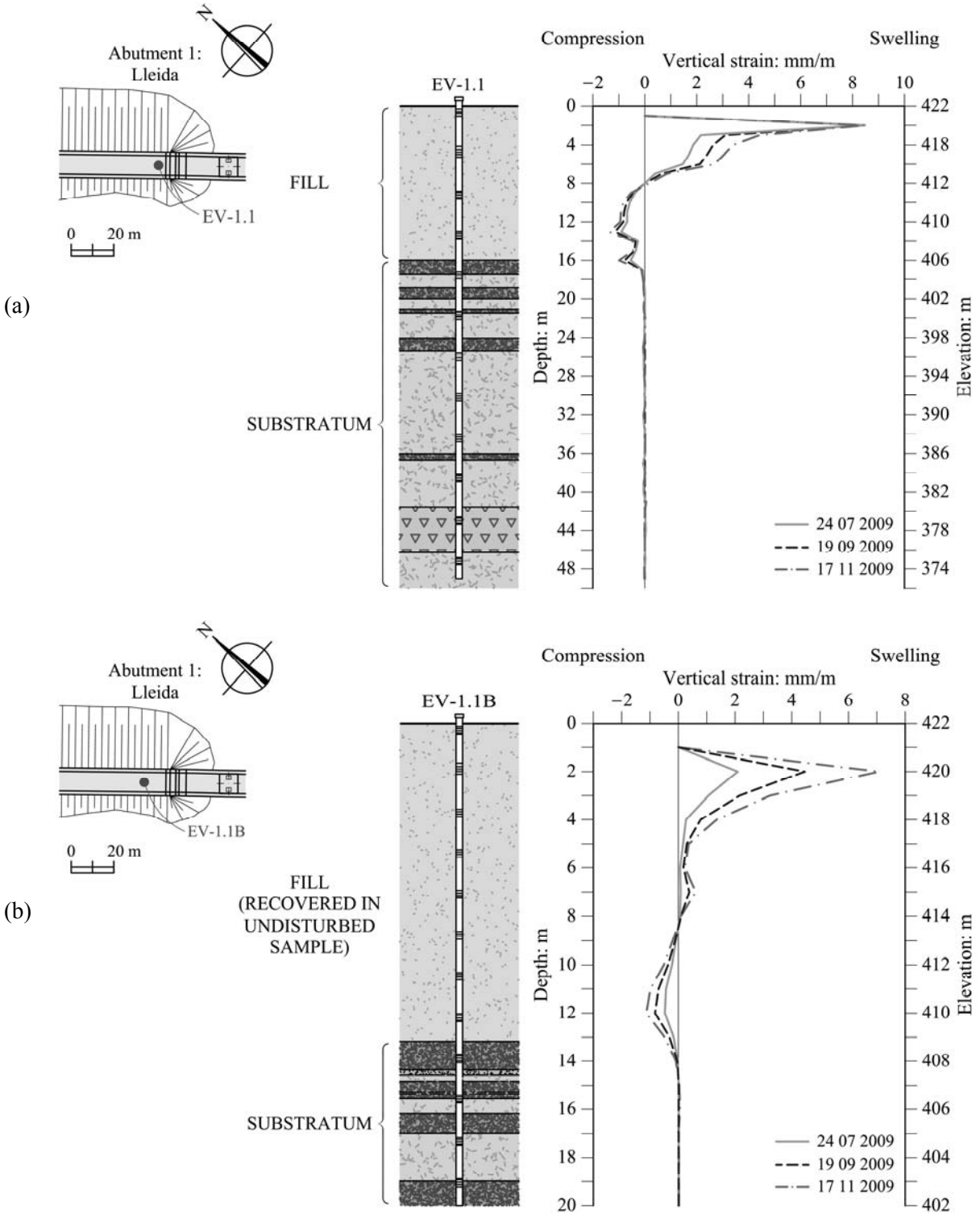

Figure 8.13. Vertical displacements measured by sliding micrometer: (a) EV-1.1, initial measurement 11 June 2009, and (b) EV-1.1B, initial measurement 25 May 209. See position in Figure 8.6

Figure 8.14. Damage observed near abutments

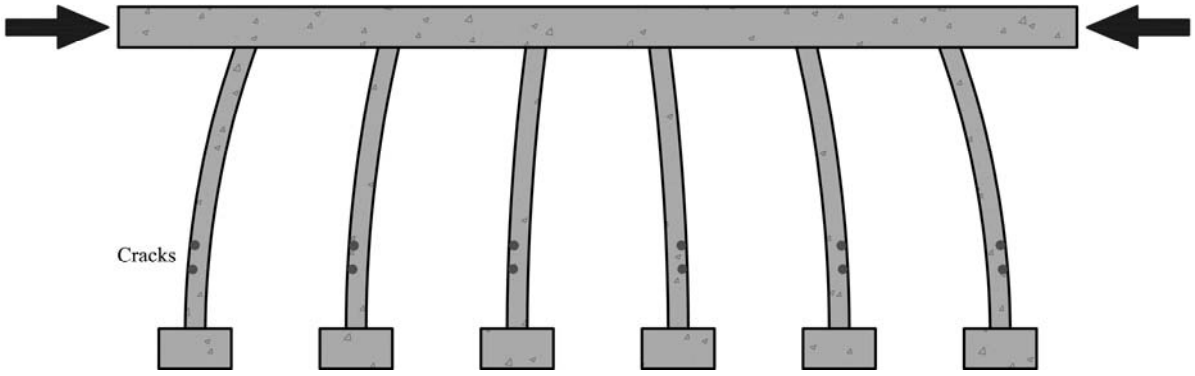

Figure 8.15. Loading and deformation situation of the bridge due to the thrusts on the abutments

8.4 Geotechnical data of the embankments

Pallaressos Bridge crosses a small valley in the eastern part of the Ebro Basin, which is filled by Tertiary deposits of Miocene age. The substratum, a sequence of horizontally deposited reddish claystone layers and sandstones poorly cemented, appears close to the surface. Thin veins of gypsum cross the claystone at regular intervals. Limestone layers of high lateral continuity are also interbedded in the sequence of claystones and sandstones. Claystone levels dominate the sequence. When intact, it reaches unconfined compression strengths in the range 10–50 MPa. However, the claystone is very sensitive to changes in water content.

The identification tests performed during the construction of the embankments indicate that the tested samples of the embankment material have sulphate contents higher than 1% in

general. The plate load tests during the construction of the embankments measured modules from 250 to 500 kg/cm^2 during loading and modules from 700 to 1500 kg/cm^2 during unloading in the embankment layers.

Compaction data taken during construction of embankments are given in Figure 8.16. Dry density-water content pairs determined on embankment lifts are plotted in the figure. Also indicated are the determined Modified Proctor Optimum values. The fill reached quite high dry densities, even if the Modified Optimum dry densities were seldom reached. On the other hand, the compaction water content was ordinarily on the dry side of optimum. Very often the degree of saturation was fairly low (< 0.7). Therefore as-compacted suction was high and water (mainly from rainfall) would tend to progressively wet the embankment.

One of the Modified Proctor Optimum points in Figure 8.16 shows an exceptionally high value of water content and a low dry density. This point was reported in the original "as built" documents. It was decided to maintain it, despite the large differences with respect to the remaining points. The plot in Figure 8.16 includes density and water content information on 24 construction layers. Interestingly, the field densities determined for the particular layer (a total of eight values) showing the exceptional density and water content values of the Modified Proctor (MP) optimum, also exhibited abnormally low density values. It is inferred that the data are correct and it may be explained by the heterogeneous nature of the source material.

Points above the $S_r = 1$ line are explained by errors in the raw laboratory data. The tests were performed at the time of construction by a Control Laboratory, and it was decided to include all of them in the plot of Figure 8.16.

Figure 8.17 shows an exposed surface of a cut through the upper part of one of the embankments. The excavation was performed during the underpinning operations described later. The picture shows two jet-grouting columns, a cement treated soil in the lower part, and the reddish compacted fill with an abundant presence of gravels and small boulders.

Samples taken in some borings were tested, and vertical profiles of some identification properties are given in Figure 8.18. The fine fraction is low-plasticity clay. The data suggest a decrease in plasticity with depth within the embankment. Water content remains below the plastic limit, except in one of the tested specimens, which has an abnormally high value in view of the compaction data given in Figure 8.16. Grain-size distribution tests provided the

following fractions (average value and range): gravel 35% (62.1-18.6%); sand 21% (35.1-10.5%) and fines content 35% (69.3-7%). The mean diameter varied widely (8.0-0.0035 mm), with an average value of 1.6 mm. Some boulders with sizes in excess of 100 mm were scattered inside the fill. They had sharp edges because they were a result of blasting the Miocene formation. Smaller-size gravels, however, had rounded edges. The main minerals identified and their approximate contents, as determined in semi-quantitative X-ray diffraction analysis, are: Carbonates (calcite and dolomite) 52%; Gypsum 20%; Clay minerals (illite and kaolinite) 18% and Quartz 10%.

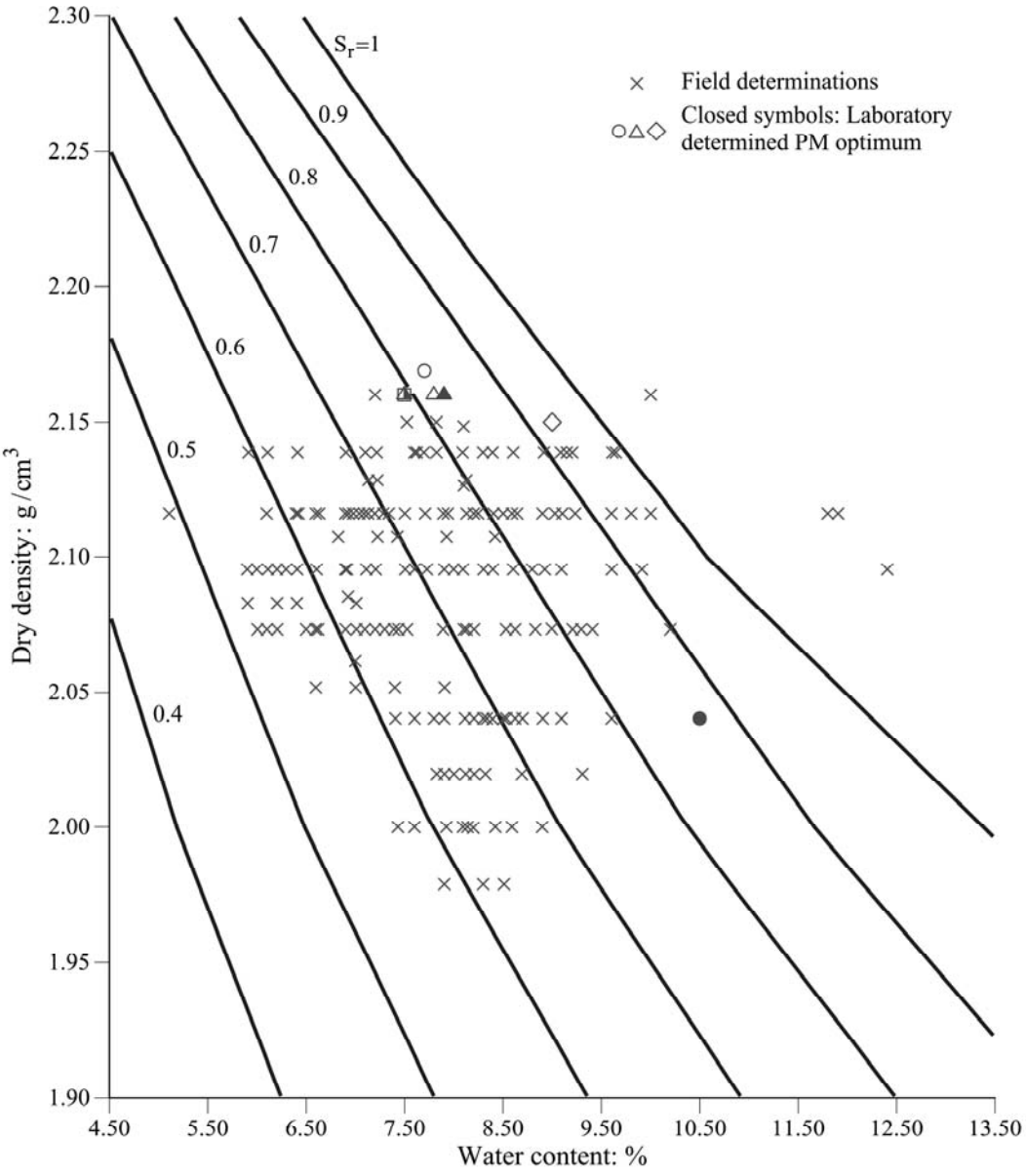

Figure 8.16. Compaction data taken during construction of embankments. Open symbols are field determinations. Closed symbols are Modified Proctor (MP) optima determined in the laboratory

Figure 8.17. View of a cut across one of the embankments made during underpinning operations. Two jet-grouting columns as well as a level of cement treated material, in the lower part, are visible. Sandstone gravels and small boulders are scattered in the compacted marl matrix

Relevant information is the variation with depth of soluble sulphates in the soil, given in Figure 8.19. It reaches values in the range 2.0–2.5% in the upper 8 m. At lower levels, the sulphate content drops to less than 0.5%. Most probably this was the result of two different source areas. It reflects the natural variation of gypsum content found in the natural formation. Data given in the introduction suggest that sulphate attack to cement is likely to develop in the upper 8 m of the embankment.

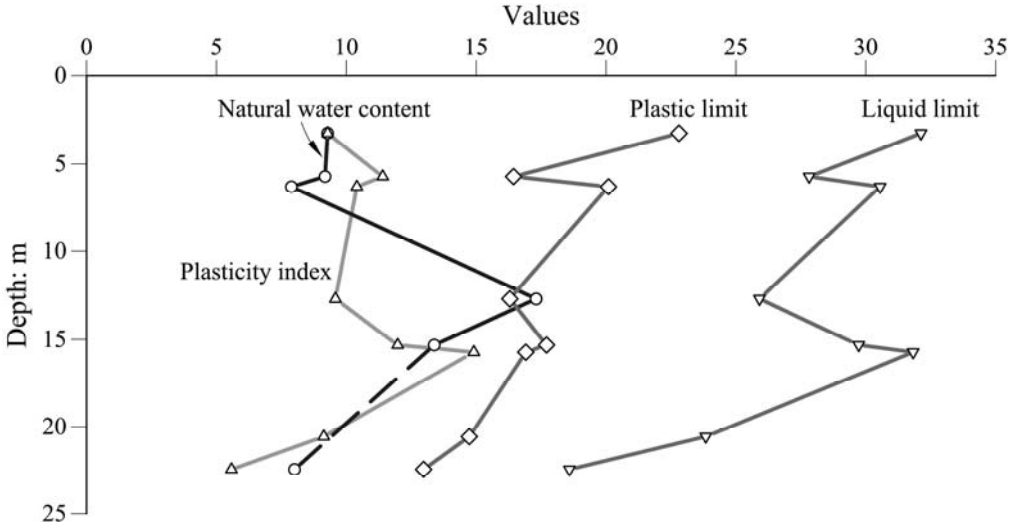

Figure 8.18. Index properties determined in samples taken in a boring drilled in Tarragona embankment (data from boring ST-1)

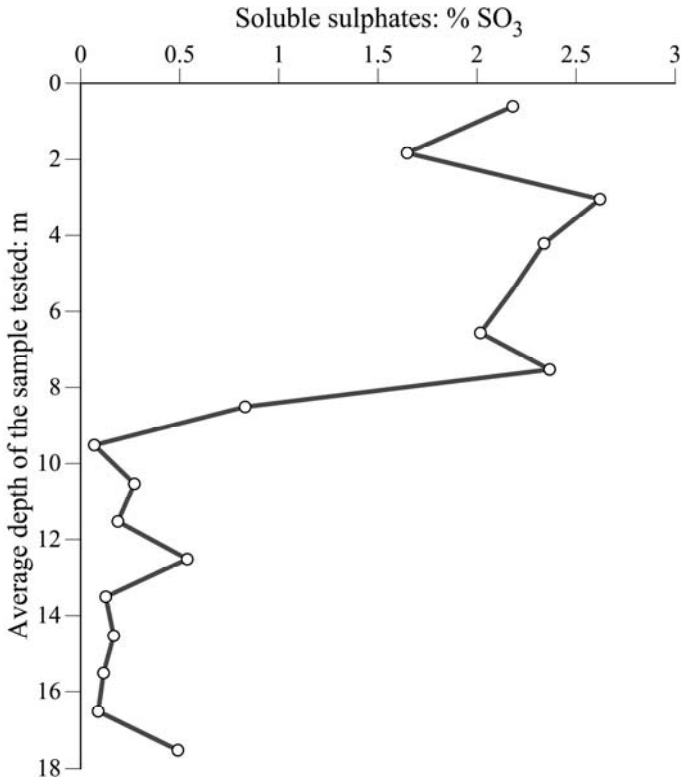

Figure 8.19. Variation of sulphate content determined in samples recovered in boring S-2.1B. Tarragona embankment

8.4.1 Swelling tests

Samples recovered in borings were difficult to test because of the presence of gravels. The following procedure was followed to approximate the conditions in the embankment. Gravels of limestone or sandstone were removed and the remaining soil was homogenised. The homogenisation was carried out in disturbed samples recovered in boring lengths of approximately 1.20 m. The resulting "soil" was compacted to the energy of Standard Proctor and a water content of 10%. A dry density very close to 2 g/cm^3 was achieved in four tested samples that extended from the surface to a depth of 4.80 m. Samples were tested in the plastic mould used for compaction (diameter 120 mm; height 160 mm). Silicon grease was previously applied to the mould inner surface. The unloaded samples were placed in a closed chamber at a constant temperature (8ºC) and the lower 20–30 mm of each sample were kept in a bath under water. Water could migrate upwards by capillary gradients. Vertical displacements were measured on the sample top.

The results are shown in Figure 8.20. The initial response reflects a "standard" swelling associated with suction reduction and clay minerals hydration, but the long-term swelling observed in all samples cannot be explained by these mechanisms. In addition, the strong swelling measured in some samples, especially in one of them (1.20–2.40 m), is not expected in a low-plasticity soil compacted at a Standard Proctor density. The mineral content of the samples before testing was not determined. Therefore the measured swelling cannot be related to some particular distribution of constituents (the compaction water content and dry density were very similar in all four samples tested). The significant result is that all tests exhibited a long-term swelling which, despite variation from test to test, was very relevant. Again, these tests are an indication of the heterogeneity of fill characteristics. The sample taken from 1.20–2.40 m, which developed the strongest swelling, was dismantled after 150 days of testing and smaller portions were subjected to X-ray diffraction and scanning electron microscopy (SEM) observations. Ettringite and thaumasite crystals were identified. They also provided strong peaks in the X-ray diffractograms. Samples collected in the embankments were also analysed, as described below.

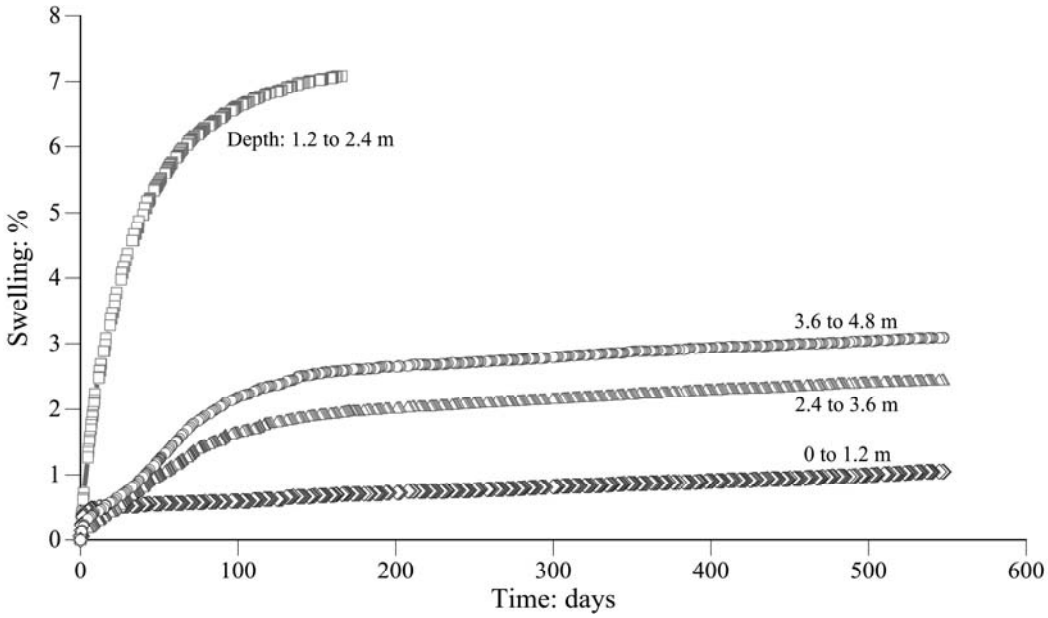

Figure 8.20. Long term swelling tests on compacted samples. Boring S-2.1B

8.5 Design and construction of a soil treatment over underpass

The second case concerns a rigid reinforced concrete caisson structure 11.2 m wide and 6.25 m high, built under the railway tracks, close to Pallaressos embankments, to allow for the

crossing of an aqueduct. The structure was capped by a layer of cement treated soil, 1.5 m thick. Above, base and ballast layers complete the layered system supporting the railway tracks. Figure 8.21 shows a cross section of the caisson. Material for the fill came from a nearby cut in the same railway line. The exposed slopes showed the soil formation: a Tertiary red claystone with abundant gypsum veins.

Periodic track levelling detected a progressive heave of the tracks above the caisson. The maximum accumulated vertical displacement measured in July 2011 was about 12 cm.

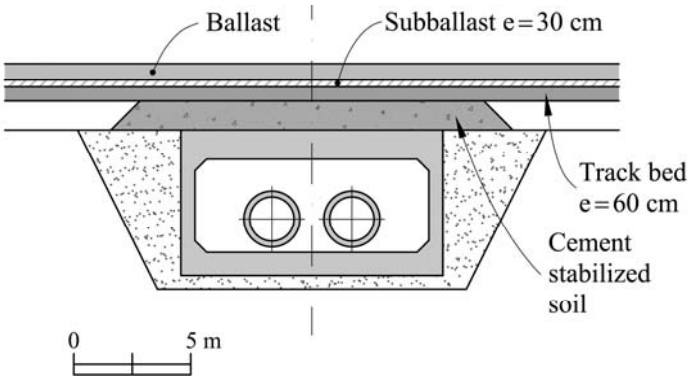

Figure 8.21. Cross section of the caisson of the underpass

8.6 Field data

Topographic levelling of the caisson didn't show any vertical displacement of the structure. This indicated that the vertical displacements measured at the rail tracks were a result of the behaviour of the material placed above the concrete caisson. A convex surface, centred in the caisson axis, was also visible in the field (Figure 8.22). In addition, the thickness of the ballast layer was noticeably lower in the bulging area, because of the necessary periodic ballast thickness correction. Two high precision (± 0.003 mm/m) vertical continuous extensometers (SL-1 and SL-2), 10 m long, were installed in boreholes located in the caisson backfill material, close to the concrete structure. Both extensometers recorded the development of vertical strains at both backfills within the upper 4 m (Figure 8.23). Figure 8.24 plots the accumulated vertical displacements measured by the continuous extensometer SL-1 within the upper 4 meters. A maximum accumulated heave rate of 1.33 mm/month was measured between 17 February 2012 and 19 April 2012 by continuous extensometer SL-1 within the upper 4 metres. A heave rate of 0.91 mm/month was recorded during the same period at the same depths in the other backfill (SL-2).

Continuous cores and undisturbed samples were recovered from boreholes performed for the installation of extensometers. A few SPT tests were also performed in borings for the installation of SL-1 and SL-2, at depths of 0.6-2.50 m. The recorded values (N = 46, 25, 39, 26, 42) reveal a compact material although the presence of gravels complicate the interpretation. A borehole 2.8 m long was also drilled above the caisson, centred along the axis of the caisson. A value N = 20 was measured in this location at a depth of 1.30-1.90 m. Interestingly, the material recovered from boreholes at depths varying from 1.2 to 2.75 m was found to be soft and wet or very wet. At those depths the existence of a heavily weathered material with presence of a mixture of cement and some sand was also observed.

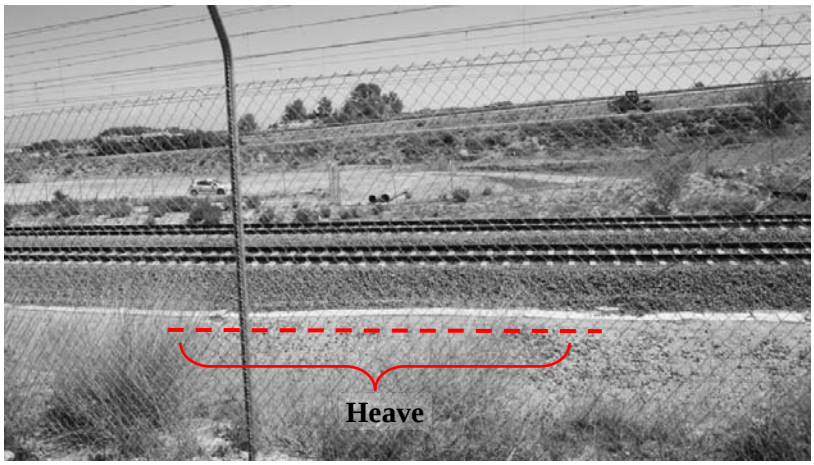

Figure 8.22. Bulge of the surface above the caisson. Observe the reduced thickness of the ballast layer

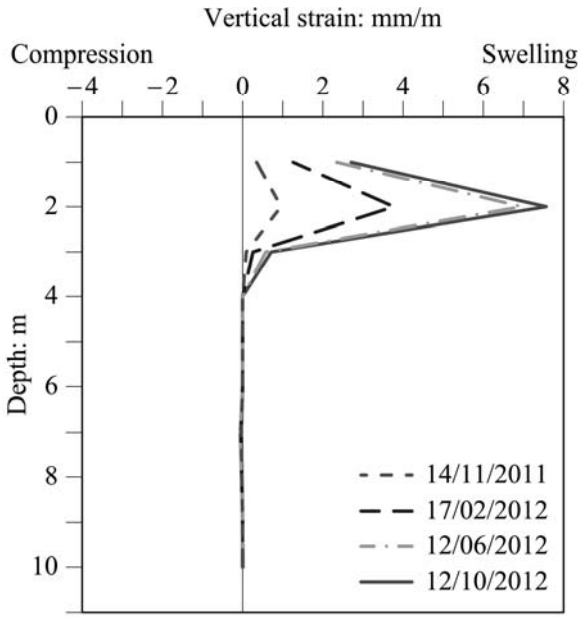

Figure 8.23. Vertical strains measured in depth along the continuous extensometer SL-1 installed within the backfill of the concrete caisson

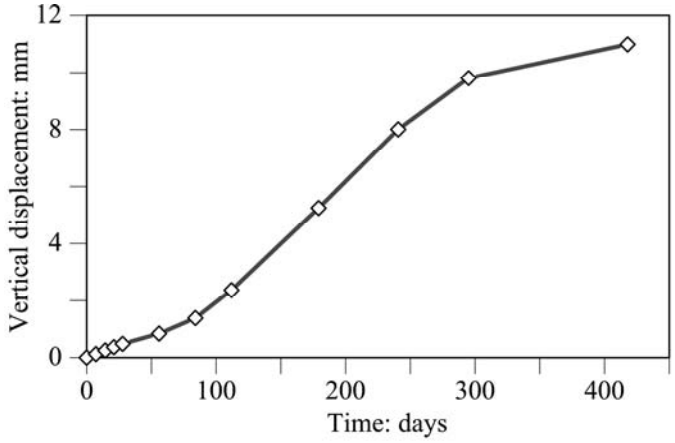

Figure 8.24. Accumulated vertical displacements measured by continuous extensometer SL-1 within the upper 4 metres

8.7 Geotechnical data. Laboratory tests

Identification tests were performed on samples recovered from boreholes drilled at the backfills and above the caisson. Sulphate and soluble salts content tests were also conducted on some of the recovered samples. The soluble sulphate content obtained in all samples is lower than 1%. The water contents in the samples tested from boreholes for the installation of SL-1 and SL-2 are respectively 8.4% and 11%. A maximum value of water content of 16.1% was measured in the laboratory in a sample recovered from the layer placed above the caisson. The values of dry density and water content in the tested samples indicate that the materials located in the upper layers in the vicinity of the caisson not only have increased in humidity but they had also lost density. The increase in humidity and the decrease in density are related to the crystal growth associated with the sulphate attack to cement.

8.7.1 Swelling tests

Free swelling tests were performed on samples prepared with the material recovered in boreholes. Two types of samples were tested with material coming from each location. Undisturbed samples as well as samples compacted at the dry density corresponding to the Normal Proctor test were tested. All samples were partially submerged in water and were placed inside a cold-storage chamber at a constant temperature of 8ºC during the test. Figure 8.25 shows the vertical swelling strains measured during the free swelling tests performed. Swelling evolves in time in all the samples tested without signs of levelling off.

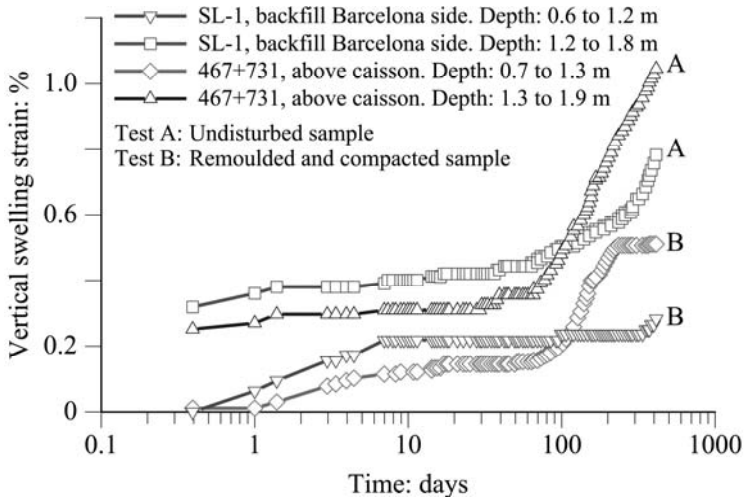

Figure 8.25. Swelling vertical strains recorded in free swelling tests

8.8 Mineral growth at Pallaressos embankments and at the treated layer over the underpass

8.8.1 Mineral growth at Pallaressos embankments

Samples for mineralogical observations were taken from several positions in the field at the area of Pallaressos embankments:

- core samples from boreholes instrumentation
- samples taken from the exposed soil or jet-grouting columns on the surface of embankments
- samples taken in excavations of the upper 5 m of the embankments during underpinning.

They were subjected to X-ray diffraction analysis and SEM-EDS (scanning electron microscopy-energy dispersed spectrometry) observations. An optical microscope with a 100× magnifying power was also employed. The results can be summarized as follows:

- Poorly cemented soil-cement mixtures or pure cement grout had a low apparent weight, a wet, sometimes muddy, consistency, and a whitish colour. Ettringite and, most notably, thaumasite were always found (Figure 8.26) The SEM photographs in Figure 8.27, Figure 8.29 and Figure 8.31 are characteristic patterns. The spectrums of the

element analysis by EDS on isolated needles corroborate the identification of ettringite and thaumasite crystals (Figure 8.28, Figure 8.30 and Figure 8.32).

– The following minerals were detected in the reddish clay matrix: calcite, gypsum, quartz, dolomite, illite (sericite) and kaolinite.

– Low-density thin flakes could be easily peeled off from the cement treated columns, which often exhibited an advanced degradation state. A white powder was observed, especially in fissures or holes. When observed by the SEM, it was identified as thaumasite crystals.

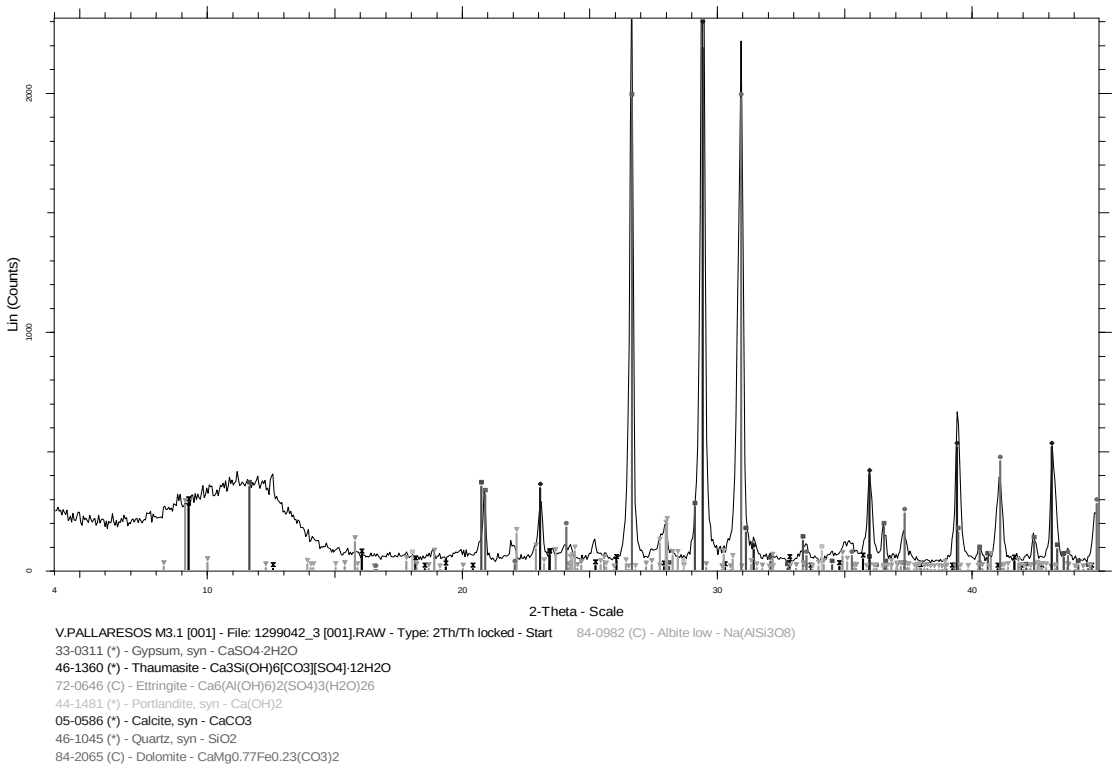

Figure 8.26. X-ray diffraction spectrogram of a sample from the mud jet-grouting treated soil material from borehole E1.1

8.8.2 Mineral growth at the treated layer over underpass

A mineralogical analysis by means of X-ray diffraction on samples recovered from the upper meters of boreholes revealed the presence of ettringite and gypsum in the material recovered from the treated (classified as low plasticity clay and sand mixtures).Calcite, quartz, dolomite and illite were also found. The presence of wet material can be probably related with the

ettringite crystal growth because the crystalline structure of ettringite crystals content a high percentage of water.

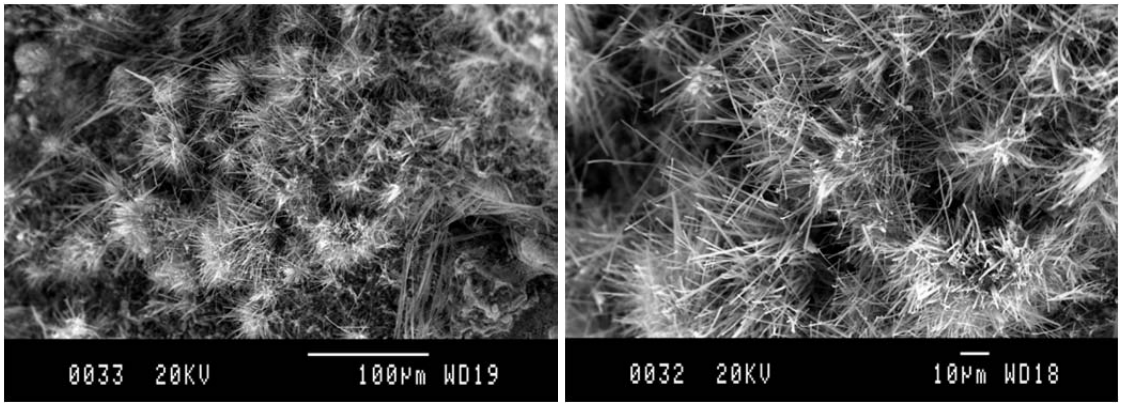

(a) (b)

Figure 8.27. Ettringite needles found in a tested sample: (a) view of an area totally occupied by ettringite crystals; (b) detail from area shown in (a)

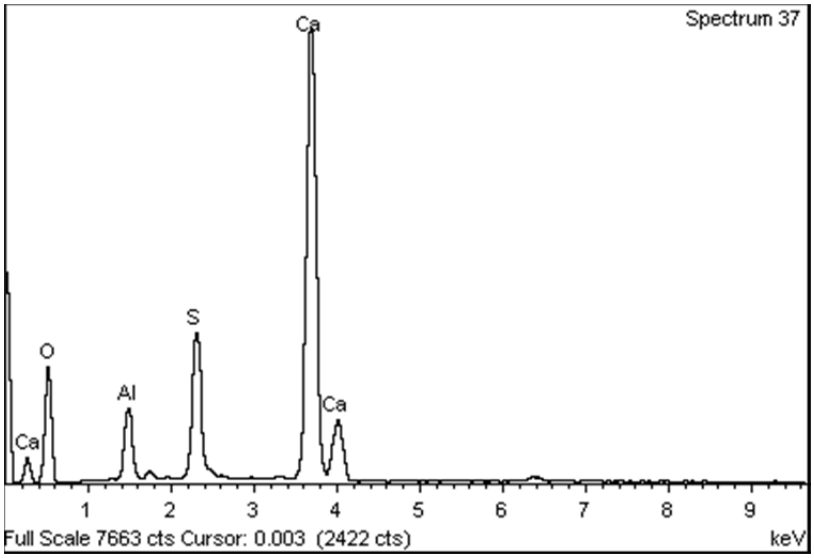

Figure 8.28 Spectrum of element analysis by means of EDS of crystal needles shown in Figure 8.27(b)

8.8.3 Discussion

The existence of thaumasite and ettringite at both cases point at the main cause of the swelling observed. Ettringite and thaumasite are rare minerals not present in the natural clay soil used for the construction of the embankments. Thaumasite is related to the formation of ettringite, which is a mineral associated with the sulphate attack to cement. The formation of thaumasite is considered a second stage of this attack. Actually, spectrograms of the treated soil present a hill shape between 2θ from 10º to 15º (Figure 8.26), which is characteristic of sulphate attack.

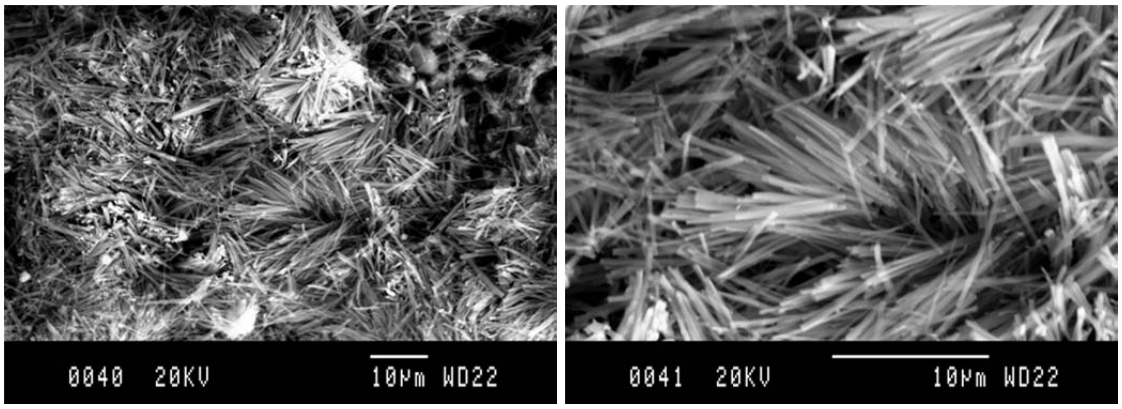

(a) (b)

Figure 8.29. Thaumasite crystals found in a tested sample: (a) view of an area totally occupied by thaumasite crystals; (b) detail of thaumasite crystals shown in (a)

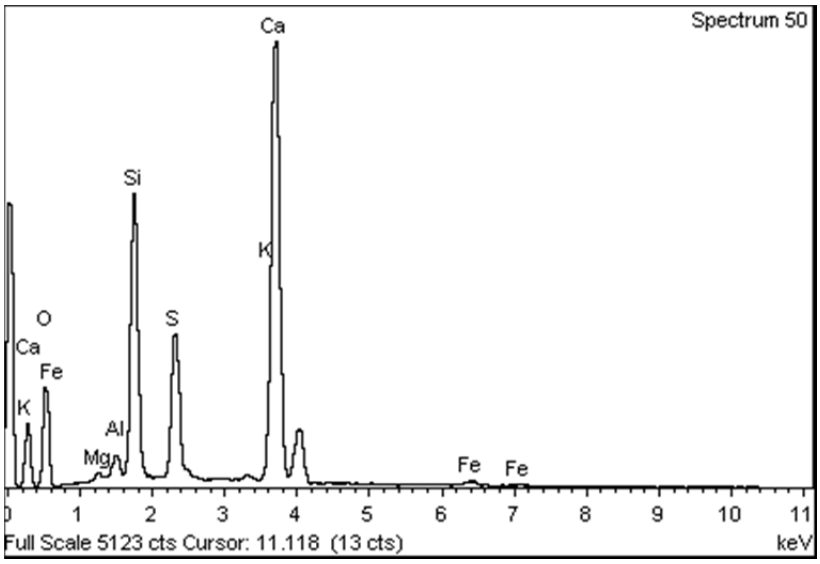

Figure 8.30. Spectrum of element analysis by means of EDS of crystal needles in Figure 8.29(b)

Sulphate attack on bases stabilized with lime or cement executed from sulphated soils has been described in the literature (Hunter, 1988, Mitchell, 1986, Mitchell and Dermatas 1992). The attack to sulphated soils treated with stabilizers made of lime or cement consists in the degradation of the cementing agents' structure and in the whole swelling, due to the formation of ettringite and thaumasite crystals. The damage due to swelling depends on the soil composition, the execution methods, the availability of water, the ionic migration and the possibility that the expansive mineral growth could be accommodated in the soil porosity (Simic, 2007). A chemical detailed description of the process of formation of ettringite and thaumasite in sulphated soils stabilised with lime or cement is presented in the following section.

8.9 Chemical reactions for the formation of ettringite and thaumasite minerals. Fundamental aspects

The chemical formulae for ettringite and thaumasite are:

– Ettringite: $Ca_6[Al(OH)_6]_2(SO_4)_3 \cdot 26H_2O$

– Thaumasite: $Ca_6[Si(OH)_6]_2(CO_3)_2(SO_4)_2 \cdot 24H_2O$

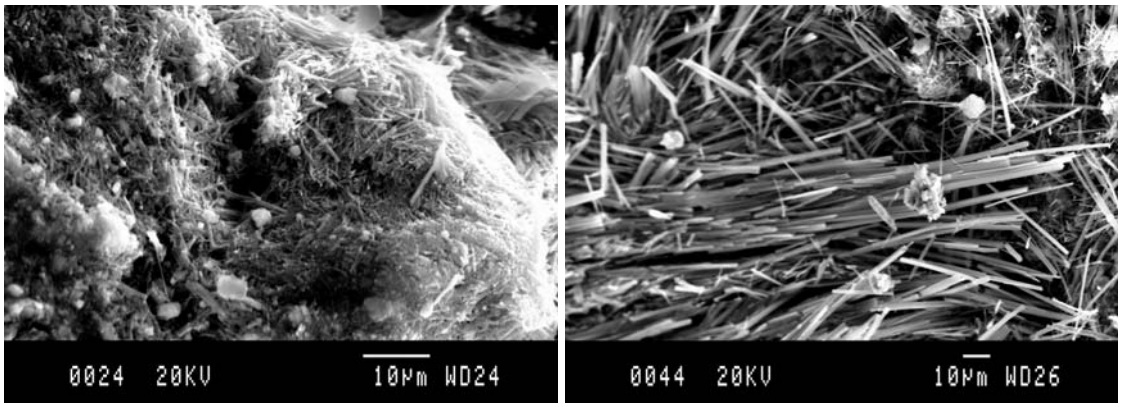

(a) (b)

Figure 8.31. Area with ettringite and thaumasite crystals found in a tested sample: (a) general view; (b) detail of flat crystals of thaumasite and ettringite needles shown in (a)

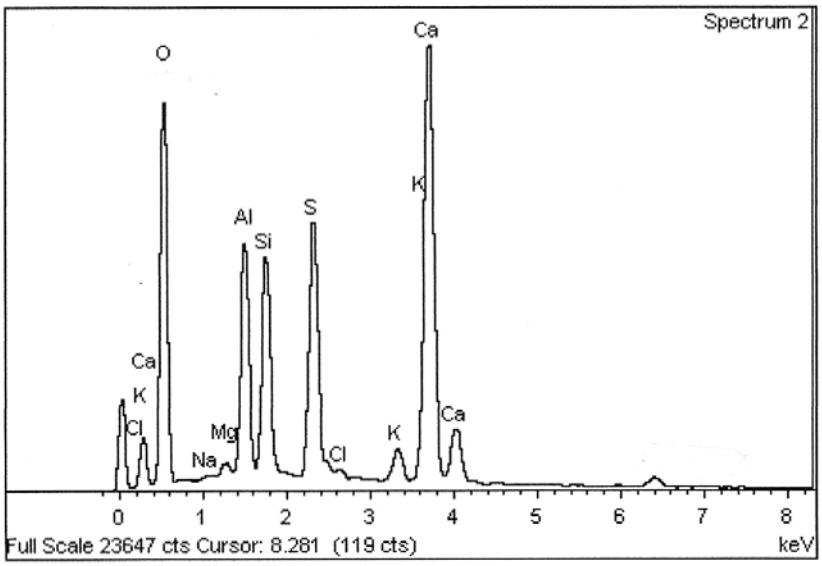

Figure 8.32. Spectrum of the element analysis by EDS of the needles in Figure 8.31 (b)

In both minerals, the presence of water is remarkable. Ettringite is a calcium aluminium sulphate hydrate. Water is predominant in its composition. Carbonates, sulphates, silicates and hydroxides make up the composition of thaumasite. The high proportion of water in

thaumasite is also remarkable; however, it is lower than in ettringite. The crystalline structure of ettringite and thaumasite is represented in Figure 8.33.

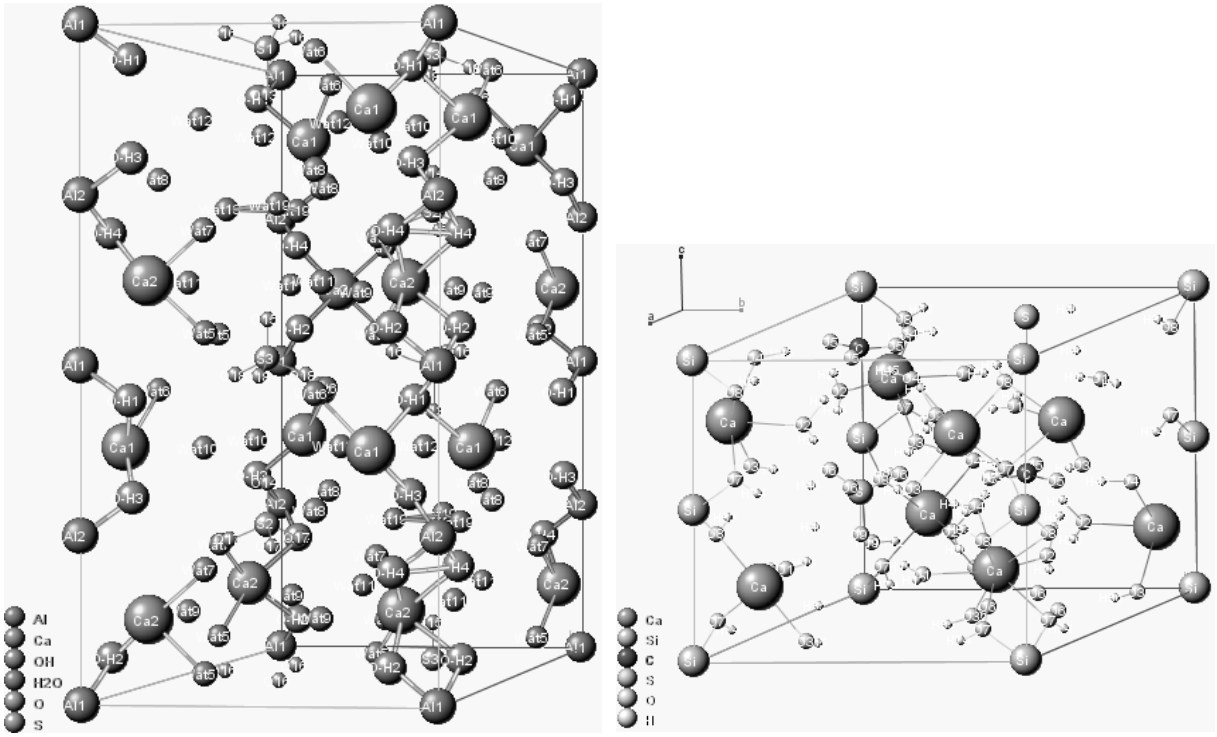

(a) (b)

Figure 8.33. Crystalline structure of: (a)ettringite; (b) thaumasite

Thaumasite growth is regarded as a secondary process once ettringite has crystallised. The chemical formulae of both minerals show the formation of ettringite and thaumasite requires the existence of calcium, carbonates, sulphates, silicates and water. Comparing the two atomic compositions, thaumasite implies the substitution of Al by Si and the presence of a carbonate component. The development of both minerals follows a complex process, which has been described by Hunter (1988), Mitchell & Dermatas (1992) and Mohamed (2000). The sequence of chemical reactions taking place in lime stabilized sulphated soils from Hunter 1988 and Mohamed (2000) is presented in Appendix 8.1. The chemical reactions involved in the formation of ettringite and the effects related with soils stabilized with cement are similar than in the soils stabilized with lime (Rajasekaran, 2005).

In lime or cement stabilised soils, the process of ettringite and thaumasite crystals formation starts by the hydration of lime or Portland cement and the ionisation of the calcium hydroxide. This increases the porosity in the treated soil and produces and alkali environment, pH reaches values up to 12.3. The Ca^{+2} ions are released from the calcium cemented agents and

are then present in the pore solution. Dissolution of clay minerals takes place at pH higher than 10.5. Therefore the highly basic environment (pH > 12) dissolves clay minerals, which provide a source for Al and Si. High pH, higher than 9, also favours the dissolution of sulphate minerals from the soil, which provides Ca^{2+} and SO_4^{2-} ions. Ettringite precipitates when aluminium released from clays, calcium from cement or lime, and sulphates from the sulphated soil (or sulphated water) combine with water molecules. Crystals develop in the pore solution (Deng & Tang, 1994; Mohamed, 2000). The availability of water for ettringite and thaumasite formations is important because it allows the transport of ions and also because ettringite and thaumasite are highly hydrated minerals and can't be formed without an important source of water.

Carbonic acid, present in the pore water, and the dissolution of calcite in that carbonic acid provide a source of carbonate ions that lead to the precipitation of thaumasite, once ettringite is present. The expansive potential of thaumasite formation has been questioned by Hunter (1988). Hunter (1988) suggests that since ettringite forms first in laboratory when alumina and silica are present in the solution, the change from ettringite to thaumasite may have taken place after the development of expansions. XRD analysis on lime stabilized sulphate bearing clay soils affected by severe expansions have identified only thaumasite crystals in damage subbases in some cases, e. g. Stewart Avenue and Owens Street in Las Vegas described by Hunter (1988); whereas only ettringite crystals have been identified in other cases, e. g. in Kansas, described by Mitchell (1986). Hunter (1988) indicates that the presence of thaumasite (and the absence of ettringite) in the damaged treated soil suggests that the transition of ettringite to thaumasite is complete. And, on the other hand, Hunter (1988) proposes that when only ettringite exists that means that the mineralogical study was carried out before the start of the transition. The dominant presence of thaumasite in the analysed samples from the embankment suggests an advanced state of sulphate attack. Bensted (2003) indicates that thaumasite can be formed by a direct reaction between calcium, sulphate, silica and carbonate ions in water solutions. This would lead to the idea that thaumasite may have originated the expansions observed in damaged soils when only thaumasite has been found. However, these reactions are unlikely or very slow (Köhler *et al*., 2006). Additionally, it has been reported that thaumasite crystallises only at temperatures not reaching 15ºC, a result that was recently challenged by Blanco-Varela *et al*. (2006), who found that thaumasite may develop at temperatures as high as 25ºC. Rajasekaran (2005) reports that ettringite appears to be more

stable above 15ºC. Therefore, the climate in Pallaressos and in the nearby cement treated stretch over caisson (a marked two-season Mediterranean environment) may explain the development of thaumasite as well as ettringite at all times throughout the year.

8.10 Chemical modelling

With the purpose of obtaining an improved understanding of the sulphate attack, a simulation of the processes taking place at the soil-cement interface was performed with the help of a general purpose transport and chemical reactions program, RETRASO (REactive TRAnsport of SOlutes: Saaltink *et al.*, 1998, 2005). RETRASO solves the coupled hydraulic transport processes and the chemical reactions. Chemical equations provide the source or sink terms (concentrations of different species) of the mass conservation equations. The set of non-linear partial differential equations is solved simultaneously by iterative procedures. The included transport processes are advection, molecular diffusion and mechanical dispersion. The code handles mineral precipitation and dissolution reaction under a large set of experimental kinetic and equilibrium laws. Kinetic laws are included in a large database. The structure of the kinetic equations was proposed by Lasaga (1984). The code can handle a number of chemical reactions (acid-base, redox, aqueous complexation, etc.) under local equilibrium.

A simple one-dimensional problem, illustrated in Figure 8.34(a), was analysed. Two porous materials, the compacted soil and a cement grout, interact through a common interface. The soil/cement properties and their “active” constituents are given in Table 8.1. Only diffuse processes are considered.

The idea was to check whether ettringite comes out naturally as a new species, and to follow its distribution in space (on both sides of the interface) and time. In addition, there was an interest in knowing the evolution of other constituents and the pH of the medium, a key piece of information to explain the sulphate attack. This geometry is especially relevant for the attack of jet grouting columns in Pallaressos embankments.

An initial pH in equilibrium was calculated for the soil and the cement pore water with the program PHREEQC (Parkhurst, 1995; Parkhurst & Appelo, 1999) considering that the aqueous solutions in soil and cement pores are in equilibrium with soil and cement respectively. PHREEQC simulates chemical reactions in aqueous solutions and allowed to determine the initial conditions (pH and chemical speciation), in the aqueous solutions

interacting at the interphase. The initial values of pH = 7.7 and pH = 12.4 were calculated for the soil and cement pore water respectively. Then, RETRASO was used to obtain the precipitated or dissolved amounts of calcite ($CACO_3$), dolomite ($CaMg(CO_3)_2$), gypsum ($CaSO_4 \cdot 2H_2O$), ettringite. They were calculated by equilibrium equations, because they result from rapid reactions. In the case of the calculation of the precipitated or dissolved amounts of kaolinite ($Al_2Si_2O_5(OH)_4$), quartz (SiO_2) and portlandite (calcium hydroxide, $Ca(OH)_2$), kinetic equations were used in RETRASO. Some results are given in Figure 8.34 for a calculation period of five years.

Table 8.1. Initial parameters for hydro-chemical analysis

Property	**Compacted soil**	**Cement**
Porosity	0.3	0.3
Diffusion coefficient, *D*	10^{-9} m^2/s	10^{-9} m^2/s
Volumetric fractions	Calcite: 0.2	Portlandite: 0.35
	Dolomite: 0.18	Quartz: 0.35
	Gypsum: 0.05	
	Kaolinite: 0.05	
	Quartz: 0.03	
Reactive surface	0.14 m^2/m^3	0.14 m^2/m^3

The pH maintains a high value on the cement side of the interface. A plume of high pH values migrates progressively towards the soil (Figure 8.34(b)). In parallel, an ettringite front advances (Figure 8.34 (c)) in the cement medium. In 5 years, a deep penetration is calculated (~ 1.5 m). The sulphate attack started (against the treated wedge and, later, against jet-grouting columns) in 2006, soon after the end of embankment construction. The calculated depth of the ettringite front in Figure 8.34 (c) suggests that the attack has currently (2014) affected the whole volume of the grouted columns. In fact, in all samples recovered at different positions, ettringite and/or thaumasite was identified.

Two additional results are shown in Figure 8.34(d)-(e): Kaolinite is being progressively dissolved in the soil, starting at the interface, because of the increase of pH at the pore water

in the soil material. The consequence is the release of Al ions, necessary for ettringite precipitation. The concentration of sulphate increases at the interface and in the immediate vicinity, which induces the precipitation of ettringite.

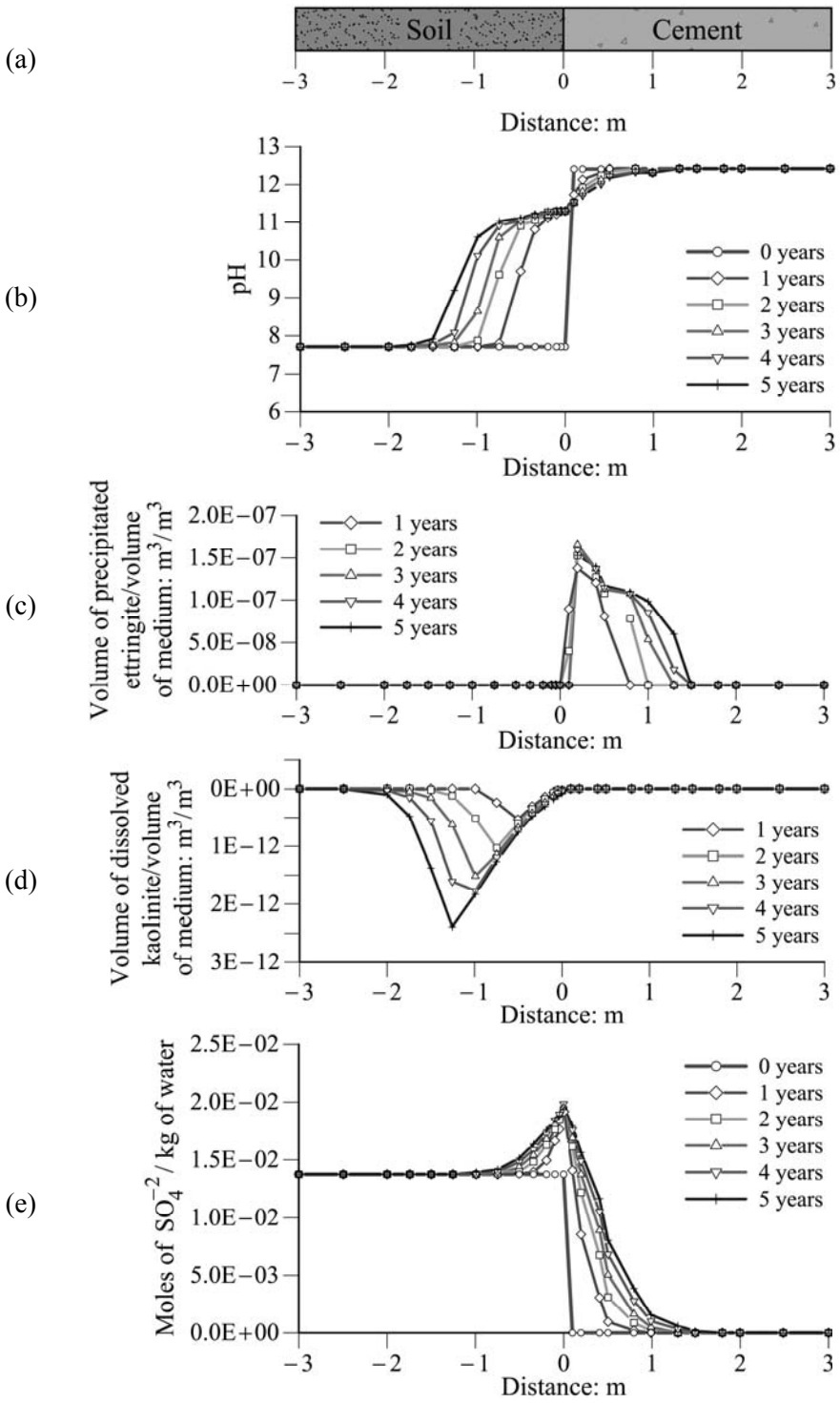

Figure 8.34. Analysis of the soil-cement reactions with the program RETRASO: (a) geometry of the problem; evolution and distribution of: (b) pH; (c) volumes of ettringite; (d) volume of kaolinite; (e) concentration of sulphate

Even if the analysis performed is quantitative, the calculated volume fraction of precipitates (or dissolved species) is not believed to be representative. The real problem is exceedingly complex: the reactive surface is unknown (a small value, 0.14 m^2/m^3, was adopted in the calculation model), there are uncertainties on the validity of the kinetic equations, the pore water was probably under significant suction values for most of the time, initial volume fractions and diffusion coefficients were estimated, etc. Therefore, no attempt was made to couple the chemical calculations with the observed heave. The measured swelling strains and their effect on the bridge were approached in a much simpler manner, as discussed below. Nevertheless, the chemical analysis performed provided a good understanding of sulphate attack.

8.11 Modelling embankment swelling

Measured swelling strains and surface heave provided data to perform a stress analysis of the embankment. A suspected passive state in the upper part of the embankment caused some concern because of a possible instability disrupting the rail tracks. Also, there was an interest of structural engineers in charge of bridge rehabilitation in estimating the existing longitudinal forces against the bridge.

A plane strain analysis was conducted (Figure 8.35). The embankment material was simulated as a Mohr-Coulomb model with parameters estimated from available design and construction data (E = 67MPa, ν =0.3, c' =5 kPa, φ' = 30º). Elastic moduli were measured in loading-reloading branches of plate-loading tests performed during embankment construction. Seven tests were performed, and the chosen value is close to the lower limit. Strength parameters are a conservative estimate of the compacted low-plasticity soil. A zero dilatancy angle was also imposed.

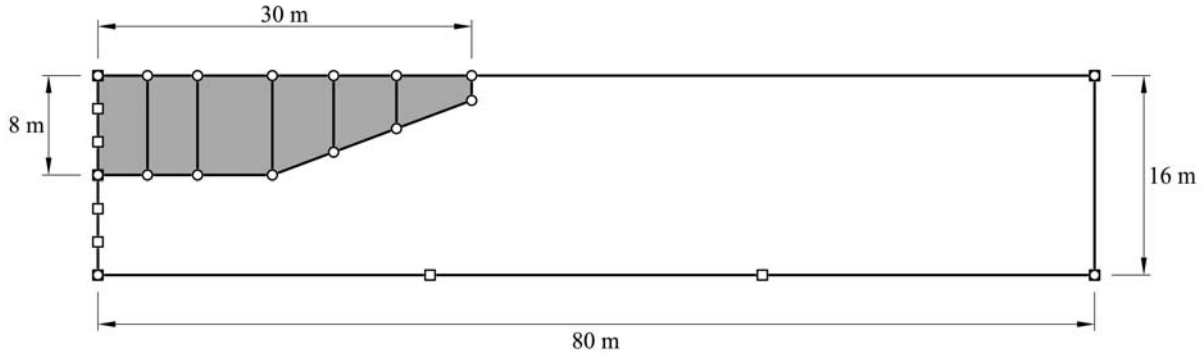

Figure 8.35. Geometry of finite-element model

Swelling was modelled by imposing a volumetric deformation distributed in the volume indicated in Figure 8.35. This active zone was divided in sectors, following the data provided by the continuous extensometers. The imposed strains were guided by two criteria: reproducing the sliding micrometer data approximately, and reproducing the measured heave at surface level.

Figure 8.36 shows the comparison of measured and calculated heave in the period 26 May 2008 to 9 December 2009. Swelling strains result in a substantial change in the initial geostatic distribution of stresses. Horizontal stresses become major principal stresses in the upper part of the embankment (Figure 8.37). Calculated stresses against the fixed bridge abutment indicated that the essentially horizontal stresses have reached a passive state. The calculation provided an estimated total force of 2.32 MN/m in the transverse direction against the bridge abutment. A discontinuity is calculated at the boundary between the swelling layer and the lower non-active soil.

Calculated stresses and forces against the bridge are most probably a lower limit to the actual values because of the conservative estimate of friction and effective cohesion, bearing in mind that the fill remains unsaturated. Increased strength would not prevent a passive state being reached, because the actual swelling experienced by the fill since the first warnings in 2006 is substantially higher than the modelled heave recorded in the shorter period analysed.

It was concluded that, in addition to the need to provide a new and stable support for the rails, the stresses against the bridge abutment should also be substantially reduced. On the other hand, there was no hope of a reduced swelling rate for the immediate future.

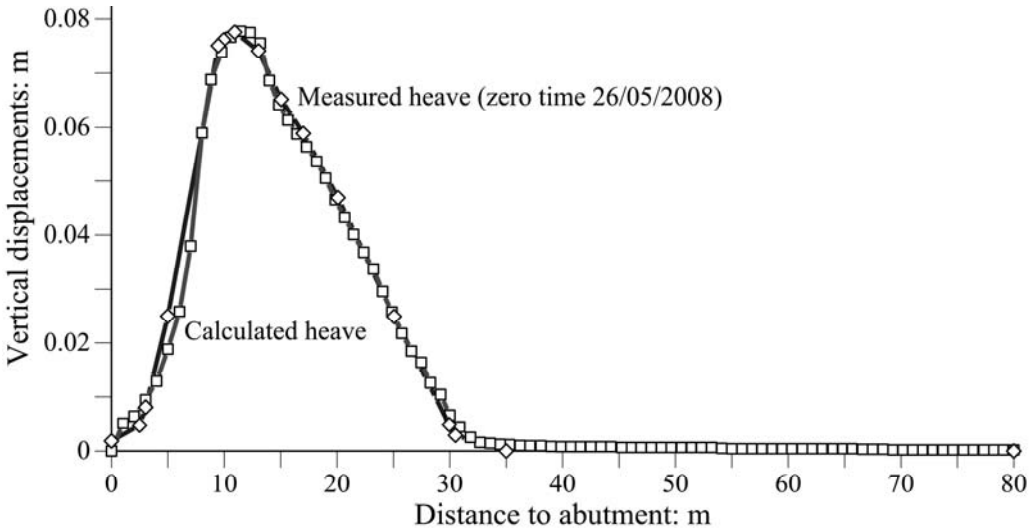

Figure 8.36. Calculated and measured vertical displacements, matching recorded swelling

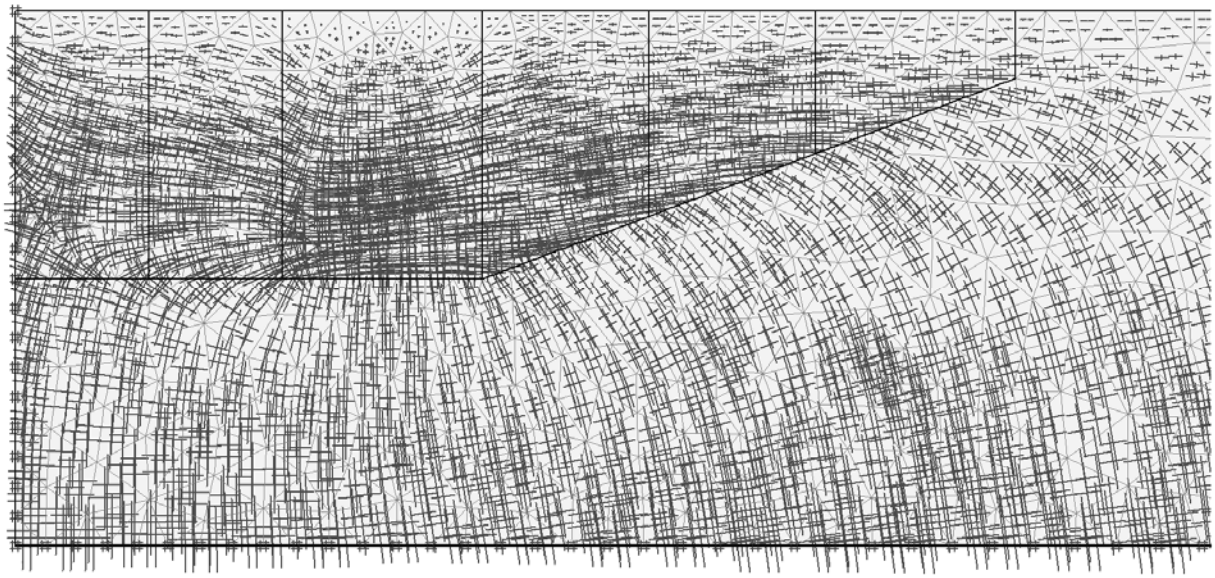

Figure 8.37. Calculated principal stresses in embankments

8.12 Remedial measures at Pallaressos embankments and at underpass

Despite the signs of a mature state of the sulphate attack (hydro-chemical calculations described; dominant presence of thaumasite), the field swelling records suggested that heave of the treated embankments could continue for years at a sustained rate. Modifying the thickness of the ballast cushion below the rail tracks could not cope with the expected medium-term heave. Forces against the abutment wall were damaging the bridge, and a passive state of stress, threatening the rail tracks, had developed in the upper part of the embankments.

It was then decided to excavate the upper 6 m of the embankments in the stretch affected by sulphate attack, and also to support the rail tracks by a structure founded on piles on both sides of the embankment. The solution is shown in Figure 8.38. Supporting piles (excavated piles, which reach the substratum) were first built in the position shown in the plan view of Figure 8.38(a). Then reinforced concrete slabs were built on the sides of the railway tracks, after enlarging the embankments in a lateral direction. Once the rail tracks were underpinned, the upper part of the embankments was excavated in stretches 9 m long, and the concrete slabs were slid into place. Figure 8.38(b) shows a longitudinal section of the solution. An open gap, 3 m thick, has been left between the lower surface of the slabs and the new upper surface of the embankments.

The solution of the heave problem above the caisson requires the removal of the cement treated layer and its substitution by a stable compacted granular material.

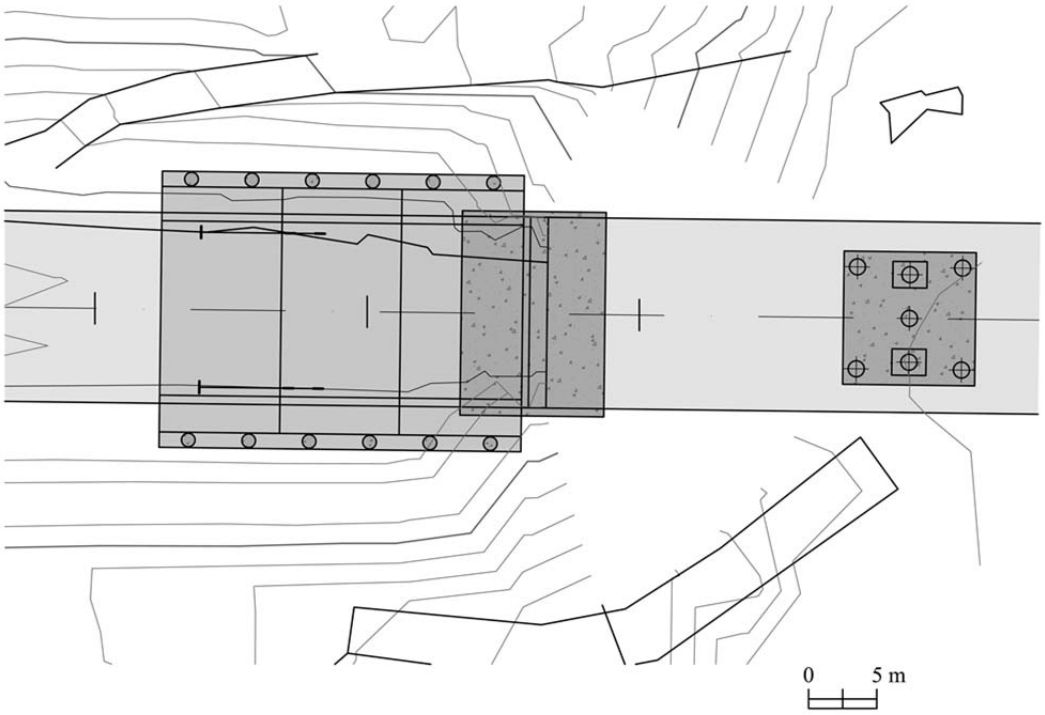

Figure 8.38. Design of repair solution: (a) plan view of slabs founded on piles; (b) longitudinal section showing excavation, underpinning of rail tracks, supporting reinforced slabs and piles

8.13 Concluding remarks

The field swelling records suggested that heave of the treated embankments and above the caisson could continue for years at a sustained rate. Modifying the thickness of the ballast cushion below the rail tracks could not cope with the expected medium term heave. In the case on embankments, the pressure developed against the bridge abutment wall was capable of damaging seriously the bridge. In addition, the vertical heave and a state of passive stresses, eventually leading to a shearing failure of the upper meters of the embankments, and

the sustained heave over the underpass posed an additional threat to the operation of the railway line.

Sliding micrometer data were conclusive in showing the extent of the swelling strains within the embankment. At the embankments, the upper 8 m had a sulphate content (2.5%) sufficiently high to explain the attack. However, solid gypsum gravels were scattered throughout the soil mass. They constitute, "de facto", a substantial increase in gypsum content, which is not accounted for in the chemical analysis of the fine fraction of the soil. Gypsum was also present in the material used in the track base. The presence of cement treated transition wedges and, specially, the installation of jet-grouted columns within the embankment triggered the attack. The growth of ettringite and thaumasite requires the presence of sulphtes, clay, a basic environment provided by cement hydration and water. All of these conditions were present in the embankments.

The potential growth of ettringite and thaumasite will continue until the exhaustion of sulphates. The availability of other chemical species (calcium, silicates, aluminium and water) seems essentially unlimited in the embankments.

The longitudinal profile of surface heave is, in part, explained by the layout of grouting columns. Friction against the abutments, enhanced by the high horizontal stresses developed in the longitudinal direction, explain the small vertical displacements measured in the vicinity of the abutment wall. The restriction to vertical heave offered by the abutment also explains, to some extent, the settlements measured by the extensometers below the upper expanding volume. But there is also the possibility of a collapse of soil as rain water migrates downwards. The compaction data given in Figure 8.16 indicate that a significant proportion of the embankments was initially under high suction. The confining stress below the "active" upper part (vertical stresses in excess of roughly 170–180 kPa) is probably enough to explain some collapse strains. This aspect of the embankment behaviour has not been analysed in this Chapter, which concentrates on the chemical changes and their consequences associated with the sulphate attack on cement treated materials in the presence of clay minerals and water.

The case history described is a case of failure of the controls expected during the execution of earthworks for bridge abutments. The Spanish Standards indicate that soils containing gypsum and other salts should not be stabilised with cement. The Standards also open the possibility of using sulphate-resistant cement in cases of sulphate content in excess of 0.5%.

Many access embankments to bridges located in the very large Ebro Basin, where sulphates are widespread, have been built in recent years. Apparently, no similar reaction has been reported and no damage was observed in those cases. Standards also specify that the Director of Works should conduct a laboratory testing plan, whose scope is also defined, before authorising the initiation of fieldworks. It seems that in Pallaressos and the underpass these controls and provisions were not followed to the extent required in the case reported.

Appendix 8.1. Sequence of chemical reactions taking place in lime stabilized sulphated soils

The formation of ettringite and thaumasite requires the occurrence of the following summarised chemical reactions (Mohamed, 2000 from Hunter 1988). The reactions written below don't take into account the presence of other salts in the soil:

1) Lime hydration. Generation of an alkaline environment

$$CaO + H_2O \rightarrow Ca(OH)_2 \tag{8.1}$$

2) Ionization of calcium hydroxide; pH rises to 12.3, high alkaline environment

$$Ca(OH)_2 \rightarrow Ca^{2+} + 2(OH)^- \tag{8.2}$$

3) Dissolution of silicate clay minerals at pH>10.5 (Montmorillonite)

$$\begin{aligned} &Al_4Si_4O_{10}(OH)_2 \cdot nH_2O + 2(OH)^- + 10H_2O \rightarrow \\ &\rightarrow 2\left\{2Al(OH)_4^- + 4H_4SiO_4\right\} + nH_2O \end{aligned} \tag{8.3}$$

4) Dissociation of silicic acid

$$2H_4SiO_4 \rightarrow 2H_3SiO_4^- + 2H^+ \rightarrow H_2SiO_4^{2-} + 2H^+ \tag{8.4}$$

5) Dissolution of sulphate minerals; x=1, y=2 o x=2, y y=1

$$M_xSO_4 \cdot nH_2O \rightarrow XM^{Y+} + SO_4^{2-} + nH_2O \tag{8.5}$$

6) Ettringite formation

$$6Ca^{2+} + 2Al(OH)_4^- + 4OH^- + 3SO_4^{2-} + 26H_2O \rightarrow \\ \rightarrow \left\{Ca_6\left[Al(OH)_6\right]_2 \cdot 24H_2O\right\}(SO_4)_3 \cdot 2H_2O \quad (8.6)$$

7) Formation of carbonic acid

$$CO_2 + H_2O \rightarrow H_2CO_3 \quad (8.7)$$

8) Dissolution of calcite in carbonic acid

$$CaCO_3 + H_2CO_3 \rightarrow Ca^{2+} + 2H^+ + 2CO_3^{2-} \quad (8.8)$$

9) Thaumasite formation due to isostructural substitution as ettringite changes to thaumasite

$$\left\{Ca_6\left[Al(OH)_6\right]_2 \cdot 24H_2O\right\}(SO_4)_3 \cdot 2H_2O + 2H_2SiO_4^{2-} + 2CO_3^{2-} + O_2 \rightarrow \\ \rightarrow Ca_6\left[Si(OH)_6\right]_2 \cdot (SO_4)_2 \cdot (CO_3)_2 \cdot 24H_2O + 2Al(OH)_4^- + 4OH^- + SO_4^{2-} + H_2O \quad (8.9)$$

CHAPTER 9

Conclusions and Future research

9.1 Conclusions

This Thesis deals with the expansive mechanisms induced by crystal growth that may develop in rocks and compacted soils containing sulphates.

The risk of anhydritic rocks in engineering works

Swelling in anhydritic formations is a widespread phenomenon well known in Central Europe because a high number of tunnels crossing formations containing anhydrite have been affected by damaging expansions taking place below tunnel floor. Anhydritic formations are abundant in Spain; therefore a potential risk of sulphate-related damaging expansions in infrastructures exists. Lilla, Camp Magré, Puig Cabrer and Albertia tunnels are recent cases in Spain. Damaging expansions in sulphated rocks can also appear in deep pile foundations. The heave of Pont de Candí bridge is a relevant and unique example. Uplifts reported very recently in the towns of Staufen in Germany and Lochviller in France highlight the widespread occurrence of these phenomena.

The mechanism

The classical explanation of the direct transformation of anhydrite exposed to water into gypsum is not the mechanism that explains the expansions. It is really a question of reaching supersaturated conditions in calcium sulphate dissolved. Supersaturation resulting in gypsum precipitation can be achieved by the evaporation of groundwater but this is not enough to explain the observed magnitude of swelling. Dissolution of anhydrite results also in supersaturated conditions with respect to gypsum since the solubility of anhydrite is higher than the solubility of gypsum. This is believed to lead to large expansions observed in the cases described. The presence of fractures in the rock naturally existent or induced by excavation (tunnelling) favours the precipitation of gypsum when water and anhydrite are present.

Main observations in Lilla tunnel and lessons learned.

The development of extreme heave in Triassic sulphated rocks is known from other European tunnels; however record values of swelling pressures were reached in Lilla tunnel excavated in Tertiary Eocene clay rock deposits. Expansions in the tunnel occur mainly below the invert. Precipitation of gypsum takes place in open discontinuities induced by the stress relief generated by the excavation of the tunnel. A circular reinforced cross-section was adopted to repair the tunnel and recent measurements in the reinforced section have shown that the expansive phenomenon hasn't stopped although it is slowly reaching stationary conditions after an 8 year period of observations. The measurements in the reinforced tunnel show that the swelling phenomenon is heterogeneous, which favours the resisting capability of the circular cross section. In addition, the expansion phenomenon observed is very three-dimensional, which also helps the lining to resist stresses. Field investigation pointed out the importance of rock mass fracturing in the development of swelling.

Main observations in Pont de Candí bridge and lessons learned

Heave in Pont de Candí demonstrates that the swelling mechanism is developed if the required conditions for the occurrence of expansions are present. This is a very singular case of expansions below a deep pile foundation due to the precipitation of gypsum in discontinuities. Gypsum precipitation in fractures was found at depths where the development

of expansions in time was measured. The triggering of expansions has been associated with the construction of the bridge. The embankment built in the area of Pont de Candí has demonstrated that an increase of the effective stress applied to crystals reduces crystal growth.

Modelling gypsum crystallization at a large scale

A model has been developed for simulating the expansions in sulphated rocks due to gypsum crystal growth. The presence of soluble sulphated minerals and the occurrence of precipitation and dissolution of crystals have been considered in the formulations. The sensitivity analysis performed indicated that the initial anhydrite and gypsum content, solubility of gypsum and anhydrite and, especially, the confining stress have a relevant effect on the swelling strains calculated. The simulation of gypsum precipitation and expansions has been successful in Pont de Candí. The tool developed is believed to constitute a step forward in the analysis and prediction of swelling phenomena in sulphate bearing clay rocks

Sulphate attack in embankments

Although sulphate attack is known in treated compacted layers with lime or cement, the phenomenon has been analysed in the case of a massive attack to embankments, which implies large pressures against bridge abutments. The development of expansions due to the precipitation of ettringite and thaumasite is essentially unlimited because of the availability of the necessary components for its formation in the compacted embankments and track bases.

9.2 Future research

The mechanisms involved in the swelling behaviour are well understood, however the following topics have been selected to clarify some remaining uncertainties:

Mechanism of swelling:

Several uncertainties remain related to the control that some variables, may exert on the process of crystal growth and therefore on the swelling mechanism:

- The effect of the composition of water: there might be an effect of the chemical characteristics of the rock/soil and groundwater chemical composition, the coexistence of other dissolved salts, on the precipitation of gypsum, ettringite or

thaumasite, on the inhibition of crystal growth of those minerals and also on the kinetics of the process. Laboratory tests may be conducted to study these effects in an attempt to provide kinetic equations of precipitation and dissolution of crystals.

- The effect of the structure of the rock mass: the influence of pore size distribution and the presence of discontinuities is not completely clear in the occurrence and the dynamics of crystal growth. Laboratory tests may be designed and performed to identify the relevance of these variables on crystal growth and associated effects (swelling strains and swelling pressure).
- The effect of the non soluble clay matrix, present in the anhydritic rock analyses is not fully understood.

Modelling:

- The model developed for the simulation of expansions due to gypsum crystal growth may be generalised to include the knowledge obtainded from the investigation proposed previously in order to improve the predicting capabilities. The presence of fractures and development of discontinuities as a result of construction processes (i.e. tunnel excavation) may be also included in the model as well as the precipitation of crystals due to evaporation of sulphated water.
- The chemical proccesses of dissolution and precipitation of minerals involved in the precipitation of ettringite and thaumasite may be included within a numerical model in a coupled manner with the mechanical effects generated.

REFERENCES

Abduljauwad, S.N., Al-Sulaimani, G.J., Basunbul, I.A. & Al-Buraim, I.A. (1998). Laboratory and field studies of response of structures to heave of expansive clay. *Géotechnique* **48**, No. 1: 103-121.

ADIF (2006). *Línea de Alta Velocidad Madrid-Zaragoza-Barcelona-Frontera Francesa, Tramo: Lleida – Martorell, Subtramo IV-b. Refuerzo del revestimiento en los Túneles de Lilla, Camp Magré y Puig Cabrer (Tarragona).* Madrid, Spain: ADIF.

Aigner, T. (1990). Zyklische stratigraphie und ablagerungsbedingungen von Hauptmuschelkalk, Lettenkeuper und Gipskeuper in Nordost-Württemberg. *Geol. Ver., N. F.* **72**: 125-143.

AITEMIN (2009). *Ensayos hidráulicos de interferencia en el viaducto de Pont de Candí (Tarragona).* Madrid, Spain: AITEMIN.

Alonso, E. E. & Berdugo, I.R. (2005). Expansive behaviour of sulphate-bearing clays. Keynote Paper. *Proceedings of International Conference on Problematic Soils*, *Famagusta*, N. Cyprus. Bilsel & Nalbantoğlu (eds), Eastern Mediterranean University Press: 477– 498.

Alonso, E. E. & Olivella, S. (2008). Modelling tunnel performance in expansive gypsum claystone. *Proceedings of the 12th Conference of International Association for Computer Methods and Advances in Geomechanics (IACMAG), Goa*, 891-910 (CD-ROM).

Alonso, E. E. & Sagaseta, C. (2003). *Informe previo sobre los problemas derivados de la expansividad del terreno en los túneles de Lilla, Camp Magré y Puig Cabrer.* Barcelona, Spain: Department of Geotechnical Engineering and Geosciences, UPC.

Alonso, E. E., Berdugo I., R., Tarragó, D. & Ramon, A. (2007). Tunnelling in sulphate claystones. Invited Lecture. *Proc. 14th European Conference on Soil Mechanics and Geothecnical Engineering, Madrid*, **1**, 103–122.

Alonso, E. E., Berdugo, I., Gens, A. & Romero, E. (2004). Expansive phenomena in an instrumented tunnel excavated in anhydritic-gypsiferous argillaceus rocks. *Proceedings of the ISRM Regional Symposium EUROCK 2004 and 53rd Geomechanics Colloquy*. Salzburg **1**, 241–244.

Alonso, E. E., Gens, A. & Lloret, A. (1993). Heave of a nuclear power station founded on expansive siltstone. Unpublished.

Amstad, C. & Kovári, K. (2001). *Untertagbau in quellfähigem fels*. Zürich, Switzerland: Eidgenössisches Departement für Umwelt, Verkehr, Energie und Kommunikation (UVEK) and Bundesamt für Strassen (ASTRA).

Anadón, P., Cabrera, L., Guimerà, J. & Dantanach, P. (1985). Paleogene strike-slip deformation and sedimentation along the southeastern margin of the Ebro Basin. In: Biddle, K., Christie-Blick, N. (eds.). Strike-slip deformation, basin formation and sedimentation. Society of Economic Paleontologists and Mineralogists, Special Publication **37**, 303-318.

Anagnostou, G. (1992). *Untersuchungen zur Statik des Tunnelbaus in quellfähigem Gebirge*, Mitteilungen des Institut für Geotechnik der ETH Zürich, Vol. 201. Zurich, Switzerland: ETH.

Anagnostou, G. (1993). A model for swelling rock in tunnelling. Rock Mech. Rock Engng **26**, No. 4, 307–331.

Anagnostou, G. (2007). Design uncertainties in tunnelling through anhydritic swelling rocks. *Felsbau - Rock and Soil Engineering*, **25**, No. 4, 48–54.

Anagnostou, G. (2011). Tunnelling in anhydritic swelling rocks. *Proc. Túneles en terrenos salinos y expansivos*, Barcelona, pp. 41-56.

Anagnostou, G., Pimentel, E. & Serafeimidis, K. (2010). Swelling of sulphatic claystones – some fundamental questions and their practical relevance. *Geomechanics and Tunnelling*, **3**, No. 5, 567–573.

ASTM (2008). *Standard test methods for one-dimensional expansion, shrinkage, and uplift pressure of soil-lime mixtures*, ASTM D3877/08. West Conshohocken, PA, USA: ASTM International.

Ayala, F.J., Oteo, C., Ferrer. M. & Salinas, J.L. (1986). *Mapa Previsor de Riesgos por Expansividad de Arcillas en España a Escala 1:1.000.000.* Instituto Geológico y Minero de España y Centro de Estudios y Experimentación de Obras Públicas (Madrid).

Banerjee, A. & Merino, E. (2011) Terra rossa genesis by replacement of limestone by kaolinite. Part III, Dynamic quantitative model. *Journal of Geology* **119**, No. 3, 259-274.

Barton, A.F.M. & Wilde, N.M. (1971) Dissolution rates of polycrystalline samples of gypsum and orthorhombic forms of calcium sulphate by a rotating disc method. *Trans. Faraday Soc*. **67**, No. 583, 3590-3597.

Bensted, J. (2003). Thaumasite: Direct, woodfordite and other possible formation routes. *Cem. Concre. Comp.,* **25**, No. 8, 873–877.

Berdugo, I. R. (2007). *Tunnelling in sulphate bearing rocks: Expansive phenomena*. PhD Thesis, UPC, Barcelona, Spain.

Berdugo, I.R., Alonso, E.E. & Romero, E.E. (2006). Swelling mechanisms in sulphate-bearing rocks. *Proc. Eurock 2006*, Van Cotthen, Charlier, Thimus & Tshibangu eds, Taylor & Francis Grup, London: 451-454.

Berner, D. (1991). Die Geologie des Freudensteintunnels, *Ingenieurbauwerke*, DB Neubaustrecke Mannheim-Stuttgart, No. 7.

Bischoff, N. & Hagmann, C. (1977). Field instrumentation for the design of tunnels in swelling rock. *Int. Symp. für Untertagbau*, Luzern: 657-668.

Bjerrum, L. (1967). Progressive failure in slopes of overconsolidated plastic clay and clay shales. *J. Soil Mech. and Found. Div. ASCE*, 93(SM5): 3-49.

Blanco-Varela, M.T., Aguilera, J. & Martínez-Ramírez, S. (2006) Effect of cement C_3A content, temperature and storage medium on thaumasite formation in carbonated mortars. *Cement Concrete Res.*, **36**, 707–715

Charola, A. E., Pühringer, J. and Steiger, M. (2007). Gypsum: a review of its role in the deterioration of building materials. Environ. Geol. 52: 339-352.

Chiaverio F., Hürzeler D. (1996): Adlertunnel; Bergmännische Tunnelstrecke, Schweizerischer Ingenieur und Architekt, No. 18.

de Torres, T., Sánchez, A. (1990). Espesores de las facies Keuper en la rama castellana de la Cordillera Ibérica y en el dominio Pre-Bético. *In Formaciones evaporíticas de la Cuenca del Ebro y cadenas periféricas, y de la zona de Levante*, Ortí & Salvany Eds, Barcelona.

Deng, M. & Tang, M. (1994). Formation and expansion of ettringite crystals. *Cement Concrete Res.* **24**, 119–126.

DETCG (2010). *CODE_BRIGHT User's Guide*. Available on-line: https://www.etcg.upc.edu/recerca/webs/code_bright

Deu, A. (2008). Estudio experimental del crecimiento de minerales sulfatados en argilitas anhidrítico-yesíferas. Final degree Thesis, UPC-UB, Barcelona, Spain.

Dhowian, A.M., Youssef, A. & Erol, O. (1987). Swelling soil problems in Saudi Arabia. *6th International Conference on Expansive Soils, New Delhi*: 17-22.

DIT-UPC (2002). *CODE_BRIGHT, a 3-D program for thermo-hydro-mechanical analysis in geological media: User's guide*, Centro Internacional de Métodos Numéricos en Ingeniería (CIMNE), Barcelona.

Einfalt, H. C. & Götz, H. P. (1976). Contribution to: Behaviour of anhydrite after addition of water. *Bulletin – International Association of Engineering Geologists*, **13,** No. 1, 69–70.

Einfalt, H. C. (1975). *Ergebnisse der Untersuchungen an den Calciumsulfaten aus dem Gipskeuper Stuttgarts*. Stuttgart, Germany: Ministerium für Wirtschaft, Mittelstand und Verkehr.

Einfalt, H. C. (1979). Umwandlung von Anhydrit in Gips: Mechanismus und Einflussfaktoren. *Ber. Nat. Tag. Ingenieurgeologie Fellbach* **2**, 153–158.

Einstein, H. H. (1979). Tunneling in swelling rock. *Underground Space* **4**, No.1: 51-61.

Einstein, H. H. (1996). Tunneling in difficult ground: swelling behaviour and identification of swelling rocks. *Rock Mechanics and Rock Engineering*, **29**, No. 3, 113–124.

Esteban, F. (1990). *Caracterización experimental de la expansividad de una roca evaporítica: Identificación de los mecanismos de hinchamiento*. PhD. Thesis. Universidad de Cantabria, Spain.

Fecker, E. (1992). Untersuchung von schwellvorgängen und erprobung von auskleidungskonzepten beim Freudensteintunnel. *Taschenbuch für den Tunnelbau 1996*, pp. 16-20. Essen, Germany: Verlag Glückauf.

Flatt, R. J. 2002. Salt damage in porous materials: how high supersaturations are generated. *Journal of Crystal Growth* **242**: 435–454.

Fletcher, R. C. & Merino, E. (2001). Mineral growth in rocks: Kinetic-rheological models of replacement, vein formation, and syntectonic crystallization. *Geochimica et Cosmochimica Acta* **65**, No. 21, 3733-3748.

Freyer, D. & Voigt, W. (2003). Crystallization and Phase Stability of CaSO4 and CaSO4 – Based Salts. Invited review. *Monatshefte für Chemie* **134**, 693–719.

Götz, H. P. (1972). Zur frage der sohlhebungen im Gipskeuper. *Proceedings of the international symposium on underground construction*, Lucerne, pp. 128–132.

Grob, H. (1972). Schwelldruck im Belchentunnel. *Proceedings of the international symposium on underground construction*, Lucerne, pp. 99–119.

Grob, H. (1976). Swelling and heave in swiss tunnels. *Bulletin - Association of Engineering Geologists* **13**: 55-60.

Hauber, L. (1996). Die Geologie des Adlertunnels. *Schweizer Ingenieur und Architek*. **18**, 341-344.

Henke, K.F. (1976). Magnitude and rate of heave in tunnels in calcium sulphate bearing rocks. *Bulletin International Association of Engineering Geologists* **13**, 61-64.

Holliday, D.W. (1970). The petrology of secondary gypsum rocks: a review. *Journal of Sedimentary Petrology,* **40**, No. 2, 734–744.

Huder, J. & Amberg, G. (1970). Quellung in Mergel, Opalinuston und Anhydrit. *Schweizerische Bauzeitung, Jhrg.* **88**, 43.

Hunter, D. (1988). Lime-induced heave in sulphate-bearing clay soils. *J. Geotech. Eng., ASCE*, **114**, 150–167.

Iberinsa (2006). Technical report – personal communication.

IGME (1981). Map of distribution of Triassic outcrops in Spain.

Jeschke, A.A., Vosbeck, K., & Dreybrodt,W. (2001) Surface controlled dissolution rates of gypsum in aqueous solutions exhibit nonlinear dissolution kinetics. *Geochimica et Cosmochimica Acta*, **65**, No.1, 27-34.

Jordan P. & Nüesch, R. (1989). Deformation structures in the Muschelkalk anhydrites of the Schafisheim Well (Jura Overthrust, Northern Switzerland). *Ecologae Geologicae Helvetiae* **82**, No.2, 429-454.

Julivert, M. (1954). Estratigrafía del Eoceno-Oligoceno entre el Francolí y el Anoia. *Instituto Geología Diputación Provincial Barcelona, Memorias y Comunicaciones* **11**, 5-22.

Kirschke, D. (1987). Laboratory and in situ swelling test for the Freudenstein tunnel. *Proc. 6th ICRM, Montreal*, v 3: 1492-1496.

Kirschke, D., Kovari, K. & Prommersberger, G. (1991). Bemessungsgrundlagen und Konstruktion der Sohle des Freudensteintunnels. Ingenieurbauwerke, DB Neubaustrecke Mannheim-Stuttgart, Nr. 7.

Köhler, S., Heinz, D. & Urbonas, L. (2006). Effect of ettringite on thaumasite formation. *Cem. Conc. Res.*, **36**, 4, 697–706.

Kolymbas, D. (2005). *Tunnelling and tunnel mechanics: a rational approach to tunnelling*. Berlin, Germany: Springer-Verlag.

Kontrec, J., Kralj, D. & Brečević, L. (2002). Transformation of anhydrous calcium sulphate into calcium sulphate dihydrate in aqueous solutions. *Journal of Crystal Growth*, **240**, No. 1-2, 203-211.

Kovári, K. & Amstad, C. (1982). A new method of measuring deformations in diaphragm walls and piles, *Géotechnique* **32**, No. 4, 402–406, http://dx.doi.org/10.1680/geot.1982.32.4.402.

Kovári, K. & Amstad, C. (1993). Decision making in tunnelling based on field measurements. In *Comprehensive rock engineering: principles, practice & projects*, Oxford-Pergamon Press.

Kovári, K. & Descoeudres, F. (2001). *Tunnelling Switzerland*. Swiss Tunnelling Society, Swiss. ISBN 3-9803390-6-8.

Kovári, K., & F. Chiaverio (2007). Modular yielding support for tunnels in heavily swelling rock. *Proceedings STUVA Conference 07, Cologne*, 1-7.

Kovári, K., Amstad, C. & Anagnostou, G. (1988). Design/construction methods: tunnelling in swelling rocks. In *Key questions in rock mechanics (Proc. of the 29th U.S. Symp. Rock*

Mech. Minnesota) (eds. P. A. Cundall, R. L. Sterling and A. M. Starfield), pp. 17–32. Rotterdam, the Netherlands: Balkema.

Krause, H. & Wurm, F. (1975). Geologische Grundlagen und Untersuchungen zum Problem der Sohlhebungen in Keupertunneln Baden-Württembergs, *Strassenbau und Strassenverkehrstechnik* **184**.

Krause, H. (1976). Sulphate rocks in Baden-Württemberg and their importance in relation to civil engineering. *Bulletin - Association of Engineering Geologists* **13**: 45-49.

Krause, H. (1977). Zur geologie und statistik des tunnelbaus in Baden-Württemberg unter besonderer berücksichtigung der Keupertunnel, *Jh. geol. Landesamt, Baden-Württemberg* **19**, 35-57.

Kuhnhenn, K., Bruder, J. & Lorscheider, W. (1979). Sondierstollen und Probestrecken für den Engelber-Basistunnel, *Proceedings 2nd German Congress on Engineering Geology*, DGEG Essen.

Kurz, G. & Spang, J. (1984). Instandsetzung und Erneuerung der Blähstrecke des Kappelesbergtunnels, Bautechnik **11**: 365-376.

Langmuir, D. 1997. *Aqueous environmental geochemistry.* Upper Saddle River: Prentice Hall.

Lasaga, A.C. (1984). Chemical kinetics of water-rock interactions. *Journal of Geophysical Research* **89**, No. B6, 4009-4025.

Lippmann, F. (1976). Corrensite, a swelling mineral, and its influence on floor heave in tunnels in the Keuper formation. *Bulletin - Association of Engineering Geologists* **13**, 65-68.

Lombardi, G. (1979). Rock Mechanics at the CERN Proton-Antiproton Facilities, *4th. Int. Congress on Rock Mechanics*, *Montreux*, 3: 433-436.

Madsen ,F. & Nüesch, R. (1990). Langzeitverhalten von Tongesteinen und tonigen Sulfatgesteinen, Mitteil. des Inst. für Grundbau und Bodenmechanik Nr. 140, ETH, Zürich.

Madsen, F., Flückiger, A., Hauber, L., Jordan, P.& Vögtli, B. (1995). New investigations on swelling rocks in the Belchen tunnel, Switzerland, *Proc 8th International Congress on Rock Mechanics, Gifu*, **1**: 263-267.

Madsen, F.T. & Nüesch, R. (1991). The swelling behaviour of clay-sulfate rocks. *Proc. 7th Int, Congr. on Rock Mech, Aachen* **1**, 285-288.

Marí, A. & Pérez, G.A. (2003). *Refuerzo del revestimiento de los túneles de Lilla y Camp Magré para la Línea de Alta Velocidad Madrid-Zaragoza-Barcelona-Frontera Francesa. Tramo Lleida-Martorell. Provincia* de Tarragona. Barcelona, Spain: Department of Construction Materials, UPC.

Mitchell, J.K. & Dermatas, D. (1992). Clay soil heave caused by lime-sulphate reactions, In *Innovations and uses for lime* (eds D. D. Walker Jr, T. B. Hardy, D. C. Hoffman and D. D. Stanley), ASTM STP 1135, pp. 41–64. West Conshohocken, PA, USA: ATM International.

Mitchell, J.K., 1986. Practical problems from surprising soil behaviour. *J. Geotech. Eng., ASCE* **112**, 259-289.

Mohamed, A. M. O., 2000. The role of clay minerals in marly soils on its stability. *Engineering Geology* **57**, No. 3-4, 193-203.

Nagel, D. (1986). Sohlhebungen in den Keupertunneln von Baden-Württemberg, *Tunnelbau, Kontakt & Studium, Band* **184**, 110-125.

Nahon D. & Merino E. (1997) Pseudomorphic replacement in tropical weathering: Evidence, geochemical consequences, and kinetic-rheological origin. *American Journal of Science* **297**, 393-417.

Nancollas, G.H., Reddy, M.M & Tsai, F. (1973) Calcium Sulfate Dihydrate Crystal Growth in Aqueous Solution at Elevated Temperatures. *Journal of Crystal Growth* **20**, No. 2, 125-134.

Noher, H.P., Kister, B. & Vögtli, B. (2006). Swelling – a geotechnical problem at the Adler Tunnel, Switzerland – monitoring results and their interpretation. *Proc Eurock 2006*, Van Cotthen, Charlier, Thimus & Tshibangu eds, Taylor & Francis Grup, London: 337-342.

Nüesch, R. & Ko, S.C. (2000). Influence of mineralogical composition to experimental swelling behaviour of shaley anhydrite clay. *Applied mineralogy*, Rammlmair et al (ed), Balkema, 611-616.

Nüesch, R., Steiner, W. & Madsen, F.T. (1995). Long time swelling of anhydritic rocks: Mineralogical and microstructural evaluation. *Proc 8th Int Congr Rock Mech*, **1**: 133-138.

Oldecop, L. & Alonso, E. E. (2012). Modelling the degradation and swelling of clayey rocks bearing calcium-sulphate. *International Journal of Rock Mechanics & Mining Sciences* **54**, 90–102.

Olivella, S., Carrera, J., Gens, A. & Alonso, E. E. (1994). Non-isothermal multiphase flow of brine and gas through saline media. *Transport in Porous Media*, **15**, 271–293.

Olivella, S., Gens, A., Carrera, J. & Alonso, E. E. (1996). Numerical formulation for a simulator (CODE_BRIGHT) for the coupled analysis of saline media, *Engineering Computations*, **13**, No 7, 87–112.

Ortí, F. (1977). Aproximación al estudio petrográfico de las microestructuras de las rocas de yeso secundario y a su origen. *Revista del Instituto de Investigaciones Geológicas de la Diputación Provincial de Barcelona* **32,** 87-152.

Ortí, F., Rossell, L., Salvany, J.M., Ingles, M., Permanyer, A. & Gracia, J. (1989). Sedimentología y diagénesis como criterios de prospección de recursos en el Terciario evaporítico de la Cuenca del Ebro. *Proc. 12th Congr. Esp, sedimentología*, Bilbao, 253-262.

Panet, M. (1995) *Le calcul des tunnels par la méthode convergence-confinement*, Paris, France: Presses de l'ENPC, Paris.

Parkhurst, D. L. & Appelo, C. A. J. (1999). *User's guide to PHREEQC (version 2): A computer program for speciation, batch-reaction, one-dimensional transport, and inverse geochemical calculations,* Water-Resources Investigations Report 99-4259. Denver, CO, USA: Earth Science Information Center, US Geological Survey.

Parkhurst, D.L. (1995). *User's guide to PHREEQC-A computer program for speciation, reaction-path, advective-transport, and inverse geochemical calculations*, Water-Resources Investigations Report 95-4227. Denver, CO, USA: Earth Science Information Center, US Geological Survey.

Paul, A. & Walter, F. (2004). Messung der Spannungsänderung im Fels und an Felsbauwerken mit Druckkissen (Measurement of stress changes in rock and rock mass and structures with pressure cells). *Bautechnik* **81**, No. 8, 639–647.

Paul, A. & Wichter, L. (1996). Das langzeitverhalten von tunnelbauwerken im quellenden gebirge - neuere messergebnisse vom Stuttgarter Wagenburgtunnel, *Taschenbuch für den Tunnelbau*, pp. 1154. Essen, Germany, Verlag Glückauf.

Pérez, A.D. (1991). *El Trias de Facies Germánica del sector Central de la Cordillera Bética*. PhD Thesis Universidad de Granada.

Pimentel, E. (2003). Swelling behaviour of sedimentary rocks under consideration of micromechanical aspects and its consequences on structure design. *Proc. GTMM 2003: Geotechnical measurements and modelling* (eds O. Natau, E. Fecker and E. Pimentel), *Karlsruhe*, 367-374.

Pimentel, E. (2007): Quellverhalten von Gesteinen Erkenntnisse aus Laboruntersuchungen. Quellprobleme in der Geotechnik, *Mittelungen der Schweizerischen Gesellschaft für Boden- und Felsmechanik* **154**, 13-20.

Pina, C. (2009). Nanoscale dissolution and growth on anhydrite cleavage faces. *Geochim. Comochim. Acta* **73**, No. 23, 7034-7044.

Pina, C., Becker, U. & Fernández, L. (2000). Epitaxial growth of gypsum on anhydrite: in situ AFM observations and computer calculations. *Journal of Conference Abstracts* **5**, No. 2, 801.

Pineda, J. (2012). *Swelling and degradation of argillaceous rocks induced by relative humidity effects: an experimental study*. PhD Thesis. UPC.

Plaza, A. (2008). Análisis del comportamiento de un túnel excavado en rocas altamente expansivas. Final degree Thesis, UPC-UB, Barcelona, Spain.

Prieto, M., Putnis, A. & Fernández, L. (1990). Factors controlling the kinetics of crystallization: supersaturation evolution in porous medium. Application to barite crystallization. *Geological Magazine* **127**, 485-495.

Prommersberger, G. & Kuhnhenn, K. (1989). The Freudenstein tunnel: tunnel construction in swelling rocks. *Proc. Rapid Excavation and Tunneling Conference*: 678-700.

Puppala, A.J., Wattanasanticharoen, E. & Punthutaecha, K. (2003). Experimental evaluations of stabilisation methods for sulphate-rich expansive soils. *Ground Improvement*, **7**, No.1, 25–35.

Putnis, A., Prieto, M. & Fernández, L. (1995). Fluid supersaturation and crystallization in porous media. *Geological Magazine* **132**, 1-13.

Rajasekaran, G., (2005). Sulphate attack and ettringite formation in the lime and cement stabilized marine clays. *Ocean Engineering*, **32**, 1133–1159.

Rajasekaran, G., Murali, K. & Srinivasaragahvan, S. (1997). Effect of chlorides and sulphates on lime treated marine clays. *Soils and Foundations,* **37**, No. 2, 105–115.

Riba, O. & Macau, F. (1962). Situación, Características y extensión de los Terrenos Yesíferos en España. *I Coloquio sobre Obras Públicas en los Terrenos Yesíferos*. Servicio Geológico de Obras Públicas (Madrid).

Saaltink, M., I., Ayora, C. & Olivella, S. (2005). *User's guide for RetrasoCodeBright (RCB)*. Departament of Geotechnical Engineering and Geo-Sciences, Technical University of Catalonia. Institute of Earth Sciences Jauma Almera, Spanish Research Council (CSIC), Barcelona. 111 p.

Saaltink, M.W., Ayora, C. & Carrera, J. (1998). A mathematical formulation for reactive transport that eliminates mineral concentration. *Water Resour. Res.*, **34**, No. 7, 1649–1656.

Sahores, J. (1962). *Contribution à l'étude des phénomenes mécaniques accompagnant l'hydratation de l'anhydrite*. PhD Thesis, Faculté des sciences de l'Université de Toulouse, France.

Salvany, J.M. (1989). *Las formaciones evaporíticas del terciario continental de la cuenca del Ebro en Navarra y La Rioja*. PhD Thesis Universidad de Barcelona, Spain.

San Dimas, L.F. (2002). *Lilla tunnel: technical report*. Madrid, Spain: Gestor de Infraestructuras Ferroviarias.

Sass, I. & Burbaum, U. (2010). Damage to the historic town of Staufen (Germany) caused by geothermal drillings through anhydrite-bearing formations. *Acta Carsologica*, **39**, No. 2, 233–245.

Sauter, S., Alonso, E.E. and Ramon, A. (2012). Efecto de la expansión profunda sobre cimentaciones por pilotes. *Proceedings of the SEMR and SEMSIG 9th National Symposium*, Sevilla, 385-397.

Scherer, G.W. (1999). Crystallization in pores. *Cement and Concrete Research* **29:** 1347-1358.

Scherer, G.W. 2002. Stress from crystallization of salt in pores. In Proc. *9th Int. Cong. Deterioration and Conservation of Stone.* Amsterdam: V. Fassina.

Schlenker B. (1971). Petrographische Untersuchungen am Gipskeuper und Lettenkeuper von Stuttgart, Oberrhein. *Geol. Abh*. 20, 69-102.

Sener (2006). Technical report – personal communication.

Serrano, A., Oteo, C., Dapena, E. & Martín Viñas, J. (1981). Análisis de los fenómenos de expansión de una formación de margas yesíferas. *Bol. Inf. Lab. Carret. y Geot.* **146**, 9–16.

Sherwood, P.T. (1962). Effect of sulphates on cement and lime stabilized soils. *Highwaay Res. Bull.,* **353**, 98–107.

Simic, D., (2007). Experiencias del tratamiento con cal en las autopistas M-50 y R-4. *II Jornada sobre materiales marginales en obras viarias,* Sevilla, Spain

Snedker, E.A. (1996). M40: Lime stabilization experiences. In *Lime Stabilization*. (eds C. D. F. Rogers, S. Glendinning and N. Dixon), pp. 142–158. London, UK: Thomas Telford.

Steiner, W. (1993). Swelling rock in tunnels: rock characterization, effect of horizontal stresses and construction procedures. *Int. J. Rock Mech. Min. Sci. & Geomech. Abstrs*, **30**, No. 4, 361-380.

Steiner, W., Kaiser, P.K. & Spaun, G. (2011). Role of brittle fracture on swelling behaviour: evidence from tunnelling case histories. *Geomechanics and Tunnelling* **4**, No. 2, 17-32.

Tarragó, D. (2006). Degradación mecánica de arcillitas sulfatadas y su efecto sobre la expansividad. Final degree Thesis, UPC-UB, Barcelona, Spain.

Thut, A., Naterop, D., Steiner, P. & Stolz, M. (2007). *Tunnelling in Squeezing Rock-Yielding Elements and Face Control*. Solexperts document: 8p.

Werder, F. (1989). *Sanierungs- und erneuerungsarbeiten im Belchentunnel (N2),* Dokumentation D 037. Zurich, Switzerland: Schweizerischer Ingenieur- und Architektenverein.

Wichter, L. (1985). Results of long-term measurement in the Wagenburg tunnel in Stuttgart. *Tunnel*, **4**, 254-257.

Wittke, M. (2006). Design, construction, supervision and long-term behaviour of tunnels in swelling rocks. *Proc EUROCK 2006: Multiphysics Coupling and Long Term Behaviour in Rock Mechanics, Liège*, 211–216.

Wittke, W. & Pierau, B. (1979). Fundamentals for the design and construction of tunnels in swelling rock. *Proc. Int. Congr. on Rock Mechanics*, Montreux **2**, 719–729.

Wittke, W. & Wittke, M. (2005). Design, construction and supervision of tunnels in swelling rocks. *Underground space use: Analysis of the past and lessons for the future*, Taylor & Francis Group, London, Erdem & Solak (eds): 1173-1178.

Wittke, W. (1990). *Rock mechanics: theory and applications with case histories*. Springer-Verlag, Berlin.

Wittke, W. (2000). *Stability analysis for tunnels*. Verlag Glückauf GmbH, Essen.

Wittke-Gattermann, P. & Wittke, M. (2004). Computation of strains and pressures for tunnels in swelling rocks. *Tunnelling and Underground Space Technology* **19**: 422–423.

Wittke-Gattermann, P. (1998). Bemessung von Tunneln in quellendem Gebirge. *Forum für junge Geotechnik-Ingenieure*, 25. Baugrundtagung, Stuttgart.

Wittke-Gattermann, P. (1998). Verfahren zur Berechnung von Tunnels in quellfähigem Gebirge und Kalibrierung an einem Versuchsbauwerk. *Geotechnical engineering in research and practice*, WBIPRINT. **1**. Essen: Glückauf.

Wüst, R.A.J. & McLane, J. (2000). Rock deterioration in the Royal Tomb of Seti I, Valley of the Kings, Luxor, Egypt. Engineering Geology **58**: 163–190.

Young, R.G. (2004). Swelling of Sunshine clay and stability of roads. RFT Report **A21**: 214-219.

Zanbak, C. & Arthur, R. C. (1986). Geochemical and engineering aspects of anhydrite/gypsum phase transitions. *Bulletin of the Association of Engineering Geologists* **23**, No. 4, 419-433.